Are all lobes made equal? Comparing the sedimentological processes and depositional architecture of submarine lobes in different palaeogeographic and sequence stratigraphic positions

Yvonne Therese Spychala

Submitted in accordance with the requirements for the degree of
Doctor of Philosophy

The University of Leeds
School of Earth and Environment

April 2016

The candidate confirms that the work submitted is her own, except where work which has formed part of jointly-authored publications has been included. The contribution of the candidate and the other authors to this work has been explicitly indicated below. The candidate confirms that appropriate credit has been given within the thesis where reference has been made to the work of others.

The work in Chapter 4 and 5 of the thesis has appeared in publication as follows:

Spychala, Y.T., Hodgson, D.M., Flint, S.S., and Mountney, N.P., 2015, Constraining the sedimentology and stratigraphy of submarine intraslope lobe deposits using exhumed examples from the Karoo Basin, South Africa: Sedimentary Geology, v. 322, p. 67-81.

Spychala, Y.T., Hodgson, D.M., Stevenson, C.J., Flint, S.S. (accepted), Aggradational lobe fringes: The influence of subtle intrabasinal seabed topography on sediment gravity flow processes and lobe stacking patterns: Sedimentology. DOI: 10.1111/sed.12315

As the primary author, I was responsible for data collection, processing, collation and interpretation, and writing of the manuscript. The contribution of the other authors was limited to discussion of the data and editorial suggestions.

Acknowledgements

Abstract

Submarine lobes are high aspect ratio sand-rich deposits fed by sediment gravity flows via channels. They are a major component of submarine fans, the largest depositional bodies on the planet, and therefore represent an important archive of palaeo-environmental change. Basin-floor, or terminal, lobes, are well-studied. Here, lobes in other geographical positions and the influence of confinement (especially when subtle and dynamic) and stratigraphic position on submarine lobe geometry, stacking patterns, and sedimentary facies are investigated.

Extensive outcrop exposures and near-outcrop research boreholes from Permian fine-grained basin-floor and intraslope lobes in the Karoo Basin (South Africa) allow spatial and stratigraphic variability in sedimentary facies and architecture to be constrained. One hundred and seventy outcrop logs (~6.9 km total length) and 11 core logs (~1 km) from Units A and E, Laingsburg depocentre and Fan 4, Tanqua depocentre, were integrated to enable the analysis of different lobe types within a physical hierarchy and enabled detailed facies distribution trends, stacking patterns and depositional models to be established.

The main outcomes of the study are: 1) recognition criteria for three distinctive lobe fringe settings: frontal, lateral and aggradational lobe fringes; observed differences between frontal and lateral lobe fringe deposits are controlled by flow processes, while aggradational lobe fringes form in response to subtle confinement by intrabasinal slopes; 2) the documentation of lobe stacking patterns within lobe complexes and complex sets. Karoo lobes show a range of stacking patterns that are controlled by seabed topography and sediment supply; 3) the evaluation of hybrid bed distribution that indicates strong geographic but weak stratigraphic trends at different hierarchical scales. Lobe stacking patterns are shown to be a major control in these trends; and 4) the comparison of depositional models established from basin-floor and rare examples of exhumed intraslope lobe complexes that show distinct differences.

Table of Contents

List of Tables

List of Figures

Preface

The thesis comprises three chapters that were prepared for publication in international peer-reviewed journals. At time of thesis submission the status of the manuscripts is as following:

1. Chapter 3: **Spychala, Y.T**., Hodgson, D.M., Prélat, A., Kane, I.A., Flint, S.S., and Mountney, N.P., *in review*, Frontal and lateral submarine fringes: Comparing sedimentary facies, architecture and flow processes. Journal of Sedimentary Research.

   Author Contributions:

   a. Spychala, Y.T. – Main author. Responsible for data collection, processing, collation and interpretation, and writing of the manuscript.
   b. Hodgson, D.M. – In depth discussion and detailed review of the manuscript
   c. Prélat, A. – Discussion and detailed manuscript review. Provision of additional data
   d. Kane, I.A. – Discussion and detailed manuscript review
   e. Flint, S.S.- Discussion and manuscript review
   f. Mountney, N.P. – Discussion and manuscript review

Submitted: 17th February 2016

2. Chapter 4: **Spychala, Y.T**., Hodgson, D.M., Stevenson, C.J., and Flint, S.S., *accepted*, Aggradational lobe fringes: the influence of subtle intrabasinal topography on sediment gravity flow processes and lobe stacking patterns. Sedimentology.

   Author Contributions:

   a. Spychala, Y.T. – Main author. Responsible for data collection, processing, collation and interpretation, and writing of the manuscript.
   b. Hodgson, D.M. – In depth discussion and detailed review of the manuscript

    c. Stevenson, C.J. – Discussion and detailed manuscript revision

    d. Flint, S.S. – Discussion and manuscript review

Submitted: 25th September 2015

Resubmitted: 7th March 2016

Accepted: 19th July 2016

Available Online: 29th July 2016

3. Chapter 5: **Spychala, Y.T**., Hodgson, D.M., Flint, S.S., and Mountney, N.P., 2015, Constraining the sedimentology and stratigraphy of submarine intraslope lobe deposits using exhumed examples from the Karoo Basin, South Africa: Sedimentary Geology, v. 322, p. 67-81.

    Author Contributions:

    a. Spychala, Y.T. – Main author. Responsible for data collection, processing, collation and interpretation, and writing of the manuscript.

    b. Hodgson, D.M. – In depth discussion and detailed review of the manuscript

    c. Flint, S.S. – Discussion and manuscript review

    d. Mountney, N.P. – Discussion and manuscript review

Submitted: 30th January 2015

Resubmitted: 30th March 2015

Accepted: 31st March 2015

Available online: 10th April 2015

"The real voyage of discovery consists not in seeking new landscapes, but in having new eyes."

-Marcel Proust

Chapter 1

Introduction

1.1 Background

Submarine lobes are high aspect ratio sand-rich deposits that are fed by turbidity currents and debris flows via channels in deep-marine settings. Submarine lobes have been identified within various deep-water settings, including the basin-floor (e.g. Harms, 1974; Twichell et al., 1992; den Hartog Jager et al., 1993; Sixsmith et al., 2004; Gervais et al., 2006; Deptuck et al., 2008; Jegou et al., 2008; Prélat et al., 2009, Migeon et al., 2010; Prélat et al., 2010; Macdonald et al., 2011; Prélat & Hodgson, 2013; Grundvåg et al., 2014; Picot et al., 2016), the base-of-slope (Posamentier & Kolla, 2003, Deptuck et al., 2008; Morris et al., 2014a) and on the continental slope (e.g. Prather et al., 1998; Fiduk et al., 1999; Adeogba et al., 2005; Li et al., 2010; Pirmez et al., 2012; Prather et al., 2012 a, b; Oluboyo et al., 2014; Ortiz-Karpf et al., 2015). Their facies associations and distributions, architecture and stacking patterns are controlled by the topographical configuration of the seabed, sediment supply system and slope maturity (disequilibrium/equilibrium). Submarine lobes are a major component of submarine fans, the largest depositional bodies on the planet, and therefore represent an important archive of palaeo-environmental change. Submarine lobe deposits are also of economic interest because of their potential as hydrocarbon reservoirs.

Over the last decade, outcrop studies (e.g. Prélat et al., 2009; Macdonald et al., 2011; Etienne et al., 2012; Grundvåg et al., 2014), geophysical studies (e.g. Gervais et al., 2006; Deptuck et al., 2008, Migeon et al., 2010; Gamberi & Rovere, 2011; Gamberi et al., 2011; Prather et al., 2012 a, b; Oluboyo et al., 2014), numerical and stochastic modelling (Pyrcz et al., 2005; Groenenberg et al., 2010) and flume tank experiments (e.g. Ouchi et al., 1995; Baas et al., 2004; Fernandez et al., 2014) have been undertaken to constrain the hierarchy, geometries and stacking patterns of submarine lobe deposits. More recent studies established a more detailed hierarchy of lobe sub-environments (Gervais et al., 2006; Deptuck et al., 2008, Saller et al., 2008; Prélat et

al., 2009; Mulder & Etienne, 2010; Prélat et al., 2010; Bernhard et al., 2012; Etienne et al., 2012; Grundvåg et al., 2014).

Outcrop and subsurface studies have highlighted that hybrid beds are an important component of lobe deposits (Ito, 2008; Hodgson, 2009; Talling et al., 2012a; Etienne et al., 2012; Grundvåg et al., 2014; Patacci et al., 2014; Collins et al., 2015; Fonnesu et al., 2015). The range of hybrid bed types has been studied by several authors (e.g. Lowe & Guy, 2000; Haughton et al., 2003; Talling et al., 2004; Ito, 2008; Davies et al., 2009; Haughton et al., 2009; Hodgson, 2009; Magalhaes & Tinterri, 2010; Kane & Pontén, 2012; Patacci et al., 2014; Fonnesu et al., 2015) and several flow processes have been proposed for their deposition (e.g. Wood & Smith, 1958; Nelson et al., 1992; Masson et al., 1997; Lowe & Guy, 2000; Haughton et al., 2003; Talling et al., 2004; Ito, 2008; Davies et al., 2009; Haughton et al., 2009; Hodgson, 2009; Baas et al., 2009; Sumner et al., 2009; Baas et al., 2011; Kane & Pontén, 2012; Patacci et al., 2014). However, quantification of stratigraphic and geographic trends are poorly constrained.

The research presented in this thesis builds strongly on outcomes from the LOBE Phase 1 project, which focused on developing models for the depositional architecture and stratigraphic evolution of submarine lobe deposits (cf. Prélat et al., 2009, 2010; Prélat & Hodgson, 2013) based on field and core data in the Karoo Basin, South Africa, and complementary process-based numerical models (cf. Groenenberg et al., 2010).

1.2 Thesis aims

The principal objective of this thesis is to refine and extend depositional and stratigraphic models established in the LOBE 1 project. As well as basin-floor or terminal lobes, which the first phase of the project focussed on, other geographic positions of submarine lobes have been identified within deep-water systems, but their deposits are poorly constrained in terms of detailed sedimentology. Furthermore, the influence of confinement (especially when subtle and dynamic) and stratigraphic position on submarine lobe geometry, stacking pattern, and facies are still poorly understood. Basin-floor lobes and intraslope lobes have been identified in the Laingsburg (Laingsburg and Fort Brown Formations) and Tanqua (Skoorsteenberg Formation) depocentres of the Karoo Basin, South Africa. Extensive and well-

preserved outcrops enable the analysis of different lobe types in various hierarchical and temporal scales, and enable detailed facies distribution trends, stacking patterns and depositional models to be established.

In this context, the thesis is focussed around key research questions. These are outlined in detail as follows, and will be returned to at the end of the thesis (Chapter 7):

Question 1: *What are the sedimentological and stratigraphic expressions of lobe fringes?*

Rationale: Submarine lobe fringe deposits are heterolithic successions that can be rich in hybrid beds (e.g. Haughton et al., 2003; Ito, 2008; Haughton et al., 2009; Davis et al., 2009, Hodgson et al., 2009; Talling et al., 2012a; Etienne et al., 2012; Grundvåg et al., 2014; Patacci et al., 2014; Collins et al., 2015; Fonnesu et al., 2015). They represent the marginal parts of lobe complexes, or can stratigraphically separate lobe axis deposits through compensational stacking (Prélat et al., 2009; Prélat & Hodgson, 2013). Lobe fringe deposits are the least well studied sub-environments of lobes despite 1) showing the widest range of facies configurations and 2) their potential to act as stratigraphic traps being encased within hemipelagic mudstones at the margins of lobe complexes. Testing and evaluating the temporal and spatial variability of lobe fringe successions could help improve reconstructions of deep-water fans, provide suitable building blocks for reservoir modelling and reduce uncertainty in the evaluation of subsurface stratigraphic traps (e.g. Biddle & Wielchowsky, 1994; Etienne et al., 2012; Bakke et al., 2013; Collins et al., 2015; Grecula et al., 2015).

Lobe fringe facies associations include: 1) thick-bedded structureless or planar laminated sandstones that pinch and swell and can comprise thick debrites; 2) argillaceous and clast-rich hybrid beds; and 3) thin-bedded current ripple-laminated sandstones and siltstones. Depending on the distribution of these facies major heterogeneities can be created within a lobe complex. For example, hybrid beds can introduce reservoir heterogeneities on a bed scale due to the vertical juxtaposition of reservoir and non-reservoir lithologies (Davies et al., 2009; Haughton et al., 2009). Differences between down-dip and across-strike facies transitions in lobe deposits have been documented (e.g. MacPherson, 1978; Pickering, 1981, 1983), which could lead to distinctive facies trends in the lobe fringes. However, detailed depositional architecture, recognition criteria and variability between frontal (down-dip) and

across-strike (lateral) lobe fringe environments remain poorly constrained. In addition, even subtle basin confinement could influence lobe fringe facies and stacking patterns as these are deposited by stratified flows. Several authors (Smith, 1987 a, b; Wilson et al., 1992; Smith, 2004 b) described an example of subtle topography and its influence on the Welsh Basin Silurian sandstone systems, where sand-prone lobe deposits laterally grade or transition into mud-rich turbiditic 'levee-like' constructional features due to the influence of faults. These features are interpreted as lobe fringes (Smith, 1987 a, b; Wilson et al., 1992; Smith, 2004 b). The sedimentology of these lobe fringes has not yet been constrained in detail, regarding sedimentary facies, processes and stacking patterns.

Establishing criteria for the identification of different lobe fringe settings could improve interpretation of palaeogeographic setting and degree of basin confinement

To document the variability in the expression of lobe fringes, outcrop and core data from two well-constrained Permian basin-floor fans (Fan 4, Skoorsteenberg Formation, and Unit A, Laingsburg Formation) in the Karoo Basin have been assessed. Specific aims are 1) to establish characteristic facies associations that distinguish different lobe fringe settings, and 2) to discuss the role of confinement in the distribution and character of lobe fringes.

Question 2: *What is the range of stacking patterns that can be constrained from lobe complexes and lobe complex sets?*

Rationale: Stacking patterns of lobes are proxies for the relationship between sediment supply and seabed topography during the deposition of lobe complexes and lobe complex sets (Piper & Normark, 1983; Mitchum & Van Wagoner, 1991; Schlager, 1993; Twichell et al., 2005; Picot et al., 2016). Traditionally, the existence of thickening upward cycles in lobes was interpreted as evidence that progradational stacking was the prevalent stacking pattern in submarine lobes (e.g. Mutti, 1974; Ricci Lucchi, 1975). Since then, several types of stacking patterns have been documented from lobe successions (e.g. Gervais et al., 2006; Amy et al., 2007; Deptuck et al., 2008; MacDonald et al., 2011; Prather et al., 2012b; Prélat & Hodgson, 2013, Burgreen & Graham, 2014; Grundvåg et al., 2014; Picot et al., 2016): compensational, aggradational, and longitudinal, with either basinward (progradational) and landward

(retrogradational) trends. Compensational stacking describes the tendency of sediment to fill topographic lows created by preceding deposits (Mutti & Sonnino, 1981; Straub et al., 2009), while aggradational stacking occurs where avulsion is not possible due to confinement (Burgreen & Graham, 2014). Longitudinal stacking is controlled by basin confinement (which limits space for lateral migration), and sediment supply (Amy et al., 2007; Prather et al., 2012b; Grundvåg et al., 2014). There is a continuum between these stacking patterns and a lobe complex set, which is formed by several genetically related lobe complexes within the same lowstand systems tract, can display different stacking patterns depending on the area of study and data type/resolution (e.g. well logs, core and outcrop).

Understanding stacking patterns from 1D data, for example core and well logs, or from limited 2D data, for example outcrops, will help to evaluate the nature of seabed topography and the sediment supply during the development of lobe complexes and lobe complex sets. Detailed sedimentological facies and geometry studies enable the determination of the influence of seabed topography during the deposition of a lobe complex. Integration of data with regional studies can constrain the overall nature of the system (prograding or retrograding) and therefore provide a qualitative idea of sediment supply over time.

An extensive data set including basin-floor and intraslope lobe deposits from the Tanqua depocentres (Fan 4, Skoorsteenberg Formation) and Laingsburg depocentre (Unit A, Laingsburg Formation, and Units D/E and E, Fort Brown Formation) has been evaluated to constrain dominant stacking patterns and their controlling factors. Specific aims are: 1) to document the range of stacking patterns observed in the Karoo Basin; 2) to provide recognition criteria for each stacking pattern that can be used in 1D and 2D data sets; and 3) discuss allogenic and autogenic controls on stacking patterns.

Question 3: *What is the stratigraphic and geographic distribution of hybrid beds in submarine lobes?*

Rationale: Hybrid bed deposits comprise a division that was deposited by a turbulent flow and a division that was deposited by a debritic flow and have been recognized as an important part of the rock record in lobe deposits(e.g. Ito, 2008; Hodgson, 2009;

Talling et al., 2012a; Etienne et al., 2012; Grundvåg et al., 2014; Patacci et al., 2014; Collins et al., 2015; Fonnesu et al., 2015). The distinction of their flow processes and their quantitative importance in the overall succession is important from a hydrocarbon exploration perspective because they affect reservoir quality. Over the last decade, many studies have focused on establishing recognition criteria and classifications for hybrid beds (e.g. Haughton et al., 2003; Talling et al., 2004; Ito, 2008; Davies et al., 2009; Haughton et al., 2009; Hodgson, 2009; Magalhaes & Tinterri, 2010; Kane & Pontén, 2012; Patacci et al., 2014; Fonnesu et al., 2015) and their detailed process sedimentology (e.g. Haughton et al., 2003; Talling et al., 2004; Baas et al., 2009; Sumner et al., 2009; Baas et al., 2011). It has been proposed that hybrid beds are more common in distal fan and lobe settings, although they can also occur in proximal areas (Talling et al., 2004; Ito, 2008; Hodgson, 2009; Pyles & Jennette, 2009; Talling et al., 2012a; Etienne et al., 2012; Kane & Pontén, 2012; Grundvåg et al., 2014; Collins et al., 2015; Fonnesu et al., 2015; Southern et al., 2015). Several authors (e.g. Haughton et al., 2009; Hodgson, 2009) suggested, that hybrid bed deposits are preferentially developed in deposits of fan initiation and retreat phases during periods of disequilibrium over steep, out-of-grade slopes. However, the majority of studies are of a qualitative nature and therefore distribution trends maybe biased. Quantitative analysis can enable unbiased interpretations that are important to evaluate hybrid bed occurrence and distribution in submarine lobes. Such an approach will aid the understanding of heterogeneities within lobe deposits in a more predictable manner than qualitative data alone and can provide modellers with essential values to constrain geological and reservoir models.

The well-constrained data set of submarine basin-floor lobes in the Karoo Basin (Fan 4, Skoorsteenberg Formation, and Unit A, Laingsburg Formation) enabled a quantitative study that focuses on both stratigraphic and palaeogeographic trends. Studies of palaeogeographic trends will test the hypothesis that hybrid beds are more common in distal lobe settings, whereas studies of stratigraphic trends will determine if the occurrence of hybrid beds is more common in the initiation and growth phase of a lobe complex and complex set (e.g. Haughton et al., 2003, 2009; Hodgson, 2009).

Question 4: *Can we apply concepts established from basin-floor lobes to lobe deposits in different stratigraphic and geographical settings?*

Rationale: Depositional and stratigraphic models of basin-floor lobes from the Karoo Basin, South Africa, act as analogues for a wide range of lobe deposits that are not necessarily in the same stratigraphic and geographical settings. Lobe deposits have been observed from various other settings, including on the continental slope (e.g. Prather et al., 1998; Fiduk et al., 1999; Adeogba et al., 2005; Li et al., 2010; Pirmez et al., 2012; Prather et al., 2012 a, b; Oluboyo et al., 2014; Ortiz-Karpf et al., 2015) and at the base-of-slope (Posamentier & Kolla, 2003; Deptuck et al., 2008 Morris et al., 2014a). They can be influenced by confinement in tectonically active settings or be deposited on the slope where accommodation is created by tectonics, halokinesis, mud diapirism or slide scars (e.g. Booth et al., 2003; Adeogba et al., 2005; Marchès et al., 2010; Li et al., 2012; Morris et al., 2014a; Oluboyo et al., 2014; Ortiz-Karpf et al., 2015). Testing the exportability of the conceptual models and quantitative data from unconfined basin-floor lobes is an important step in establishing important similarities and differences between different lobe types. The identification of these differences can be used to aid the identification of other lobe types (e.g. intraslope lobes) in less well constrained subsurface and outcrop datasets.

The extensive data set of basin-floor lobes (Fan 3, Tanqua depocentre, Prélat et al., 2009; Unit A, Laingsburg depocentre, Prélat & Hodgson, 2013) as well as new findings presented in this thesis allow comparison to intraslope lobe deposits of the Fort Brown Formation (Unit D/E and E) and recognition criteria for intraslope lobes to be determined.

1.3 Thesis outline

This thesis includes three manuscripts that have been accepted, or submitted, for publication in international peer-reviewed journals (Chapter 3-5). It also contains one chapter that is in preparation for submission (Chapter 6).

Chapter 2: *Submarine lobes: Hierarchy, anatomy and environments.* This chapter summarizes the current understanding of the sedimentology of submarine lobes. This

is followed by an introduction to the field area, where the following studies were carried out, and a summary of methods used within.

Chapter 3: *Frontal and lateral submarine lobe fringes: Comparing sedimentary facies, architecture and flow processes.* – submitted to the Journal of Sedimentary Research. This chapter assesses the difference between frontal and lateral lobe fringes for the first time using the palaeogeographically well-constrained Fan 4 succession of the Skoorsteenberg Formation, Karoo Basin, South Africa. This chapter also discusses the control on these differences by flow processes and the implications of confinement to lobe fringe distribution patterns.

Chapter 4: *Aggradational lobe fringes: the influence of subtle intrabasinal topography on sediment gravity flow processes and lobe stacking patterns.* – accepted at Sedimentology. This chapter examines the influence of a gentle intrabasinal slope on the depositional architecture of submarine lobe deposits. Modifications to lobe fringe facies and their stacking patterns are assessed and the nature of the confining slope evaluated.

Chapter 5: *Constraining the sedimentology and stratigraphy of submarine intraslope lobe deposits using exhumed examples from the Karoo Basin, South Africa.* – published in Sedimentary Geology. This chapter presents the detailed sedimentology of intraslope lobes (facies, lobe environments and stacking patterns). The characteristics of intraslope lobes are compared to those of basin-floor lobes in the discussion and the creation of accommodation for lobe deposition on the slope is evaluated.

Chapter 6: *Is hybrid bed distribution in basin-floor fans predictable?* – in preparation for submission. This chapter tests the predictability of hybrid beds within basin-floor lobe successions. In this quantitative study, that integrates outcrop and core data, geographical and stratigraphical trends of hybrid bed distribution have been evaluated.

Chapter 7: This chapter provides an extended discussion that addresses the key research questions presented in Chapter 1. Findings from research presented in chapters 3-6 are collated and synthesised to answer these questions. This chapter also includes the conclusions and wider implications of the research. Finally, possible future research foci are proposed.

Chapter 2

Submarine lobes: Hierarchy, anatomy, environments and processes

This chapter provides additional background knowledge that underpin the Chapters 3-6, which have been written as manuscripts. It covers the sedimentology and stratigraphy of submarine lobes, subaqueous gravity flow processes, the geological setting of the study area and finally a detailed summary of the methodologies used.

2.1 Sedimentology of submarine lobes

Submarine lobes are defined as convex-upward deposits that are located down-dip of a submarine channel-mouth (e.g. Normark, 1970; Mutti, 1974; Pickering, 1981; Swart, 1994; Deptuck et al., 2008). A geographically defined channel-lobe transition zone (CLTZ) can exist between channel and lobe deposits (Bouma et al., 1985; Wynn et al., 2002; Macdonald et al., 2011). Traditionally, lobe deposits have been described as simple radial (lobate) bodies that thin and fine from an apex (e.g. Normark, 1970; Mutti, 1977; Normark, 1978; Lowe, 1982; Bouma, 2000) and have a convex-upward or lensoidal shape in cross-section (Swart, 1994; Bouma, 2000; Deptuck et al., 2008; Saller et al., 2008). Over the last decades, however, it has been recognized that the anatomy of lobe deposits is more complicated in terms of morphology, sub-environments and stacking patterns (e.g. Nelson et al., 1992; Twichell et al., 1992; Bouma & Rozman, 2000; Gervais, 2006; Hodgson et al., 2006; Deptuck et al., 2008; Prélat et al., 2009; Groenenberg et al., 2010; Etienne et al., 2012; Burgreen & Graham, 2014, Grundvåg et al., 2014). The range of lobe settings, hierarchy, environments, stacking patterns and dimensions is reviewed in the following section:

2.1.1 Lobe settings

Lobes have been observed from various settings, including the basin-floor, the base-of-slope and on the continental slope (Fig. 2.1). Basin-floor or terminal lobes can represent the dominant component of submarine fan successions and criteria for their recognition are well established (e.g. Harms, 1974; Twichell et al., 1992; Hartog

Jager et al., 1993; Sixsmith et al., 2004; Gervais et al., 2006; Deptuck et al., 2008; Jegou et al., 2008; Prélat et al., 2009, Migeon et al., 2010; Prélat et al., 2010; Macdonald et al., 2011; Prélat & Hodgson, 2013; Grundvåg et al., 2014).
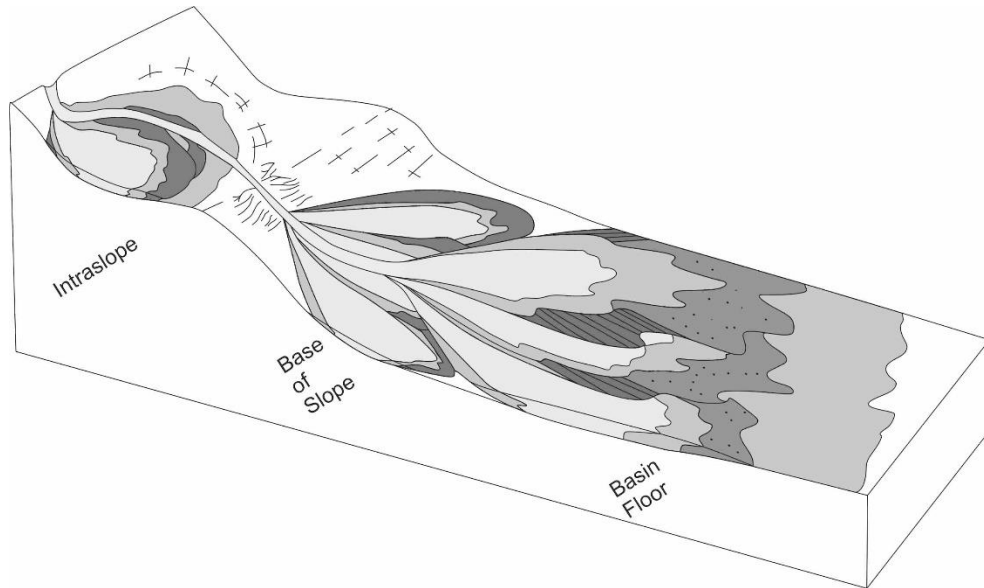
Figure 2.1. Lobe settings including the slope, the base of slope and the basin floor.

Examples of base-of-slope lobe deposits include "toe-of-slope lobes" (Deptuck et al., 2008) and the so-called frontal lobes of Posamentier & Kolla (2003) and Morris et al. (2014a) and are deposited over a zone that lies on the lower slope and the basin-floor. Not much is known about the detailed sedimentology of base-of-slope lobes as they are partially preserved in outcrop (Morris et al., 2014a), commonly channelized and misinterpreted as being part of the levee or channel-mouth bars. Intraslope lobes are deposited in areas of slope accommodation. They are also referred to as perched lobes and transient fans. Documented examples include studies from the Gulf of Mexico (Prather et al., 1998; Fiduk et al., 1999; Pirmez et al., 2012; Prather et al., 2012b), the Niger Delta continental slope offshore Nigeria (Adeogba et al., 2005; Li et al., 2010; Barton, 2012; Prather et al., 2012a), the Lower Congo Basin, offshore Angola (Oluboyo et al., 2014), the Algarve Margin, offshore Portugal (Marchès et al., 2010), the Gioia Basin, southeastern Tyrrhenian Sea (Gamberi and Rovere, 2011; Gamberi et al., 2011) and the Baiyun Sag, South China Sea (Li et al., 2012).

2.1.2 Lobe hierarchy

Hierarchical schemes aid comparison of scales, processes, and stacking patterns across different datasets and have been developed for the component architectural elements in a range of siliciclastic settings including fluvial, submarine channel/levee, and aeolian dune deposits (e.g. Allen, 1966; Mutti & Normark, 1987; Miall, 1988; Pickering & Clark, 1996; Sprague et al., 2003).

Over the recent years, it has been recognized that lobe deposits show a hierarchical structure (Gervais et al., 2006; Deptuck et al., 2008, Saller et al., 2008; Prélat et al., 2009; Mulder & Etienne, 2010; Prélat et al., 2010; Bernhard et al., 2012; Etienne et al., 2012; Grundvåg et al., 2014). A fourfold hierarchy of lobes in the Karoo Basin was proposed by Prélat et al. (2009): 1) a 'bed' represents a single depositional event; 2) one or more beds stack to form a 'lobe element'; 3) several lobe elements that are divided by thin siltstone intervals form a 'lobe'; 4) one or more related lobes stack to form a 'lobe complex' (Fig. 2.2).
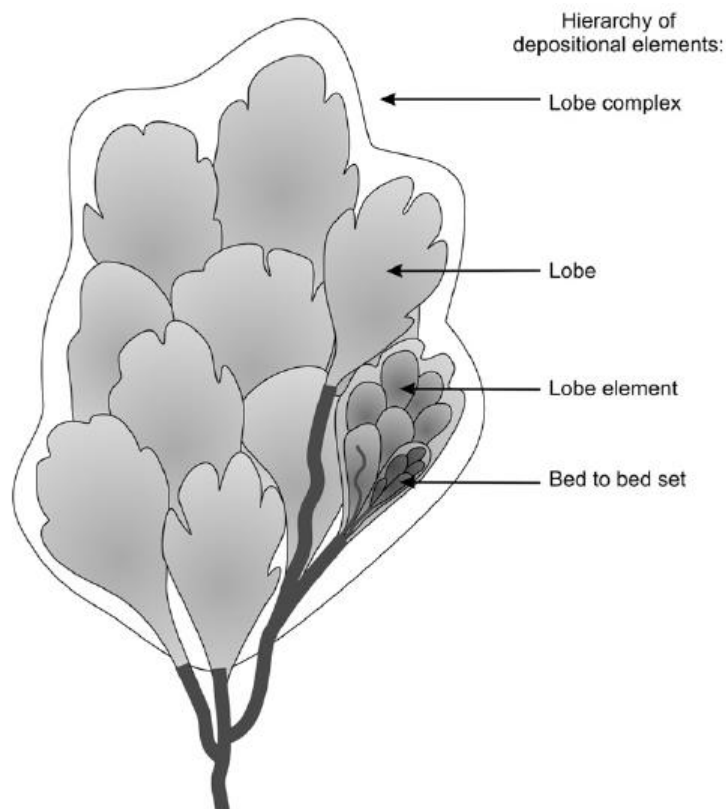
Figure 2.2. Hierarchy of depositional elements of lobes in plan view. The fourfold hierarchy comprises: bed/bed sets, lobe element, lobe and lobe complex (from Prélat et al., 2010).

Lobe complexes are deposited as packages during discrete periods of channel activity or growth phases and bounded by fine-grained strata due to avulsion (cf. Feeley et al., 1985; Deptuck et al., 2008; Prélat et al., 2009) or changes in relative sea level (Flint et al., 2011). Their size, shape and architectural complexity depends on the period prior to avulsion (or abandonment; Deptuck et al., 2008). The hierarchy can be expanded by adding a fifth hierarchical unit, the 'lobe complex set', which is formed by several related lobe complexes within the same lowstand systems tract. Similar hierarchy divisions have been used by several authors (cf. Table 2.1) to describe depositional variability of lobes across different scales. Etienne et al. (2012) stated that the highest complexity in architecture and facies can be found on bed and lobe scale, whereas the laterally extensive outcrops on lobe complex scale appear to possess 'sheet-like' geometries.

Authors	Data set	Hierarchy				
Prélat et al., 2009 Grundvåg et al., 2014	outcrop	bed/bedset	lobe element	lobe	lobe complex	lobe complex set
Mulder & Etienne, 2010 Etienne et al., 2012a,b	outcrop	bed	lobe element	lobe	lobe system	lobe complex
Gervais et al., 2006 Bourget et al., 2010	geophysical	elementary sedimentary body		internal unit	lobe	lobe complex
Deptuck et al., 2008 MacDonald et al., 2011	geophysical and outcrop	bed	lobe element	composite lobe	lobe complex	
Jegou et al., 2008	geophysical		subunit	channel-mouth lobe	channel-mouth lobe complex	
Saller et al., 2008	geophysical		sheetlike splay elements	lobe	fan	

Table 2.1. Comparison of hierarchies used to describe lobe deposits in outcrop and in geophysical studies.

2.1.3 Lobe environments

Traditionally, authors distinguished between a thick-bedded lobe body and a thin-bedded lobe fringe (e.g. Pickering, 1981; Deptuck et al., 2008; Hadelari et al., 2009). However, lobe deposits show more complexity and thus require further sub-division. Prélat et al. (2009) established four sub-environments for lobe deposits that are characterized by specific facies associations and thickness trends, termed lobe axis, lobe off-axis, lobe fringe and lobe distal fringe (Fig. 2.3). This terminology has been adapted by several authors working with outcrops in different basin settings, e.g. the Magallanes Basin (Bernhardt et al., 2012).
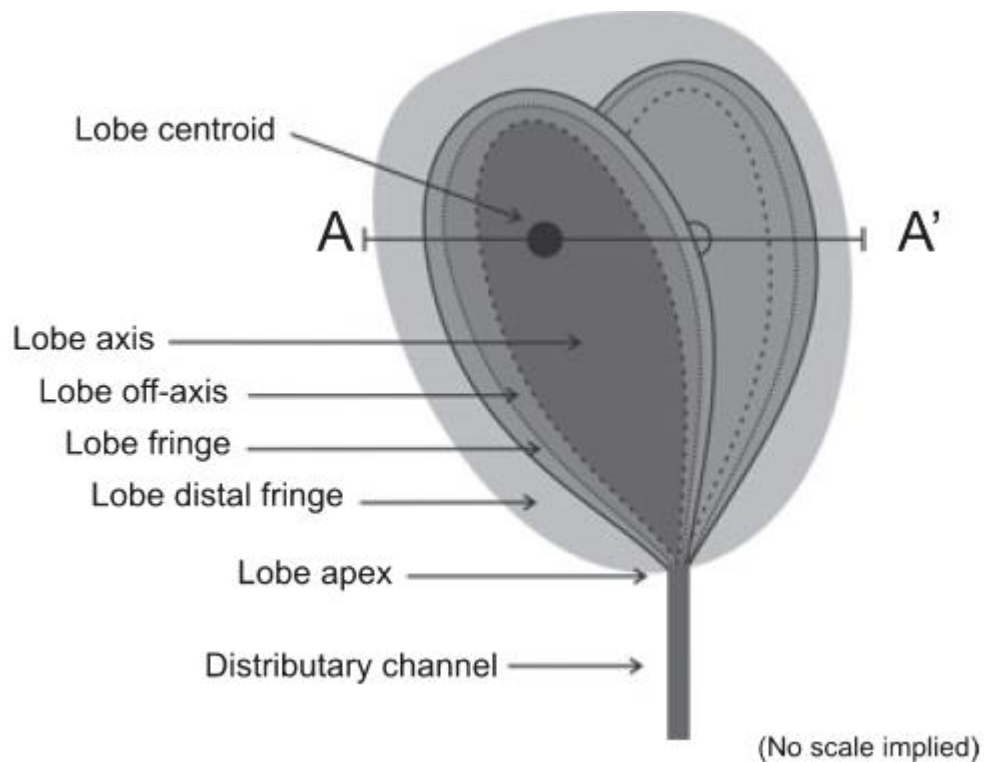
Figure 2.3. Lobe sub-environments. From proximal to distal: lobe axis, lobe off-axis, lobe fringe and lobe distal fringe (Prélat et al., 2009)

Thick-bedded sand-prone deposits that commonly show amalgamation define **the lobe axis**. The lobe axis represents the most proximal area to the feeder-channel channelization and scouring is commonly identified (Bouma, 2000; Deptuck et al., 2008; Bourget et al., 2010; Grundvåg et al., 2014). The deposits of the lobe axis are laterally extensive down-dip and across strike for several hundred metres and generally show tabular geometries. Units of high amalgamation (high amalgamation zones) can be traced into non-amalgamated medium-bedded units of the lobe off-axis towards the frontal and lateral margin of the lobe deposits. (Fig. 2.4)

Figure 2.4. Example of lobe axis deposits from the Laingsburg Formation, Karoo Basin, South Africa. Geologist (1.65 m) for scale.

The **lobe off-axis** is characterized by medium-bedded sand-prone deposits that are either amalgamated or layered. The beds commonly show abundant sedimentary structures (planar lamination, ripple lamination, climbing-ripple lamination and wavy lamination). Lobe off-axis deposits are characterized by 50-85% sandstone. They show tabular geometries in outcrop and can be traced out for several hundred metres in both dip and strike directions (Fig. 2.5).

Figure 2.5. Example of lobe off-axis deposits from the Laingsburg Formation, Karoo Basin, South Africa. Geologist (1.70 m) for scale.

The **lobe fringe** displays a heterolithic character as medium-bedded deposits from the lobe-axis generally thin and fine frontally and laterally basinward and turbidites can be replaced by hybrid beds. Lobe fringe deposits are characterized by 20-50% sandstone. At outcrop, lobe fringe deposits can show either tapering or pinch-and-swell geometries. The pronounced pinch-and-swell geometries give the impression of lenticular bodies, even though no evidence of truncation is observed (Bouma & Rozman, 2000; Groenenberg et al., 2010). The lateral extent of lobe fringe deposits is variable and ranges from a few (1-2 km) to several (up to 5 km) kilometres. The term of 'interlobes' has been used to describe facies that correspond to these lobe fringe characteristics (e.g. Carr & Gardner, 2000; Prélat et al., 2009). A more detailed study on lobe fringe sedimentology is presented in Chapters 3 and 4 (Fig. 2.6). The transition from lobe fringe to lobe distal fringe environment marks the sand pinchout of the system.

Figure 2.6. Heterolithic deposits of lobe fringes. An example from the Skoorsteenberg Formation, Karoo Basin, South Africa. Logging pole for scale.

The **lobe distal fringe** environment is dominated by siltstone deposits with rare intercalated sandstone beds (< 20% sandstone). Siltstones can aggrade to bedded successions of several metres. Lobe distal fringe deposits form an extensive 'halo' around the main sand-prone lobe body and extend for several kilometres (Fig. 2.7).

Figure 2.7. Siltstone is the dominant facies in the distal lobe fringe setting. An example from the Fort Brown Formation, Karoo Basin, South Africa. Logging pole for scale.

2.1.4 Lobe stacking patterns

In general, three types of stacking patterns can be observed: compensational, aggradational stacking and longitudinal stacking. Stacking patterns are dependent on the confinement of the basin, avulsion of the feeder-channels and sediment supply.

Compensational stacking describes the tendency of sediment to fill topographic lows created by preceding deposits (Mutti & Sonnino, 1981; Straub et al., 2009). Therefore, subsequent lobes will avoid the depositional relief created by underlying lobes, if sufficient accommodation is present to do so. Compensational stacking can occur across many scales from bed to lobe complex scale (Deptuck et al., 2008; Prélat et al., 2013) to lowstand systems tracts (van der Merwe et al., 2014). Migration of lobe deposition can be lateral or longitudinal (progradational or retrogradational; Gervais et al., 2006). Aggradational stacking occurs where avulsion is not possible due to the scale of confinement (Burgreen & Graham, 2014) and is commonly observed with lobes deposited in highly confined settings, e.g. mini-basins and ponded basins (e.g. Burgreen & Graham, 2014). Longitudinal stacking patterns can be either progradational (basinwards) or retrogradational (landwards). Progradational stacking has been described with basin configurations that limited the space for lateral

migration of lobes, increased rates of sedimentation due to shelf edge progradation and initiation of larger volume flows, and/or high sediment supply rates resulting in rapid shelf-margin accretion (Grundvåg et al., 2014). Progradational stacking patterns are associated with indicators of erosion and bypass of sediment farther into the basin, such as distributary channels, scours and megaflutes (Macdonald et al., 2011; Grundvåg et al., 2014). Landward stacking has been observed in highly confined basins, e.g. the Peïra Cava Basin, France (Amy et al., 2007) and the Brazos-Trinity system, Western Gulf of Mexico (Prather et al., 2012b). The landwards shift in deposition has been inferred to be caused by aggradation in the depocentre and an up-slope migration of the slope break (Amy et al., 2007).

2.1.5 Lobe shapes and dimensions

Lobes are described as having lenticular convex-upward cross-sections (Normark, 1970; Swart, 1994; Bouma, 2000; Deptuck et al., 2008; Saller et al., 2008) and elongated ellipse to equidimensional plan view shapes (Vernai, 1998; Kenyon et al., 2002; Jegou et al., 2008; Saller et al., 2008). Bouma (2000) suggested that the minor convexity of lobe deposits maybe too subtle to be observable in the field and therefore lobe deposits will exhibit apparently tabular geometries. More recently, it has been observed that lobes can show finger-like patterns at their most distal setting (Twichell et al., 1992; Prélat et al., 2009; Groenenberg et al., 2010).

Areal dimensions of lobes are highly variable. They can be between 4-50 km long, 4-18 km wide and 2-47 m thick (Pickering, 1981; Swart, 1994; Vernai, 1998; Carr & Gardner, 2000; Deptuck et al., 2008; Jegou et al., 2008; Saller et al., 2008; Prélat et al., 2009, Prélat & Hodgson, 2013; Grundvåg et al., 2014; Marini et al., 2015). Generally, there are two populations of lobes: 1) thin but areally extensive; and 2) thick but areally smaller. These two populations correspond to unconfined and confined lobes (Prélat et al., 2010; Fig. 2.8). However, Prélat et al. (2010) showed that their volumes are similar ranging from 0.4- 3.5 km^3. This similarity in volumes has been suggested to be due to autogenic factors like the filtering of sediment load or avulsion and migration in the system (Prélat et al., 2010).
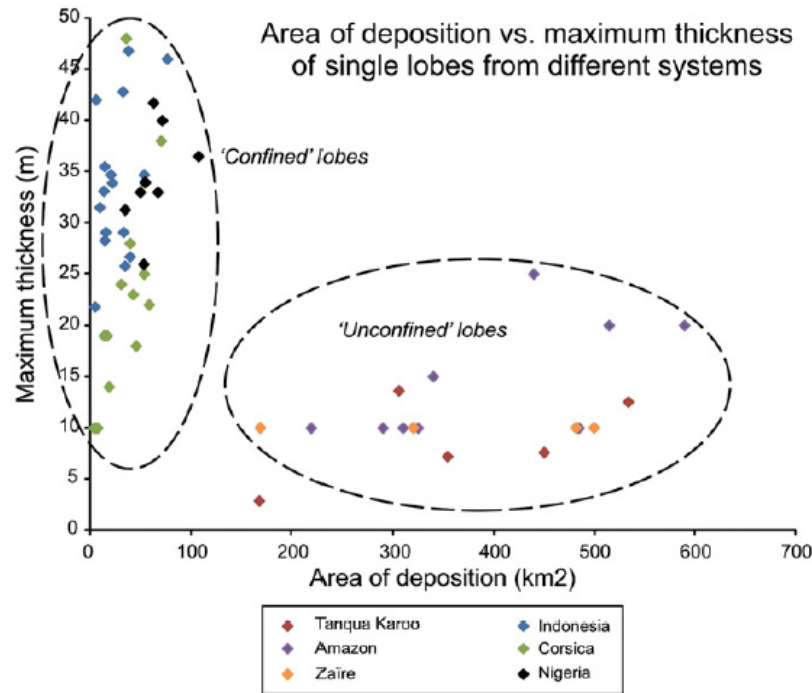
Figure 2.8. Plot of area of deposition versus maximum thickness. Two populations can be identified: 1) thinner more extensive lobes- unconfined; and 2) thicker less extensive lobes-confined. From Prélat et al., 2010.

2.2 Subaqueous sediment gravity flows

Sediment gravity flows (slides, slumps, debris flows and turbidity currents; Middleton & Hampton, 1973) contribute to the formation of canyons, channel-levee systems and lobes (Normark & Piper, 1972; Mutti, 1992). Therefore, understanding the initiation, characteristics and dynamics of such flows is paramount for interpreting their deposits. Sediment gravity flows are defined as mixtures of particles and fluid that are transported downslope because their density is greater than that of their ambient fluid. Sediment gravity flows are typically interpreted by their deposits (Mulder, 2011). These interpretations are tested by scaled experiments in the laboratory (e.g. Kuenen & Migliorini, 1950; Kuenen, 1950, 1951; Luthi, 1980, 1981; Baas et al., 2009, Sumner et al., 2009). Direct observations of sediment gravity flows, specifically turbidity currents, are extremely hard to obtain and still remain rare (e.g. Talling et al., 2012a, 2013; Peakall & Sumner, 2015). Several classifications have been established and are based on the interpreted rheology of the flows (e.g. Dott; 1963, Mulder & Cochonat, 1996), on their particle- support mechanism (e.g. Middleton & Hampton, 1973; Lowe, 1979; Stow, 1996), their flow concentration (Mulder & Alexander, 2001) and on their deposits (e.g. Bouma, 1962; Mutti & Ricci Lucchi, 1975; Pickering et al.,

1989). Generally, two types of flows are described: cohesive (viscous) and non-cohesive flows. The former is characterised by its matrix strength due to cohesion of fine particles, are commonly referred to as debris flows, while the latter is characterised by the behaviour of discrete particles, and includes a process continuum from sediment slides to turbidity currents (Mulder & Alexander, 2001). Initiation of sediment gravity flows can be due to transformation of submarine landslides into laminar and later turbulent flows, direct input from continental rivers or resuspension of sediment near the shelf edge by oceanographic processes (Piper & Normark, 2009). Submarine landslides transforming into debris flows and/or turbidity currents (Hampton, 1972; Hampton et al., 1996; for more detailed discussion see Chapter 2.2.3) can be caused by overloading and oversteepening of the shelf and submarine slope, seismic triggers, fluid escape (cf. the Storegga slide; Bugge, 1983; Mienert et al., 2005).

2.2.1 Turbidity currents and turbidites

Turbidity currents are defined as flows where fluid turbulence acts as the main particle transport mechanism (Middleton & Hampton, 1973; Lowe, 1982; Middleton, 1993; Simpson, 1997; Kneller & Buckee, 2000; Meiburg & Kneller, 2010; Mulder, 2011). The turbulence of the current is generated by the forward motion of the current along the lower boundary, the circular motion in the frontal part of the flow and shear between the flow and the ambient fluid (Meiberg & Kneller, 2010). Generally, turbidity currents can be divided into three types (Fig. 2.9): turbulent surges (lasting hours to days), longer duration surge-like flows, and quasi-steady flows (lasting weeks to months). Turbulent surges and surge-like flows are initiated by failure on the shelf and slope, whereas quasi-steady flows are associated with river flux. Flow duration has been linked to the resulting deposits. Surge-like turbidity currents are interpreted to deposit (complete) Bouma-Sequences, whereas quasi-steady flows can deposit coarsening-up units that are capped by fining-up units and may comprise thick units of uniform character (Kneller, 1995; Kneller & Branney, 1995; Mulder & Alexander, 2001).

Anatomy

Turbidity currents start in the form of a surge, regardless of their type, and rapidly develop into a current that consists of a head (and neck), a body and a tail (Middleton, 1966a,b; Edwards, 1993;).

The head has a bulge-like shape. It develops due to the strong mixing of sediment and ambient fluid. The head is mainly erosional, producing structures like grooves and flute marks (Allen, 1971a; Middleton, 1993), the most concentrated and transports the coarsest grains of the flows (cf. Stow, 1996). The head is where entrainment of
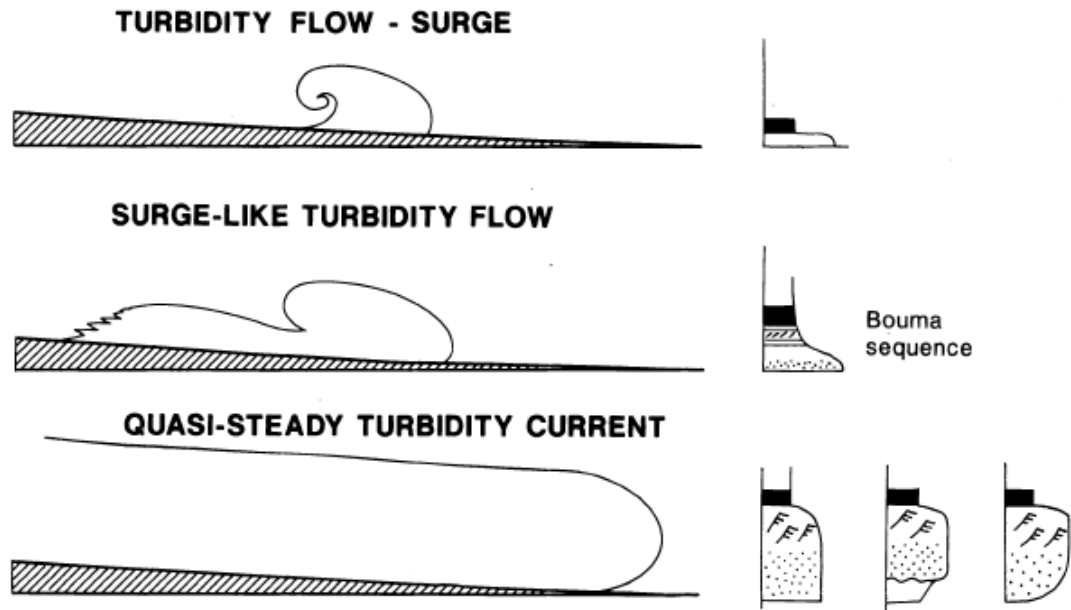
Figure 2.9. Types of turbidity currents and their associated deposits (modified from Mulder & Alexander, 2001).

underlying substrate takes place. Circular movement to the top and the front characterises the dynamics of the flow head (Mulder, 2011).

The body is sometimes connected to the head by a neck (Mulder, 2011). Main transport mechanism in the body is sediment suspension supported through friction between the ambient fluid and the overriding bed (cf. Stow et al., 1996). The body is mainly depositional and transports the bulk of the sediment. Flow thickness in the body is approximately constant.

The tail represents the dilute part of the turbidity current and transports the finer grained part of the sediment (Mulder, 2011). The sediment settles due to energy loss during downslope movement.

Dynamics of subaqueous turbidity currents

To compare laboratory flow experiments with outcrop deposits, non-dimensional numbers were introduced to define the state of the flow (Reynolds Number), the flow regime (Froude Number) and the stability of the flow interface (Richardson Number):

The Reynolds Number is defined as

$$Re = \frac{UH}{v}$$

Where *U* is the mean velocity of the flow, *H* is the thickness of the flow body and *v* is the kinematic viscosity. The Reynolds number defines the state of flow. If *Re* is < 500 the flow is laminar, between 500-2000 the flow is transitional and >2000 the flow is turbulent (cf. Lowe and Guy, 2000). Laminar flows are dominated by viscous forces and characterised by smooth, fluid motions, whereas turbulent flows are dominated by inertial forces and characterised by eddies, vortices and othe flow instabilities (Grant, 1958).

The Froude Number is defined as

$$Fr = U/\sqrt{g'H}$$

Where *U* is the mean body velocity, *H* is the thickness of the flow body and *g'* is the reduced density ($g' = \Delta\rho/\rho$), that results due to the supporting fluid being water. The Froude number defines the flow regime. If *Fr* is <1 a flow is subcritical, if *Fr*= 1 a flow is critical and finally if *Fr* is >1 a flow is supercritical. A hydraulic jump is defined by the transition from *Fr* > 1 to *Fr* < 1. Super critical flows are thin, dense flows with high velocities (Komar, 1971). When a flow passes from supercritical to subcritical conditions its velocity decreases, turbulence is generated, and density is decreased by entrainment of ambient water (Ellison & Turner, 1959; Komar, 1971). Therefore, subcritical flows are thick, less-dense, low-velocity flows.

The Richardson Number is defined as

$$Ri = 1/Fr^2$$

It describes the stability of the flow and is used to quantify the entrainment of water within the flow.

Velocity and density stratification

Turbidity currents show velocity and density stratification. Generally, both decrease upwards. The flow velocity profile is characterised by two regions: the lower and upper region (Fig. 2.10). The lower region (near-wall region) comprises the lower part of the turbidity current and has a positive velocity gradient. The maximum velocity value marks the boundary to the upper region (shear layer) which is characterised by a negative velocity profile. The upper region is generally thicker that the lower region (by 5 to 10 times; Stacey & Bowen, 1988). Drag forces control the exact height of the velocity maximum, and thus the boundary between the regions (Fig. 2.10). Density stratification is dependent on the distribution of the suspended sediment throughout the current. Some authors (Britter & Simpson, 1978; Simpson & Britter, 1979) suggested that a flow comprises two parts: a thin and dense basal layer and a more dilute upper layer mixed with ambient fluid. However, it has been shown that flow density decreases upwards, i.e. finer grains are suspended in the more dilute upper region, whereas coarser grains are dominantly in the dense basal layer (Hess & Normark, 1976; García, 1994; Klauke et al, 1997; Peakall et al., 2000; Migeon et al., 2012). Concentration profiles of turbidity currents are dependent on their dynamics. Thus, low-concentration and weakly depositional currents have a smoother concentration profile than erosional currents or currents with high rates of entrainment of ambient fluid (cf. García, 1990,1993, 1994; Altinakar et al., 1996; Peakall et al., 2000). Stratification of turbidity currents is an important factor as it enables flow spilling and stripping in submarine channel-levee settings (Peakall et al., 2000; Kane et al., 2007; Mulder, 2011) and on topographic highs (Sinclair & Tomasso, 2002).
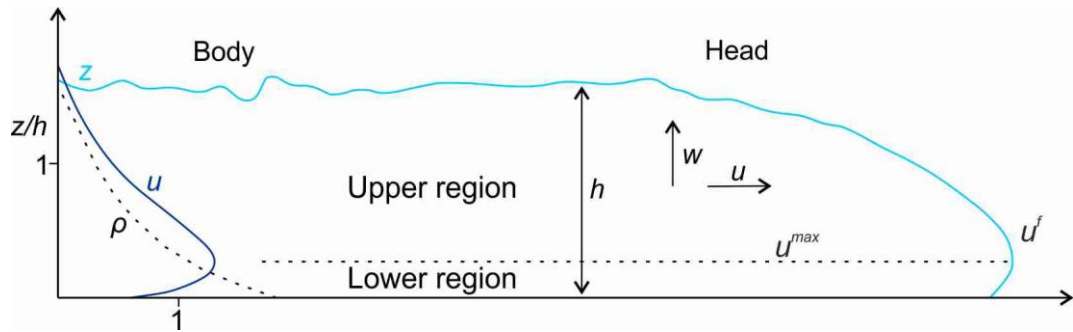
Figure 2.10. Schematic of a turbidity current showing the two regions of the flow and generalized velocity and density profiles (modified from Meiburg & Kneller, 2010).

Low-density vs high-density turbidity currents

In the rock record, turbidity current deposits are commonly distinguished by their character and interpretation to be formed by low-density or high-density turbidity currents (Fig. 2.11). Low-density turbidity currents are thought to be fully turbulent near the bed (Lowe, 1982; Mulder & Alexander, 2001). They display low sediment fallout rates and sediment settling is not hindered due to grain-to-grain interactions (Fig. 2.11). Low-density turbidity currents form deposits that comprise several sedimentary structures: 1) planar laminations, both from lower-flow-regime (Bouma, 1962) and upper-flow-regime (Allen, 1982; Southard, 1991); 2) ripple cross-lamination; and 3) dunes (at very low fallout rates). They tend to form beds that have thicknesses below 0.5 m (Ricci Lucchi, 1967; Talling et al., 2007) and a tapering shape, whereas the mud intervals that cap these deposits thicken slightly distally (Mutti, 1992; Kane et al., 2007; Talling et al., 2007).

The term of high-density turbidity currents was introduced by Kuenen (1948, 1950, 1951) and Kuenen & Migliorini (1950) and describes turbidity currents where hindered settling is an important factor near the bed. This occurs at sediment concentrations that exceed 9%Vol (Bagnold, 1962) as grain-to-grain interactions, excess pore pressure and increased fluid viscosity become important additionally to fluid turbulence (Kuenen, 1950, 1951; Bagnold, 1954; Lowe, 1982). Aggradation rates from high-density turbidity currents are higher than those of low-density turbidity currents. Increased sediment concentration damps the flow turbulence, especially near to the bed (Kneller & Branney, 1995; Fig. 2.11). Therefore, bedload reworking is mostly prevented and predominantely structureless deposits are formed. Sedimentary structures that can form from high-density turbidity currents are: 1) planar laminations; and 2) stepped planar laminations. Generally, deposits from high-

density turbidity currents show broad thickness maxima and tabular geometries (cf. Talling et al., 2012a).

However, Peakall & Sumner (2015) argue that there is a discrepancy between the values for sediment concentration in high-density currents (>9% Vol; Kuenen, 1966; Mulder and Alexander, 2001; Talling et al., 2012a) based on experiments and rocks and estimated concentrations in modern systems (0.2-2.5% Vol; Pirmez & Imran, 2003; Konsoer et al., 2013). The authors suggest this could be due to the issue of flow stratification as rock-based estimated only incorporate the *in-situ* deposited flow closest to the bed sediment interface raising the question if high-density and low-density currents truly exist or reflect the remnant of interpretation from deposits.
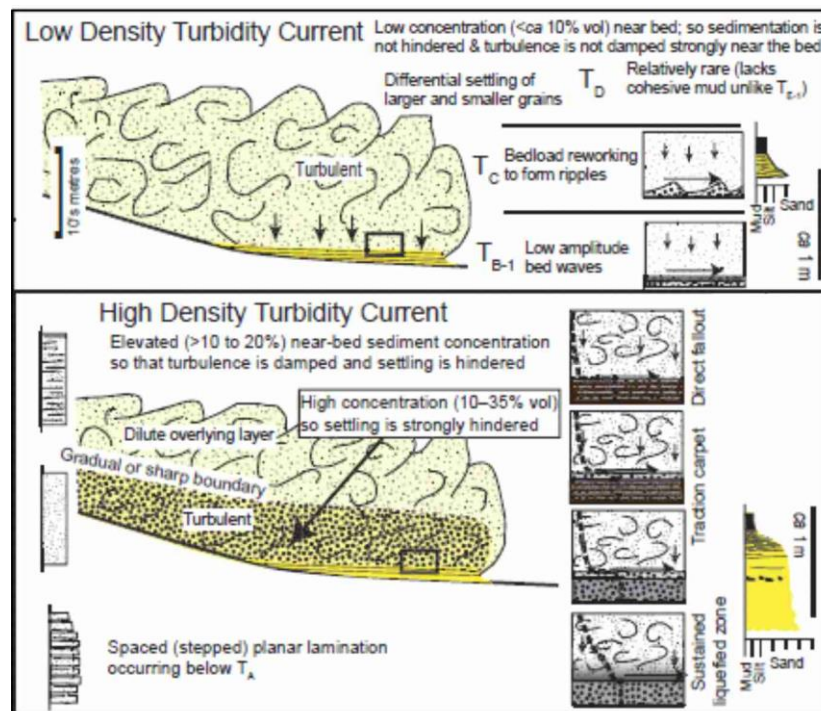
Figure 2.11. Summary of low-density and high-density currents showing transport phase, depositional phase and deposit characteristics (Modified from Talling et al., 2012a)

2.2.2 Debris flows and debrites

Submarine debris flows are high concentration flows and interpreted to be characterised by mainly laminar particle transport (Johnson, 1970; Hampton, 1972; Enos, 1977). Debris flows initiate from one or more submarine landslide or failure which undergo remoulding and incorporation of water (Hampton, 1972; Iverson, 1997). Debris flows are charcaterised by 1) surges (Hampton, 1972; Coussot & Meunier, 1996; Iverson, 1997) 1) movement along shear planes (Hampton, 1972;

Coussot & Meunier, 1996), 2) their liquid-like state (Iverson, 1997), and 3) multimodal grain size distribution (Hampton, 1972; Coussot & Meunier, 1996; Iverson,1997). The behaviour of debris flows is influenced by the combination of grain-friction, grain-collision, viscous fluid flow and suspension provided through yield-strength (Johnson, 1970; Hampton, 1972; Iverson, 1997).

Debris flow are able to transport clasts and blocks depending on their matrix strength and buoyancy. Commonly, the largest clasts are moved to the surface and front of debris flows (Hampton, 1972; Coussot & Meunier, 1996; Iverson, 1997). Internal shear in debris flows can enable syn-sedimentary deformation of transported clasts and blocks and form inverse grading (Mulder, 2011). The deposits of debris flows, debrites, form by *en masse* freezing of the flow (Hampton, 1972; Couusot & Meunier, 1996; Talling et al., 2012b). Typically, debrites are poorly sorted, lack sedimentary structures that are created by bedload reworking, show sharp grain-size breaks on their top boundaries, display chaotic distribution of clasts in a fine grained matrix, and commonly have a high mud content. Their shape is highly irregular, creating relief on the slope and basin floor. Debrites tend to pinch out abruptly independently of the underlying seabed topography (Amy et al., 2005).

Two end members of debris flows exist: cohesive debris flows (with mud-rich matrix) and non-cohesive debris flows (only sand matrix, no cohesive mud particles). Between those two end members a continuum of composition can occur. Cohesive debris flows are subdivided into high-strength, moderate-strength and low-strength debris flows depending on their ability to support mud clasts. High-strength debrites are very thick (>2 m) and occur mainly on the continental slope (Johns et al., 1981; Laberg & Vorren, 2000; Talling et al., 2013). Moderate-strength debris flow deposit thinner deposits (< 2m) and are described from the continental slope and in distal fan and lobe settings (Wood & Smith, 1958; Talling et al., 2004; Haughton et al., 2009). Moderate-strength debris flows are more likely to entrain ambient fluid and undergo successive dilution that can generate associated turbidity currents (cf. Talling et al., 2012b). Deposits from low-strength debris flows do not contain mud clasts, solely outsized sand grains. They tend to be very extensive and very thin. Non-cohesive debris flows deposit structureless sandstones that are characterised by their chaotic distribution of clasts, their abrupt pinchout independent of the underlying seabed topography, contorted patches of outsized grains and irregular grading (Talling et al., 2012b).

2.2.3 From debris flows to turbidity currents

Debris flows can transform into turbidity currents downslope. Generally, there are three mechanisms observed (Marr et al., 2001; Mohrig & Marr, 2003; Felix & Peakall, 2006): 1) grain-by-grain erosion of sediment on the surface of a debris flow (Hampton et al., 1972; Marr et al., 2001; Mohrig et al., 1998); 2) shearing of thin sediment layers from the head of the debris flow (Hampton et al., 1972; Marr et al., 2001); and 3) turbulent mixing at the head of the debris flow causing dilution and local transformation to a turbidity current (Allen,1971b; Hallworth et al., 1993; Marr et al., 2001). Felix & Peakall (2006) suggest that density and viscousity of the parent debris flow govern the resulting turbidity current. For example a dense and viscous debris flows is described to undergo only minor transformation at the surface. This results in dilute turbidity currents. Less dense and viscous debris flows are postulated to undergo different transformations (breaking up of mass, breaking of internal waves, and mixing) throughout and transformed to turbidity currents entirely.

2.2.4 Types and flow processes of hybrid beds

Generally, hybrid beds comprise a division that was deposited by a turbulent flow and a division that was deposited by a cohesive flow. This means that the deposit comprises a sharp based, commonly structureless and dewatered sandstone that is overlain by poorly sorted argillaceous divisions that can contain terrestrial plant fragments, muddy sandstones that are rich on mudstone chips and terrestrial plant fragments, muddy sandstones with contorted texture (Haughton et al., 2003; Ito, 2008; Davies et al., 2009; Haughton et al, 2009; Hodgson, 2009; Jackson et al., 2009; Magalhaes & Tinterri, 2010; Kane & Pontén, 2012) or mudclast-rich, well sorted sandstones (D3 of Hodgson, 2009). Contacts between the two divisions are either irregular with evidence of liquefaction and upward sand injection, or very sharp. Over the last decade, hybrid beds have been identified as an important component of lobe deposits. Several authors have studied them in detail in outcrop and core data sets (Haughton et al., 2003; Ito, 2008; Davies et al., 2009; Haughton et al., 2009; Hodgson, 2009, Jackson et al., 2009; Magalhaes & Tinterri, 2010; Kane & Pontén, 2012; Patacci et al., 2014; Fonnesu et al., 2015) and established different classification schemes. Flume tank experiments have been carried out to confirm and verify process models

that have been postulated from these data sets (Baas et al., 2009; Sumner et al., 2009).
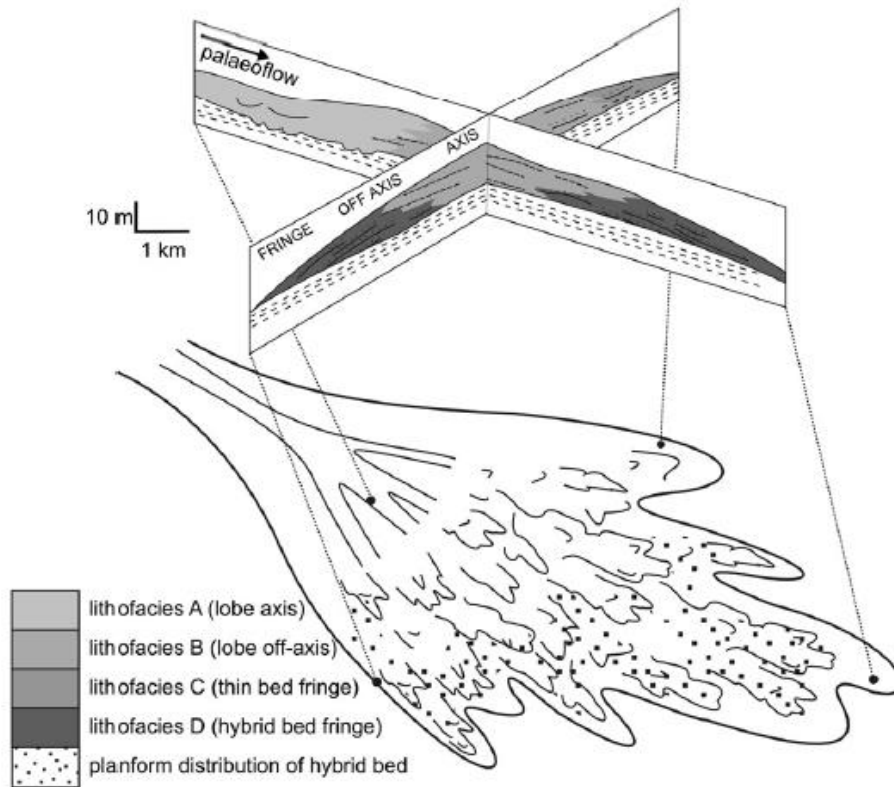
Figure 2.12. Schematic map and fence diagram illustrating the distribution of hybrid beds with lobe deposits (from Hodgson, 2009).

Overall, it has been established that hybrid beds dominantly occur in lobe fringe settings (Fig. 2.12; Hodgson, 2009; Pyles & Jennette, 2009; Kane & Pontén, 2012; Talling et al., 2012a; Etienne et al., 2012; Grundvåg et al., 2014; Patacci et al., 2014; Collins et al., 2015; Fonnesu et al., 2015) and are commonly observed during fan initiation and retreat (Haughton et al., 2009; Hodgson, 2009). Where hybrid beds have been observed in more proximal lobe settings (Ito, 2008; Jackson et al., 2009; Patacci et al., 2014; Southern et al. 2015) enhanced erosion and deceleration have been invoked due to processes occurring in the channel-lobe transition zone and confinement. Frontal confinement is proposed to enhance flow transformation as it favours deceleration and mud-erosion processes (Magalhaes & Tinterri, 2010; Patacci et al., 2014). Many models for the generation of hybrid beds have been proposed (cf. Haughton et al., 2003; Talling et al., 2004; Haughton et al., 2009; Talling et al., 2013). Generally three models are preferentially invoked for the formation of hybrid bed deposits:

1) Co-generated by independent flows: In this model independent debris flows and turbidity currents are developed by the failure of the slope and juxtaposed to form a bed with a clean sandstone division and a chaotic muddy division (Wood & Smith, 1958; Nelson et al., 1992; Masson et al., 1997).

2) Longitudinal evolution from a high-density turbiditity current (*sensu* Haughton et al. 2003; Fig. 2.13): In this scenario part of a turbidity current undergoes flow transformation through the successive entrainment of mudstone clasts due to erosion. The mudclasts are successively broken apart within the turbidity current. Eventually, the mud particles overload a section of the flow or suppress turbulence, transforming a section of the flow to a laminar clast-rich flow that is retarded compared to the forerunning turbulent section (Haughton et al., 2003; Talling et al., 2004; Ito, 2008; Davies et al., 2009; Haughton et al., 2009; Hodgson, 2009; Magalhaes & Tinterri, 2010; Patacci et al., 2014).

3) Vertical segregation supersaturated flows (*sensu* Baas et al., 2009; Fig. 2.13): In this model a supersaturated turbidity current transforms into a quasi-laminar flow through vertical segregation of grains due to deceleration. This turbidity current is characterised by higher clay concentration. During flow transformation it undergoes a transitional stage where a basal shear layer enhances turbulence and a plug flow develops (Baas et al., 2009; Sumner et al., 2009; Baas et al., 2011; Kane & Pontén, 2012; Kane et al., in review).

Interpretation (Haughton et al., 2009)	Interpretation (Baas et al., 2011)
Suspension fallout, some shearing	Suspension fallout, some shearing
Traction by dilute turbulent wake	Traction by dilute turbulent wake
Cohesive debris flow, locally modified by sand injection from beneath, and partly reworked at top	Cohesive debris flow with QLPF behaviour, locally modified by sand injection from beneath, and partly reworked at top
Transitional flow (*sensu* Lowe & Guy, 2000) with intermittent turbulence suppression due to near-bed dispersed clay and internal shearing	Transitional flow (*sensu* Baas et al, 2009) with modulated turbulence (TETF, LTPF or UTPF), scouring and reworking the underlying sand
Progressive aggradation beneath a non-cohesive high-density turbidity current	Rapid aggradation from turbulent or transitional sediment gravity flow that is supersaturated with sand due to insufficient turbulence and cohesive support

Figure 2.13. Schematic log of idealized hybrid event bed with inferred processes of formation of H1 to H5 divisions, based on Haughton et al. (2009) and Baas et al. (2011). QLPF: quasi-laminar plug flow; TEFT: turbulence-enhanced transitional flow; LTPF: lower transitional plug flow; UTPF: upper transitional plug flow. Modified after Haughton et al. (2009) and Baas et al. (2011).

2.3 Geological setting of the study area

2.3.1 Karoo Basin
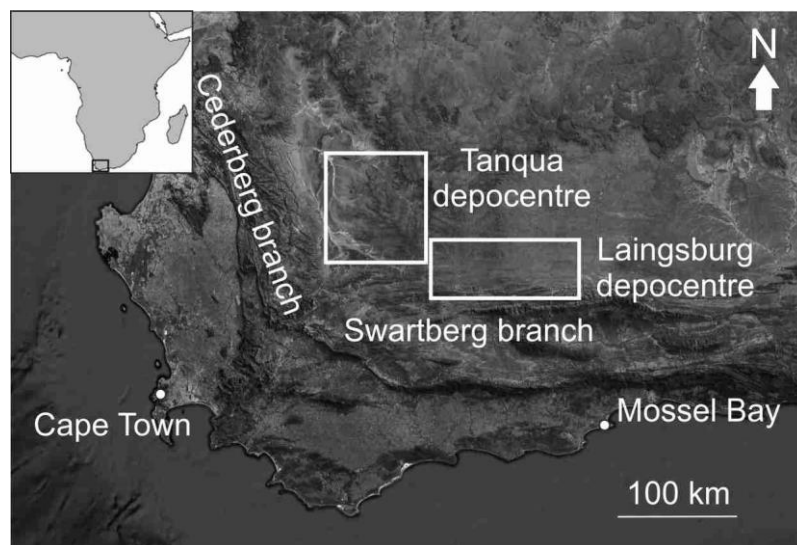
Figure 2.14. Locations of the Tanqua and Laingsburg depocentre adjacent to the Cape Fold Belt branches.

The Late Carboniferous to Early Jurassic Karoo Basin lies inboard of the Cape Fold Belt. The basin is framed by the two branches of the Cape Fold Belt to the west (Cederberg branch) and south (Swartberg branch; Fig. 2.14). The two branches coalesce in the Hex River Mountains. There, the occurrence of linear anticlinal structures separate the Tanqua and Laingsburg depocentres (van der Werff & Johnson, 2003). The Karoo Basin formed as part of broad area of subsidence parallel to the palaeo-Pacific margin of Gondwana (Visser, 1997). Traditionally, the Karoo Basin is interpreted as a retroarc foreland basin with loading of the Cape Fold Belt as main factor of subsidence in the Permian (Visser & Prackelt, 1996; Visser, 1997; Catuneanu et al., 1998, 2005; Gamundi & Rossello, 1998). More recent tectonic reconstructions (Pysklywec & Mitrovica, 1999; Tankard et al., 2009) and geochemical studies (Fildani et al., 2007, 2009; McKay et al., 2015) point to lithospheric deflection, due to subduction driven mantle flows, as key factor for subsidence during the Permian. This means that the Cape Fold Belt was not emergent at the time of deep-water to shelf-deposition. Tankard et al. (2009) suggest that the Cape orogeny started in the Early Triassic. At this time effects from flexural thrust loading (Pysklywec & Mitrovica, 1999) dominated subsidence.

Deposits of the Karoo Supergroup fill the Karoo Basin. The Karoo Supergroup is divided into the Dwyka Group, the Ecca Group and the Beaufort Group. The late Carboniferous to early Permian Dwyka Group encompasses glaciomarine deposits (massive diamictites, stratified diamictites and mudstone). Their maximum thickness in the Karoo Basin is about 800 m and represents deposition during four major glacial/deglacialcycles (Visser, 1997). The Permian Ecca Group comprises a shallowing upward succession of deep-water to deltaic deposits, which is described in detail below for the Tanqua and Laingsburg depocentres. The Late Permian to Early Triassic Beaufort Group consists of fluvial deposits (e.g. Gulliford et al., 2014; Jirah & Ribidge, 2014; Wilson et al., 2014). The Beaufort Group is the final major sedimentation stage of the Karoo Basin, which was subsequently uplifted (Pysklywec & Mitrovica, 1999).

2.3.2 Tanqua depocentre
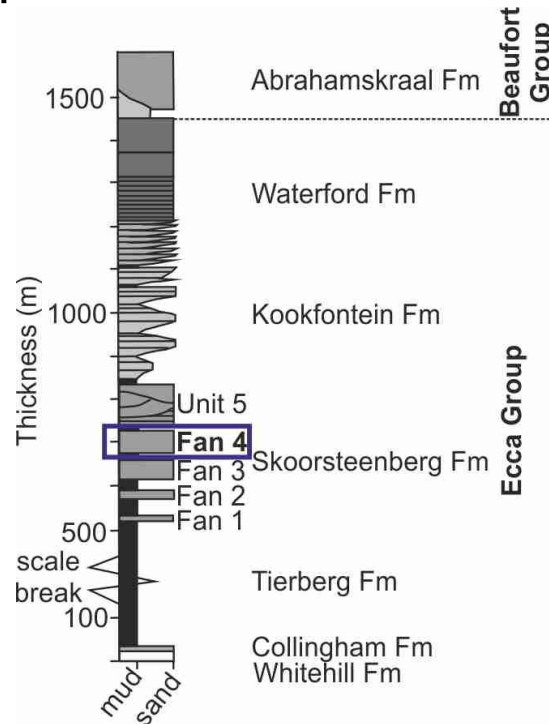
Figure 2.15. Stratigraphy of the Tanqua depocentre. Chapter 3 presents data from Fan 4, Skoorsteenberg Formation (marked with blue box).

In the Tanqua depocentre, the Ecca Group is up to 1350 m thick (King et al., 2009). It comprises the fine-grained Whitehill and Collingham Formations, >600 m of basinal mud- and siltstones of the Tierberg Formation (Hodgson et al., 2006; Fig. 2.15), clastic deep-water deposits of the Skoorsteenberg Formation (Wickens, 1994; Morris et al., 2000; Bouma & Rozman, 2000; Goldhammer et al., 2000; Rozman, 2000; Johnson et al., 2001; van der Werff & Johnson, 2003a,b; Sullivan et al. 2004; Wild et al., 2005; Hodgson et al., 2006, 2009; Prélat et al., 2009; Jobe et al., 2012; Hofstra et al., 2015, Kane at al., in review; Fig. 2.15), slope and shelf deposits of the Kookfontein Formation (Wild et al., 2009; Oliveira et al., 2010; Dixon et al., 2012; Laugier & Plink-Björklund, 2016; Fig. 2.15) and shoreface/deltaic deposits of the Waterford Formation (Fig. 2.15). Radiometric dates of ashes from the Collingham Formation (270 Ma, Turner, 1999) and ages of fossil assemblages (255 Ma) from the overlying Beaufort Group (Rubidge, 1991), bracket the deep-water to fluvial succession to a 15 My period.

The Skoorsteenberg Formation (450 m thick; Bouma & Wickens, 1991; Wickens, 1994; Johnson et al., 2001) encompasses four basin-floor systems (Fan 1-4) and a base-of-slope system (Unit 5; Fig. 2.14). Each of these systems is 20–60 m thick and separated by 20–75 m thick claystone and siltstone intervals (Johnson et al., 2001).

Each fan is interpreted as a low-frequency lowstand system tract, whereas the mud- and siltstone dominated intervals represent the associated transgressive and highstand system tracts (Johnson et al., 2001; Hodgson et al., 2006).
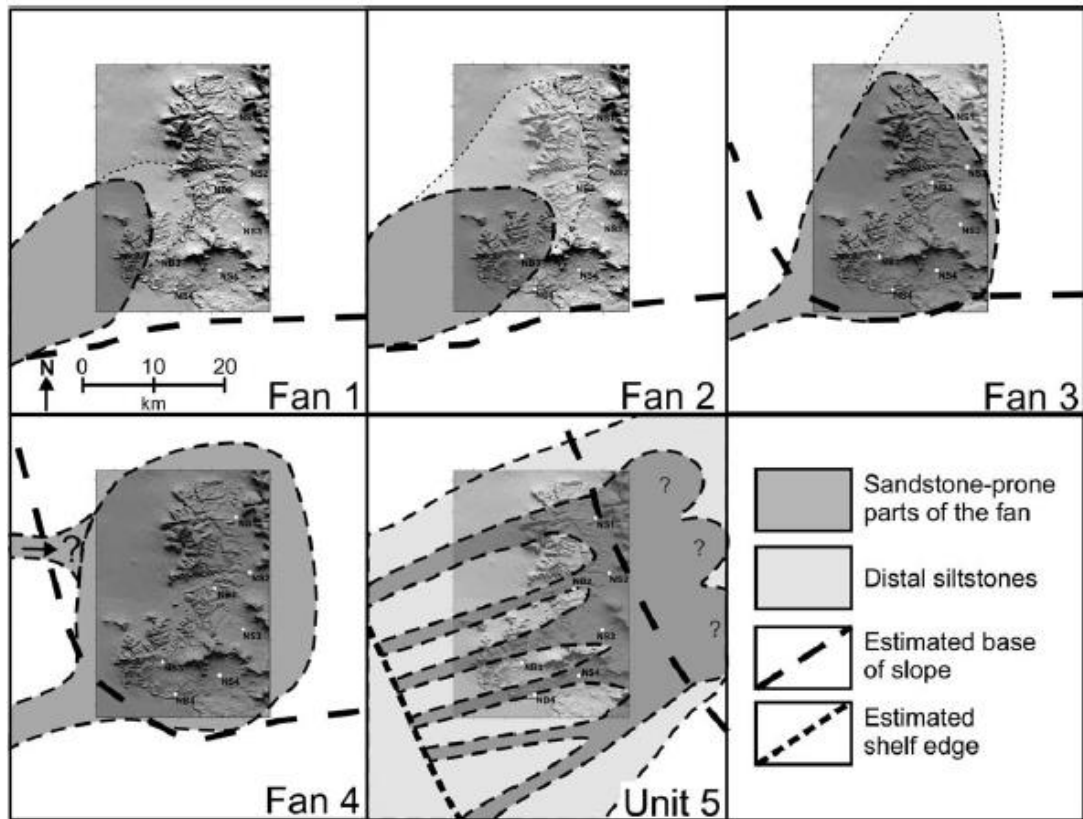
Figure 2.16. Palaeogeographic reconstructions of the outlines of Fan 1-4 and Unit 5 (from Hodgson et al., 2006)

Only the distal pinchout area of Fan 1 is exhumed in the Tanqua depocentre (Fig. 2.16). Deposits are up to 20 m thick, comprising three sand-prone units separated by two siltstone units, and stacked progradationally (Hodgson et al., 2006). Palaeoflow was dominantly to the northwest.

Fan 2 comprises mid-to outer fan deposits. Its maximum thickness is 42 m and comprise three sand-prone unit that are separated by intercalated mudstone and siltstone intervals (Rozman, 2000; Johnson et al., 2001; Hodgson et al., 2006). Architectural elements include heterolithic and sandstone channel-, scour-fills and 'sheets'. Fan 2 exhibits progradational stacking patterns. Palaeoflow was dominantly to the northwest (Fig. 2.16).

Fan 3 is the most studied system of the exhumed deep-water deposits of the Tanqua depocentre (e.g. Bouma & Rozman, 2000; Morris et al., 2000; van der Werff &

Johnson, 2003 a,b; Hodgson, 2006; Luthi et al., 2006; Prélat et al., 2009; Jobe et al., 2012; Hofstra et al., 2015; Kane et al., in review). It is 36 km long and 15 km wide (van der Werff & Johnson, 2003 a,b; Fig. 2.16). Its maximum thickness of 55 m is in the south, thinning occurs over a distance of 28 km to the north (Johnson et al., 2001; Hodgson et al., 2006). Architectural elements include channels, lobes and scours. Similar to Fan 1 and 2, Fan 3 exhibits progradational stacking patterns.

Fan 4 shows a maximum thickness of 65 m and is built up by channels in the south and lobes to the north (Johnson et al., 2001). Palaeocurrents and thickness distributions indicate that sediment was sourced from two directions (Fig. 2.16), from the southwest and west (Dudley et al., 2000; Hodgson et al., 2006). General palaeocurrent orientations are to the east and northeast (Wickens & Bouma, 2000; Hodgson et al., 2006). Fan 4 is divided into two sand-rich units named the lower and upper sandstone divisions (Wickens & Bouma, 2000; Hodgson et al., 2006) separated by a mudstone and siltstone package that is up to 6 m thick in the south and thins and fines northward. Fan 4 exhibits aggradational to progradational stacking patterns. Fan 4 is the focus of studies in Chapter 3.

Deposits of Unit 5 (formerly Fan 5) are dominated by channel- and scour-fill deposits that represent slope-channel complexes (Johnson et al., 2001; Hodgson et al., 2006; Oliveira et al., 2009). Unit 5 is 80-100 m thick (Hodgson et al., 2006). Its deposition marks a period of abrupt slope progradation due to increased sediment supply and change from point- sourced basin-floor fans to line-sourced slope system (Hodgson et al., 2006; Fig. 2.16).

2.3.3 Laingsburg depocentre

In the Laingsburg depocentre, the Ecca Group is up to 1300 m thick (van der Merwe et al., 2009, 2010, 2011). The basal deposits comprise the mud-prone Prince Albert and Whitehill Formations and silt-prone turbidites of the Collingham Formation (Viljoen 1992, 1994; Fig. 2.17a). The Prince Albert, Whitehill and Collingham Formations have a cumulative thickness of 350 m (van der Merwe et al., 2010). They are overlain by the 280-380 m thick basin-plain deposits (siltstones, sandstones and mass transport deposits) of the Vischkuil Formation (van der Merwe et al.,2009, 2010, 2011; Fig. 2.17b) followed by the deep-water deposits of the Laingsburg Formation (e.g. Grecula et al., 2003a,b; Sixsmith et al., 2004; Prélat & Hodgson, 2013; Brunt et

al., 2013a; Hofstra et al., 2015; Fig. 2.17b), the slope deposits of the Fort Brown Formation (e.g. Figueiredo et al., 2010; Di Celma et al., 2011; Hodgson et al., 2011; Brunt et al., 2013b; Morris et al. 2014a,b; Fig. 2.17b) and shoreface/deltaic deposits of the Waterford Formation (Jones et al., 2013, 2015; Fig. 2.16).
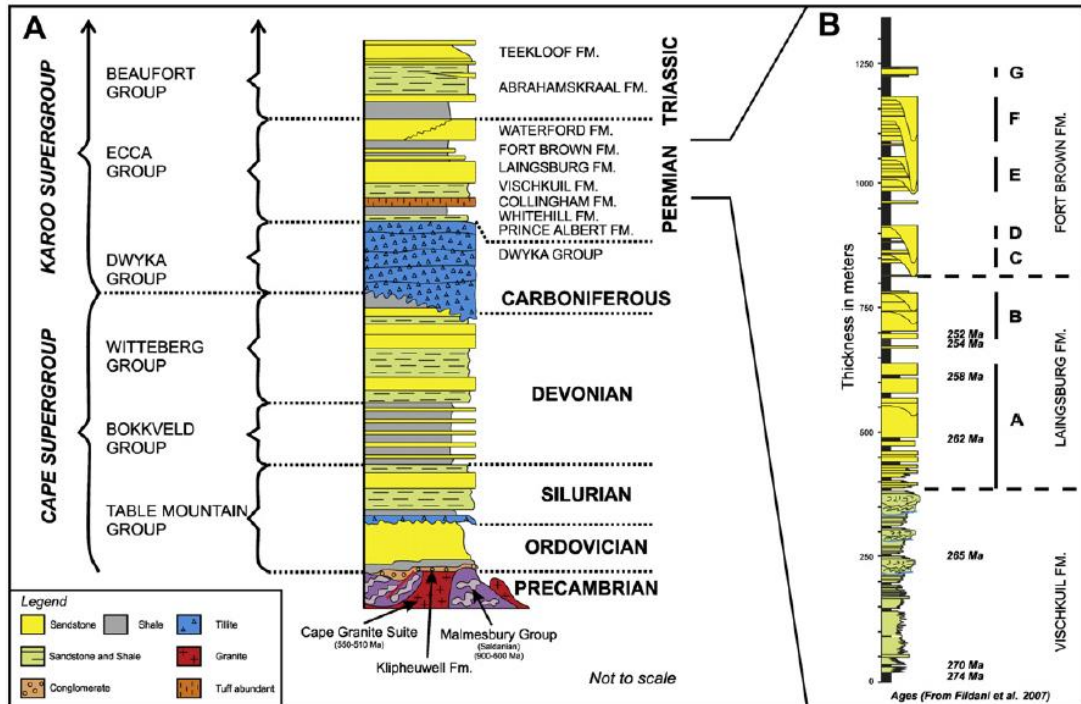
Figure 2.17. A: Lithostratigraphy of the Western Cape (redrawn after Wickens, 2004). B: Stratigraphy of the study section in the Laingsburg depocentre. Unit A of the Laingsburg Formation was the focus of studies presented in Chapter 4 and 5 and Unit E of the Fort Brown Formation of the study presented in Chapter 6. From Flint et al., 2011.

Pb/U ages obtained from zircon grains in volcanic ashes constrain part of the chronology for the deep-water strata: 275±1.5 Ma for the upper Collingham Formation; 267.9±2.6 Ma for the Vischkuil Formation; and 254±3.2 Ma for the mudstone between Units A and B (Fildani et al., 2007; 2009).

The Laingsburg Formation is subdivided into Unit A (sand-prone basin floor fan; Sixsmith et al., 2004; Prélat & Hodgson, 2013) and Unit B (base-of-slope deposits; Grecula et al., 2003a,b; Pringle et al., 2010; Brunt et al. 2013a). The stratigraphy of Unit A was subdivided by Sixsmith et al. (2004) into seven sandstone-prone subunits called A.1 to A.7 from base to top, separated by regional hemipelagic mudstone horizons. Recently, the stratigraphy of Unit A has been revised by Prélat & Hodgson (2013) and A.4 and A.7 were incorporated as lobe complexes into A.5 and A.6, respectively, as no true claystone separate them. Unit A is the focus of the study

presented in Chapter 4. Unit B is divided into three depositional sequences (B1, B2 and B3). The subunits represent a lobe complex, channel systems and an overlying levee system marking the progradation of the system (Flint et al., 2011). Units A (150 to 300 m) and B (200 m) are separated by a 40 m thick hemipelagic mudstone and (muddy) siltstone, which contains a thin sand-prone unit referred to as the A/B Interfan (Grecula et al., 2003a,b, Flint et al., 2011).

The Fort Brown Formation is divided into Unit C-F. The units are separated by thick regional mudstone horizons. Several interfans (B/C, D/E) are intercalated with these mudstone horizons (Figueiredo et al., 2010; Flint et al., 2011). Units C and D are interpreted to represent lower to middle slope settings. Unit C represents a levee-confined channel system with occurrence of frontal lobe deposits (Pringle et al., 2010; Hodgson et al., 2011; Morris et al., 2014b). It is 45 m thick and can be divided into three subunits (C1, C2 and C3) separated by hemipelagic mudstone intervals (Di Celma et al., 2011; Hodgson et al., 2011). Unit C is separated from Unit D by a 21 m thick mudstone. Unit D represents an entrenched channel-system that shows complicated stratigraphy with multiple erosion surfaces and abrupt sedimentary changes (Hodgson et al., 2011). The system cuts down (to a maximum of <100 m) into Unit C (Flint et al., 2011; Brunt et al., 2013b). Units E-G represent deposits from middle to upper slope settings. Unit E is 40-100 m thick and divided into three depositional cycles (E1, E2 and E3). Deposits of E1 are interpreted as intraslope lobes, whereas deposits of E2 and E3 represent a levee confined channel-belt and a larger channel-levee system (Figueiredo et al., 2010; Flint et al., 2011). Unit E (and intrafan D/E) is the focus of the study presented in Chapter 6). Unit F can be divided into three depositional sequences (F1, F2 and F3) as well. F1 comprises lobe fringe deposits, F2 deposits of an entrenched slope valley system and F3 deposits of a levee-confined slope valley. F2 cuts down ~150 m and removes locally the whole of Unit E (Figueiredo et al., 2010, 2013; Flint et al., 2011). These composite sequences (Flint et al., 2011) have been mapped over a 2500 km^2 area, from entrenched channels through channel-levee systems to basin-floor lobe complexes (van der Merwe et al., 2014), which provides an excellent palaeogeographic context for more detailed work.

2.4 Methodology

The following studies (Chapters 3-6) are dominantly based on data that have been collected during field and core logging seasons. Detailed methods of data collection are outlined below and summarised in the corresponding chapters. Appendix A includes detailed information on the creation of isopach maps and statistical analysis.

2.4.1 Outcrop data

Outcrop data were collected from the Tanqua and Laingsburg depocentres of the Karoo Basin, South Africa. Methods used in the field include logging, outcrop sketching, photo panelling, measuring of palaeoflow directions and kinematic indicators and walking out of surfaces for in field correlation.

Altogether 170 sections (6.9 km in cumulative thickness) were logged during the course of the project. Logging was executed at resolutions of 1:50 and 1:25, depending on the envisaged use of the log. Shorter detailed logs have permitted the creation of detailed sedimentological models that account for facies distributions and small-scale geometries. Individual bed-by-bed logs record grain size, thickness, grading, sedimentary structures and the nature and extent of bounding surfaces. In a first step, well-exposed outcrops were sketched to gain a first idea of internal geometries. Where applicable photo panelling was used to support the identification of larger outcrop geometries. Photo panels were printed out and annotated in the field. Palaeoflow measurements were collected from ripple lamination, climbing-ripple lamination and tool marks. In total 1345 measurements were collected and restored. Key stratigraphic surfaces (such as bed bases and erosion surfaces) and prominent beds (marker horizons) were established and walked out systematically in order to achieve a robust correlation of the internal stratigraphy of the studied units and document longitudinal facies variabilities.

2.4.2 Core data
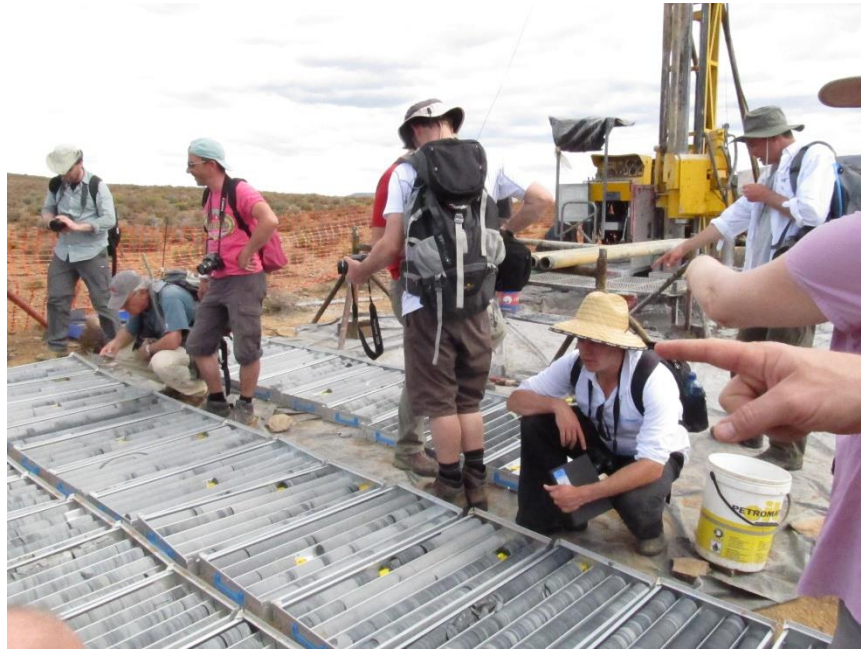
Figure 2.18. LOBE 2 sponsors visiting BK drill site during sponsors' trip in 2013.

During the course of the Lobe2 project seven new near-outcrop research boreholes were drilled (Fig. 2.18). Four cores were collected from the Tanqua depocentre (OR, KK, BK and GBE) and three from the Laingsburg depocentre (BSL, DK and ZKNL). The cores were stored near Stellenbosch for logging and photography. In total 782 m of core was logged at 1:4 scale. Later, they were redrawn at 1:50 scale for correlation purposes with the collected outcrop dataset. Bed-by-bed core logs record grain size, thickness, grading, sedimentary structures, bioturbation and the nature of bounding surfaces. For confident identification of mud-rich hybrid beds and banded facies a Dinocam (a handheld digital microscope) was used to establish relative clay content comparison (Fig. 2.19). During the course of logging, pictures of the different core facies and prominent beds were taken. After completion of core logging the entire core dataset was systematically photographed by a professional (example photograph see Fig. 2.20).

Figure 2.19. Usage of the Dinocam to look at banded facies in the core store.
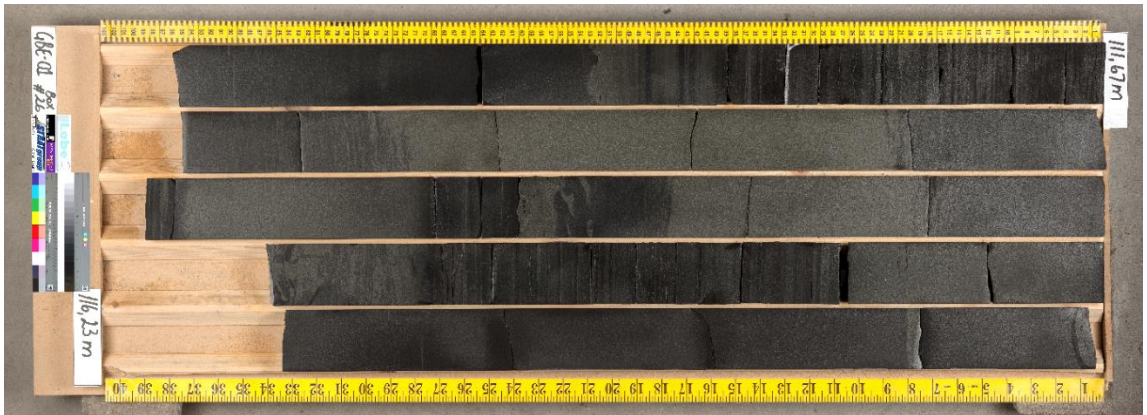
Figure 2.20. Representative example core photography from GBE core.

Chapter 3

Frontal and lateral submarine lobe fringes: comparing sedimentary facies, architecture and flow processes

3.1 Abstract

Submarine lobe fringe deposits are heterolithic successions that may comprise a high proportion ofhybrid beds. The identification of lobe fringe successions aids interpretation of palaeogeographic setting and degree of basin confinement. Here, for the first time, the sedimentological and/or architectural discrimination between frontal and lateral lobe fringe deposits is investigated. Extensive outcrop and core data for Fan 4, Skoorsteenberg Formation, Karoo Basin, South Africa, allow facies changes from axis to fringe settings of lobes and lobe complexes in both down-dip (frontal) and across-strike (lateral) directions to be tightly constrained over a 800 km^2 study area. Fan 4 comprises three sand-prone divisions that form compensationally stacked lobe complexes, separated by thick packages of thin-bedded siltstone and sandstone intercalated with (muddy) siltstone, interpreted as lobe complex fringes. Lobe-fringe facies associations comprise: 1) thick-bedded structureless or planar laminated sandstones that pinch and swell, and are associated with underlying debrites; 2) argillaceous and mudclast-rich hybrid beds; and 3) current ripple-laminated sandstones and siltstones. Typically, frontal fringes contain high proportions of hybrid beds and transition from thick-bedded sandstones over length-scales of 1 to 2 km. In contrast, lateral fringes tend to be current ripple-laminated and transition to thick-bedded sandstones in the lobe axis over several kilometres. The distinct difference in facies association is considered to be controlled by flow processes. Preferential deposition of hybrid beds in frontal fringe positions is probably related to the dominantly downstream momentum of the high-density core of the flow. In contrast, the ripple-laminated thin beds in lateral fringe positions are interpreted to be deposited by more dilute (marginal) low-density (parts of) flows. The palaeogeographic constraints allow criteria to be established to discriminate between different fringe settings and to constrain the rates of facies transitions. These are critical to improving palaeogeographic reconstructions of submarine fans at outcrop and in the subsurface, and will help to reduce uncertainty during hydrocarbon field appraisal and development.

3.2 Introduction

Traditionally, submarine lobe deposits are described as simple radial bodies that thin and fine from an apex (e.g. Mutti, 1977; Normark, 1978; Lowe, 1982; Bouma, 2000). However, it has been recognized that the anatomy of lobe deposits is more complicated in terms of facies distribution and geometry (e.g. Nelson et al., 1992; Twichell et al., 1992; Bouma & Rozman, 2000; Gervais et al., 2006; Hodgson et al., 2006; Deptuck et al., 2008; Prélat et al., 2009; Groenenberg et al., 2010; Etienne et al., 2012). Prélat et al. (2009) proposedfour sub-environments for lobe deposits that are characterized by specific facies associations and thickness trends, termed lobe axis, lobe off-axis, lobe fringe and lobe distal fringe (Fig. 3.1a).
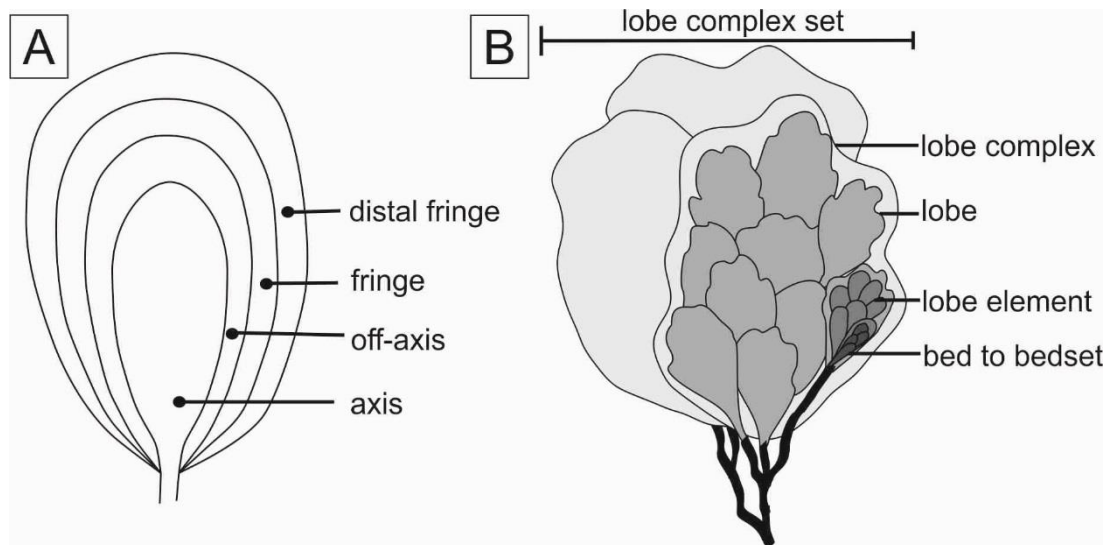
Figure 3.1. A: Simplified lobe model indicating the different lobe sub-environments (redrawn from Prélat et al., 2009). B: Plan from view of fivefold lobe hierarchy: bed to bed set, lobe element, lobe, lobe complex and lobe complex set (modified from Prélat et al., 2010).

Placing constraints on the temporal and spatially variability of lobe fringe successions would help improve reconstructions of deep-water fans, provide suitable building blocks for reservoir modelling and reduce uncertainty in the evaluation of subsurface stratigraphic traps (e.g. Biddle & Wiechowsky, 1994; Etienne et al., 2012; Bakke et al., 2013; Collins et al., 2015; Grecula et al., 2015). Hybrid beds (e.g. Haughton et al., 2003; Talling et al., 2004; Haughton et al., 2009; Davis et al., 2009) and heterolithic deposits, dominated by thin-bedded turbidites, have been associated with lobe fringe

environments (Ito, 2008; Hodgson, 2009; Talling et al., 2012a; Etienne et al., 2012; Grundvåg et al., 2014; Patacci et al., 2014; Collins et al., 2015; Fonnesu et al., 2015). Previous work on lobe fringe successions has focused on pinch-out geometries (e.g. Rozman, 2000; Marini et al., 2011; Etienne et al., 2012; Nagatomo and Archer, 2015). Some authors (e.g. MacPherson, 1978; Pickering, 1981, 1983) have documented differences between down-dip and across-strike facies transitions in lobe deposits. However, detailed depositional architecture, recognition criteria and facies variability between down-dip (frontal) and across-strike (lateral) lobe fringe environments remain poorly constrained.

The aim of this integrated outcrop and core study is to assess the difference between frontal and lateral lobe fringes using the palaeogeographically well-constrained Fan 4 succession of the Skoorsteenberg Formation, Karoo Basin, South Africa. Specific research objectives are: 1) to establish the characteristic facies associations that distinguish the different lobe fringe settings, 2) to interpret flow processes that produce the observed facies variability; 3) to discuss the role of confinement in the distribution and character of lobe fringes; and 4) to assess the implication of the results for subsurface applications.

3.3 Geological Setting

The Karoo Basin has been interpreted as a retroarc foreland basin connected to a magmatic arc and fold-thrust belt (Cape Fold Belt) (Visser & Prackelt, 1996; Visser, 1997; Catuneanu et al., 1998). Alternatively, Tankard et al. (2009) argue that subsidence during the early, deep-water, phase of deposition, which is the focus of this study, pre-dates the effects of loading by the Cape Fold Belt, and was induced by dynamic topography associated with mantle flow processes coupled to distant subduction of the palaeo-Pacific plate (Pysklywec & Mitrovica, 1999). The basin-fill comprises the Karoo Supergroup and records sedimentation from Late Carboniferous to Early Jurassic. The Karoo Supergroup comprises the glacial Dwyka Group, the deep- to shallow-marine Ecca Group and the non-marine (fluvial) Beaufort Group. The Ecca Group, which is the focus of this study, represents a shallowing-upward succession of sediments from deep-water to fluvial settings (Flint et al., 2011).
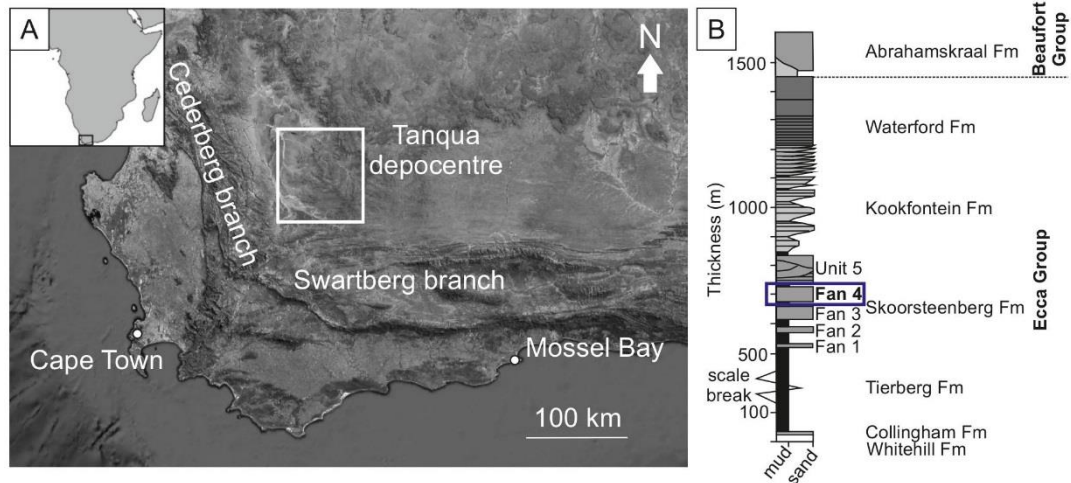
Figure 3.2. The Tanqua depocentre inboard of the Cape Fold Belt (Cederberg and Swartberg branches). The square indicates the location of the study area. B: Stratigraphy of the Tanqua depocentre. The Skoorsteenberg Formation. overlies the Tierberg Formation., and is overlain by the Kookfontein Formation (redrawn from Wild et al., 2009). This study focuses on Fan 4. Images taken from Google Earth.

The Tanqua depocentre is located in the southwest of the Karoo Basin adjacent to the Cederberg branch of the Cape Fold Belt (Fig. 3.2a). Here, the Lower Ecca Group comprises the Prince Albert Formation (shallow-marine), the Whitehill Formation (deep-marine) and the Collingham Formation (deep-marine), and the Upper Ecca Group comprises the Tierberg Formation (basin-plain), the Skoorsteenberg Formation (basin-floor to base-of-slope), the Kookfontein Formation (slope to shelf-edge) and the Waterford Formation (shoreface) (Fig. 3.2b; Bouma & Wickens, 1991; Wickens, 1994).

The Skoorsteenberg Formation (450 m thick; Bouma & Wickens, 1994) is subdivided into five sand-prone bodies. The lower four sandstone bodies (Fans 1-4) have been interpreted as basin-floor fans (Wickens & Bouma, 2000, Johnson et al.,2001), whereas the fifth (Unit 5) has been interpreted as a lower slope to base-of-slope system (Wickens & Bouma, 2000; Wild et al., 2005 Hodgson et al., 2006). Although a submarine fan represents a system built up by channels and lobes, 'Fan' is retained here as a lithostratigraphic descriptor for consistency with previous literature. Individual preserved fans are up to 65 m in thickness, with gradational to sharp bases and tops (Johnson et al., 2001) separated by mudstones and siltstones (Van der Werff & Johnson, 2003a). Each fan is interpreted as a lowstand systems tract, with the overlying fine grained deposits of regional extent representing the related

transgressive/highstand systems tract (Goldhammer et al., 2000; Johnson et al., 2001; Hodgson et al., 2006; Hodgson, 2009).

This study focusses on the lobe deposits of Fan 4, a lobe complex-set (Fig. 3.1b), in an 800 km^2 study area (Fig. 3.2a). Fan 4 is up to 65 m thick (Johnson et al., 2001) and is characterised by a high amount of amalgamation in the Skoorsteenberg area (Fig. 3; Dudley et al., 2000). Palaeocurrents and thickness distributions indicate that sediment was sourced from two directions, from the southwest and west (Dudley et al., 2000; Hodgson et al., 2006) in contrast to the underlying fans (Fan1-3) that are supplied solely from the SW. General palaeocurrent orientations are to the east and northeast (Wickens & Bouma, 2000; Hodgson et al., 2006). Fan 4 is divided into two sand-rich units named the lower and upper sandstone divisions (Wickens & Bouma, 2000; Hodgson et al., 2006) separated by a mudstone and siltstone package that is up to 6 m thick in the south and thins and fines northward. The upper division thickens to the north where the lower division thins, which was suggested by Hodgson et al. (2006) to indicate compensational stacking. The stratigraphy of Fan 4 has been revised to show that the lower sandstone division comprises one sand-prone lobe complex, whereas the upper division comprises two sand-prone lobe complexes, separated by thin-bedded heterolithic lobe complex fringe strata.

3.4 Methodology

For this study, 24 log sections were measured in strategically chosen locations (Fig. 3.3) in order to collect a data set that provides 3D constraint and that comprises lithology, palaeocurrent measurements and bed thickness data. Detailed bed-by-bed sections (see section locations on Fig. 3.3; ranging from 3 to 60 m in length and totalling 510 m in cumulative thickness) record grain size, sedimentary structures and bounding surfaces of beds. Logs were recorded at 1:25 scale in the field. Four newly drilled (see well locations on Fig. 3.3), near-outcrop cores intersect Fan 4 (212 m total thickness) and were logged at 1:4 scale. These data were augmented with three core logs (see locations of NOMAD wells on Fig. 3.3; 128 m cumulative thickness) and 19 logs collected during previous research (Hodgson et al., 2006; Prélat et al., 2009) (Fig. 3.3). Outcrop sections and core logs were redrawn at 1:50 scale for correlation purposes. The base of the mudstone and siltstone interval that separates the lower
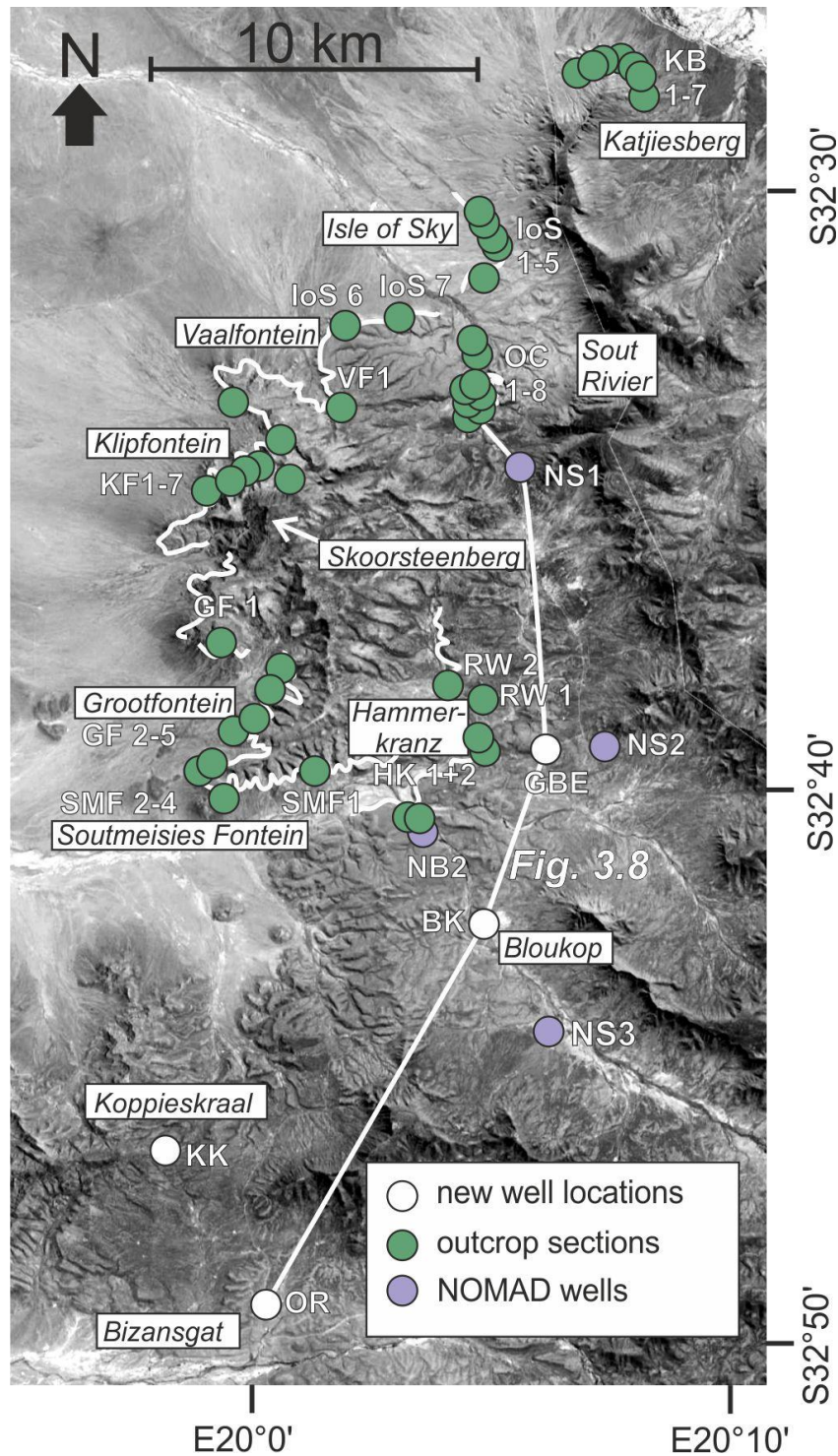
Figure 3.3. Locations of recently cored wells, outcrops, NOMAD well locations and previous studies' outcrop sections used in the study. Fan 4 outcrops are marked in white. Images taken from GoogleEarth. A larger scale map of the Tanqua depocentre can be found in the back of the thesis as a pull-out.

and upper sandstone division of Fan 4 was used as a marker interval. Palaeocurrent measurements (108 in total) were collected from current ripple-laminated strata, climbing ripple-laminated strata, and flutes and grooves preserved as casts on bed

bases. To determine facies associations and architectures of frontal and lateral lobe fringe deposits, the hierarchy and palaeogeography of Fan 4 needed to be revised to improve the spatial understanding of lobe distribution.

3.5 Model of lobe anatomy

3.5.1 Hierarchy

A fourfold hierarchy of lobes in the Tanqua was proposedby Prélat et al. (2009): 1) a 'bed' represents a single depositional event; 2) one or more beds stack to form a 'lobe element'; 3) several lobe elements that are divided by thin siltstone intervals form a 'lobe'; 4) one or more lobes stack to form a 'lobe complex' (Fig. 3.1b). The hierarchy can be expanded by adding a fifth hierarchical unit, the 'lobe complex set', which is formed by several lobe complexes within the same lowstand systems tract (Fig. 3.1b). Prélat and Hodgson (2013) demonstrated that extensive meter-thick, thin-bedded units between sand-rich lobes, originally referred to as 'interlobes' by Prélat et al. (2009), represent the distal fringes of lobes. Typically, these are separated from sand-rich lobe deposits (axis and ff axis) across abrupt surface interpreted to mark up dip channel avulsion (Prélat and Hodgson, 2013). Thicker and more extensive thin-bedded successions can be interpreted as the fringes of lobe complexes (Prélat and Hodgson, 2013).

3.5.2 Sedimentary facies and facies associations

Aspects of the sedimentary facies and related environments of deposition of the Skoorsteenberg Formation have been described in detail previously (e.g. Morris et al., 2000; Johnson et al., 2001; van der Werff & Johnson 2003a; Hodgson et al., 2006; Luthi et al. 2006; Prélat at al., 2009; Hodgson, 2009, Jobe et al., 2012; Hofstra et al., 2015). Individual facies encountered in both outcrop (Fig. 3.4a-f) and core (Fig. 3.5a-f) datasets are summarized in Table 3.1. The facies combine into common facies associations representing different lobe environments: lobe axis, lobe off-axis, lobe fringe and lobe distal fringe (Fig. 3.1). The boundaries between these environments are transitional. This fourfold division was introduced by Prélat et al. (2009) and has been applied to several outcrop studies (e.g. Etienne et al. 2012; Prélat & Hodgson,

2013; Grundvåg et al., 2014; Chapter 4-6). Lobe dimensions from several studies of sand-rich systems (Jegou et al., 2008; Saller et al., 2008; Deptuck et al., 2008; Prélat et al., 2009; Sømme et al., 2009) show that these bodies have elongate shapes with length-to-width ratios of 1.7 – 3.6 (Prélat et al., 2010). Average dimensions of lobes in the Tanqua depocentre are 27 km (length) × 13 km (width) × 5 m (thickness) (Fan 3, Prélat et al., 2009). Similar dimensions are expected for the lobes of Fan 4 as it was deposited under similar conditions (e.g. relative unconfined, grain size range), and similar lobe dimensions are identified across different unconfined systems (Prélat et al., 2010).

Lobe axis. Lobe axis deposits are dominated by thick-bedded structureless sandstone (F1; Figs.3.4a, 3.5a; Table 3.1) with planar laminated (F2; Figs. 3.4b, 3.5b; Table 3.1) and banded sandstone (F3; Fig. 3.5c; Table 3.1) in minor proportions. The lobe axis setting is characterized as 85-100% sandstone. Multiple zones of amalgamation may occur (Prélat et al., 2009) and can form packages up to 8 m thick where there is scouring at the base of the lobe. The deposits of the lobe axis are laterally extensive down-dip and across strike for several hundred metres and generally show tabular geometries (Fig. 3.4a). Units of high amalgamation can be traced into well-bedded units of the lobe off-axis towards the frontal and lateral margin of the lobe deposits.

Lobe off-axis. Lobe off-axis deposits comprise well stratified medium-bedded structured sandstone (F2; Table 3.1) and are typically 2 to 4 m thick. Lobe off-axis deposits are characterized by 50-85% sandstone. They show tabular geometries in outcrop and can be traced out for several hundred metres in both dip and strike directions.

Lobe fringe. Lobe fringe deposits comprise a range of facies, including structureless sandstone (F1), hybrid beds (F4; Figs. 3.4c,d; Table 3.1), debrites (F5; Fig. 3.5e; Table 3.1) and heterolithic packages (F6; Figs. 3.4d, 3.5e). Lobe fringe deposits are characterized by 20-50% sandstone. Typical thicknesses range between 0.1 and 2 m. Several metre thick successions (>2 m) are interpreted as fringes to lobe complexes; such accumulations can be walked out into thick lobate sandstone units without truncation (cf. Prélat and Hodgson, 2013). At outcrop, lobe fringe deposits can show either tapering or pinch- and- swell geometries. The pronounced pinch- and- swell geometries give the impression of lenticular bodies, even though no evidence of truncation is observed (Bouma & Rozman, 2000; Groenenberg et al., 2010). The lateral extent of lobe fringe deposits is variable and ranges from a few to

several kilometres. The transition from lobe fringe to lobe distal fringe environment marks the sand pinchout of the system.

Lobe distal fringe. The lobe distal fringe environment is dominated by siltstone deposits (F7; Figs. 3.4e; 3.5g; Table 3.1). Some thin very fine-grained sandstone beds are intercalated in these siltstone-prone packages (<20% sandstone). Siltstones can aggrade to form bedded successions of several metres. Lobe distal fringe deposits form an extensive 'halo' around the main sand-prone lobe body and extend for several kilometres. Their dimensions have not been established.

In summary, lobe axis and off-axis deposits build the core of a lobe body and are dominated by structureless and structured sandstone. Sandstone percentage decreases towards the lobe fringe and is lowest in distal lobe fringe environments.

3.6 Architecture

3.6.1 Thickness distribution and palaeoflow directions

Fan 4 is subdivided into a lower and upper sand-prone division, separated by a thin-bedded heterolithic division (Fig. 3.6, 3.7a). The two sand-prone divisions of Fan 4 show different thickness trends and palaeocurrent patterns and are separated by an extensive fine grained division.

The lower sand-prone division has a maximum thickness of ~25 m in the southern part of the study area (Fig. 3.6). Thinning is documented to the north and the northeast. The lower division records palaeoflow to the northeast but this trend is more northwards in the northern part of the study area (Fig. 3.6). Correlation panels (Fig. 3.7) show that down-dip pinch-out of lobe deposits occurs in several areas, such as around BK, NB2, GBE, OC7 and Ios6 area (Fig. 3.7).

Lithofacies	Grain size	Thickness range	Description	Process interpretation	Depositional environment
Structureless sandstone (F1)	fs to vfs	0.2–2.0 m	Sharp, erosive or loaded base; flute and tool marks common; form high amalgamation units; dewatering common at the base; up to 5% mudstone chips and carbonaceous material in matrix	Deposited by high-density turbidity currents (Kneller & Branney, 1995) with high aggradation rates (Arnott & Hand, 1989; Leclair & Arnott, 2005; Talling et al., 2012)	Commonly deposited in lobe axis setting, but also observed in lobe fringe settings
Structured sandstone (F2)	fs to vfs	0.1 to 0.7 m	Planar, current-ripple, low angle climbing-ripple or wavy laminations; normal grading; bed bases are sharp or loaded; bed tops are sharp and flat or undulating; may contain carbonaceous material at the top	Deposited by low-density turbidity currents. Planar and current-ripple lamination produced by reworking through dilute flows along the bed (Allen, 1982; Southard, 1991; Best and Bridge, 1992). Climbing-ripple lamination forms under bedload transport associated with high aggradation rates (Allen, 1973; Hunter, 1977; Jobe et al., 2012). Wavy or sinusoidal lamination indicate deposition from waning currents with very high rates of suspension fallout (Allen, 1973; Jopling & Walker, 1968; Hunter, 1977)	Deposited in lobe off-axis setting
Banded sandstone (F3)	fs to vfs	0.1 to 1.5 m	Couplets of dark and light bands; Light bands comprise 'clean' sandstone; dark bands are mud-rich and can comprise mudstone chips and carbonaceous material; band thickness varies from 0.2 to 1 cm; bands can be continuous or discontinuous over the distance of several metres	Deposited by transitional flows. Fluctuations of clay content of near-bed layers result in flows alternating between fully turbulent and more cohesive viscous types, thereby depositing alternating clean and argillaceous sand laminae (Lowe & Guy, 2000; Davis et al., 2009; Haughton et al., 2009)	Observed at the boundary between lobe-axis to off-axis settings
Hybrid beds (F4)	fs to vfs	0.05 to 1.5 m	Consists of two divisions. Lower division: well sorted and 'clean' with mudstone chips to the top; Upper division can be: 1) mudstone- and siltstone-clast rich with clean matrix; 2) argillaceous, poorly sorted sandstone with a swirly and patchy fabric comprising mudstone chips and carbonaceous material; or 3) argillaceous, micaceous, poorly sorted, clast-rich sandstone	Deposited from strongly stratified flows (e.g. Kane and Pontén, 2012; Talling, 2013) and from co-genetic turbidity currents (lower division) and cohesive debris flows (upper divisions) (Haughton et al., 2003; Talling et al., 2004; Haughton et al., 2009, Hodgson, 2009). Hybrid beds with an upper clast-rich division are interpreted to be formed as a suspension deposit from a purely turbiditic current (Hodgson, 2009) due to local entrainment of heterolithic material.	Deposited in lobe fringe environments
Debrites (F5)	fs to vfs	0.2 to 3 m	Poorly sorted; mud-rich; outsized quartz grains (ufs); variable amount of mudstone chips, siltstone clasts and carbonaceous material	Deposited by en masse freezing of debris flows (Iverson, 1997; Talling et al., 2012).	not indicative of any environment
Heterolithic packages (F6)	vfs and silt	0.05 to 0.3 m	Sandstone beds show planar, wavy, current-ripple, and stoss-side preserved climbing-ripple lamination; . Siltstones are stuctureless to planar laminated; normal grading; sharp bed bases; undulating tops due to preservation of ripple crests	Deposits of distal, sluggish, low volume flows (cf. Jobe et al., 2012). Ripple laminations form beneath dilute turbulent flows via reworking of the bed under moderate aggradation rates, whereas climbing-ripple lamination forms under high aggradation rates (Allen, 1971; Allen, 1982; Southard, 1991)	Deposited in lobe fringe environments
Siltstone (F7)	fine to coarse silt	0.01 to 0.2 m	Structureless; planar laminated or current-ripple laminated (where sandy); bioturbation is common;	Deposited by dilute turbidity currents. Planar lamination is a product of traction (Stow and Piper, 1984; Mutti, 1992; Talling et al., 2012). Structureless beds are formed by direct suspension fallout (Bouma, 1962)	Deposited in lobe distal fringe environments
Claystone (F8)	clay	0.005 to 0.02 m	Commonly silty; concretions associated with distinctive horizons	Suspension fall-out	Hemipelagic background deposits

Table 3.1. Summary of sedimentary facies of Fan 4.
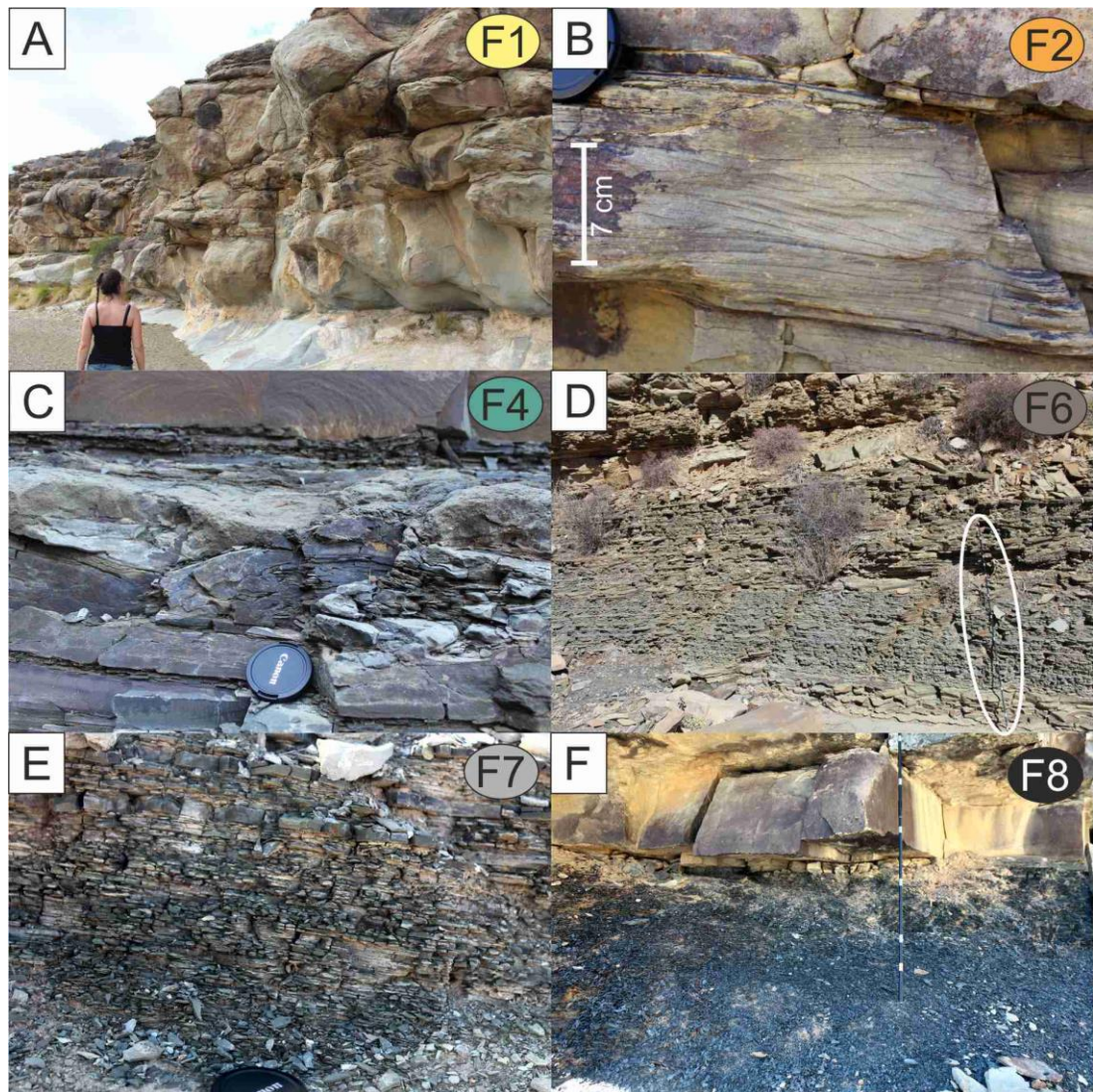
Figure 3.4. Representative outcrop photographs of observed facies. A: Structureless thick-bedded sandstone (F1). Person as scale (~ 1.7 m); B: Structured medium-bedded sandstone (F2). C: Hybrid bed (F4) with lower clean division and upper mudstone clast –rich division, Lens cover as scale (~7 cm diameter); D: Thin-bedded heterolithic strata (F6). Logging pole (1.8 m) as scale; E: Thin-bedded siltstone (F7). Lens cover as scale (~7 cm diameter); F: Mudstone (F8) horizon overlain by sandstone. Logging pole as scale (10 cm increments).
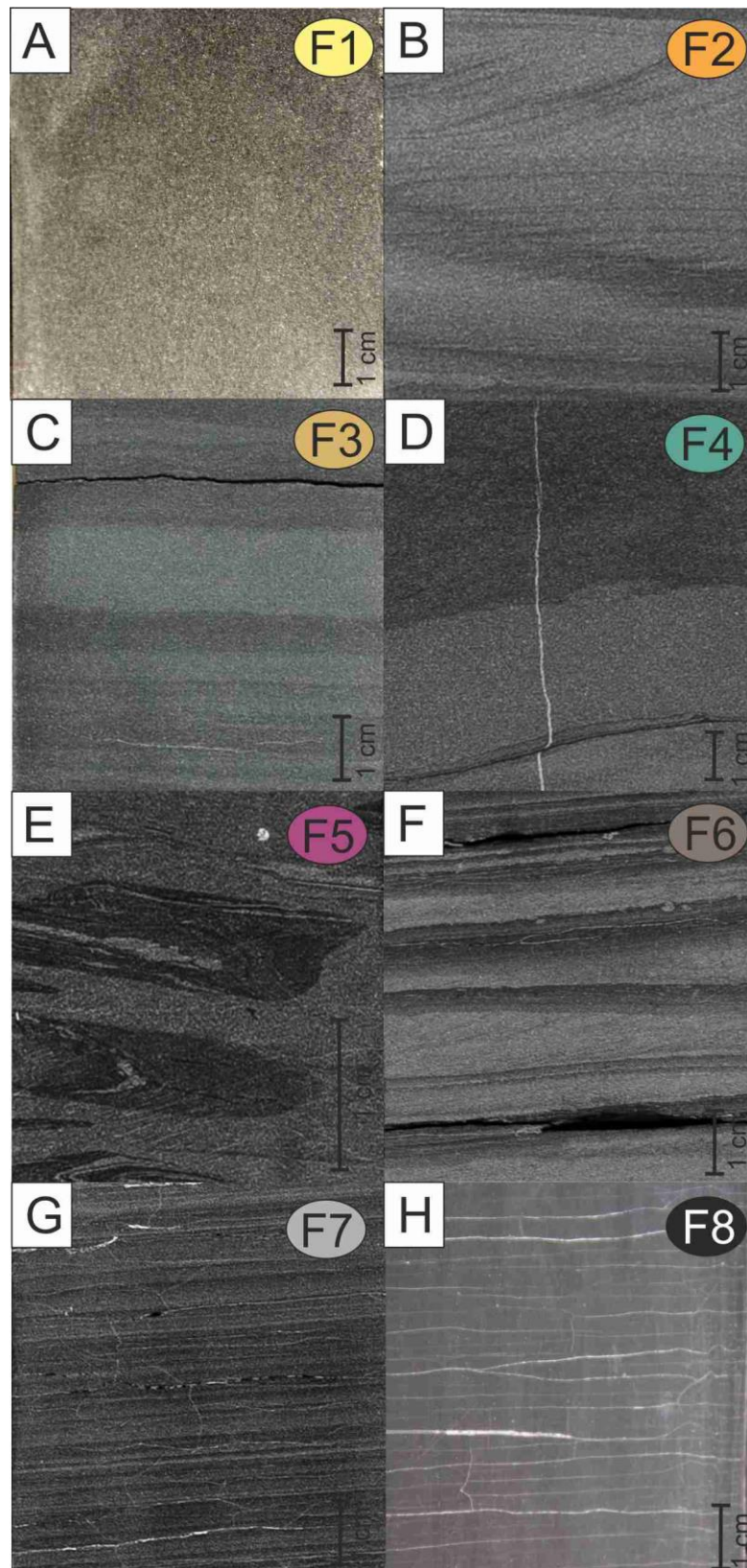
Figure 3.5. Representative core photographs of observed facies. A: Structureless sandstone (F1); B: Structured sandstone (F2); C: Banded sandstone (F3); D: Hybrid bed (F4) with lower clean sandstone division and upper argillaceous sandstone division; E: Debrites (F5); F: Heterolithic package (F6); G: Siltstones (F7); H: mudstone (F8).
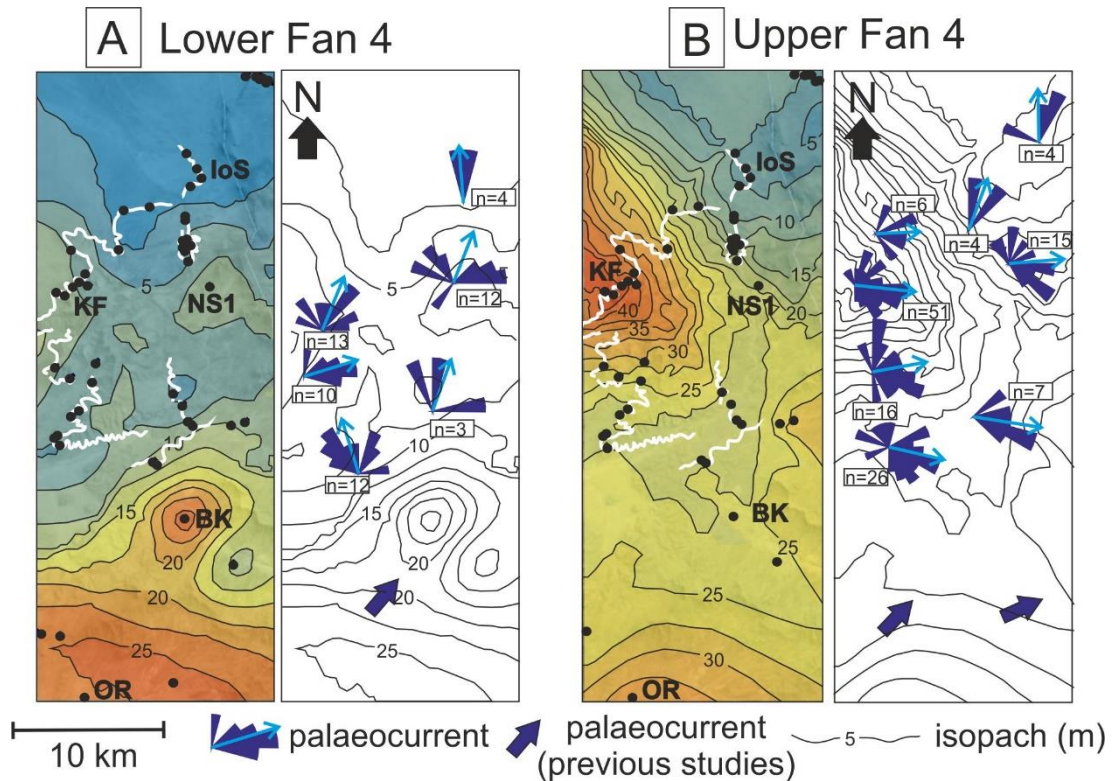
Figure 3.6. Isopach and palaeocurrents maps for A. Lower and B. Upper Fan 4. Contours are in metres. Palaeocurrents from previous work based on Hodgson et al. (2006).

The final sand-pinch out to the northeast occurs in the Vaalfontein- Sout Rivier area (Fig. 3.3). Notable lateral thinning across strike towards the east (NS3; Fig. 3.3) can be observed (~5.5 m/km). Thin (< 2 m thick) siltstone deposits are deposited farther to the north where they thin gradually.

The thin-bedded heterolithic division that separates the lower and upper sand-prone divisions of Fan 4 thins and fines over 30 km from Bizansgat in the S (~6 m) gradually to Sout Rivier in the N (~0.7 m) (Fig. 3.8).

The upper sand-prone division of Fan 4 has a more complicated thickness and palaeoflow distribution. There are two areas that show high thickness values (Fig. 3.6). Maximum thickness in the southern study area is ~35 m (Bizansgat) from where the division thins to the north and northeast, with palaeoflow trends that conform to the northeasterly to northerly trends of the lower division and of underlying Fan 3 (cf. Wickens & Bouma, 2000; Hodgson et al., 2006; Prélat et al., 2009). In the area around Skoorsteenberg (Fig. 3.3), the upper division is 47 m thick (Fig. 3.6) with palaeoflow trends that record a radial spread of directions to the east, northeast and southeast (Fig. 3.6; cf. Hodgson et al., 2006). Thinning occurs to the southeast and northeast,

with the rate of thinning to the northeast being highest (~6.9 m/km). The most northeastern outcrops around Katjiesberg (down-dip) are characterized by highly variable thicknesses that range between 2 and 14 m and these reflect a pinching and swelling trend of the deposits, and record dominantly northward palaeocurrents (Fig. 3.6b). Correlation panels (Fig. 3.7) show that the oldest deposits pinch-out in the Sout Rivier area, and the youngest deposits do not reach as far as the Katjiesberg area. Therefore, an overall basinward to landward stacking pattern is constrained.

3.6.2 Hierarchy of Fan 4

Thicknesses, facies associations and palaeocurrents indicate that the lower division of Fan 4 comprises one lobe complex (Fig. 3.8a, LC1) that was fed by flows from the southwest. The heterolithic succession that separates the lower and upper sand-prone divisions of Fan 4 comprises thin-bedded silty mudstone, siltstone and sandstones (heterolithic deposits) (Fig. 3.8b, c). The facies association, the lack of hemipelagic claystone, and the thickness patterns, collectively suggest this succession most-likely represents the distal fringe of a lobe complex.

The associated sand-prone deposits of this lobe complex (LC2) are inferred to be located to the west, beyond the outcrop exposure. Palaeoflow and thickness trends suggest two distinct sediment entry points for the upper sand-prone division of Fan 4 (Wickens & Bouma, 2000; Dudley et al., 2000; Hodgson et al., 2006).The upper part of Fan 4 comprises two sand-prone lobe complexes (LC3 and LC5). They both have maximum thicknesses in the Skoorsteenberg area, and are separated by a ~3 m thick extensive thin-bedded unit that is interpreted as the fringe of another lobe complex (LC4; Fig. 3.8a).
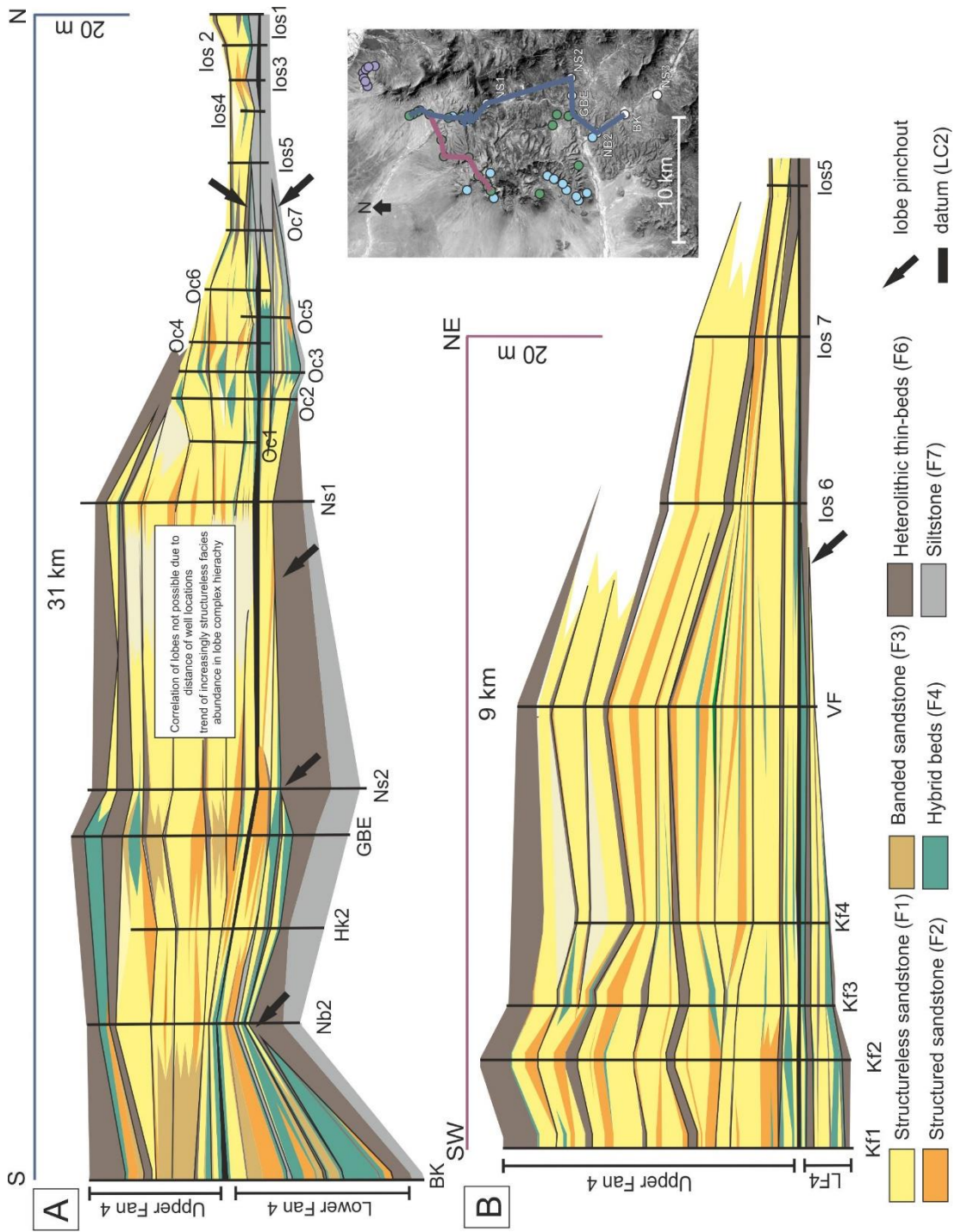
Figure 3.7. Correlation panels of Fan 4. Top: Correlation of a S-N transect from Bloukop (BK) to Isle of Sky (Ios). Bottom: SW-NE correlation from Klipfontein (Kf) to Isle of Sky (Ios). The base of the mudstone and siltstone interval (black unit) that separates the Lower and Upper Fan 4 is used as datum.
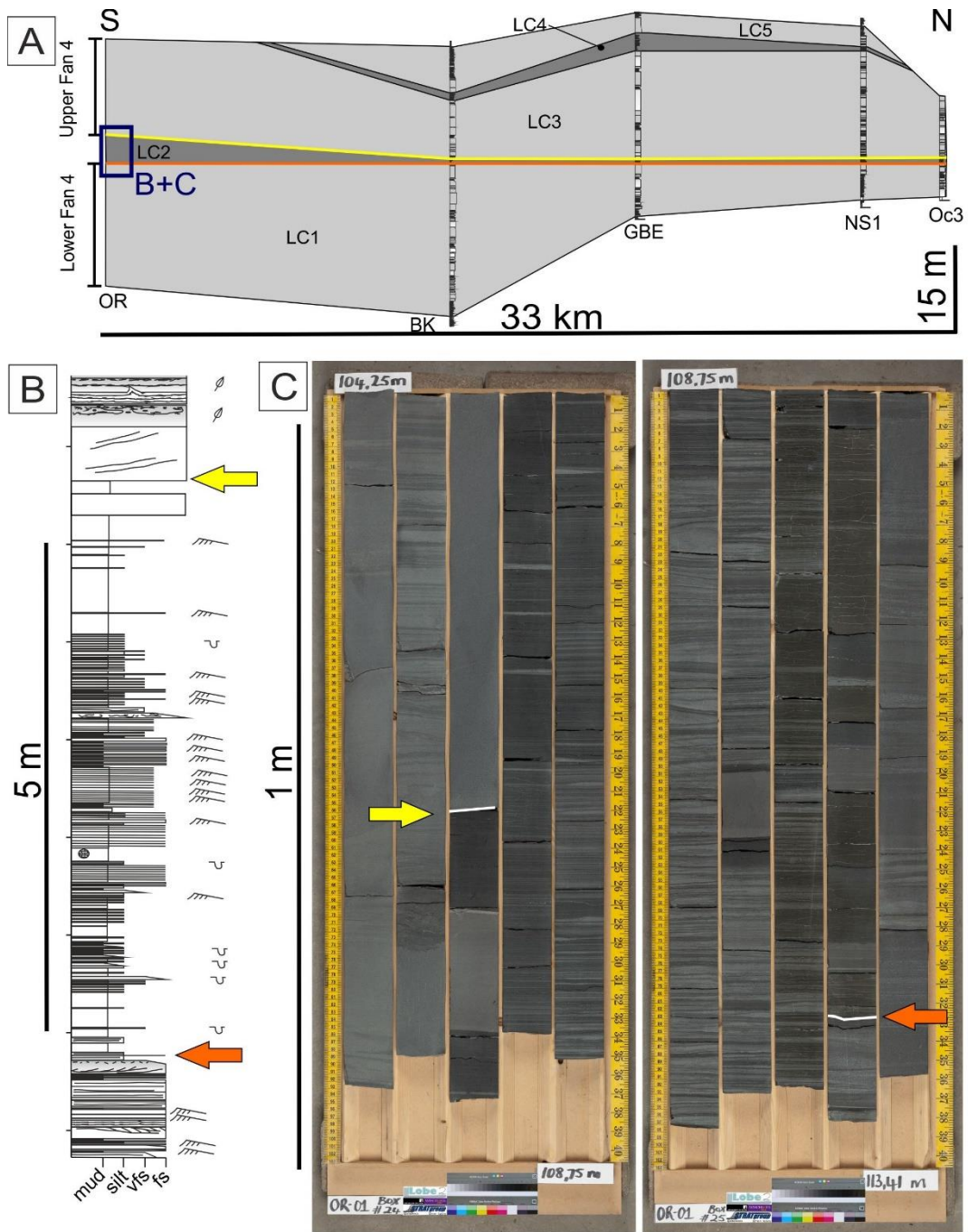
Figure 3.8. A: Hierarchical model of Fan 4. Location of panel is marked in Fig. 3.3. Fan 4 consists of two sand-prone divisions that are separated by a thin-bedded heterolithic lobe fringe complex. Lower Fan 4 comprises one lobe complex (LC1), and upper Fan 4 comprises two lobe complexes (LC3 and LC5) and a fringe complex (LC4). Blue square marks zoom-in area of B and C. B: Close-up of the LC2 deposits in the OR well (see Fig. 3.3 for location). C: Corresponding core photographs.

3.6.3 Facies distribution

Successive lobe deposits in weakly confined settings build lobe complexes that commonly exhibit compensational stacking patterns driven by avulsion of distributive channels (Pickering, 1981; Deptuck et al. 2008; Prélat et al., 2009; Prélat and Hodgson, 2013) (Fig. 9a-d). The distribution of sedimentary facies are described from LC1 (lower division; Fig. 10a) and LC 3-5 (upper division; Fig. 10b).

In the southern part of the study area, where LC1 is thickest, the deposits are dominated by structureless (F1) and structured sandstone (F2; see Table 3.1; F1+F2> 75%; Fig. 3.10a). The proportion of hybrid beds (F4) increases northwards where they can represent up to 50% of the thickness (e.g. Vaalfontein). Heterolithic deposits (F6) dominate the basal part of LC1 around the NB2, NS2 and NS1 well locations (see location of the well on Fig. 3.3). The NS3 well is represented by heterolithic deposits (~70%), siltstone (~10%) and mudstone (~20%) (Fig. 3.11). Structureless sandstones are present in the northern part of the study area in highly variable proportions (15% to 50% of deposits) (Fig. 3.10a). Sandstone-pinchout occurs in the Sout Rivier area (Fig. 3.7). Northwards, the deposits of LC1 consist entirely of thin-bedded siltstones.

The upper part of Fan 4, which comprises LC3, 4, and 5, is characterised by a higher proportion of structureless sandstone. The southern study area is marked by structureless (F1), structured (F2) and banded sandstones (F3), which represent the bulk of deposits (50 to 75%; Fig. 3.10b). Hybrid beds (F4) contribute 20% of the facies composition in Koppieskraal; elsewhere they contribute less than 10%. Heterolithic deposits (F6) contribute 15 to 35% towards the central study area but less than 10% in the southern study area (Fig. 3.10b). The northern study area is dominated by structureless sandstone deposits (more than 50%) with the highest proportion observed in the Skoorsteensberg area (up to 80%; Fig. 3.10b). Structured sandstone is a minor contributor (~ 15%). Hybrid beds represent less than 10% of deposits, whereas heterolithic deposits commonly represent 10 to 15%. In the Katjiesberg area in the northeast, almost no heterolithic deposits are present (<2%) but thin-siltstone deposits are intercalated with structureless sandstone and hybrid beds.
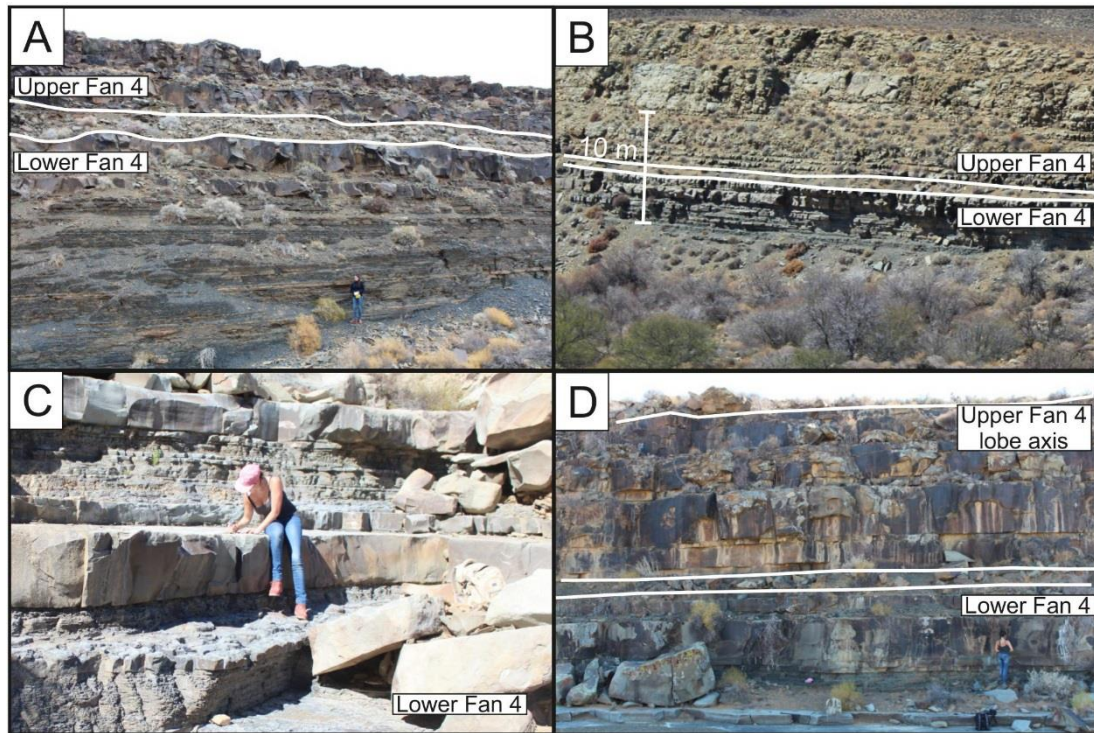
Figure. 3.9. Representative photographs of lobe successions in the field area. A: Lobe fringe deposits of lower Fan 4 overlain by lobe axis and off-axis deposits of upper Fan 4. Person as scale (~1.7 m); B: Lobe fringe deposits of lower Fan 4 overlain by lobe axis and off-axis deposits of upper Fan 4 C: Lower Fan 4. Hybrid beds are separated by thin-bedded siltstone successions. Person as scale (~1.7 m). D: Thick-bedded lobe axis deposits of Upper Fan 4. Person as scale (~1.7 m).

3.6.4 Fan 4 palaeogeographic reconstruction

Integration of palaeoflow directions, thickness map and facies distribution have enabled reconstruction of the lower (LC1) and upper (LC3-5) divisions of Fan 4. Palaeoflow directions for LC1 are both to the north and northeast (Fig. 3.6)), whereas sediment entered from the southwest (e.g. Dudley et al., 2000; Hodgson et al., 2006). This means that the northward pinchout represents a frontal fringe and the eastern termination a lateral pinchout at the scale of the lobe complex (Fig. 3.7). Younger lobe deposits of LC1 successively pinchout farther to the north, which is consistent with a progradational stacking pattern, and frontal pinch-out at the scale of a lobe. The frontal sand pinchout of LC1 in the Sout-Rivier area (Fig. 3.2) is associated with a pinch-and-swell geometry of lobes and predominantly structureless sandstone and hybrid beds (Fig. 3.7). A 'halo' of thin-bedded siltstone, that represents distal lobe fringe deposits, is deposited farther to the north. Deposits across strike (lateral) to the east are dominated by heterolithic deposits (NS3; Figs. 3.10a, 3.11). The change in facies is associated with thinning of LC1. Therefore, the deposits observed in NS3
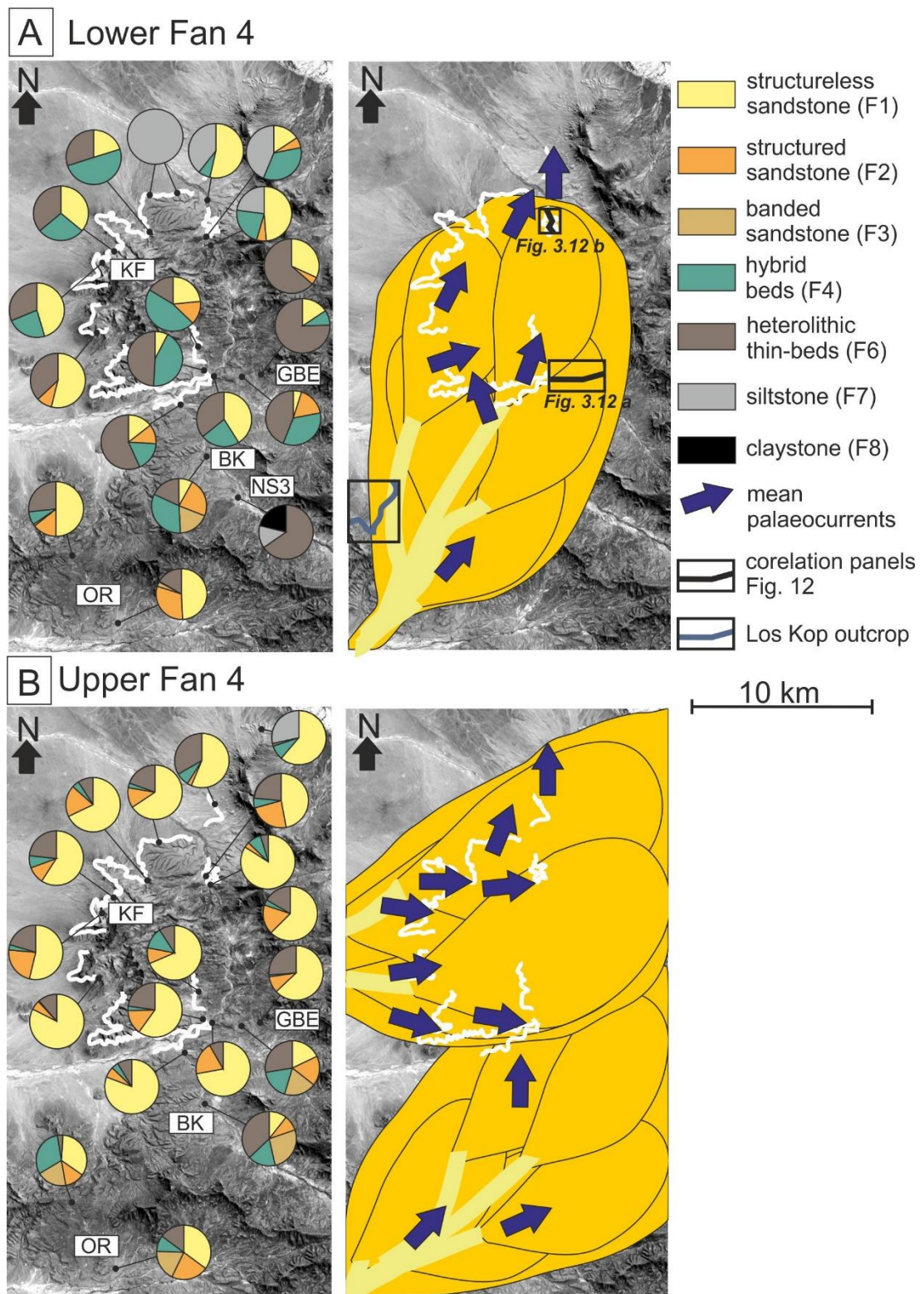
Figure 3.10. Facies distributions and palaeogeographic reconstruction for the lower and upper Fan 4. A.: Lower Fan 4 consists of one lobe complex that progrades northward. OR: Ongeluks River; BK: Bloukop; KF: Klipfontein. B: Upper Fan 4 comprises four lobe complexes; the southern lobe complex prograded to the northeast, whereas the northern lobe complexes are characterised by weaker compensational stacking patterns. Both divisions show different distribution patterns in relation to their stacking patterns and sediment source.

represent several lateral lobe fringes that stack to form the lobe complex fringe. Similar facies changes have also been identified on the western margin of LC1 by Hodgson et al. (2006) in the Los Kop area (marked in Fig. 3.10a).

The upper division of Fan 4 comprises two sand-rich lobe complexes, LC3 and LC5, separated by an extensive thin-bedded heterolithic interval interpreted as the lobe complex fringe, LC4. LC3 has two thick and axial zones, in the Bizansgat and in the Skoorsteensberg area (Figs. 3.6, 3.8). The facies distribution patterns and palaeoflow (Fig. 3.1) indicate that deposition could have been by two coeval systems with different entry points. The deposits are treated as a single lobe complex, because no bounding surface or extensive thin-bedded units separating the two thick and axial areas has been observed that could have been the result of avulsion. Facies distributions indicate that the southern part of lobe complex (LC3) was strongly compensational on lobe scale (Fig. 3.10), whereas the northern part of LC3 and LC5 show dominantly aggradational stacking patterns of lobes (Figs. 3.9, 3.10). Facies changes (e.g. F1 and F3) can be explained by compensational stacking on lobe element-scale (Prélat et al., 2009; Etienne et al., 2012; Prélat & Hodgson, 2013) and scouring and amalgamation in axial lobe environments. Abrupt facies changes from heterolithic deposits (distal lobe fringes) to sand-prone lobes suggest sufficient space for lateral compensation. In the down-dip direction (Katjiesberg; for location see Fig. 3.3) of LC3, structureless sandstone, siltstone and hybrid bed deposits that show pinch-and-swell geometries are observed (Fig. 3.12, 3.13) dominate the lobe complex. These are interpreted as stacked frontal lobe fringe deposits.
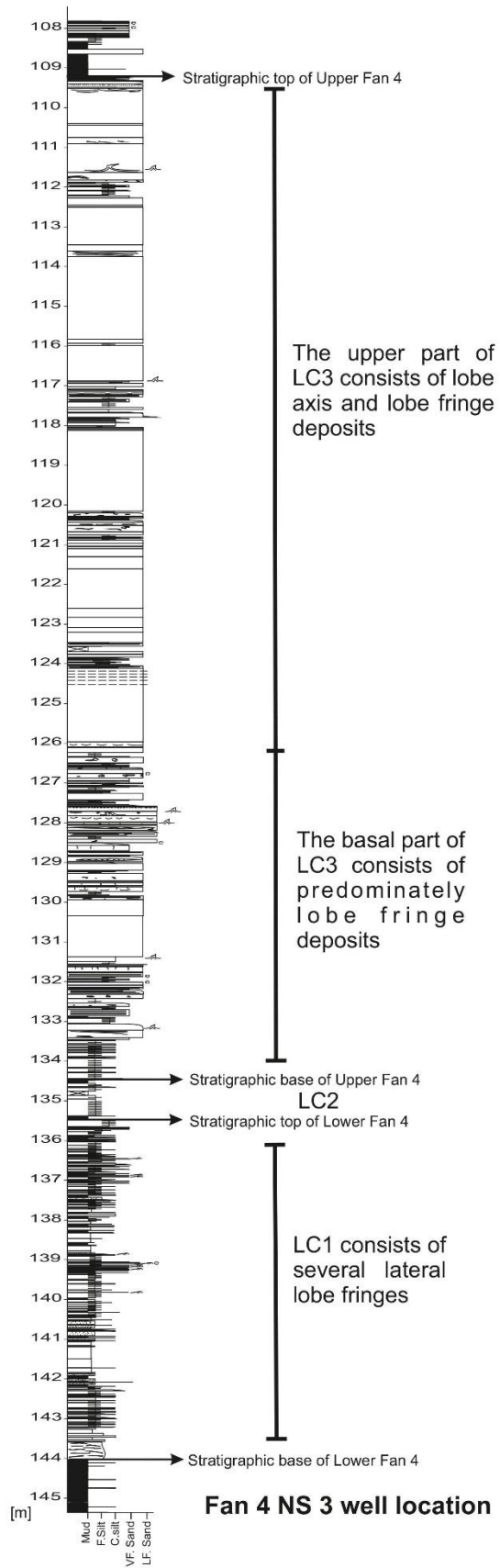
Figure 3.11. Well core log through Fan 4 (NS3; see Fig.3.3). The lower division of Fan 4 comprises solely thin-bedded heterolithic deposits, siltstones and mudstones of lobe fringe setting. The upper division of Fan 4 consists of interbedded structureless sandstone, hybrid beds and heterolithic packages.

3.7 Lobe fringe associations

Palaeogeographic reconstruction of the Fan 4 lobe complex 1 (LC1) shows that lateral and frontal lobe complex fringe environments can be well constrained using isopach maps and palaeocurrents (Fig. 3.10). Integration of these data with mapped sand pinch-outs enables the relative position and orientation of individual lobe bodies to be determined with confidence (Fig. 3.10). Generally, their dip direction is to the N, whereas their strike direction is to the E and W. Figure 12 depicts characteristic transitions in facies at lateral (Fig. 3.12a) and frontal (Fig. 3.12b) lobe fringes in LC1, which are described in detail below. Frontal and lateral lobe fringe environments are shown to display characteristic facies associations and geometries that are summarized in Table 3.2.

Characteristics	Frontal lobe fringe	Lateral lobe fringe
Bed thickness	highly variable; 0.1-1.5 m	0.05-0.2 m
Average grain size/ sand vs silt	25-45% silt	60-80% silt
Outcrop geometries	tabular to lenticular	tabular
pinchout geometries	finger-like with abrupt pinchout	wedge shaped; gradual
Current ripple lamination?	rare	common
Climbing-ripple lamination?	rare	rare
Multi-directional palaeoflow indicators?	rare	common
Hybrid beds?	common	rare
Climbing bedforms?	rare	rare
Debrites?	rare	rare

Table 3.2. Recognition criteria of frontal and lateral lobes for outcrop and core.
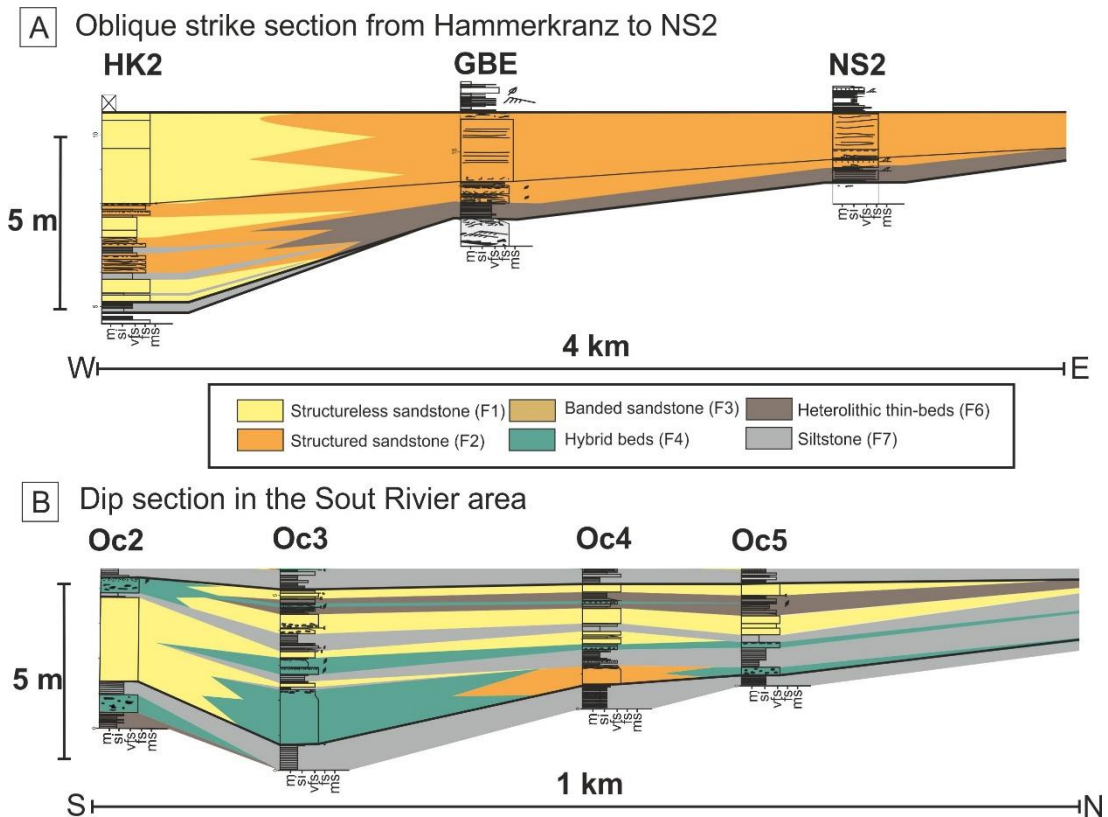
Figure 3.12. Dip and strike facies transition of individual lobes within LC1 of Fan 4. A: Strike section in the Gemsbock Valley (see Figure 3.10 for location). Lithology changed from structureless sandstone to structured sandstone to heterolithic deposits. B: Dip section on the Sout Rivier area (see Figure 3.10 for location). Lithology is dominated by structureless sandstone, hybrid beds and siltstone.

3.7.1 Lateral lobe fringe

Figure 3.12a shows a correlation panel of a single lobe from Hammerkranz to NS2 in LC1 (Figs. 3.3 and 3.10a). The lobe is defined by sharp lower and upper changes in facies to distal lobe fringe successions. Using the well-constrained palaeogeographic map of LC1, this is a lateral transition from axial lobe deposits (dominated by F1 and F2) to a succession that is dominated by structured sandstone and heterolithic deposits. The lobe thins from 5.5 m in the axial position to 1.9 m in the lateral position in 4 km (0.9m/km rate of thinning). The lower part of the lobe exhibits a transition into thin-bedded lobe fringe deposits, and the upper part of the lobe exhibits a transition to traction dominated sandstones. Bed amalgamation is not observed.

The NS3 core (Fig. 3.11) shows an example of the lateral margin of a lobe complex (LC1) where all lobes pass stratigraphically into an aggradational stack of fringe deposits. The integration of observations of the detailed facies transition and the lobe fringe-dominated succession in NS3 allows the following characteristics for lateral

lobe fringes to be established. The lateral lobe facies association is dominated by thin-bedded (>0.2 m) heterolithic deposits of structureless or planar laminated siltstone, and wavy, ripple and climbing-ripple laminated very-fine grained sandstone (Figs. 3.14a, b, 3.15b; Table 3.2). Rare, individual debrites are present (Fig. 3.15b). Lateral lobe fringe deposits experience gradual decrease in sand-content (~50% at the transition of the lobe-off axis to ~20% at transition to distal lobe fringe) and bed thickness (average bed thickness of 0.6 m in lobe off axis to average bed thickness of 0.1 m in lateral lobe fringe). Therefore, pinch-out occurs over several kilometers through thinning and fining of the deposits. In outcrop (e.g. LC4; Fig. 3.14b), lateral lobe fringes commonly show tabular geometries at the scale of observation (Figs. 3.14a, b; Table 3.2). A similar facies transition to a lateral fringe in a lobe was well constrained in the underlying Fan 3 by Prélat et al. (2009, their Lobe 6).

3.7.2 Frontal lobe fringe

Figure 3.12b shows a correlation panel of a single lobe from OC2 to OC5 in LC1 (Fig. 3.7 and 3.10a). The lobe is identified by abrupt lower and upper contacts to lobe distal fringe deposits. Using the well-constrained palaeogeographic map of LC1, this marks the frontal transition from axial lobe deposits (dominated by F1) to a succession marked by hybrid bed deposits, structureless sandstone and siltstone beds. Sandstone deposits show a high degree of amalgamation in OC2, and become progressively less amalgamated down-dip, and increasingly intercalated with thin-bedded siltstone units (Fig. 3.12b; Fig. 3.15a). The lobe deposits exhibit a pinch-and-swell geometry (thickening from 2.5 m in OC2 to 3.2 m in OC3 and then thinning to 2 m in OC5; Fig. 3.12b). The sand pinch-out of the lobe occurs abruptly within few hundred meters.

Similar facies associations and geometries are observed in the frontal pinch-out of lobe deposits in termination of LC3. The frontal lobe fringe facies association is characterized by dewatered, structureless or planar laminated fine-grained sandstones (Figs. 3.14c, d, 3.15a) associated with hybrid beds and rare thick debrites (Table 3.2). Commonly, the sandstone and hybrid beds of frontal lobe fringes exhibit depositional pinch-and-swell geometries (Fig. 3.13), which are underlain by siltstones but without any basal truncation. In map view, the pinch-and-swell geometries are mapped as irregular finger-like bodies aligned with palaeoflow (Bouma & Rozmann, 2000; Van der Werff & Johnson, 2003b; Prélat et al., 2009; Hodgson, 2009;

Groenenberg et al., 2010). The dimensions of these fingers are 200-300 m in strike width and 1.5 to 2.0 km in dip length. When sand pinch-out occurs overlying sand-prone strata, pronounced fingers do not develop. The percentage of structureless sandstone within the frontal lobe fringe remains high (10 to 50%) up to the point of sandstone pinch-out. Commonly, sandstone pinch-out is abrupt, but deposition of thin-bedded siltstones typically continue for several kilometres farther.

3.8 Discussion

Lobes do not show simple thinning and fining trends in all directions away from their apex (cf. Groenenberg et al., 2010). Despite showing the widest range of facies, lobe fringes are the least well studied sub-environments of lobes. Observations of their complexity have already been made by MacPherson (1978) and Pickering (1981; 1983), who demonstrated the significant variability of lobe (or fan) fringe facies. The process reasons behind the observed differences in lateral and frontal lobes fringes, and the subsurface implications of improved identification of fringe setting, are discussed below.

3.8.1 Controls on lobe pinch-out geometries

Generally, lateral lobe fringes are predominantely characterised by deposits from low-density turbidity currents, whereas frontal lobe fringes are dominated by deposits from high-density turbidity currents and other high-concentration flows (structureless sandstones, debrites and hybrid beds; Talling et al., 2012). Lateral lobe fringes fine and thin as they taper away from lobe axis environments (Fig. 3.15b). In contrast, basal lobes in the frontal fringes of lobe complexes show abrupt thinning and facies changes (Fig. 3.15a). Controls on this distinctive geometry in frontal lobe position could reflect 1) influence of underlying seabed topography or 2) flow processes and interactions with substrate. Finger-like pinchouts of frontal lobes are observed within successive lobes of multiple different lobe complexes within the Tanqua depocentre (Bouma & Rozman, 2000; Rozman, 2000; Prélat et al., 2009; Groenenberg et al., 2010). Similar terminations have also been observed within other basin-floor lobe systems (Nelson et al., 1992; Twichell et al., 1992), albeit occasionally misinterpreted as channel-forms (e.g. Van der Werff & Johnson, 2003b) due to their elongated shape in planform view and their convex-up form in outcrop. Therefore, flow processes can
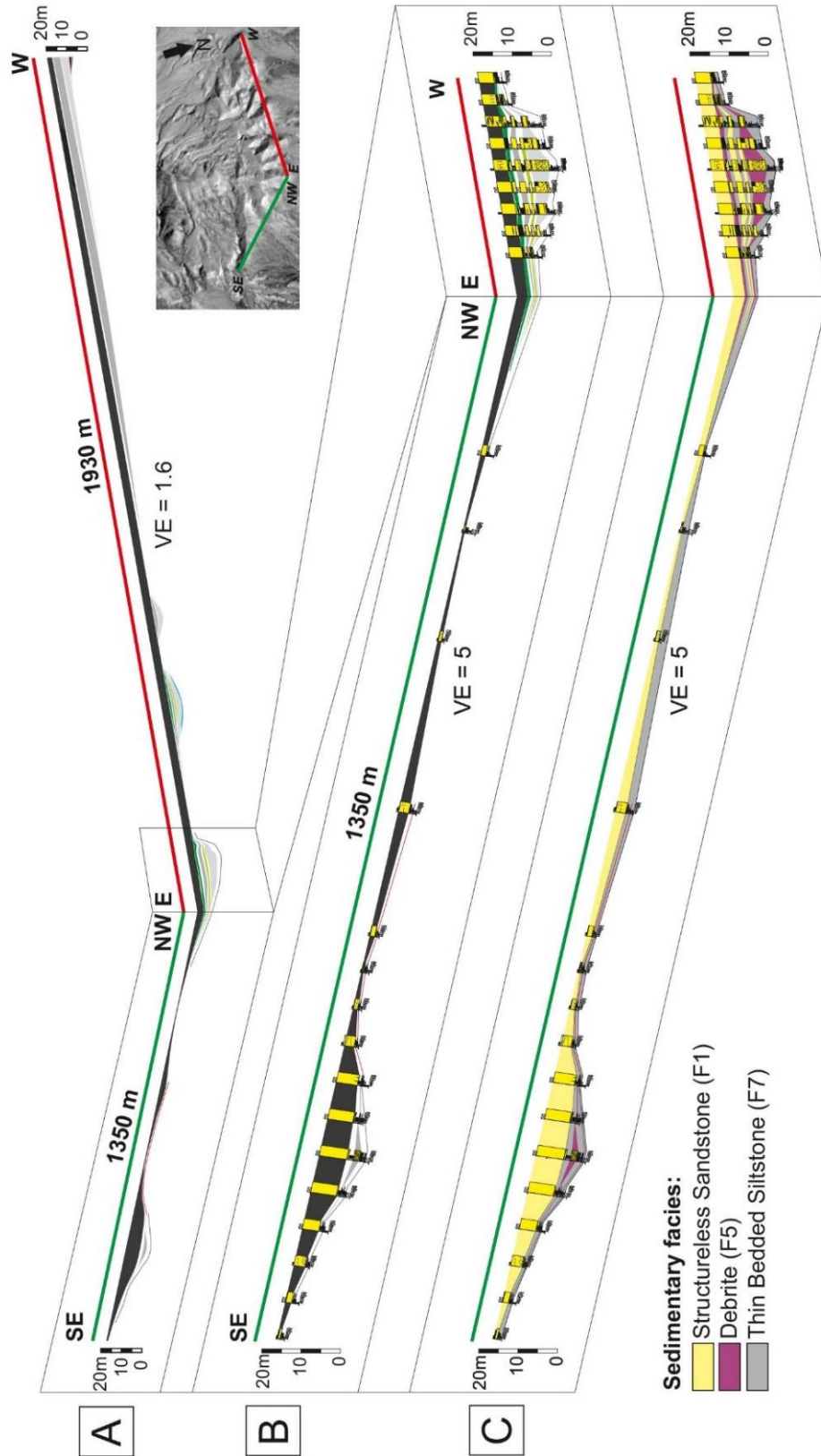
Figure 3.13. Correlation panels for frontal lobe pinchout area around Katjiesberg. A: Areal correlation of four pinchout fingers. B: Zoom into the northwestern-southeastern part of the correlation panel. C: Sedimentary facies of the pinchout fingers. They are composed of structureless sandstone deposits, debrites and siltstone deposits.
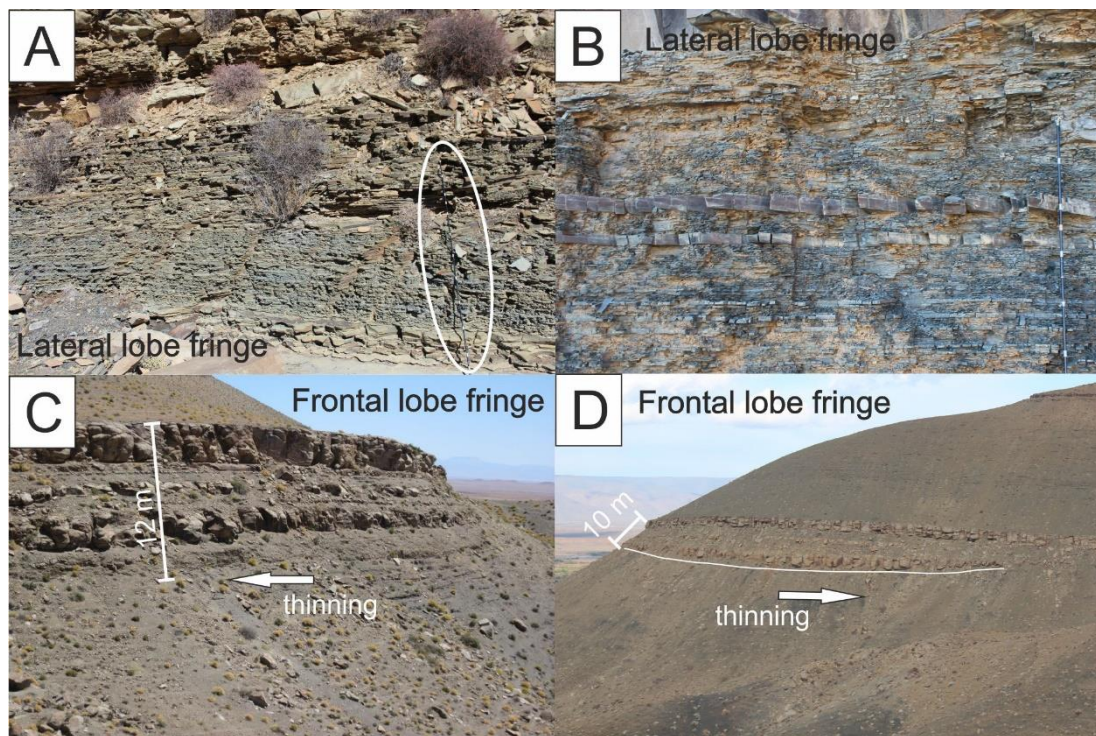
Figure 3.14. Representative lobe fringe photographs. A: Frontal lobe fringe deposits at Katjesberg. B: Frontal lobe fringe deposits at Katjesberg. C: Lateral lobe fringe deposits at Klipfontein. Logging pole as scale. D: Lateral lobe fringe deposits at Hammerkranz. Logging pole as scale.

be invoked as the key factor (Fig. 3.16b). Groenenberg et al. (2010) did not support the presence of pre-existing seabed topography as the main influencing factor because of the common occurrence of finger like bodies in several basal lobes over several lobe complexes. The repeated formation of seabed relief in a radial finger-like pattern prior to initiation of each lobe complexes, was viewed as highly unlikely.

Hybrid beds have been reported to be associated with distal lobe settings (Haughton et al., 2003; Talling et al., 2004; Ito, 2008; Hodgson, 2009; Talling et al., 2012a; Grundvåg et al., 2014; Patacci et al., 2014; Collins et al., 2015; Fonnesu et al., 2015) and their cohesiveness is suggested to control the abrupt pinch-out of deposits in this setting (Groenenberg et al., 2010). In frontal lobe fringes, there is evidence that relatively distal turbidity currents eroded and entrained substrate material, preserved as mud-clasts and dispersed mud (Hodgson 2009, Kane et al., in review). The combined effects of flow deceleration, and increased flow concentration through entrainment, led to enhanced flow stratification and the development of a dense,
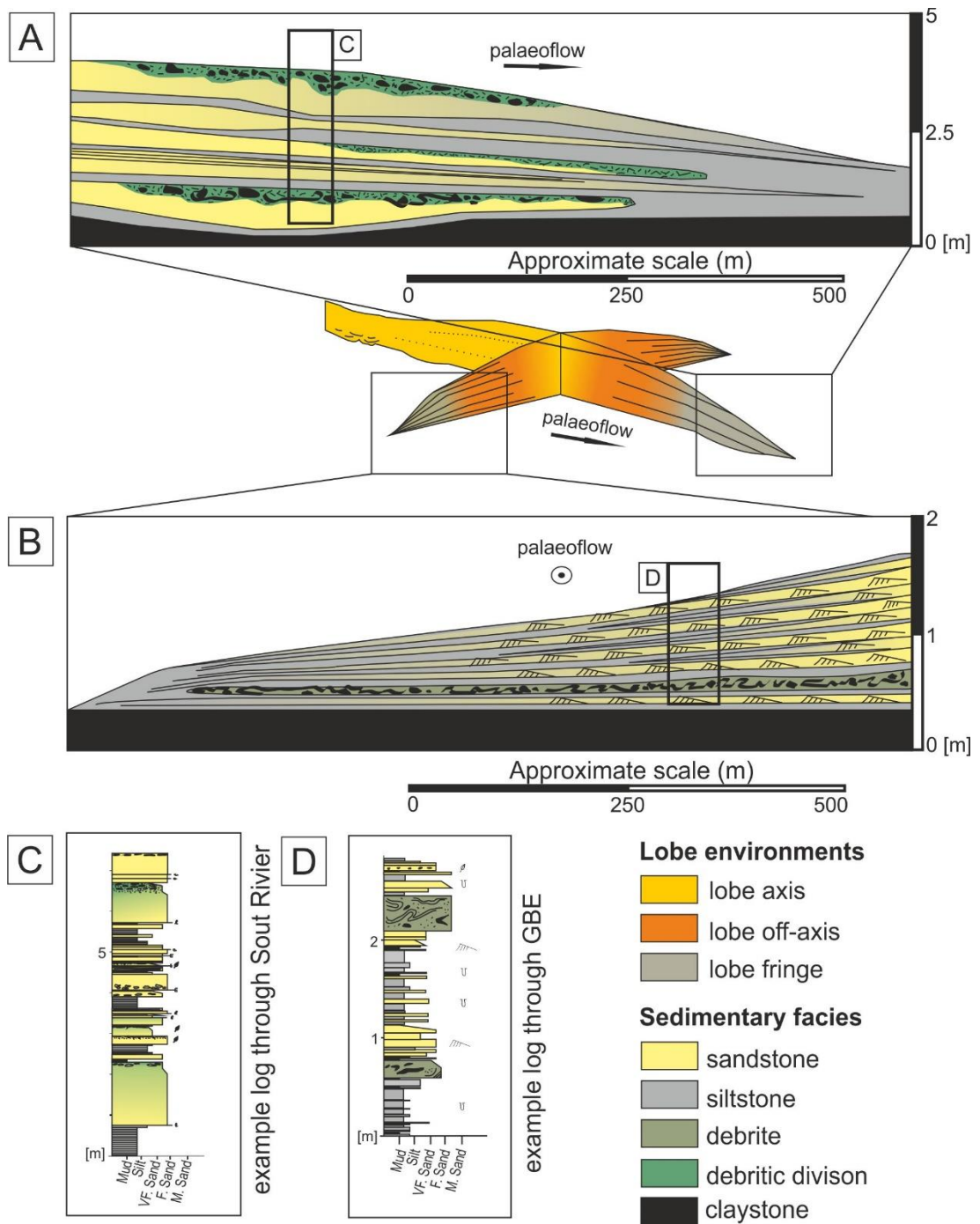
Figure 3.15. Simplified anatomy of frontal lobe fringe deposits. B: Simplified anatomy of lateral lobe fringe deposits. C: Example log showing a vertical section through a frontal lobe fringe in the Sout Rivier area. D: Example log showing a vertical section through a lateral lobe fringe in the Gemsbock East core.

cohesive basal layer (e.g. McCave & Jones, 1988; Kane & Pontén, 2012; Talling et al., 2013; Kane et al., in review). The development of a dense basal layer in the flow may have suppressed upward transfer of turbulence resulting in the collapse of the upper part of the flow (McCave & Jones, 1988; Kane et al., in review). The collapse of the upper part of the flow may account for the abrupt pinchout of both the lower

and upper parts of hybrid beds in distal settings. The principal alternative, that turbidity currents fractionated their suspended load and split into forerunning turbidity currents with trailing debris flows (depositing turbidites with linked debrites, Haughton et al., 2003; Haughton et al., 2009), may account for thicker debrites, that are observed to be deposited within the finger-like structures (see Fig. 3.12c). These may have over-run, or taken a different course, to their forerunning turbidity currents. Deposits of high-density turbidity currents are able to create their own pathways and become successively more elongated down-dip, forming finger-like bodies. These finger-like structures of frontal lobes are connected by thin-beds creating a webbed bird's foot geometry in planform (Fig. 3.13, 3.16a). This accords with results by Groenenberg et al. (2010) from process-based numerical modelling of lobes, who suggested that depositional relief of preceding lobes could help to focus these types of flow into distal areas. Elongated beds have been produced experimentally by Luthi (1981) showing that velocity of the turbidity currents was highest along the central axis. The frontal pinchout of lobe complexes is accompanied by abrupt thickness decrease and occurs over a few hundred metres (Fig. 3.15a).

The lateral fringe forms a wedge-like geometry that thins away from the lobe axis and off-axis (Fig. 15b) as deposits fine gradually over a few kilometres (Fig. 3.16a). Lateral lobe fringe deposits dominantly record the accumulated products of low-density turbidity currents. Luthi's (1981) experiments show that flow velocities are lowest in these flow marginal areas, and the flow thickness decrease is greatest laterally away from the central flow axis. Depositional relief of preceding lobe deposits probably had a relatively minor influence on low-density flows, as these can surmount seabed topography (e.g., Brunt et al., 2004; Bakke et al., 2013). Their run-out distance is therefore primarily dependent on their thickness and volume (Wynn et al., 2002). The deposits of the low-density turbidity currents probably form laterally extensive radial deposits which are higher in proportion at the lateral fringe, owing to the forward momentum and lack of lateral spreading of the higher concentration flows. In the frontal fringe setting, the low-density turbidity currents, for the most-part, out ran the flows responsible for depositing the hybrid beds. Thin stand-alone debrites recorded in the lateral fringe deposits are inferred to have by-passed the majority of the lobe to be deposited in its fringe (Talling et al., 2012b; Ducassou et al., 2013).
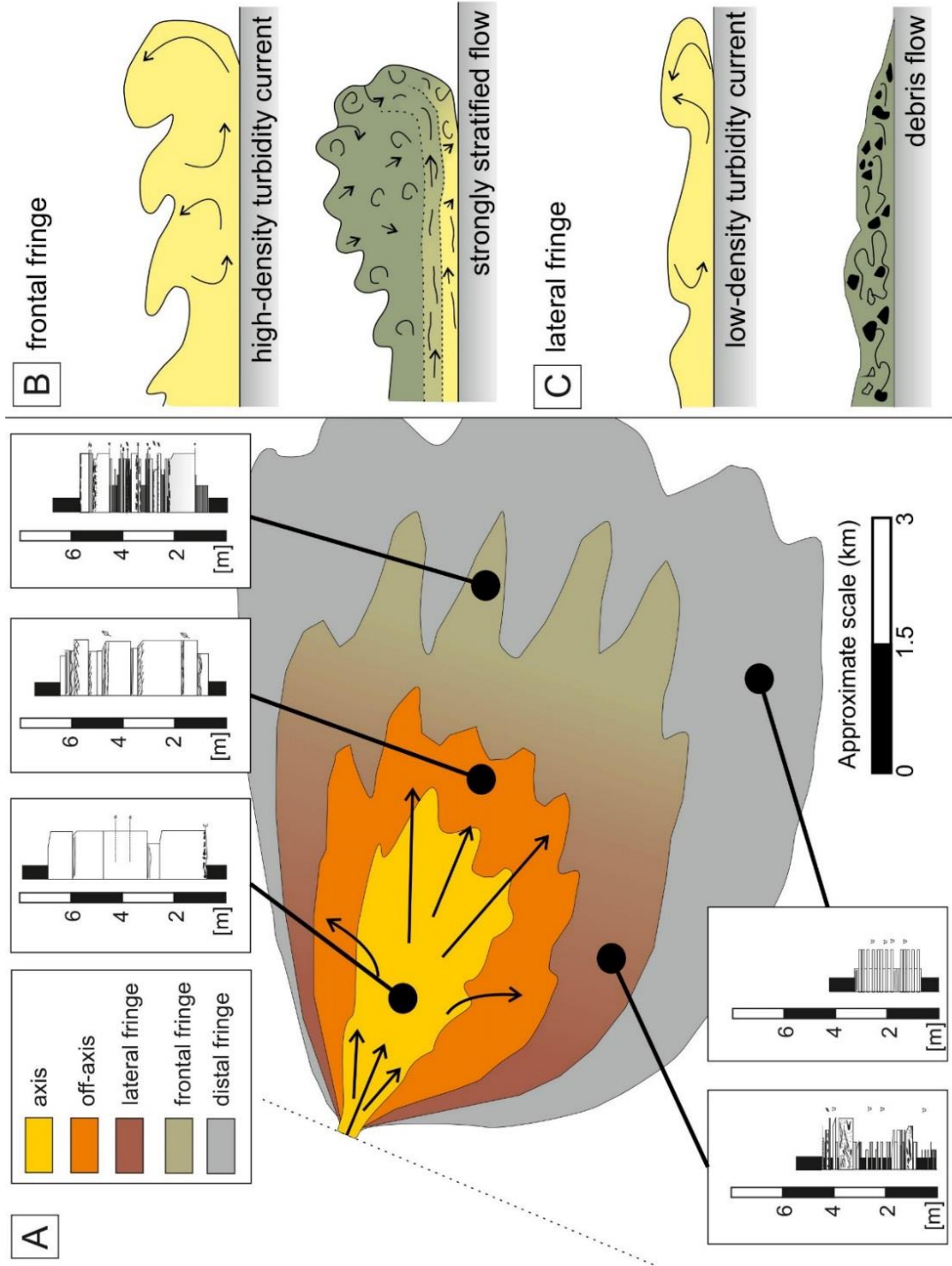
Figure 3.16. Simplified plan view of a lobe marking the distribution of lobe sub-environments and example logs for each sub-environment. B: Dominant flow processes to deposit frontal lobe fringes: High-density turbidity currents and strongly stratified flows. C: Low-density turbidity currents and debris flow deposit lateral lobe fringes. C is modified from Kane et al. (in review).

3.8.2 Role of confinement

The presented configuration of lobe fringe evolution has been documented in a relatively unconfined basin-floor setting. In basins where lobes do not feel basin confinement, compensational stacking will result in alternating successions of lobe axis and off-axis environments, and facies within lobe fringes and distal fringes (Prélat & Hodgson, 2013). Therefore, it is possible that frontal and lateral lobe fringes will be present in a 1D section through a lobe complex. Flow confinement has been documented to be an important autogenic factor in the control of dispersal patterns and lobe stacking patterns (e.g. Piper & Normark, 1983; Smith & Joseph, 2004; Amy et al., 2004, Twichell et al., 2005; Macdonald et al., 2011; Southern et al., 2015; Marini et al. 2015).

With increased seabed confinement lobes will be forced to aggrade or stack longitudinally over compensational stacking, leading to clearer segregation of frontal and lateral lobe fringes. Even subtle intrabasinal slopes, with angles as small as a fraction of a degree, have been shown to modify stacking patterns and facies distribution considerably. Chapter 4 shows that an intrabasinal slope (< 0.5°) in the Laingsburg depocentre, Karoo Basin, led to aggradational stacking of lateral lobe fringes in multiple stacked lobe complexes, compared to compensational stacking patterns in the unconfined part of the basin. The lateral lobe fringe facies association reflects the overall aggradational trend with sedimentary features such as climbing bedforms and predominant climbing-ripple lamination. Similar observations have been made from the Silurian sand-prone deep-water systems of the Welsh Basin (cf. Smith, 1987a,b; Wilson et al., 1992; Smith, 2004b). It is not clear if there are distinctive lateral or frontal facies trends in more highly confined basin settings; this is an area that warrants further investigation.

3.8.3 Subsurface implications

Differences in sedimentology and architecture of lobe fringes encompass several implications for subsurface applications. Facies recognition criteria established in this study can help determine internal division of lobe complexes in 1D datasets, e.g. core data, and help improve palaeogeographic reconstruction. Stacking of

fringe types are a helpful indicator of seabed topography. In an unconfined setting, vertical stacking of frontal and lateral lobe fringes is possible, whereas in settings influenced by relief thicker successions of frontal fringes (hybrid bed-rich deposits) and lateral fringes (thin-bedded heterolithic deposits) can be predicted depending on the location of the data point.

Lobe fringe deposits form heterogeneities within deep-water fan deposits (e.g. Etienne et al., 2012; Collins et al., 2015; Grecula et al., 2015). Generally, frontal lobe fringes have higher sandstone percentages (~50%). However, the high proportion of hybrid beds means that permeability values are likely to be considerably lower than within structureless and structured sandstones. This conforms to conclusions of Marchand et al. (2015) who observed that the presence of silt-sized particles and ductile, platy shaped grains in distal sand-rich successions decreases reservoir quality. Thick-bedded deposits can be expected in frontal lobe fringes, but amalgamation is rare. Lateral fringe deposits gradually decrease in sand-content (~50% at transition structured sandstones of the lobe-off axis to ~20% at transition to distal lobe fringe) and bed thickness. Vertical amalgamation is not observed. Permeability and porosity values are expected to be relatively low, and decrease gradually as the deposits thin and fine. Lobe fringes have the potential to be stratigraphic traps (*sensu* Levorsen, 1936) with their confining element being lateral depositional changes especially at the margins of a lobe complex that are encased by hemipelagic deposits. Lateral lobe fringes are dominated by their lateral gradation of sandstone to silty mudstone with widespread waste zones (cf. Rittenhouse, 1972; Biddle & Wielchowsky, 1994). Frontal lobe fringes, however, are characterised by their abrupt pinchout style (cf. Rittenhouse, 1972; Biddle & Wielchowsky, 1994) and are connected to the high-quality reservoir sandstones of the lobe axis and lobe off-axis up-dip. Therefore, in consideration with respect to successful stratigraphic trap mechanism, frontal fringes are considered more prospective.

3.9 Conclusions

Lobe fringe deposits are the least well studied sub-environments of lobes despite showing the widest range of facies. An integrated outcrop and research borehole data set uses thickness and grain-size trends, facies distribution and depositional geometries, to constrain two distinctive lobe fringe settings; frontal lobe fringe and lateral lobe fringe. Frontal lobe fringes are characterised by structureless sandstone

and hybrid bed deposits. They can exhibit elongated finger-like shapes with abrupt sandstone pinchout. Lateral fringes are dominated by heterolithic traction-influenced deposits that gradually thin and fine to form a simple taper. Therefore, lobes do not show simple thinning and fining trends in all directions away from their apex, and have a morphology that resembles a webbed bird's foot.

Facies associations and geometries of the two lobe fringe sub-environments are controlled by flow processes. Frontal lobe fringes are characterised by deposits of the highest energy parts of turbidity currents that passed through the axis of the lobe, and maintained the highest momentum, whereas lateral fringes are dominated by deposits from low-density turbidity currents that are prone to tractional reworking. Distinguishing frontal and lateral fringes improves prediction of facies distributions, and their stacking patterns and better reconstruction of lobe systems even without well-exposed outcrops arranged in 3D distributions. Compensational stacking of lobes in unconfined settings can lead to stratigraphic alternations of frontal and lateral lobe fringes in lobe complexes, whereas it is speculated that in confined settings aggradational to longitudinal stacking of frontal and lateral fringes will result in stronger spatial segregation. The development of recognition criteria to distinguish between frontal and lateral lobe fringes will help to support palaeogeographic reconstructions, and inform the appraisal of stratigraphic trap prospects in the subsurface.

Chapter 4

Aggradational lobe fringes: the influence of subtle intrabasinal seabed topography on sediment gravity flow processes and lobe stacking patterns

4.1 Abstract

Seabed topography is ubiquitous across basin-floor environments, and influences sediment gravity flows and dispersal patterns. The impact of steep (several degrees) confining slopes on sedimentary facies and depositional architecture has been widely documented. However, the influence of gentle (fraction of a degree) confining slopes is poorly understood, largely due to outcrop limitations. Here, exceptional outcrop and research borehole data from Unit A of the Permian Laingsburg Formation, South Africa, provides the means to examine the influence of subtle lateral confinement on flow behaviour and lobe stacking patterns. The dataset describes the detailed architecture of subunits A.1-A.6, a succession of stacked lobe complexes, over a palinspastically restored 22 km across-strike transect. Facies distributions, stacking patterns, thickness and palaeoflow trends indicate the presence of a southeast facing low angle (fraction of a degree) lateral intrabasinal slope. Interaction between stratified turbidity currents with a thin basal sand-prone part and a thick mud-prone part and the confining slope result in facies transition from thick-bedded sandstones to thin-bedded heterolithic lobe fringe-type deposits. Slope angle dictates the distance over which the facies transition occurs (100s m to km). These deposits are stacked vertically over tens of metres in successive lobe complexes to form an aggradational succession of lobe fringe. Extensive slides and debrites are present at the base of lobe complexes, and are associated with steeper restored slope gradients. The persistent facies transition across multiple lobe complexes, and the mass flow deposits, suggests that the intrabasinal slope was dynamic and was never healed by deposition during Unit A times. This study demonstrates the significant influence that even subtle basin-floor topography has on flow behaviour and depositional architecture in the Laingsburg depocentre, Karoo Basin; presenting a new

aggradational lobe fringe facies association and recognition criteria for subtle confinement in less well-exposed and subsurface basin fills.

4.2 Introduction

The behaviour of sedimentary gravity flows is strongly influenced by underlying seabed topography over a wide range of vertical and horizontal scales. Seabed topographic configurations control the general dispersal patterns of sediment and distribution of facies (e.g. Piper & Normark, 1983; Kneller & McCaffrey, 1999; Smith & Joseph, 2004; Amy et al., 2004, Smith, 2004a; Twichell et al., 2005; Bersezio et al., 2009; Wynn et al., 2012; Stevenson et al., 2013). The origin of seabed topography may be related to active or inherited tectonic features (e.g. Piper & Normark, 1983; Wilson et al., 1992; Haughton, 2000; Laursen & Normark, 2003; Hodgson & Haughton, 2004; Zakaria et al., 2013; Lin et al., 2014), salt and mud diapirism (e.g. Fusi & Kenyon, 1996; Stewart & Clark, 1999; Rowan et al., 2003; Lopez-Mir et al., 2014), and depositional and erosional relief (e.g. Normark et al., 1979; Pickering & Corregidor, 2005; Normark et al., 2009; Dakin et al., 2013; Ortiz-Karpf et al., 2015; Chapter 5). The impact of static and dynamic seabed topography on depositional architecture and dispersal patterns on the continental slope has been widely documented in subsurface datasets (e.g. Prather et al., 1998; Fiduk et al., 1999; Smith & Møller, 2003; Marchès et al., 2010; Gamberi & Rovere, 2011; Kilhams et al., 2012; Yang & Kim, 2014; Prather et al., 2016). Underlying inherited structures can also exert long-term influence in a basin through differential compaction (e.g. Parker Gay, 1989; Nygård et al., 2002; Færseth & Lien, 2002).

The interaction of turbidity currents and seabed topography results in a wide range of onlap configurations (e.g. Puigdefàbregas et al., 2004; Smith & Joseph, 2004; Gardiner, 2006; Bersezio et al., 2009; Marini et al., 2015). Understanding sedimentary facies changes and organisation of sub-seismic elements at onlaps can be used to reconstruct the palaeogeographic configurations and tectonic history of sedimentary basins. Smith & Joseph (2004) illustrated a continuum of onlap configurations from abrupt to aggradational onlap as a function of coeval aggradation on the bounding slope and the basin-floor. They inferred that abrupt onlap occur with high slope angles, when little or no coeval sediments are deposited on the slope. Aggradational onlaps occur when aggradation rates on the slope are high associated with a

progressive facies change towards the lateral slope (Smith & Joseph, 2004). Smith (2004b) illustrated low-gradient lateral bounding slope scenarios to explain thick intervals of 'lobe fringe' thin-bedded heterolithics, in belts several kilometres wide, adjacent to basin-floor lobe complexes.

The influence of high amplitude palaeo-seabed topography and their associated high degree of confinement on turbidity currents and their depositional architecture is well constrained from outcrop studies in small basins (Pickering & Hilton, 1998; Sinclair, 2000; Haughton, 2000; Sinclair & Tomasso, 2002 , Amy et al., 2004; Hodgson & Haughton, 2004; Smith & Joseph, 2004; Amy et al., 2007; Aas et al., 2010; Etienne, 2012; Etienne et al., 2012; Yang & Kim, 2014; Marini et al., 2015). The angle of confining slopes interpreted from outcrop are commonly higher [e.g. 4-10° in the Grès d'Annot sub-basins (Puigdefàbregas et al., 2004; Amy et al., 2007); 5-10° in the Cengio Turbidite System (Bersezio et al., 2009); >10-12° in the Castagnola Turbidite System (Southern et al., 2015)] than the range of slopes identified on reflection seismic and multibeam data (e.g. Gervais et al., 2006; Heiniö & Davies, 2007; Hanquiez et al., 2010; Prather et al., 2012a; Stevenson et al., 2013b). The effects of confining topography are less well documented from moderately confined basins (associated with aggradational onlap and bounding slope degrees of <5-1°) (Bailleul et al., 2007; Pyles, 2008; Pyles & Jennette, 2009; Burgreen & Graham, 2014) and remain poorly constrained in weakly confined basins (bounding slopes <1°; Smith, 1987 a, b; Wilson et al., 1992; Smith, 2004 b; Sixsmith et al., 2004), because the recognition of low-gradient slopes requires inference from isopach and facies trends or exceptionally extensive undeformed outcrops. General recognition criteria were established by Smith (2004 b): 1) palaeoflow parallel to the strike of the palaeoslope, and 2) lateral replacement of sand-prone lobe complexes by thin-bedded turbidites.

This integrated outcrop and borehole study aims to examine the influence of a gentle lateral intrabasinal slope (fraction of a degree) on the depositional architecture of submarine lobe deposits in Unit A of the Laingsburg Formation, Karoo Basin, South Africa. The objectives are to 1) examine the distribution of facies associations within the deposits of Unit A; 2) reconstruct the palaeogeography during deposition; 3) establish diagnostic criteria for aggradational lobe fringe facies association; and 4) discuss the implications of the long-term interaction of turbidity currents and seabed topography in a continuum of systems between confined and unconfined settings.

4.3 Geological and stratigraphic setting

The Karoo Basin has been interpreted as a retroarc foreland basin connected to a magmatic arc and fold-thrust belt (Cape Fold Belt) (Visser & Prackelt, 1996; Visser, 1997; Catuneanu et al., 1998). More recently, Tankard et al. (2009) suggested that subsidence during the early, deep-water, phase of deposition pre-dates the effects of loading by the Cape Fold Belt, and was induced by dynamic topography through mantle flow processes coupled to distant subduction (Pysklywec & Mitrovica, 1999). The basin-fill comprises the Karoo Supergroup and records sedimentation from Late Carboniferous to Early Jurassic. The Karoo Supergroup comprises the glacial Dwyka Group, the deep- to shallow-marine Ecca Group and the non-marine/fluvial Beaufort Group. The Ecca Group represents a shallowing-upward succession of sediments from deep-water to fluvial settings (Flint et al., 2011).
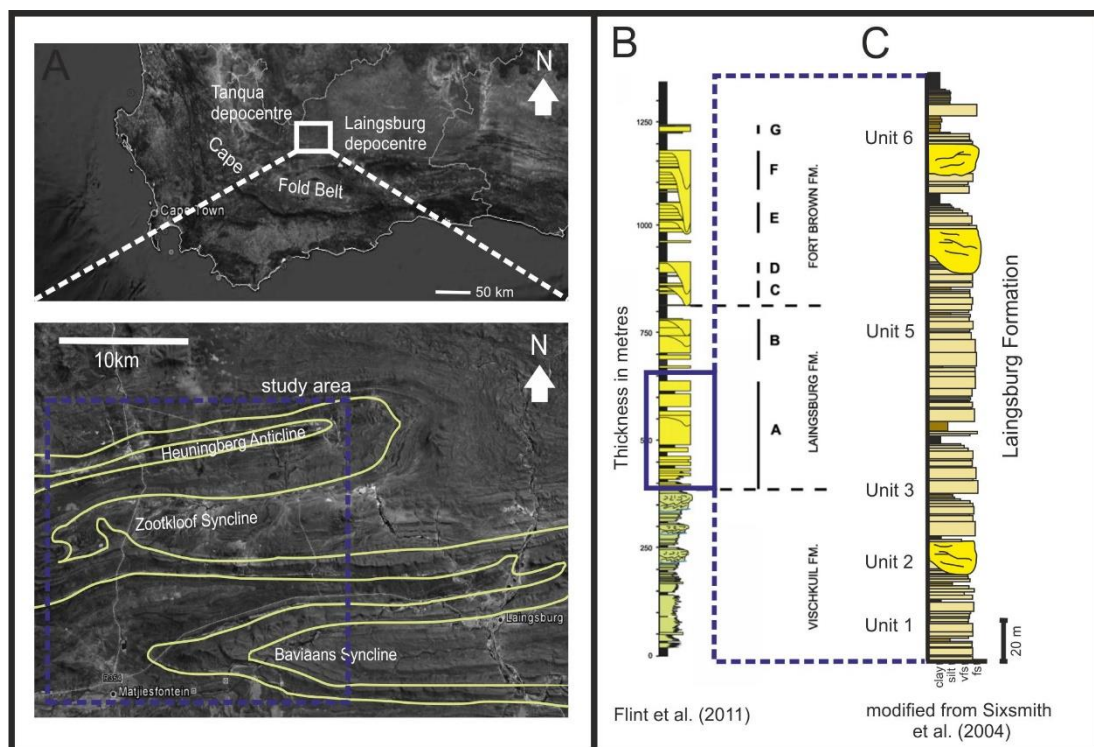
Figure 4.1. A: The Laingsburg depocentre inboard of the Cape Fold Belt. The blue dashed square indicates the area of study. B: Stratigraphy of the Laingsburg depocentre. The Laingsburg Fm. overlies the Vischkuil Fm. and is overlain by the Fort Brown Fm. (Flint et al., 2011). C: Unit A comprises six subunits, separated by regional hemipelagic mudstone horizons (modified from Sixsmith et al., 2004). Images taken from Google Earth.

4.3.1 Stratigraphy of the Laingsburg depocentre

The Laingsburg depocentre is located in the southwestern part of the Karoo Basin (Fig. 4.1a). The deep-water stratigraphy comprises mud-prone distal basin-floor fan deposits of the Permian Vischkuil Formation (van der Merwe et al., 2009) overlain by the 550 m-thick sand-prone Laingsburg Formation, the focus of this study (Fig. 4.1b). The Laingsburg Formation is overlain by the Fort Brown Formation, a 400 m thick channelized submarine slope succession (Di Celma et al., 2011; Flint et al., 2011; Hodgson et al., 2011). The Permian Laingsburg Formation is subdivided into Unit A (sand-prone basin floor fan; Sixsmith et al., 2004; Prélat & Hodgson, 2013) and Unit B (base-of-slope deposits; Grecula et al., 2003b; Brunt et al., 2013a). A 40 m thick hemipelagic mudstone and (muddy) siltstone separates Units A (up to 300 m) and B (up to 200 m), which contains a thin sand-prone unit referred to as the A/B Interfan (Grecula et al., 2003b).

The stratigraphy of Unit A was subdivided by Sixsmith et al. (2004) into seven sandstone-prone subunits called A.1 to A.7 from base to top, separated by regional hemipelagic mudstone horizons. Flint et al. (2011) reassessed the sequence stratigraphy of Unit A through interpretation of relative thicknesses of hemipelagic mudstone and stacking patterns. Unit A comprises three composite sequences. Subunits A.1 to A.3 show a progradational stacking pattern, and together with the overlying hemipelagic mudstone form the first composite sequence. The second composite sequence, which consists of subunits A.4 and A.5 and the overlying hemipelagic mudstone, has the most channel-fills and marks the most basinward advance in sedimentation in Unit A. The third composite sequence includes subunits A.6 and A.7 and with the overlying 40 m-thick mudstone marks an overall retrogradational stacking pattern. The three composite sequences make up the Unit A composite sequence set (Flint et al., 2011). In agreement with Prélat & Hodgson (2013), subunits A.4 and A.7 have been re-interpreted as lobe complexes within Subunits A.5 and A.6 respectively, as there is no true hemipelagic mudstone separating them (Fig. 4.1c). Palaeocurrents in Unit A show local complexity, but are dominantly to the NE (Sixsmith et al., 2004).

4.4 Methodology and data set

For this study, 21 detailed (1: 50 scale) bed-by-bed sections (each ranging from 140 to 300 m), recording grain size, sedimentary structures and bounding surfaces of beds, were measured to establish a S-N strike transect as well as W-E dip-sections to construct correlation panels (Fig. 4.2). For correlation purposes, facies associations were defined to represent particular sedimentary environments. All correlation panels use the base of Unit A.6 as a datum, because it is present in all outcrops, and the thickness and facies of Unit A.6 shows the least variation over the study area. More than 750 palaeocurrent measurements collected from ripple lamination and tool marks in sandstone beds, and from thrust planes and fold vergence in chaotic and folded deposits, were restored. Outcrop data were integrated with a recently drilled near-outcrop research borehole (ZKNL, Figs. 4.2 and 4.3 a-g) strategically sited to enhance the existing dataset. For isopach map purposes, thickness data were combined with existing thickness datasets of Unit A (Sixsmith, 2000, Sixsmith et al., 2004; Prélat & Hodgson, 2013).
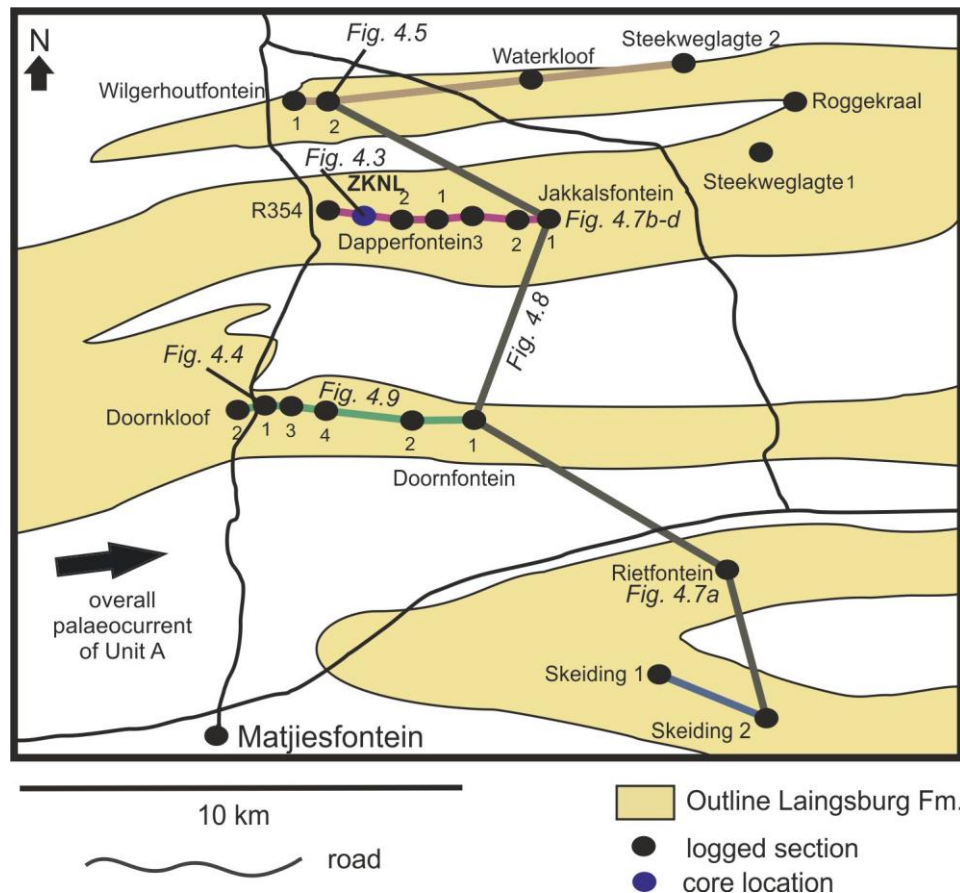
Figure 4.2. Log locations and lines of correlated sections. The grey line indicates the S-N transect (Fig. 4.8), blue, violet, green (Fig.4.9) and beige lines indicate dip-section correlation panels. Black dots indicate logged sections, blue dot the location of the ZKNL core. A larger scale map of the Laingsburg depocentre can be found in the back of the thesis as a pull-out.

4.5 Facies association

Unit A is interpreted as a basin-floor fan system composed of tabular sandstone-rich units that are locally cut by sandstone-rich channel-fills (Sixsmith et al., 2004). The sand-rich units (30-110 m thick) are laterally extensive (kilometres) and are intercalated with thin-bedded siltstone units. The facies associations, bounding surfaces, and geometrical characteristics are consistent with an interpretation as basin-floor lobe deposits (Prélat et al., 2009), and show a variety of bed thickness patterns controlled by compensational stacking across multiple scales (Prélat & Hodgson, 2013). The basin-floor lobes stack to form lobe complexes (Prélat et al., 2009).

4.5.1 Structureless and parallel laminated thick-bedded sandstones (lobe axis):

This facies association is characterised by thick-bedded (>0.5 m – 2 m) weakly normally graded upper to lower fine-grained sandstones that are usually structureless but may show faint parallel lamination (Table 4.1). Bed bases are sharp, loaded or erosional. Beds stack to form 5-8 m thick amalgamated units. Amalgamation surfaces are indicated by discontinuous layers of mudclasts or subtle grain size breaks. In core, dewatering features are common in the lower part of thick sandstone beds. Mudstone clasts are common near bed bases and rarely dispersed through the whole bed. Typically, the sandstone beds are laterally extensive for kilometres (up to 1.5 km) and display tabular geometries. Locally, there is evidence for confinement on a channel-scale such as lenticular geometries, truncation or margin collapse. Some packages of thick-bedded sandstone form large (up to 7 m high) symmetrical deformed features with vertical to overturned bedding that are laterally traceable (over 10s of metres) into undeformed successions along the outcrop.

Thick-bedded structureless and parallel laminated sandstone beds are interpreted to be deposited by high density turbidity currents (Kneller & Branney, 1995) with high aggradation rates (Arnott & Hand, 1989; Leclair & Arnott, 2005; Talling et al., 2012a). Planar laminations that are produced by high density currents are associated with thick-structureless sandstones. Their geometry, thickness and facies conform to a lobe-axis interpretation (Prélat et al., 2009). Lenticular structureless sandstone beds (100-200 m in width) with basal erosion surfaces are interpreted to be deposited in channel-environments. Scours in Unit A have a more complex geometry and in-fill (cf. Hofstra et al., 2015). Units with vertical to overturned bedding are interpreted to be formed *in-situ* by dewatering (Oliveira et al., 2009).

4.5.2 Structured medium to thin bedded sandstone (lobe off-axis):

Medium- to thin-bedded (0.5-0.1 m) very fine- to fine-grained sandstones display a range of sedimentary structures such as planar, wavy and occasional climbing-ripple lamination (Table 4.1). Individual beds can preserve more than one type of sedimentary structure. Structureless sandstone beds are rare. Normal grading is

common with rare inverse grading observed at bed bases. Two types of hybrid bed are observed in this facies association. 1) Hybrid beds with an upper mudclast-rich division with a clean sandstone matrix (D3 division of Hodgson, 2009). The clasts are rounded and have a narrow diameter range (< 5 cm) within individual beds and located in the upper third of the event bed. 2) Hybrid beds with an upper banded division (Lowe & Guy, 2000; H2 division of Haughton et al., 2009). Commonly, banded sandstones have a lower structureless division that can make up the bulk of the bed. The banded division comprises alternating light and dark sandstone bands. Darker bands have a clay-rich matrix and are poorly sorted, whereas light bands are quartz-rich and well sorted. Darker bands can be rich in carbonaceous material and/or mudstone chips. Light bands typically load into the dark bands. There are no grain size breaks between the individual bands. Observed banded divisions are up to 20 cm thick comprising individual bands each < 2cm thick (see M_2c and microbanded beds of Lowe and Guy, 2000). Bands are commonly planar or sub-parallel and continuous, but discontinuous bands are also observed. Structured sandstones are extensive for several hundred metres and show tabular geometries in outcrop scale.

Structured medium- to thin-bedded sandstones are interpreted to be deposited by low-density turbidity currents. Planar laminations and current ripple-laminations are produced by dilute flows, which rework sediment along the bed (Allen, 1982; Southard, 1991; Best & Bridge, 1992). Where a bed shows repetitive sedimentary structures this may indicate either long lived surging flows or collapsing flows (Jobe et al., 2012). Planar laminations deposited by low density turbidity currents are associated with thin-bedded ripple laminated sandstones. Clean sandstone beds with an upper mud clast rich division are interpreted to be the product of turbidity currents; whereby the head and body of the flows deposit clean sand with mud clasts carried towards the top and rear of the flows, to be deposited on the bed top (Hodgson, 2009). Deposition of banded divisions and their associated lower structureless division is interpreted to be by high-density turbidity currents. The banded division results from fluctuations in clay content in near-bed layers in an aggradational setting as reported during deposition of traction carpets (Lowe, 1982; Sumner at al., 2008; Talling et al., 2012a). Deposits are comparable to the H2 division of Haughton et al. (2009) and other transitional flow deposits (Lowe & Guy, 2000; Davis et al., 2009; Fonnesu et al., 2015). The facies and thickness of this association is consistent with an interpretation as deposited in the lobe off-axis (Prélat et al., 2009).

Facies association	Description	
1. Lobe- axis	thick bedded (0.5m - 2m) lower fine to upper fine sandstones structureless, dewatering features highly amalgamamated occasionally faint lamination	
2.Lobe off-axis	medium to thin bedded (0.1m - 0.5 m) very fine to lower fine sandstones planar, ripple/ climbing ripple or wavy laminations generally normal graded, sometimes inverse grading hybrid beds with upper banded division or upper clast division	
3. Lobe fringe	thin-bedded (<0.1 m) heterolithic packages planar, ripple/climbimg ripple lamination hybrid beds with upper carbonaceous or upper argillaceous clast-rich division	
4. Lobe distal fringe	thin-bedded (<0.1 m) fine to coarse siltstone mostly planar laminated sometimes with small scale ripples (< 1cm)	
5. Aggradational lobe fringe	thin-bedded (<0.1 m) siltstone, sandy siltstone and very fine sandstone dominant ripple laminated, minor planar and wavy lamination sigmoidal (or climbing) bedforms occasionally hybrid beds with upper argillaceous clast-rich division	
6. Chaotic facies	silt-prone matrix with intraformational clasts/ sandy slumps intraformatinal clast consist of folded coarse siltstone to very fine sandstone; folds are isoclinal or recumbent folded erosive based	

Table 4.1Description of the facies association defined in Unit A

4.5.3 Heterolithic packages (lobe fringe):

Thin-bedded (0.01-0.1 m) heterolithic packages (0.2 to 2.5 m thick) (Figs. 4.3 f and 4.4 a, b; Table 4.1) comprise fine and coarse siltstones (< 5 cm) interbedded with very fine- to lower fine-grained sandstone. Sandstone beds contain planar and/or current ripple laminations, with rare climbing ripple lamination. Siltstone beds are either structureless or planar laminated. Bed thickness range is narrow (5-10 cm), but 2-5 m thick packages with thickening- or thinning-upward trends occur. Two types of hybrid beds (0.05-1.5 m thick) are observed within the heterolithic packages. 1) Clean sandstone overlain by an argillaceous (muddy sand) division that is mica- and plant material-rich (D1 division of Hodgson, 2009, and H3 division of Haughton et al., 2009). Core observations show that; the fabric in the upper argillaceous division is commonly swirly and patchy. The boundary between the lower and upper division is commonly gradational. Some sand grains in the argillaceous division are coarser than in the underlying sandy division. 2) Hybrid beds with an upper argillaceous clast-rich division (D2 division of Hodgson, 2009, and H3 division of Haughton et al., 2009). The argillaceous division consists of a muddy sand matrix and subangular to subrounded intraformational mudstone clasts (cm to dm in size). No preferred orientation of the

clasts was observed. The boundary between the lower and upper division can be gradational or sharp. The underlying sandstone can show wavy or pseudo-lamination, when it contains a significant amount of mud chips. Rarely, beds show a lower clean sandstone division overlain by an argillaceous division with either intraformational mudclasts- or a carbonaceous-rich middle division and a clean sandstone upper division (cf. H4 of Haughton et al., 2009).

The heterolithic packages are interpreted as distal, sluggish, dilute flows (Stow & Bowen, 1980; Jobe at al., 2012). Ripple laminations form beneath dilute turbulent flows via bedload transport under moderate aggradation rates, whereas climbing-ripple laminations form under high aggradation rates (Allen, 1971a; Allen, 1982; Southard, 1991). Hybrid beds are interpreted to be the product of flows that transform along their length from turbidity current to debris flow (Fisher, 1983; Haughton et al., 2009; Fonnesu et al., 2015). The facies and thickness of this association are consistent with an interpretation of a lobe fringe setting (Mutti, 1977; Pickering, 1981; Prélat et al., 2009).

4.5.4 Thin-bedded siltstones (distal lobe fringe):

This association comprises thin-bedded (0.05 m) fine and coarse siltstones with rare thin (<0.05m) very fine-grained sandstones (Figs. 4.4 a, c; Table 1). The siltstones are structureless or planar to starved ripple laminated, when they display a sandy component. Observations from the core show moderate to high bioturbation in these facies associations. Thicknesses of individual intervals are variable (0.5 m to 3.5 m).

Thin-bedded siltstones are the preserved products of dilute turbidity currents. Planar laminated and rippled beds are a product of tractional reworking of the bed (Stow & Piper, 1984; Mutti, 1992; Talling et al., 2012a), while structureless beds are a product of direct suspension fallout (Bouma, 1962). The facies is typical of distal lobe fringe environments (Prélat et al., 2009). The variation in interval thicknesses is interpreted to be dependent on the number of overlapping distal lobe fringe deposits (Prélat et al., 2009).
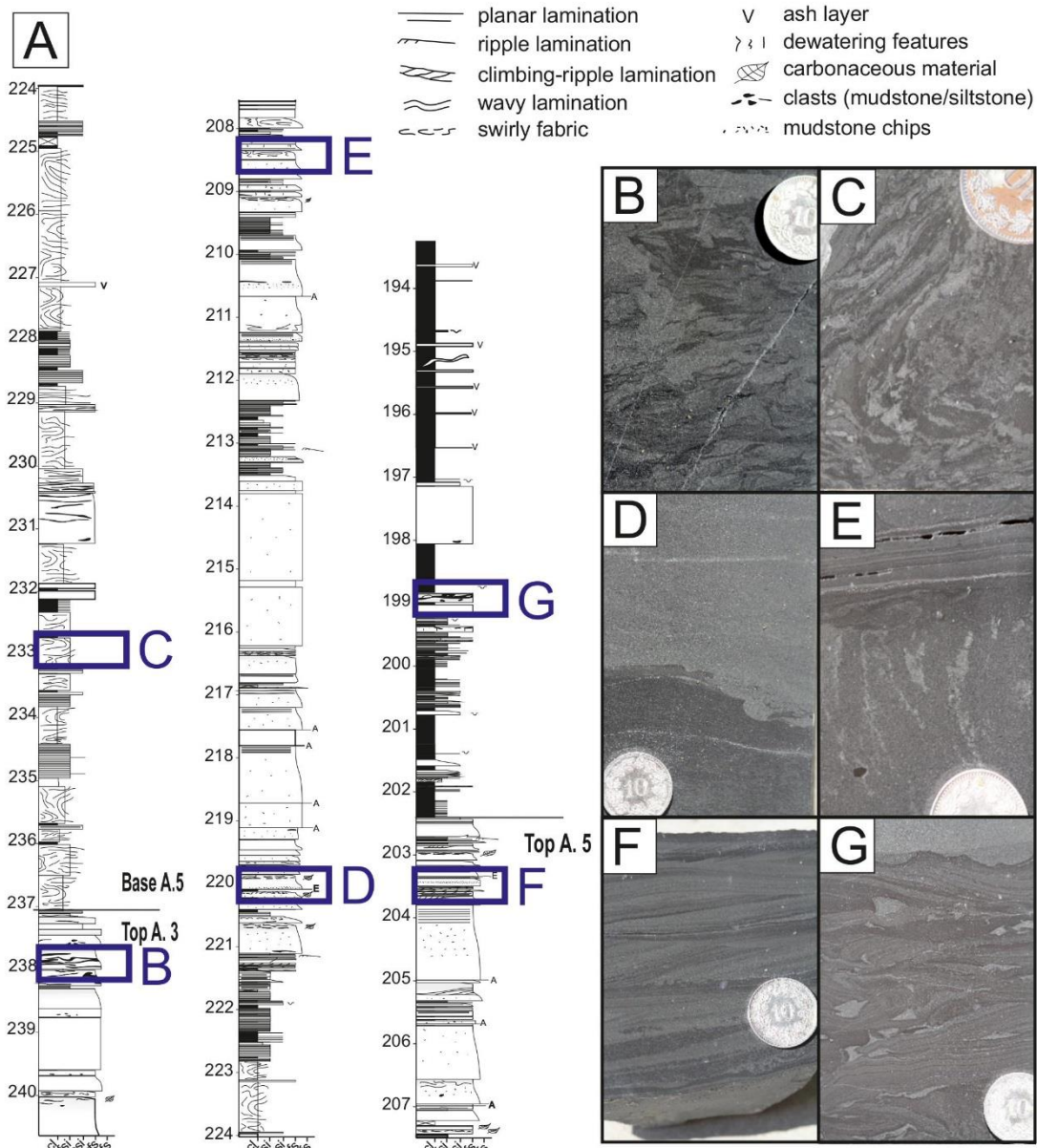
Figure 4.3. ZKNL core log and photos. A: Core log through Subunit A.5 B: Mud-streak rich sandstone on the top of A.3. Coin as scale (~1 cm diameter). C: Silt-prone syndepositional deformed interval of the chaotic facies. Coin as scale (~1 cm diameter). D: Clean sandstone loading into a debritic top of a hybrid bed. Coin as scale (~1 cm diameter). E: Dewatering features in a sandstone. Coin as scale (~1cm). F: Ripple-laminated sandstones intercalated with siltstone deposits. Coin as scale (~1 cm diameter). G: Highly sheared siltstone-prone package. Coin as scale (~1 cm diameter).
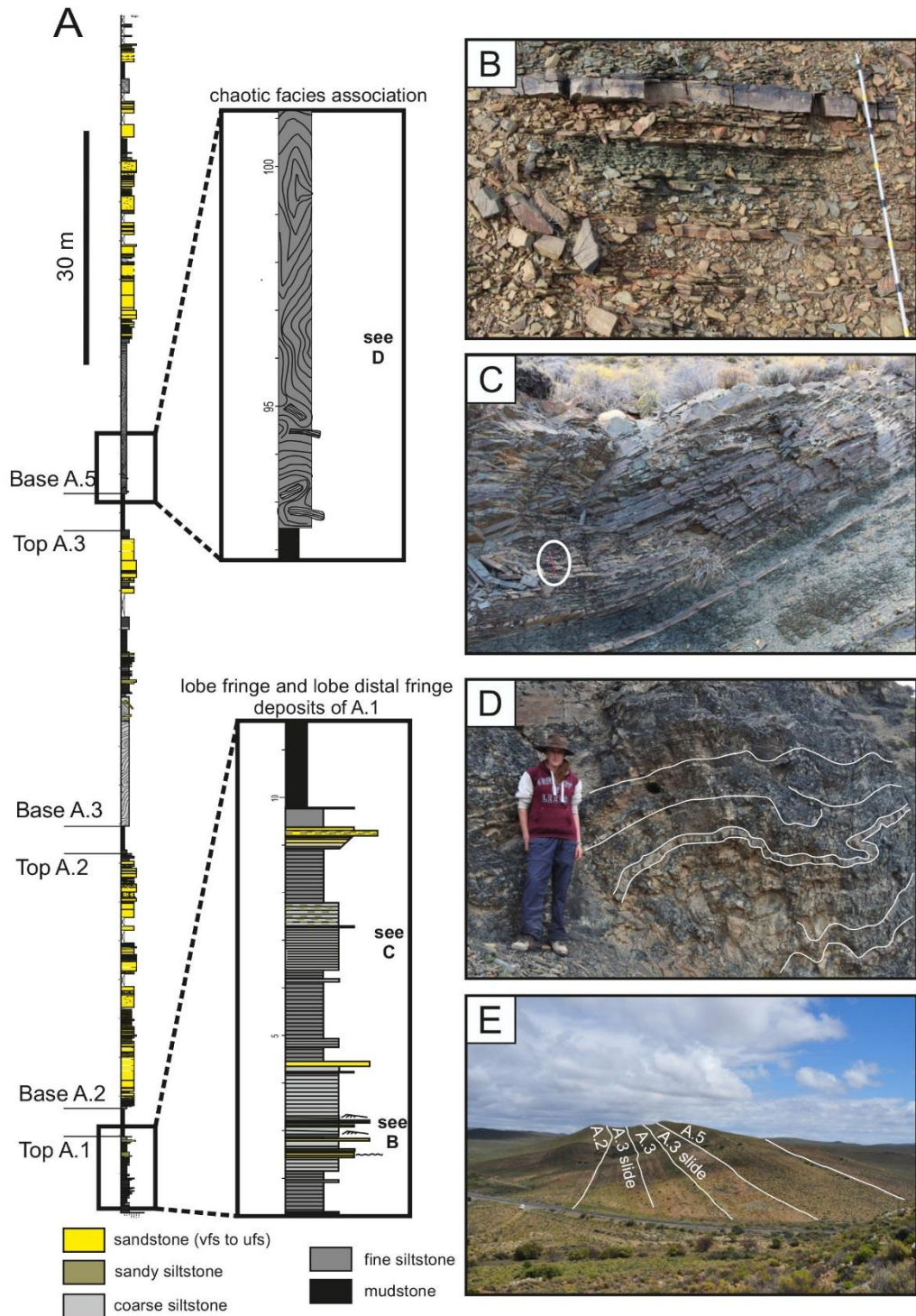
Figure 4.4. A: Sedimentary log through Doornkloof 1 section (see Fig. 4.3). Expanded parts show slide facies and lobe fringe facies. B: Thin-bedded appearance of A.1 at the lateral lobe complex margin at Steekweglagte 1. Logging pole for scale. C: Lobe fringe deposits of Subunit A.1. Pencil (~15 cm) for scale. D: Slightly deformed thin-beds in the Jakkalsfontein area. Geologist for scale (1.65 m). E: View into the Doornkloof area.

4.5.5 Structured climbing bedform dominated heterolithic packages:

Thin-bedded (0.01 to <0.1 m) fine to coarse siltstones are interbedded with sandy siltstones to very fine-grained sandstones (Figs. 4.5 a-e; Table 1). Siltstones make up the bulk of the heterolithic packages (Fig. 4.5 c). Sandstone beds show either planar, stoss-side preserved climbing- ripple or wavy lamination. Ripple morphology is preserved on bed tops, and in cross-section individual beds are sigmoidal with a long gently dipping limb and a shorter steeper limb, used to indicate a palaeoflow direction (Fig. 4.5 b). Successions of these ripples form larger dune-like features. The heterolithic package comprises multiple event beds that stack in the direction of palaeoflow (Fig. 4.5 c). Stacking patterns are dominantly aggradational (Fig. 4.5 d). The facies association includes rare hybrid beds with an upper argillaceous carbonaceous division. These heterolithic intervals are up to 10 m thick, and intercalated with thin-bedded siltstone intervals (Fig. 4.5 e).

Structured climbing bed dominated heterolithic packages indicate rapid deposition from dilute turbidity currents. Stoss-side preserved climbing-ripple lamination indicate deposition beneath energetic flows forming under high aggradation rates (Allen, 1971a; Allen, 1982; Southard, 1991).

4.5.6 Chaotic and folded facies association:

Chaotically deformed packages (up to 30 m thick) (Figs. 4.3 b, c and 4.4 a, d, e; Table 4.1) comprise isoclinal and recumbent folds of thin-bedded (cm-scale) siltstones interbedded with very fine- grained sandstones. Where folded, thin-bedded units can be partly disaggregated and encased by a poorly sorted structureless siltstone matrix. Planar, current ripple and climbing-ripple lamination can be observed in beds within the folded sandstone/siltstone packages. In core, the chaotic facies shows micro-faulting (mm-scale offsets) around folds (Fig. 4.3 c). Locally, these units are intercalated with relatively undeformed thin-bedded units (Table 4.1). Bases of chaotic and folded units are sharp to erosive, while bed tops are undulated and irregular.
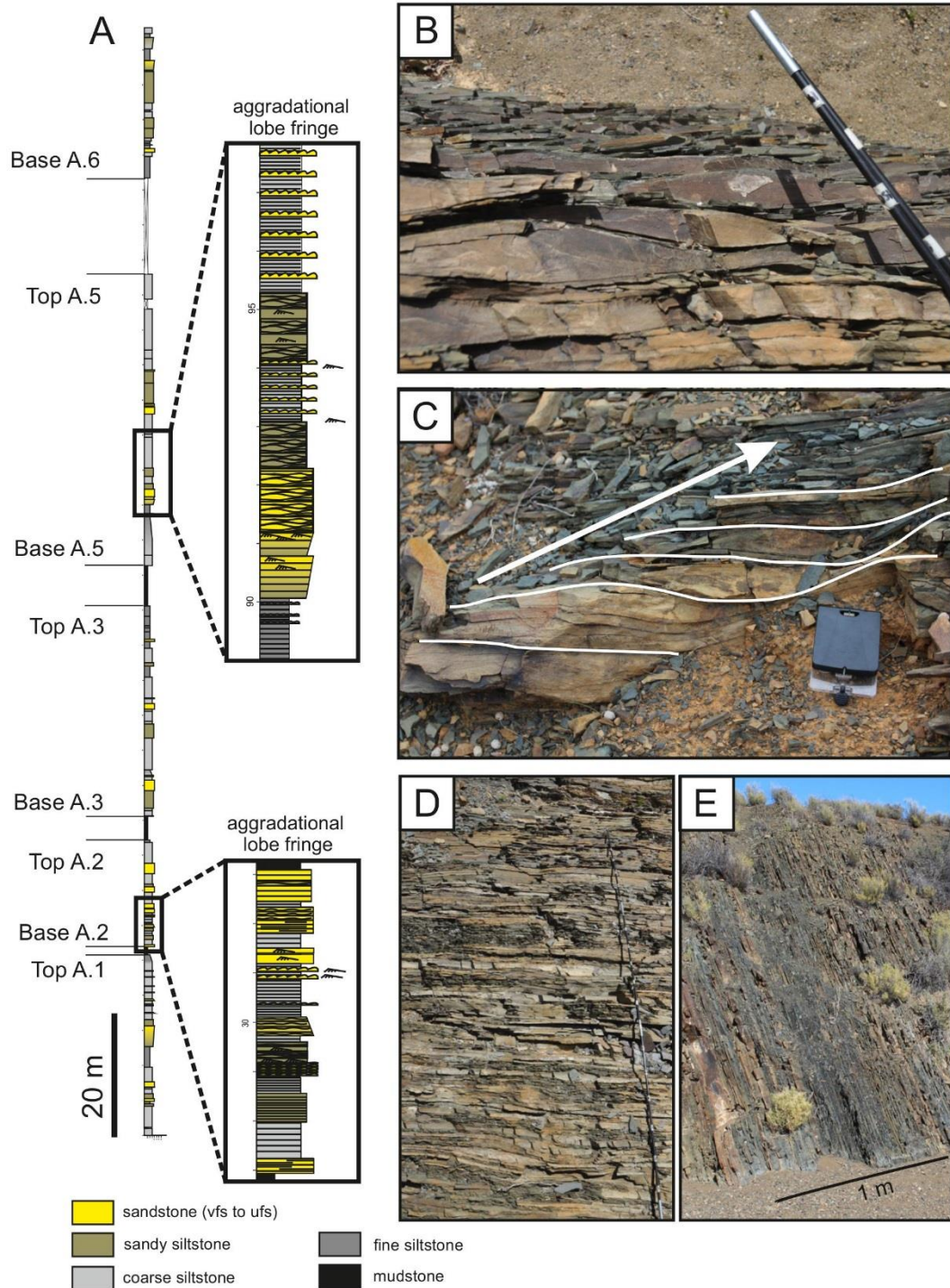
Figure 4.5. A: Sedimentary log of the Wilgerhoutfontein 2 section (see Fig. 4.3). Representative photographs to show the appearance of the aggradational lobe facies association (logging pole for scale). B: Very fine-grained sandstone beds showing sigmoidal shapes. Logging pole for scale. C: Package of climbing siltstone beds. Note the trajectory indicating flow direction. Compass for scale. D: Very fine-grained sandstone dominated package, climbing ripple laminated. Logging pole for scale. E: Thin-bedded planar laminated coarse siltstones.

The orientation of the folds does not conform to the post-depositional tectonic folding of the Laingsburg area stratigraphy. Therefore, the tight folding of the thin-bedded strata is interpreted as syn-depositional deformation due to remobilisation of local thin-bedded stratigraphy. The low amount of disaggregation supports an interpretation of slide to slump deposits, although where the matrix encases clasts of folded thin-beds a debris flow deposit interpretation is invoked (Woodcock, 1979; Prior et al., 1984; van der Merwe at al., 2009; Talling et al., 2012a). Slide deposits and debrites can be followed out for several kilometres and cover an area of at least 65 km^2.

4.5.7 Hemipelagic mudstones:

Mudstones are thin-bedded (0.5- 1cm) and commonly silty. Mudstone dominated packages can be up to 15 m thick. Calcareous concretions are common and can be associated with distinct horizons in the deposit. Thin-bedded siltstones and ash layers (< 5 cm) are locally intercalated. Clastic injection is common, especially in the mudstone horizon that separates Subunits A.5 and A.6 (Cobain et al., 2015). Mudstone packages are regional in extent and do not show thickness changes, except where eroded by remobilized chaotic and folded deposits or flows that deposit younger sand-rich deposits.

Mudstones are interpreted as hemipelagic background deposits. They can be mapped over large areas and mark episodes of sediment starvation to the basin-floor. Flint et al. (2011) interpret these to contain the deep-water expression of maximum flooding surfaces. Mudstone packages therefore serve as useful correlation intervals.

4.6 Palaeocurrents

Palaeocurrent measurements show that the mean palaeoflow direction of turbidity currents in Unit A was to the northeast (Fig. 4.6), consistent with overall northeast to east palaeocurrent measurements in the underlying Upper Vischkuil Formation (van der Merwe et al., 2009) and the overlying Unit B (Brunt et al., 2013a) and Fort Brown

Formation (Figueiredo et al., 2010; Di Celma et al., 2011; van der Merwe et al., 2014, Chapter 5). Around Jakkalsfontein and Dapperfontein, palaeocurrents are commonly to the east or show flow patterns to the southeast, especially in subunits A.3 and A.5 (Fig. 4.6). Palaeocurrent data from ripple laminations in the most northern outcrops (Wilgerhoutfontein 1+2 and Waterkloof) present a narrow spread with a dominant direction to the east. In contrast, measurements of thrust planes and fold vergence from slides indicate transport towards the southeast and southwest (Fig. 4.6).

4.7 Distribution of facies associations and their thicknesses

In the study area, Unit A comprises six facies associations (Table 4.1) with five of them representing a particular lobe sub-environment. Prélat et al. (2009) described 'lobe axis', 'lobe off-axis', 'lobe fringe' and 'distal lobe fringe' from detailed mapping of submarine lobes from the nearby Tanqua depocentre. Outcrops in the south of the study area (Skeiding and Rietfontein, Fig. 4.2) are dominated by lobe axis (Fig. 4.7 a) and lobe off-axis deposits (Sixsmith et al., 2004) separated vertically by lobe fringe associations (Fig. 4.8). This stratigraphic trend is indicative of compensational stacking patterns (Prélat & Hodgson, 2013). Outcrops in the north of the study area consist of lobe off-axis (Fig. 4.7 b) and fringe deposits intercalated with silt-prone slide deposits and debrites (Doornkloof, Doornfontein and Jakkalsfontein). Slides and debrites occur dominantly at the bases of subunits A.3 and A.5 (Fig. 4.7 d), although thin (< 5 m) localised deposits of deformed strata can be observed within the other subunits. Subunit A.3 shows large-scale dewatering structures (up to 7 m high) in its top in the Jakkalsfontein- Dapperfontein area, which are truncated by an overlying debrite at the base of A.5 (Fig. 4.7 c). Climbing-bedform dominated thin-bedded siltstone successions are only present in the northern part of the study area (Waterkloof and Wilgerhoutfontein; Fig. 4.8). The position of the lateral transition from lobe fringe to climbing thin-bedded siltstones follows a strongly aggradational pattern, with a slight northward trend through the stratigraphy from A.1 to A.6 (Fig. 4.8). Locally, hemipelagic mudstones between A.2/A.3 and A.3/A.5 are completely removed through entrainment by slides and debris flows in some localities, while the mudstone deposits between A.1/A.2 and A.5/A.6 are preserved across the whole study area (Fig. 4.8, 4.9, 4.10).
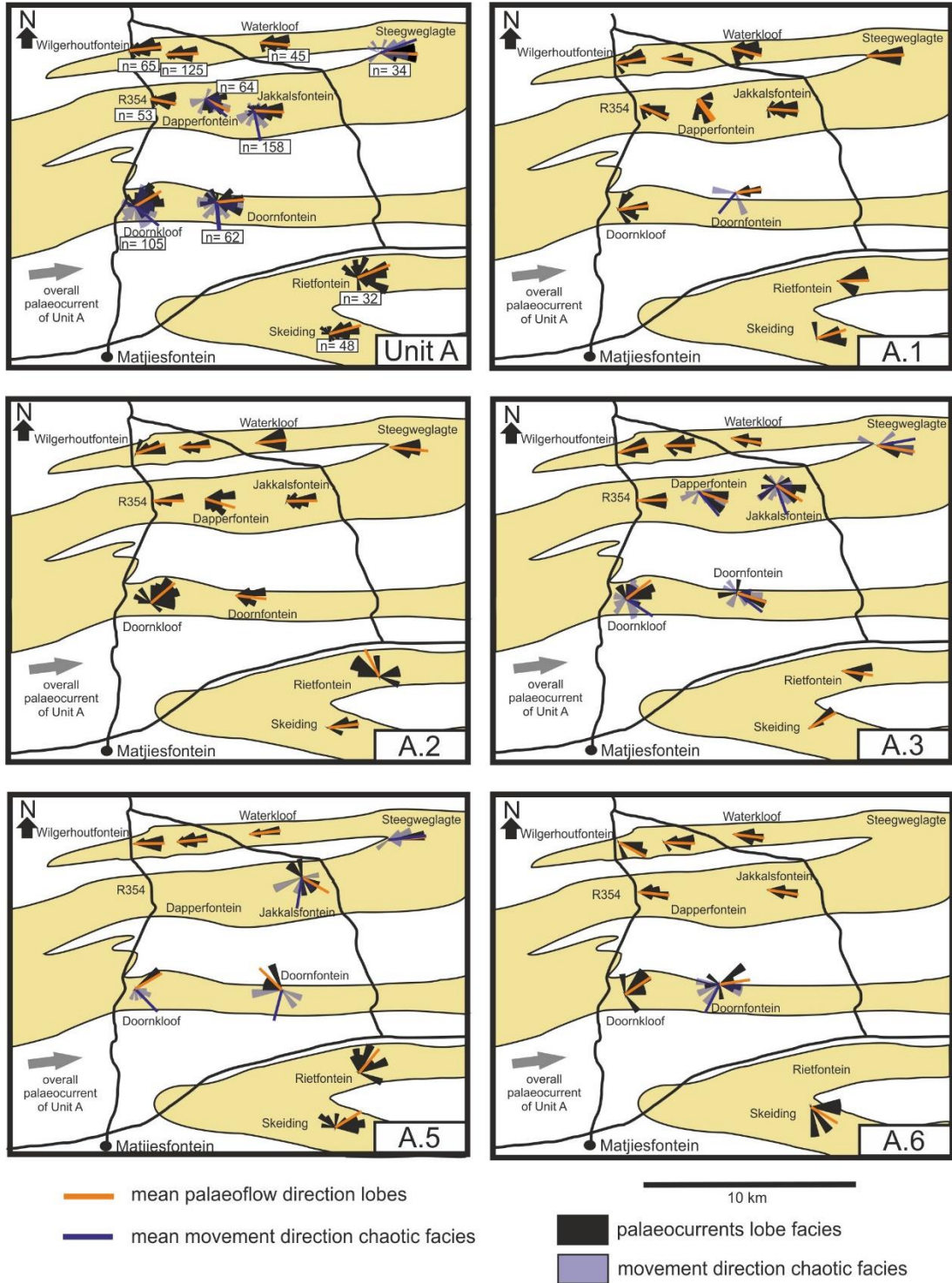
Figure 4.6. Palaeocurrents for Unit A (cumulative) and subunits A.1 to A.6. Black: palaeocurrents for lobe deposits; blue: movement direction for chaotic deposits. Orange line: mean palaeoflow direction of lobe deposits; blue line: mean movement direction of chaotic deposits.
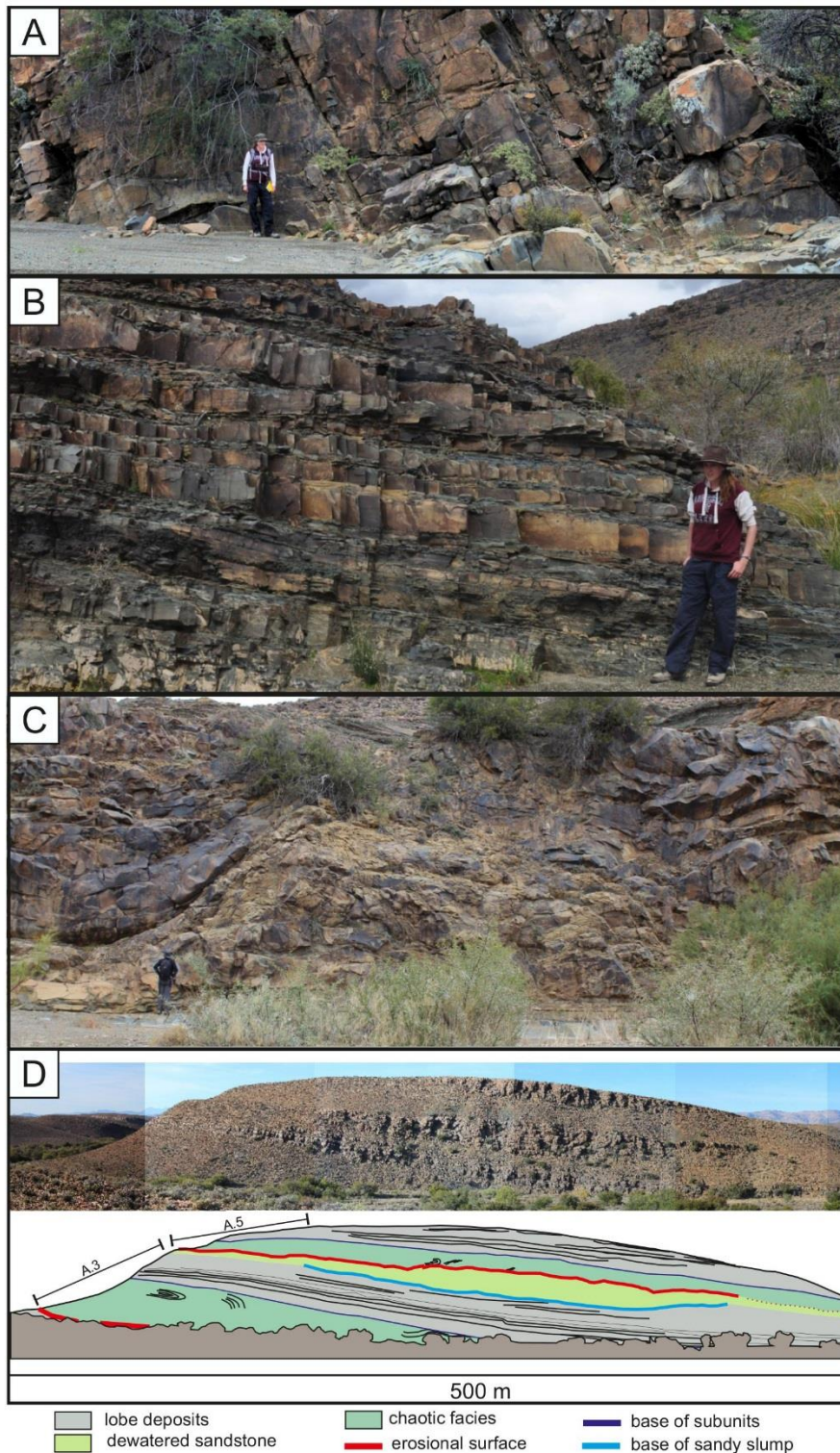
Figure 4.7. Representative photographs for Unit A, Laingsburg Fm. A: Thick-bedded structureless sandstones dominated by lobe axis deposits separated by lobe fringe thin-beds. Geologist (~1.65 m) for scale. B: Medium-bedded structured sandstones interbedded with heterolithic packages in the northern study area (Jakkalsfontein). Geologist (~1.65 m) for scale. C: Large-scale dewatering feature at Jakkalsfontein 1 in A.3. The flames are truncated by an erosion surface overlain by a debrite at the base of A.5. Geologist as scale (~1.7 m). D: Photo panel of the Jakkalsfontein area showing Subunits A.3 and A.5. Both subunits have a basal slide deposit that is overlain by bedded sandstones. The base of the A.5 slide is erosive and truncated the big-scale dewatering features at the top of A.3.

In strike section, the thickness of Unit A is 300 m in the south (Skeiding) and thins to 140 m (Jakkalsfontein) towards the north (Fig. 4.8). Whereas the thickness of subunit A.1 shows no change, A.2 show slight thinning (from ~23 m to ~15 m; Fig. 4.8), while subunits A.3 – A.5 show a pronounced thinning trend. Subunit A.5, which consists of several lobe complexes, shows the maximum amount of thinning (117 m in the south to 42 m in the north). Subunit A. 3 thins from 43 m to 30 m, whereas A.6 thins slightly from 25 m to 22 m. In depositional dip sections (Fig. 4.9), subunits A.1-A.6 maintain a similar thickness, and only minor thickness and facies changes are observed that can be accounted for by compensational stacking at subunit level. Isopach thickness maps (Fig. 4.10) show an overall shift in the main locus of deposition to the N through A.1- A.6. Subunit A.3 displays two areas of thicknesses exceeding 30 m. In the SE, the thickness conforms to lobe deposits, whereas in the NW the thickness is caused by slides and debrites at the base of A.3 (34 m thick).

4.8 Palaeogeographic reconstruction

The stratigraphic thinning to the northwest, the presence of mass flow deposits with kinematic evidence of movement to the southeast and southwest, and the thick aggradational succession of climbing ripple dominated thin-bedded siltstone facies with a narrow eastward palaeoflow direction (Fig. 4.7) in all lobe complexes point to the presence of seabed topography during deposition of Unit A (cf. recognition criteria of low-gradient slopes established by Smith (2004 b)). Based on these data, a SW-NE orientated and SE-facing intrabasinal slope has been reconstructed. The regional palaeocurrent trends in the underlying (Vischkuil Formation) and overlying (Unit B of Laingsburg Formation and Fort Brown Formation) are dominated by overall NE palaeocurrents (van der Merwe et al., 2009; Brunt et al., 2013, van der Merwe et al., 2014). This indicates that the intrabasinal slope was a lateral slope rather than the main basin margin slope. The limited amount of basinward thickness changes in subunits A.1-A.6 to the east (Sixsmith et al., 2004; Prélat & Hodgson, 2013, Fig. 4.9), suggest that the base of the intrabasinal slope ran between Matjiesfontein in the southwest and the centre of the Moordenarskaroo in the NE (Fig. 4.10).
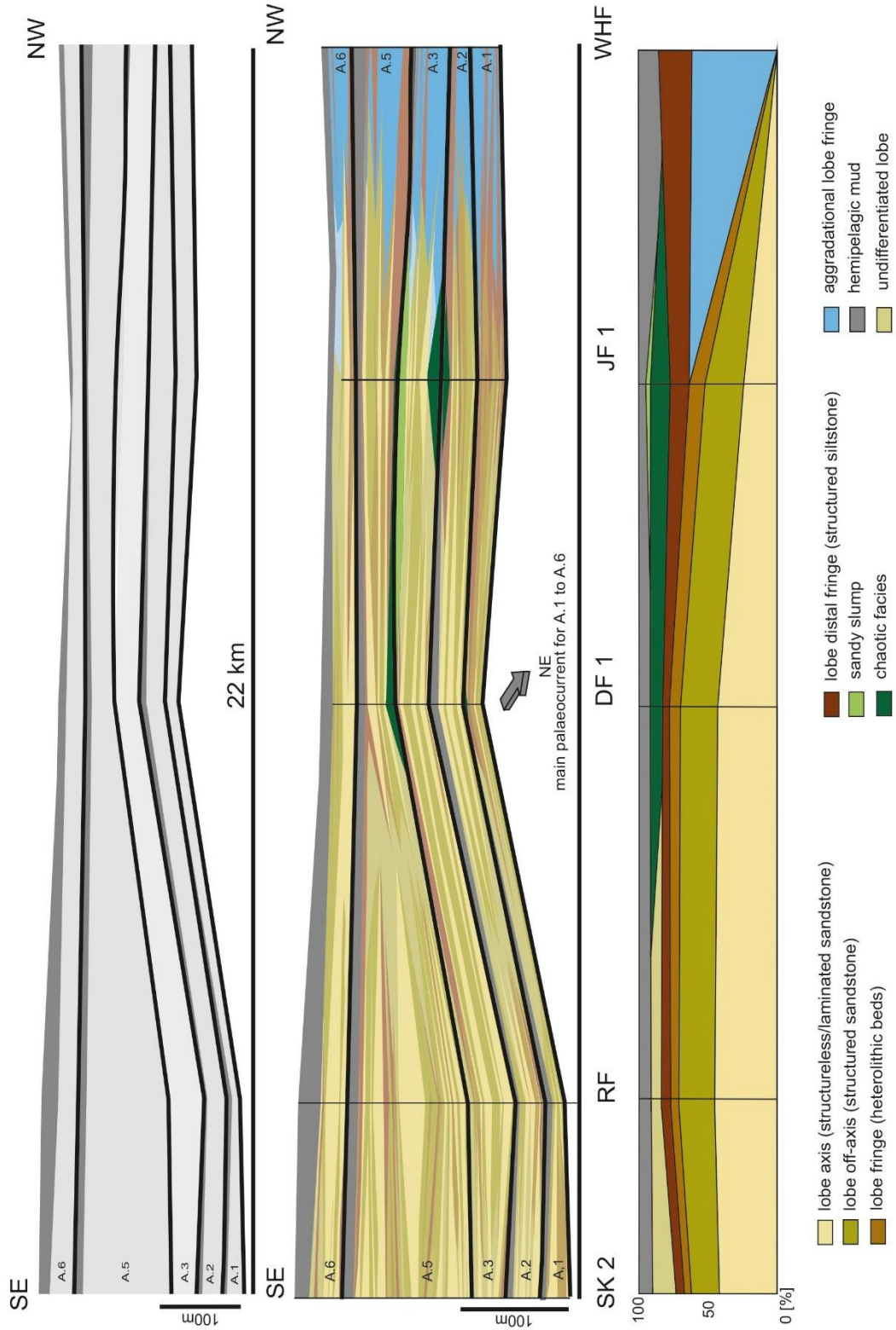
Figure 4.8. S-N transect correlation panels. Top: Correlation of subunits. Unit A thins to the north from ~270m to ~160m. Middle: Correlation of lobe sub-environments. Slide deposits occur in the Doornfontein and Jakkalsfontein areas. In the most northerly outcrop all facies associations are replaced by the aggradational lobe fringe facies association. SK2: Skeiding 2; RF: Rietfontein; DF: Doornfontein 1; JF 1: Jakkalsfontein 1; WHF: Wilgerhoutfontein. DPF: Dapperfontein, JF: Jakkalsfontein. Fig. 4.2 shows locations of transects. Bottom: Percentage of facies proportion over the transect. Note that at Wilgerhoutfontein the typical lobe environments are replaced by 'aggradational lobe fringe' facies.
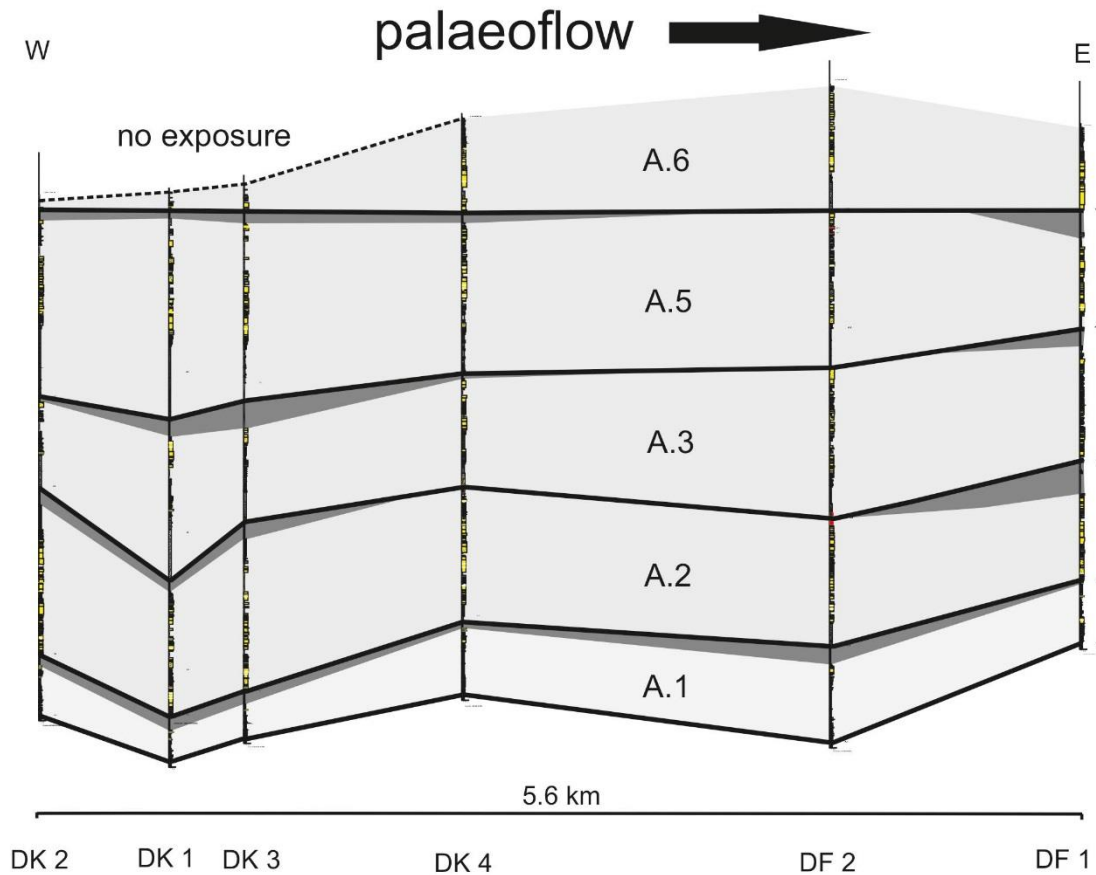
Figure 4.9. W-E transect (down-dip) correlation panel from the Doornkloof-Doornfontein area. Note that thickness remains almost the same over 5.6 km. Slight thickness changes may be due to compensational stacking of the subunits.

The southern study area is characterised by lobe complexes built through compensational stacking of lobes dominated by lobe axis and lobe off-axis deposits intercalated with heterolithic lobe fringe deposits. The northern study area consists of progressively more thin-bedded lobe fringe deposits that show aggradational stacking. Compensational stacking in the south to southeast of the study area and aggradational stacking in the northwest point to a relatively abrupt change in gradient (Fig. 4.11), associated with a break in slope.
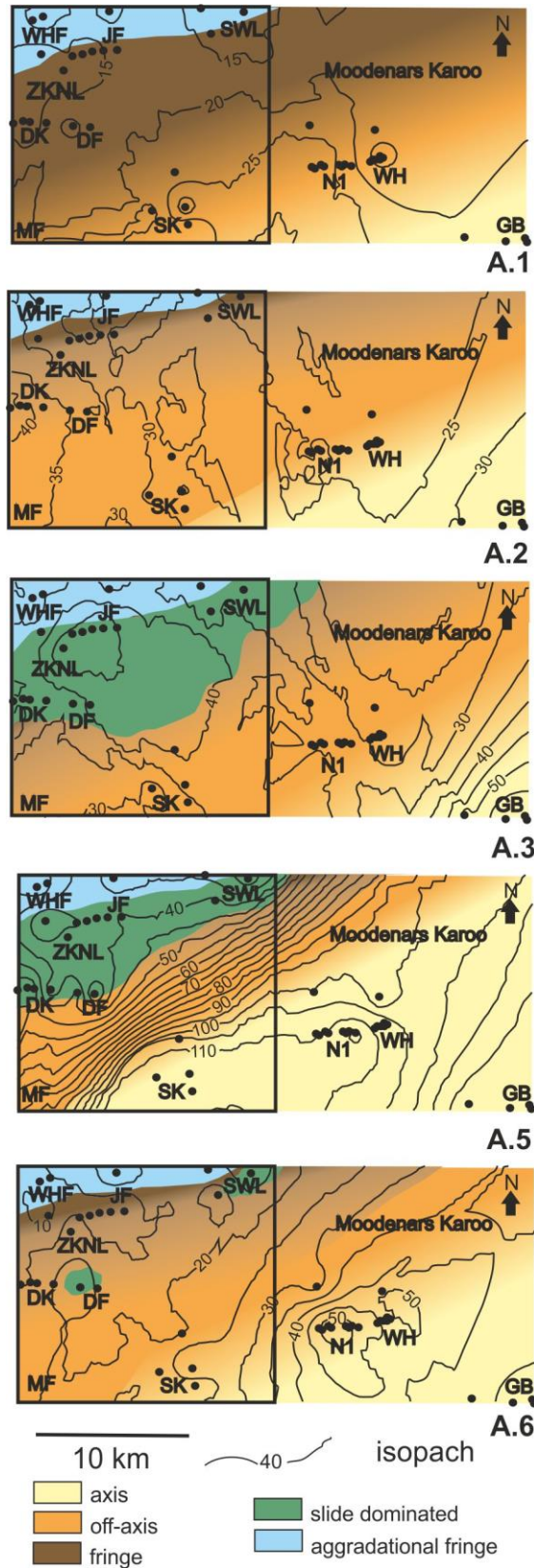
Figure 4.10. Thickness isopach and palaeoenvironmental maps for subunits A.1 to A.6. Note that A.1 and A.2 do not show specific thickness trends but do show facies trends. A.3 to A.6 thin above an SE-facing slope. DF: Doornfontein, DK: Doornkloof, GB: Geelbeck, JF: Jakkalsfontein, SK: Skeidingen, SWL: Steegweglagte, WH: Wilgerhout, WHF: Wilgerhoutfontein, ZKNL: Zoutkloof Northern Limb. MF: Matjiesfontein

Slightly more pronounced thinning of A.3 and prominent thinning of A.5 over the transect suggests that the confining slope steepens from the deposition of Subunits A.1 and A.2 to A.3 and A.5. The steepening of the confining slope is coincident with the emplacement of thick slide and debris flow deposits, which are most abundant in Subunits A.3 and A.5. The slides and debrites comprise remobilised heterolithic stratigraphy (lobe fringe deposits), dominated by thin-bedded climbing ripple laminated sandstones and the regional hemipelagic mudstones. Therefore, it is possible that the increased gradient destabilised sediments that had accumulated on the confining slope. The absence of the regional mudstone *in situ*, suggests that remobilisation happened after initiation of subunits A.3 and A.5.

4.9 Discussion

4.9.1 Aggradational lobe fringe facies association

Flow processes

Sedimentary structures indicate that very fine-grained sandstones, sandy siltstones, siltstones and mudstones with climbing bedform geometries were deposited rapidly from stratified turbidity currents with a thin basal sand-prone part and a thick mud-prone part. Due to rapid deceleration the upper parts of the flows deposited heterolithic climbing-ripple dominated facies along the intrabasinal slope (Fig. 4.11). The main sand fraction was partitioned to the south, where lobe complexes display intercalation of dominantly structureless sandstone lobe axes and structured sandstone lobe off-axes with heterolithic lobe fringes that is indicative of unconfined compensational stacking (Fig. 4.11). The thick sand-rich packages in the south grade abruptly into thin-bedded heterolithic lobe fringe facies in the northwest (against the confining slope). The lateral transition to lobe fringe from lobe axis and off-axis successions supports interpretation of the palaeo-environment of deposition being stacked lateral lobe fringes (Pickering, 1981, 1983). The lobe fringe facies association in this study differs from the lobe fringe facies association proposed by Prélat et al. (2009) from the unconfined Tanqua depocentre, largely due to the evidence for high sedimentation rates (climbing ripples and climbing bedforms) and the persistent aggradational stacking of facies over tens of metres on lobe complex scale. The narrow spread of slope sub-parallel palaeocurrents documented within these deposits

suggests minor flow deflection (Fig. 4.6). We propose the term 'aggradational lobe fringes' for this specific lobe sub-environment. The lateral facies transition between lobe axis and off-axis to fringe is governed primarily by the height of the topography relative to the thickness of the flows (Muck & Underwood, 1990; Pickering & Hilton, 1998, Wynn et al., 2012). However, flows are stratified in terms of their grain size and sediment concentration (García & Parker, 1993; McCaffrey et al., 2003; Baas et al., 2005; Kane & Pontén, 2012). In relatively unconfined basin-floor settings, flows are likely to be relatively thin (Stevenson et al., 2013b); transporting their sandy sediment only metres from the bed with the finer grained component transported in a thicker (10s metres) dilute overriding layer (Stevenson et al., 2014). The presence of subtle lateral topography on the basin-floor will therefore impose different levels of confinement on the basal and upper parts of the flows (Fig. 4.11).

Interaction of stratified flows and seabed topography

A gentle SE-facing lateral slope present during the deposition of A.2, A.3 and A.6 would confine the basal part of the flows (metres thick) and lateral pinching would occur over distances of kms. In contrast, the upper parts of flows would be able to easily surmount the topography. This generates a scenario whereby sandy lobe deposition (axis and off-axis environments) is weakly confined by the slope, whilst the fine-grained fringes deposit as if unconfined (Fig. 4.11 a). Fringe deposits from lobes that are deposited farther away from the confining slope are extensive. As they deposit from the dilute part of the flow they will contribute to the deposits on the slope. Therefore, thinning in this scenario is notably gradual (Fig. 4.11 a).

Relatively steeper slopes (subunit A.5) would confine the sandy basal parts of flows more strongly and result in lateral pinching over distances of hundreds of metres. The thicker upper parts of flows are also confined but still onlap higher up the slope and are, therefore, able to deposit drapes onto the bounding slope (cf. Smith & Joseph, 2004). This generates lobe deposits that abruptly (over hundreds of metres) transition into aggradational lobe fringe facies (Fig. 4.11 b). With continued sandy lobe deposition, compensating lobes will stack against the confining slope with aggradational lobe fringes (Fig. 4.11 b).
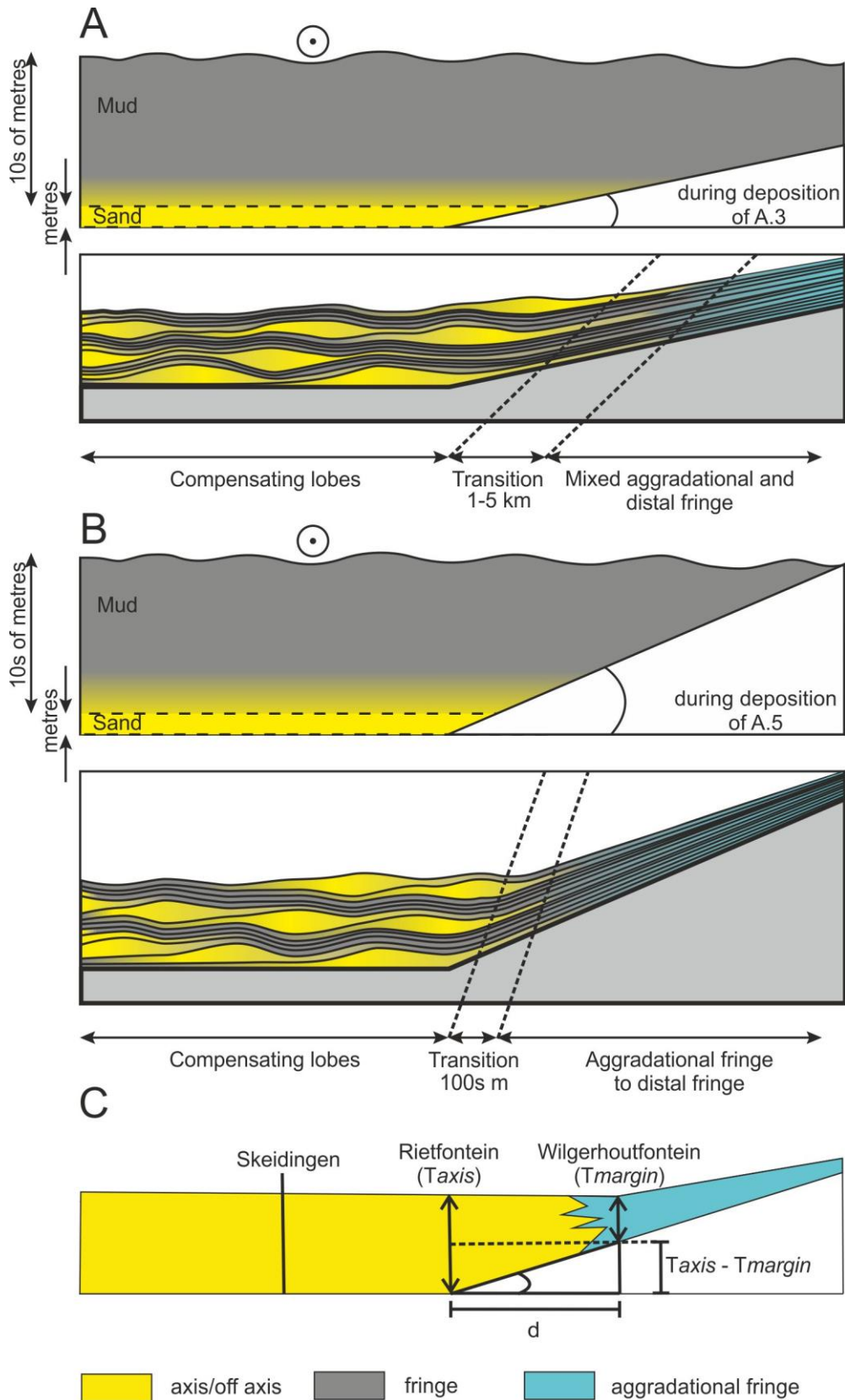
Figure. 4.11. Schematic evolution of lobes and stacking patterns within subunits (thicknesses exaggerated). A) With a gentle intrabasinal slope as during the deposition of A.3 compensational stacking pattern in the main depocentre passes into a mixed aggradational and distal fringe on the slope. The transition from lobe axis and off-axis deposits to aggradational fringe deposits occurs over kms (climbing trajectory). B) A relative steeper intrabasinal slope as present during deposition of A.5 results

in compensational stacking in the main depocentre and abrupt facies transitions (100s m; vertical trajectory) and thinning to the slope, where aggradational fringe and distal lobe fringe deposits are successively located slope-upwards. C) Estimation of slope angle using trigonometric geometries. Where T_{axis} is the thickness at Rietfontein, T_{margin} is the thickness at Wilgerhoutontein (for locations see Fig. 4.2) and d is the distance between the locations (18.7 km) along the transect corrected for post-depositional tectonic shortening.

4.9.2 Nature of the confining structure

The origin of the lateral slope, and whether it was static or dynamic, is discussed using stratigraphic evidence. The thickness trends and facies distributions (Fig. 4.10) indicate that the gradient of the confining slope increased through time from A.1 to A.5, then reducing from A.5 to A.6. The persistent lateral facies transition to thick aggradationally stacked lobe complex fringes, in a similar fashion, indicates that the slope was always present and inhibited the development of lobes. Therefore, the intrabasinal slope was dynamic rather than static. Differential compaction above syn-rift topography has been shown to have a long-lived impact on deep-water sedimentation patterns (e.g. e.g. Parker Gay, 1989; Nygård et al., 2002; Færseth & Lien, 2002). However, reduction of the slope gradient after the deposition of A.5 indicates that differential compaction above a deeper rigid block cannot be the driving mechanism for the dynamic intrabasinal slope. Syn-tectonic activity deforming the seabed has been postulated previously in the basin (e.g. Grecula et al., 2003b; Sixsmith et al., 2014). Sixsmith (2000) proposed syndepositional basin-floor deformation as a driving mechanism for thickness variations, speculating early movement on incipient structures that became the present day E-W trending folds. Sixsmith et al. (2004) inferred that Units A.1 and A.2 pinchout with an onlap against an incipient Hexberg-Bontberg-Heuningberg antiform structure (see Fig. 4.1) with Unit A.1 and A.2 pinching-out against the structure, and that Unit A thickens dramatically to the north of the Heuningberg anticline. Here, all subunits are correlated over the study area, with no evidence of any subunit pinching out across the Heuningberg anticline area. The thinning and facies trends do not coincide with the present day orientation of fold structures but are consistent with a SE-facing low gradient intrabasinal confining slope.

Timing of mass wasting processes, thickness distributions and slope angles are key indicators to determine the nature of the slope. Mass wasting events have been examined on modern seabed basin margins on slopes gradients as low as 0.05 to 1.4° (Bugge et al., 1988, Masson et al., 1998; Gee at al., 1999; Haflidason et al.,

2004; Frey-Martínez et al., 2006). The slides and debrites are located at the bases of Subunits A.3 and A.5 as slope angles increased. It is likely that much of the steepening occurred during the slow accumulation of the hemipelagic drapes that separate Subunit A.2 from A.3 and Subunit A.3 from A.5. The initiation of slides and debris flows may have been due to 1) oversteepening of the intrabasinal slope; 2) liquefaction of the underlying muddy deposits (cf. Bull et al., 2009); 3) failure through high pore pressure due to high sedimentation rates on the slope (Nygård et al., 2002), or a combination of these processes. Gee at al. (1999) reported that high pore pressures can initiate bed shearing on slopes as little as 0.05° conforming to slope angles during deposition of A.3 and A.5. For example, seismicity can increase slope gradients, liquefy strata and generate overpressure (Heezen and Ewing, 1952; Bugge et al., 1988). Therefore, punctuated mass wasting, and successive steepening of the slope and healing before the deposition of A.6 suggests an underlying tectonic driver and explains the presence of a dynamic if subtle lateral slope, with different rates of tilting and sedimentation governing its gradient at any time on the seabed.

4.9.3 Estimating the angle of the lateral slope

Estimation of palaeoslope gradients from outcrop data is problematic as many assumptions need to be made. For example, the original gradient of the seabed, the effects of differential sediment compaction, and the amount of post-depositional shortening due to tectonic activity. Although it is not possible to determine original gradient unequivocally, reconstructing an approximate slope gradient is useful in making comparisons across different systems (i.e. low gradient slope <1°; moderate gradient slope 1-5°; and high gradient slope < 5°). Although the original gradient of the seabed on the basin floor at the time of onset of accumulation of Subunit A1 cannot be determined, it was likely close to zero (van der Merwe et al., 2009). Thinning and facies distribution of Unit A, particularly of remobilised chaotic deposits, suggest that the intrabasinal slope likely dipped to the SE.

If all the thinning of subunits A.1 to A.6 across the transect from axis to margin is attributed to the presence of a seabed topography, and if the basin floor is assumed to have had no gradient at the time of accumulation, then an approximate minimum intrabasinal slope angle can be estimated using a simple trigonometric approach (see Fig. 11c):

$$\tan^{-1} = (T_{axis} - T_{margin})/d \qquad \text{[Equation 1]}$$

Where Taxis is the original accumulated thickness at Rietfontein, Tmargin is the original accumulated thickness at Wilgerhoutfontein (for locations see Fig. 2), and d is the measured distance between the locations (Rietfontein and Wilgerhoutfontein, Fig.2 along the transect, which has been corrected for post-depositional tectonic shortening (18.7 current distance; 21.3 km restored distance; Spikings et al., 2015). The results of Equation 1 have been converted into degrees.

A number of factors need to be taken into consideration when evaluating the uncertainties associated with the reconstruction of slope angles. Firstly, differential compaction will have resulted in significantly reduced thicknesses of the finer-grained lobe fringe deposits compared to the sand-rich lobe successions. Here, preserved section thicknesses have been decompacted using the approach of Sheldon & Retallack (2001) to estimate whether the effects of differential compaction have resulted in a significant error in the calculation of slope angle:

$$C = S_i/[F_o/e^{Dk})-1] \qquad \text{[Equation 2]}$$

Where C is the fraction of the original thickness, Si is initial solidity, Fo is the initial porosity, D is depth of burial in km, k is the curve-fitting constant. General values for S_i, F_o and k for marine sediments were established by Sclater & Christie (1980) and Baldwin & Butler (1985). They are displayed in Table 2. For sandstone, the following values are used: Si =0.51, Fo= 0.49, and k= 0.27 (cf. Sclater & Christie, 1980; Sheldon & Retallack, 2001). Sediments of the Karoo Basin exhibit greenschist metamorphism and were therefore buried to at least 6 km (Tinker et al., 2008; Hansma et al., 2015). The amount of compaction of the sandstone is estimated as follows:

$$C = 0.51/[0.49/e^{(6*0.27)})-1] \qquad \text{[Equation 3]}$$

This yields a value for C of 0.55 for sandstone, (i.e. the present preserved thickness has decreased by almost half compared to its original thickness). C value for siltstone and claystone are 0.42 and 0.22, respectively. Lobe axis and off-axis are dominated by sandstone and minor siltstone deposits, whereas lobe fringes are dominated by siltstone and very fine-grained sandstone deposits, and claystone is absent, meaning that decompaction has limited effects on the estimation of slope angle. Table 3 shows compacted and decompacted thicknesses, sand percentages and the variation of slope angle for all subunits. Over the whole transect (21.3 km); these thickness

variations introduce an average error (variance) in calculated slope gradient of ±0.01° over all subunits.

Second, post-depositional tectonic shortening has reduced the lateral distance of the transect from 21.3 km originally (Spikings et al., 2015) to 18.7 km today (d in Equation 1). Spikings et al. (2015) conducted mass-balanced palinspastic restoration of the Laingsburg depocentre, and calculated a post-depositional shortening of 14.2%. Adjacent mass-balanced sections from Laingsburg and Matjiesfontein indicate post-depositional shortening of 14.7 % and 9.2 %, respectively (Spikings et al., 2015). The range of shortening estimates for the area is 9.2 to 14.7 %, which results in corrected lateral distances across the transect ranging from 20.4-21.4 km. This 1000m uncertainty in the amount of shortening corresponds to an error of approximately ± 0.01° in slope gradient (Equation 1) (see Table 4).

Using Equation 1, Subunits A.2 and A.6 experienced slope angles of <0.05°, A.3 around 0.05°, whereas A.5 encountered a slope of around 0.3° (see Table 4). Slope angle values for Subunit A.1 fall within the range of error. Nonetheless, the subunit shows palaeoflow directions that are parallel to the inferred slope, suggesting that a slope may have been present at this time of deposition, but the rate of aggradation on the lateral slope was similar to the rate of aggradation on the basin-floor.

4.9.4 Grades of confinement and their influence to basin-floor lobe systems

Several ancient deep marine fans with inferred lateral confinement have been described or inferred, including the Grès d'Annot Formation (SW Alps, France), the Castagnola Formation and the Cenigo Turbidite system (Tertiary Piedmont Basin, Italy), the Mynydd Bach, Aberystwyth, Cwmystwyth and Pysgotwr Formations (Welsh Basin, Wales), Laga Formation (South Laga Basin, Central Appenines, Italy) and the Loma de los Baños Formation (Tabernas-Sorbas Basin, Spain). Most of these systems show a range of onlap geometries (Fig. 4.12).

The Grès d'Annot Formation, the Laga Formation, the Castagnola Formation, the Cenigo Turbidite systems and the Loma de los Baños Formation represent systems that were deposited under high to moderate confinement. Lateral palaeoslope values are reported between 4- 10° (Amy et al., 2007; Salles et al.,2014) for the Grès d'Annot

Formation; 6-8° (Marini et al., 2015) for the Laga Formation; 10-12° for the northern margin of the Castagnola Formation and 4° for the southern margin, respectively (Felletti, 2002; Southern et al., 2015; Marini et al., 2016); and 5-10° for the Cenigo Turbidite systems (Bersezio et al., 2009; Felletti & Bersezio, 2010). The Grès d'Annot Formation was deposited during the upper Eocene and Oligocene in an Alpine foreland setting. It crops out in synclines of the thrust belt of the SW Alps in France (Amy et al., 2004). Two styles of onlap (Fig. 4.12) were described for the sub-basins: 1) abrupt onlap (Sinclair, 2000; Etienne, 2012) and 2) aggradational onlap with draping of the confining slope (Sinclair, 2000; Etienne, 2012). The Laga Formation was reported to be deposited under changing grades of confinement (confined to semi-confined; Marini et al., 2015) in the Southern Laga Basin, Italy. The termination styles against the lateral slope comprise abrupt onlap and feather-like onlaps of thin ripple-laminated turbidites. The Tertiary Piedmont Basin (Castagnola Formation and Cenigo Turbidite systems) developed during the Alpine and Apennine orogenesis as a piggyback basin. Topographic features are complex and comprise several unconformities that resulted in modification of basin size and configuration (Felletti, 2002). Bounding lateral slopes are mostly steep and lead to abrupt onlap, but aggradational onlap has been reported to the southern basin margin with lower slope gradients (4°; Felletti, 2002). The Loma de los Baños Formation, Tabernas-Sorbas Basin, SE Spain indicates flow confinement against intrabasinal faults, such as the the El Cautivo Fault zone (Hodgson & Haughton, 2004). Hodgson & Haughton (2004) reported aggradational onlaps when flows encountered forced folds (cf. Stearns, 1978) and abrupt pinch-outs against fault scarps. Several authors (Smith, 1987 a,b; Wilson et al., 1992; Smith, 2004 b) described an example of subtle topography and its influence on the Welsh Basin Silurian sandstone systems, namely the Mynydd Bach, Aberystwyth, Cwmystwyth and Pysgotwr Formations. Sand-prone deposits laterally grade or transition into a mud-rich turbiditic 'levee-like' constructional feature due to the influence of faults. Smith (2004 b) used the geometrical model established by Smith & Joseph (2004) to illustrate the lateral facies change from lobes (Pysgotwr Formation) to thin-bedded heterolithics (Hafdre Formation).

All of the above systems include syndepositional deformed slides/slumps in proximity to the lateral slope. The slides/slumps are interpreted to be initiated through 1) gravitational instability/ re-equilibration of the slope or 2) mass dumping of sediment against the slope. Except for the Mynydd Bach Formation, the examples outlined above describe direct onlap of deposits against the confining intrabasinal slopes. In contrast, this study describes a persistent facies transition to 'aggradational lobe

fringes' against the confining slope, similar to the facies transitions reported from the Welsh Basin Silurian systems (Smith, 1987 a, b; Wilson et al., 1992; Smith, 2004 b) and in subsurface from the Ormen Lange turbidite system (Smith & Møller, 2003). The systems discussed exhibit a range of onlap geometries from abrupt to aggradational onlaps, and more subtle facies transitions against the confining slope, which form part of a continuum of possible configurations (Fig. 4.12).
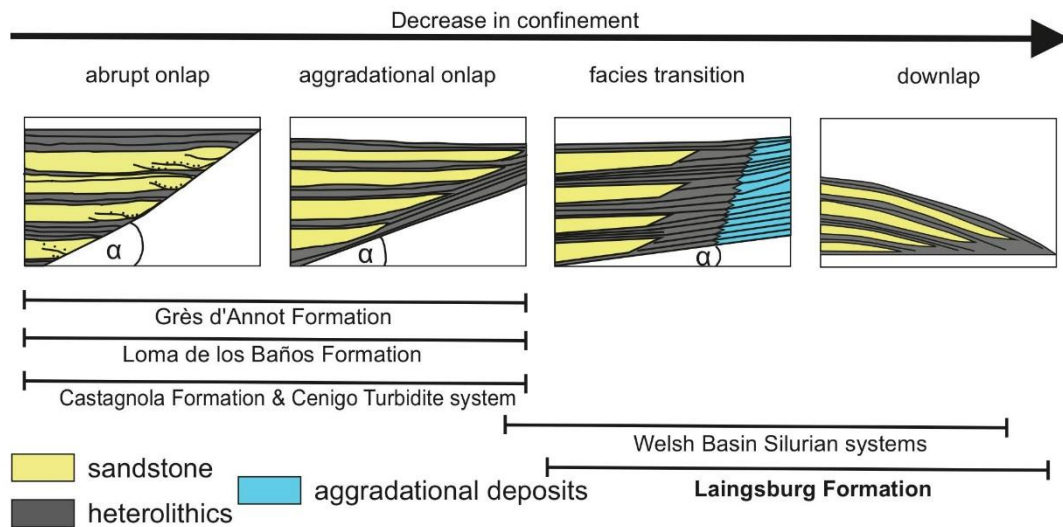
Figure 4.12. Submarine basin-floor lobes and their interaction with topographic features. 1) Low amount of aggradation on the slope compared to the basin - abrupt pinch-out against structure; 2) moderate amount of aggradation on the slope compared to the basin - aggradational onlap with draping muds; 3) low-gradient slope and high aggradation rates - facies transition and remobilisation; 4) unconfined – downlap.

4.10 Conclusions

This study uses an integrated outcrop and research borehole data set, from Unit A of the Permian Laingsburg Formation, South Africa, to examine the influence of confinement on flow behaviour, and resulting depositional architecture of basin-floor lobes and lobe complexes. Across strike changes in unit thickness, palaeocurrent patterns, and the distribution of sedimentary facies, were combined to reconstruct a laterally confining SW-facing intrabasinal slope. Although subtle, the slope influenced flow behaviour throughout the succession generating distinctive facies distributions over the study area; confining the sandstone-rich deposits to the south, where conventional lobe compensational stacking was able to take place. Against the

confining slope, sand-rich lobe facies pinch and transition laterally into thick (10s of metres) aggrading successions of thin-bedded laminated to structureless siltstones, and current/climbing-ripple laminated very fine-grained sandstones: a new facies association termed 'aggradational lobe fringes'. This transition is a result of stratified flows interacting with the slope, whereby sand (transported only meters from the bed) is confined and pinches out, whilst finer-grained sediment is held aloft in a much thicker overriding cloud and deposits much higher up the slope. Distances of facies transition depend on the slope angle. The persistent facies transition across multiple lobe complexes, and the punctuated occurrence of remobilized facies, associated with steeper slope gradients, suggests a tectonically-driven and dynamic intrabasinal slope. This study highlights that basin-floor flows are grain-size stratified with a thin basal sand-prone part and a thick mud-prone part, meaning that even subtle topography will exert a major influence on lobe architecture. Identification of thick aggradational lobe fringe successions, as a direct response to subtle dynamic intrabasinal topography, widens the range of geometric and facies-based recognition criteria of subtle confinement in basin-floor settings. The framework provided here is important for the improved recognition of lobe confinement in outcrop, and its interpretation in the subsurface.

Chapter 5

Constraining the sedimentology and stratigraphy of submarine intraslope lobe deposits using exhumed examples from the Karoo Basin, South Africa

5.1 Abstract

Intraslope lobe deposits provide a record of the infill of accommodation on submarine slopes, and their recognition enables the accurate reconstruction of the stratigraphic evolution of submarine slope systems. Extensive exposures of discrete sand-prone packages in Units D/E and E, Fort Brown Formation, Karoo Basin, South Africa, permit analysis of the sedimentology and stacking patterns of three intraslope lobe complexes and their palaeogeographic reconstruction via bed-scale analysis and physical correlation of key stratal surfaces. The sand-prone packages comprise tabular, aggradationally to slightly compensationally stacked lobe deposits with constituent facies associations that can be attributed to lobe axis, lobe off-axis, lobe-fringe and distal lobe-fringe environments. Locally, intraslope lobe deposits are incised by low aspect ratio channels that mark basinward progradation of the deepwater system. The origin of accommodation on the slope for lobe deposition is interpreted to be due to differential compaction or healing of scars from mass wasting processes. The stacking patterns and sedimentary facies arrangement identified in this study are distinct from those of more commonly recognised basin-floor lobe deposits, thereby enabling the establishment of recognition criteria for intraslope lobe deposits in other less well exposed and studied fine-grained systems. Compared to basin floor lobes, intraslope lobes are smaller volume, influenced by higher degrees of confinement, and tend to show aggradational stacking patterns.

5.2 Introduction

Basin-floor lobe deposits are the dominant component of submarine fan successions and criteria for their recognition are well established (e.g., Harms, 1974; Hartog Jager et al., 1993; Sixsmith et al., 2004; Pyles, 2008; Prélat et al., 2009, 2010; Pyles & Jennette, 2009; Kilhams et al., 2012; Etienne et al., 2012; Burgreen & Graham, 2014). By contrast, the characteristics of intraslope lobes, which are also referred to as perched lobes (Plink-Björklund & Steel, 2002; Prather et al., 2012a) and transient fans (Adeogba et al., 2005; Gamberi & Rovere, 2011), which form in areas of slope accommodation, are poorly defined (Fig. 5.1). Intraslope lobes have been identified in several subsurface geophysical studies based on multibeam bathymetric data, CHIRP profiles and seismic imaging (2D and 3D). Documented examples include studies from the Gulf of Mexico (Prather et al., 1998; Fiduk et al., 1999; Badalini et al., 2000; Pirmez et al., 2012; Prather et al., 2012b), the Niger Delta continental slope offshore Nigeria (Adeogba et al., 2005; Li et al., 2010; Barton, 2012; Prather et al., 2012a), the Lower Congo Basin, offshore Angola (Oluboyo et al., 2014), the Algarve Margin, offshore Portugal (Marchès et al., 2010), the Gioia Basin, southeastern Tyrrhenian Sea (Gamberi & Rovere, 2011; Gamberi et al., 2011) and the Baiyun Sag, South China Sea (Li et al., 2012).
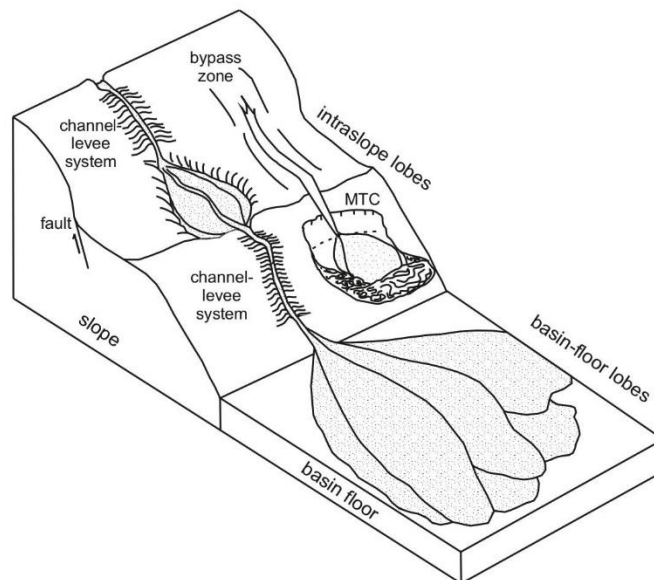
Figure 5.1. Principal features of a stepped deep-water system. Two mechanisms to generate accommodation on the slope are shown: generation of a slope step due to tectonic faulting and above a scar of a mass transport complex (MTC).

The geophysical expression of intraslope lobes is described as layered (high amplitude reflectors) to transparent seismic facies by most authors (Booth et al., 2003; Adeogba et al., 2005; Li et al., 2012), though Marchès et al. (2010) report cases that are represented by chaotic seismic reflectors. These seismic facies have been interpreted as channel-lobe systems and associated mass transport deposits, respectively. Different mechanisms are invoked to explain the development of intraslope accommodation needed for intraslope lobe deposits to form, including tectonics (Marchès et al., 2010; Li et al., 2012), mud diapirism (Adeogba et al., 2005), halokinesis (Booth et al., 2003; Oluboyo et al., 2014) or slide scars (Morris et al., 2014a). Several commonly observed features of intraslope lobes are considered as diagnostic indicators: 1) a smaller lateral extent and lower aspect ratio than basin floor lobes (Plink-Björklund & Steel, 2002; Deptuck et al., 2008); 2) common evidence for incision due to their transience that is linked to a lower base level on the basin floor (Adeogba et al., 2005; Flint et al., 2011; Barton, 2012; Prather et al., 2012b) or to slope profiles that are not in equilibrium (Ferry et al., 2005); 3) association with mass transport complexes (MTCs) (Adeogba et al., 2005; Gamberi & Rovere, 2011; Li et al., 2012); 4) deposits delimited by onlap and downlap terminations (Booth et al., 2003; Li et al., 2012); 5) prevalence of coarse sand sediment that is deposited in response to hydraulic jumps due to a break-in-slope related to a stepped slope profile (Komar, 1971; Ferry et al., 2005); and 6) mounded or tabular morphologies (e.g., Oluboyo et al., 2014).

Intraslope lobes are important features in the reconstruction of the evolution of the slope and the analysis of sediment dispersal patterns, and indicate the presence of an uneven slope profile during deposition. Although attempts have been made to determine the importance of submarine slope deposits within a source-to-sink system (Eschard et al., 2004), intraslope lobes have rarely been identified in outcrop studies (Plink-Björklund & Steel, 2002; Sinclair & Tomasso, 2002; Beaubouef et al., 2007; Figueiredo et al., 2010; Bernhardt et al., 2012; van der Merwe et al., 2014). Therefore, the sub-seismic depositional architecture of intraslope lobes can be considered as one of the missing pieces in understanding the stratigraphic record of deep-marine systems and their preserved successions.

Extensive fieldwork carried out in the Laingsburg depocentre of the Karoo Basin, South Africa (e.g. Grecula et al., 2003a; Sixsmith et al., 2004; Di Celma et al., 2011; Flint et al., 2011; Hodgson et al., 2011; Brunt et al., 2013a; Morris et al., 2014b; van

der Merwe et al., 2014) has established the stratigraphic and palaeogeographic framework in detail and enables the identification of lobes that were deposited in a slope setting. In this study, we focus on a more detailed characterisation of some of the intraslope lobes of the Karoo Basin. Specific objectives are: 1) to determine the characteristic facies associations and anatomies of the intraslope lobes in the study area; 2) to compare their characteristics with those of basin floor lobes, and 3) to discuss the origin of the transient slope accommodation. The establishment of recognition criteria for the identification of intraslope lobes will help reduce uncertainties in the interpretation of depositional environments observed in core and outcrop where the palaeogeographic context is not clear.

5.3 Geological and Stratigraphic Settings

The evolution of the Karoo Basin has long been associated with a magmatic arc and the tectonics of a fold-thrust belt (Cape Fold Belt; Fig. 5.2a), thus characterising it as a retroarc foreland basin (Visser & Prackelt, 1996; Visser, 1997; Catuneanu et al., 1998). Recent studies (e.g., Tankard et al., 2009) suggest that an early phase of subsidence enabled a basin fill that pre-dates the initiation of the Cape Orogeny, and was induced by dynamic topography. This topography is thought to have been derived from the coupling of mantle flow processes to distant subduction of the palaeo-Pacific Plate (Pysklywec & Mitrovica, 1999).

The Laingsburg depocentre is located in the south-western part of the Karoo Basin and adjacent to the present-day Cape Fold Belt (Flint et al., 2011). The stratigraphic unit of study is the Fort Brown Formation of the Ecca Group, which is exposed along the limbs of large, post-depositional folds (Fig. 5.2b). The Fort Brown Formation is a 400 m-thick submarine slope succession (Di Celma et al., 2011; Flint et al., 2011; Hodgson et al., 2011) that overlies the Laingsburg Formation, a 550 m-thick sand-rich basin floor and base-of-slope succession (Sixsmith, 2000; Grecula et al., 2003a; 2003b; Sixsmith et al., 2004; Brunt et al., 2013b). The Fort Brown Formation is divided into Units C to G (Flint et al., 2011; van der Merwe et al., 2014). These sand prone-units are each separated by regional hemipelagic claystones that locally include additional thin (1-15 m-thick) intercalated sand-prone units informally referred to as interfans (B/C interfan and D/E interfan) (Grecula, 2003a; Hodgson et al., 2011). The sequence stratigraphy of the Fort Brown Formation has been proposed by Flint et al. (2011) to comprise two composite sequence sets, the lower one containing units
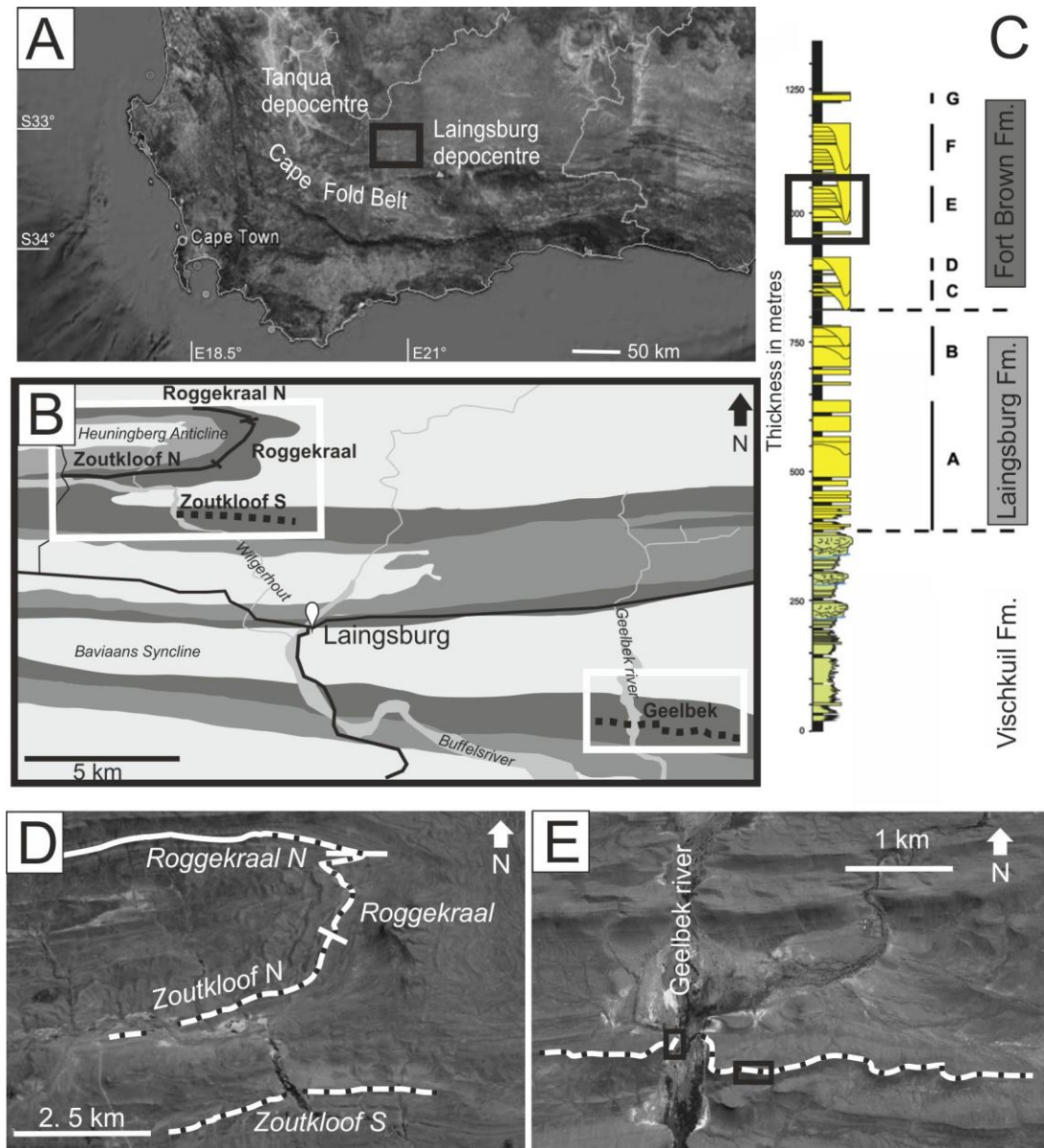
Figure 5.2. A) The Laingsburg depocentre is located inboard of the Cape Fold Belt. Black square indicates the area of study. Satellite images taken from Google Earth. B) Location of detailed study areas: Roggekraal and Zoutkloof in the North, Geelbek in the South. Shading corresponds to colours of boxes in C. White boxes represent the outlines of the study areas shown in D and E. C) Schematic stratigraphic log sections of the Fort Brown Formation., Laingsburg Formation. and Waterford Formation. (Flint et al., 2011). Units D/E and E are highlighted by the black square. D) Detailed view of the Zoutkloof and E) Geelbek study areas. White lines indicate outcrop exposure, black dots indicate positions of logged sections, and black boxed areas of detailed correlation panels (Figure 5.7).A more detailed location pull-out location map can be found at the back of the thesis.

B/C, C and D and the upper one containing units D/E, E and F. Each individual unit represents a lowstand sequence set, with subunits. For example Unit E is divided into Subunits E1, E2, and E3 based on the occurrence of claystone layers of regional mapped extent. Each subunit is interpreted as a lowstand systems tract. In this framework, the regional claystones that separate the units are interpreted as

associated transgressive (TST) and highstand (HST) sequence sets and the equally widespread claystones between sub-units are interpreted as combined transgressive and highstand systems tracts that record the deep-water expression of maximum flooding surfaces (Flint et al., 2011). Limited chronostratigraphic age control in the Fort Brown Formation (McKay et al., 2015) precludes establishment of the duration of depositional sequences.

This study focuses on two areas. Exposures of the Unit D/E interfan and Subunit E1 in the NW area of Zoutkloof (Fig. 5.2b) have been interpreted previously as lobes that formed in a slope setting (Figueiredo et al., 2010), but have not been hitherto characterised in detail. Four correlation panels were constructed (Zoutkloof S, Zoutkloof N, Roggekraal and Roggekraal N) to illustrate down-dip and strike variations in the successions. Unit E2 in the Geelbek area (Fig. 5.2b) comprises tabular sand-rich deposits, which, based on a detailed regional dataset, are interpreted to be intraslope lobes that formed above a stepped slope profile up-dip of a ramp dominated by sediment bypass (van der Merwe at al., 2014). The existence of these intraslope lobe deposits demonstrates the location and timing of slope accommodation and can be used to constrain the stratigraphic evolution of the Laingsburg submarine slope system.

5.4 Methodology and Data Set

For this study, 125 measured sections (each ranging from 3 to 36 m in length and totalling 2.8 km in cumulative thickness) were logged at 1:50 scale in the field, recording grain size, sedimentary structures and the nature and extent of bounding surfaces. In the Zoutkloof area (Fig. 5.2b,d), 80 sedimentary logs and 422 palaeocurrent measurements from ripple lamination and climbing-ripple lamination were collected over three large, adjacent fold limbs to reconstruct the large-scale geometries of exhumed intraslope complexes (Fig. 5.2b). In the south-eastern study area (Geelbek area; Fig. 5.2b,e), 45 sedimentary logs and 173 palaeoflow measurements were collected from ripple lamination, climbing ripple lamination and tool marks along an oblique dip section. In areas of specific interest, 11 additional detailed short sections were measured and correlated (Fig. 5.2e). This has permitted the development of a detailed sedimentological model to account for facies distributions and small-scale geometries. Correlation panels for the Geelbek area are hung from the regional claystones separating subunits E2 and E3. The Zoutkloof

correlation panels are hung from the base of Unit D/E that overlies a regional claystone above Unit D.

5.5 Facies associations

Six facies associations are identified based on inferred sedimentary processes and depositional environment. Five of the six facies associations represent particular lobe sub-environments (lobe axis, lobe off-axis, lobe fringe and distal lobe fringe) and have been modified from Prélat et al. (2009) according to the observed facies in the intraslope lobe deposits. FA1-5 represent lobe axis to lobe distal fringe, whereas FA 6 represents hemipelagic background sedimentation.

5.5.1 FA 1: Thick-bedded sandstone

Observations. This facies association is dominated by structureless, 0.7 to 2.5 m-thick beds of lower to upper fine-grained sandstone that commonly contain parallel lamination with some lenticular mudstone chips (mm-sized) aligned parallel to the laminae. Overall, beds are moderately to well sorted. Most beds lack grading, though weak normal grading is observed towards the tops of some beds that consist of 2 to 10 cm-thick caps of mica-rich, moderately sorted silty sandstone. Intraformational mudclasts are rarely observed at bed bases. Bed bases are sharp, loaded or erosive and can preserve tool marks. Bed amalgamation is common and can lead to > 10 m-thick packages of structureless sandstones (high-amalgamation zones; Fig. 5.3a). Amalgamation surfaces are indicated by discontinuous layers of mudclasts or subtle grain size breaks. Amalgamated sandstone packages can overlie surfaces that truncate underlying strata by up to 5 m. These surfaces are mantled with thin layers of mudstone clast conglomerates. Thick-bedded sandstones show tabular geometries. They are laterally extensive for up to 6 kms.

Interpretation. Thick-bedded, structureless and amalgamated sandstones with weak normal grading are interpreted to be the deposits of high-density turbidity currents (Kneller & Branney, 1995) with high aggradation rates (Arnott & Hand, 1989; Leclair & Arnott, 2005; Talling et al., 2012a). Their geometries, thickness and facies conform to lobe- or channel-axis settings (e.g., Prélat et al., 2009; Brunt el al., 2013a).

5.5.2 FA 2: Medium- to thin-bedded structured sandstone

Observations. This facies association comprises lower fine- to very-fine-grained, normally graded sandstone beds that are well sorted. Bed thicknesses range from 0.1 to 0.7 m. Sedimentary structures present include planar lamination, wavy lamination, current-ripple lamination and climbing-ripple lamination (Fig. 5.3b). Climbing-ripple lamination can be observed with supercritical angles of climb whereby stoss sides are preserved. The majority of beds contain two or more of these sedimentary structures. A common pattern is the vertical repetition of climbing-ripple laminations that are transitional to wavy laminations. Ripple foresets can be draped by thin (<0.1 cm thick) silty laminae. Individual beds can preserve multiple flow directions. Carbonaceous material and mud chips are dispersed in the sandy matrix. Bed bases are sharp or loaded. Medium- to thin-bedded sandstones show tabular geometries and can be traced for kms down-dip and in strike.

Interpretation. This facies association is interpreted to be deposited by low-density turbidity currents in a lobe off-axis setting. Bedforms such as planar lamination and current-ripple lamination are produced beneath dilute turbulent flows, which rework sediment along the bed (Allen, 1982; Southard, 1991; Best & Bridge, 1992). Beds with opposing palaeocurrent indicators suggest reflection and deflection of the flow (Edwards et al., 1994). Beds with repeating patterns of climbing-ripple and wavy lamination are interpreted to indicate highly unsteady flow behaviour due to either long-lived surging (Jobe et al., 2012).

5.5.3 FA 3: Interbedded thin-bedded sandstones and siltstones

Observations. This facies association comprises thin-bedded (0.01 to 0.2 m), very-fine-grained sandstone interbedded with sandy siltstone and coarse to fine siltstone. Sandstone beds show planar, current-ripple or wavy lamination, whereas siltstone beds commonly display planar lamination with rare isolated starved ripple forms at their base where there is a sand component to the siltstone (Fig. 5.3c). Contacts between sandstone and siltstone beds are sharp, undulating or loaded. Stoss-side preservation of climbing ripple lamination in sandstone beds is observed in 2D, and ripple geometries are locally preserved as sigmoid-shaped bedforms where 3D

observations are possible (see Kane & Hodgson (2011) Fig. 12b). Commonly, interbedded sandstones and siltstones form stacked, aggradational packages up to 5 m thick, which internally show no discernible trends in grain size or bed thickness. Individual packages dominantly comprise ripple and climbing-ripple laminated sandstones in their lower part and planar laminated sandstones in their upper part.

Interpretation. Ripple lamination formed due to reworking by dilute turbulent flows with moderate aggradation rates, whereas climbing-ripple lamination is indicative of high aggradation rates (Allen, 1971a; Allen, 1982; Southard, 1991). Ripple and planar laminated packages correspond with T_C and T_D divisions of Bouma (1962). This facies association is interpreted as a combination of deposition from sluggish, small-volume flows (Jobe et al., 2012) and flows that underwent rapid deceleration that led to high rates of sediment fallout. This implies that some flows were responding to changes in confinement, similar to flows that undergo expansion and rapid deposition when exiting channel confinement (e.g. Morris et al., 2014b). Observed facies and thicknesses of this facies association conform to an interpretation of a lobe-fringe setting.

5.5.4 FA 4: bipartite beds

Observations. Bipartite sand-prone beds (0.01 to 1.5 m thick) are composed of a lower and upper division. The well sorted lower division comprises relatively clean, structureless sandstone with low mud content. The upper division comprises poorly sorted mica-rich argillaceous sandstone that contains sand grains that are coarser than in the lower division, and varied proportions of subangular to subrounded mudstone clasts (mm to cm sized), mudstone chips and carbonaceous material (plant fragments) (Fig. 5.3d). Mudstone clasts show no preferred orientation. Typically, the boundary between the lower and upper divisions is gradational. Bed bases are sharp, whereas bed tops can be undulose.

Interpretation. Bipartite beds are interpreted to be the result of a juxtaposition of a high-density turbidity current and a genetically linked cohesive debris flow - a type of hybrid bed (Haughton et al., 2009). Several authors have identified an increase in the number of turbidites with linked debrites in distal parts of basin floor lobes (e.g. Ito, 2008; Hodgson et al., 2009; Talling et al., 2012a; Grundvåg et al., 2014). Therefore, bipartite beds are interpreted to be deposited in lobe-fringe settings.
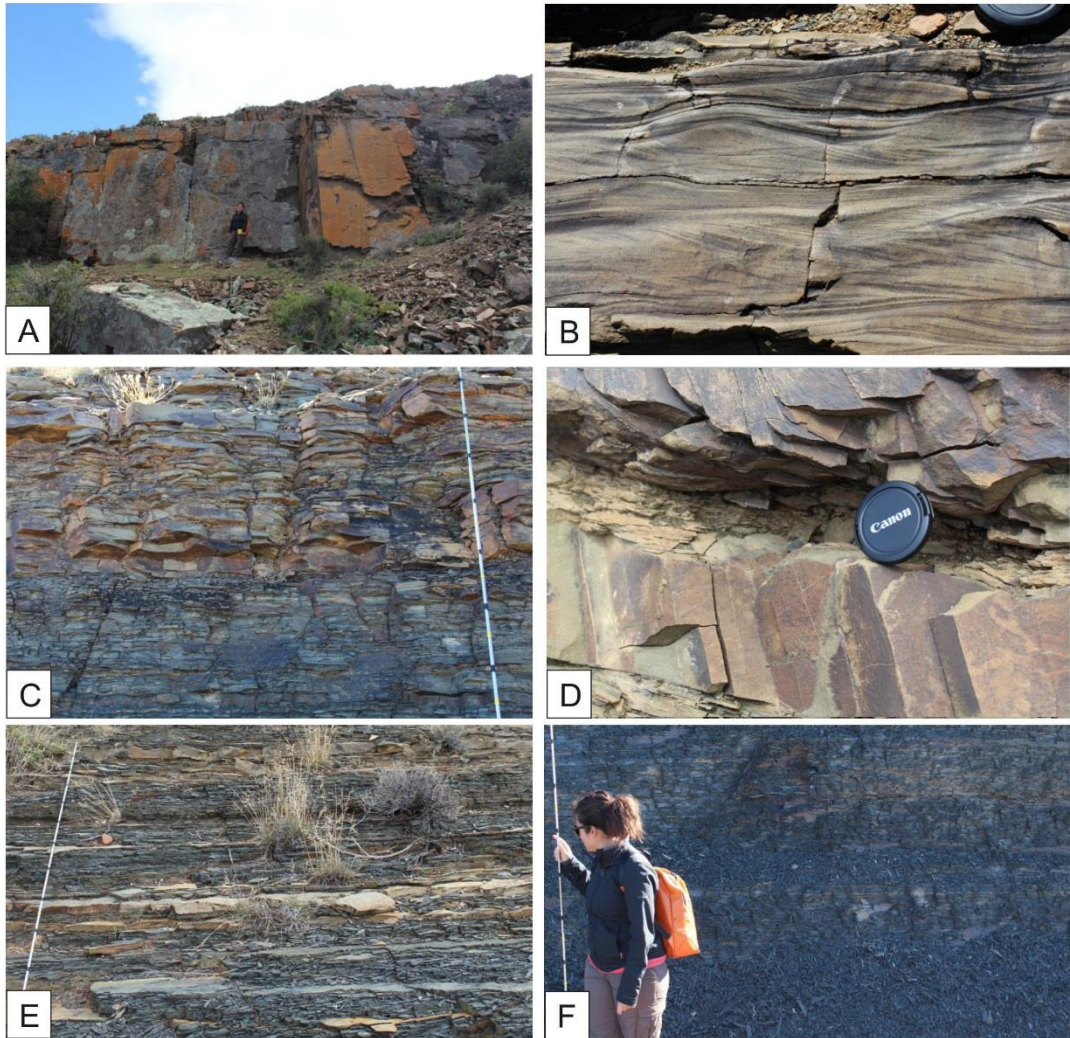
Figure 5.3. Representative photographs of sedimentary facies observed in the Zoutkloof area. A) Thick-bedded amalgamated sandstones of the lobe axis (FA 1). Geologist for scale (1.6 m). B) Climbing ripple-laminated, medium bedded, fine-grained sandstones, with some stoss-side preservation, in lobe off-axis (FA 2). Camera lens cover for scale. C) Heterolithic packages of thin-bedded sandstones and siltstones in the lobe fringe (FA 3). Logging pole (0.5 m) with 10 cm gradations as scale. D) Hybrid bed (FA 4). Camera lens cover as scale. E) Siltstone package with intercalated sandstones (FA 5). Logging pole (2 m) with 10 cm gradations as scale. F) Silty claystones (FA 6). Geologist for scale (1.6 m).

5.5.5 FA 5: thin- bedded siltstone

Observations. Thin-bedded (sandy), fine- to coarse-grained siltstones (0.05 to 0.1 m) form metre-scale packages with rare thin (>0.05 m), very fine-grained sandstones that are well sorted (Fig. 5.3e). Typically, beds are structureless or planar laminated and some incorporate mudstone chips (up to 20% of the bulk volume). Some sandy

siltstone beds show isolated starved ripple forms at their base. Thin-bedded siltstones can show minor bioturbation.

Interpretation. Siltstone deposits are interpreted as the preserved products of dilute turbidity currents in distal lobe-fringe settings. Structureless beds are attributed to direct suspension fallout (Bouma, 1962), whereas planar laminated beds are produced by traction (Stow & Piper, 1984; Mutti, 1992; Talling et al., 2012a).

5.5.6 FA 6: regional claystone

Observations. Homogenous intervals of (silty) claystone (Fig. 5.3f) are up to 22 m thick. Layers of concretions are common and tend to be associated with distinct horizons in the deposits. Claystone intervals are laterally extensive for tens of kilometres, except where eroded by channelised flows. Thin (<10 cm) ash layers and thin-bedded (mm-scale) graded siltstone units are locally intercalated with the claystones.

Interpretation. Claystones are interpreted as hemipelagic background deposits. Where mapped over large areas, they mark episodes of sediment starvation to the deep basin, and are interpreted to contain the deep-water expression of maximum flooding surfaces (e.g., Flint et al., 2011). Such packages therefore serve as useful correlation intervals.

5.6 Architecture

Unit D/E and Subunits E1 and E2 of the Fort Brown Formation have been recognized as tabular, sand-prone units within the submarine slope succession (Grecula et al., 2003b; Figueiredo et al., 2010). Flint et al. (2011) placed these packages into the overall sequence stratigraphic framework and van der Merwe et al. (2014) confirmed their palaeogeographic position on the slope. For the first time, the distribution of architectural elements and facies associations of these units are presented and discussed.

The identification of architectural elements is based on cross-sectional geometry, spatial extent, distribution of sedimentary facies and bounding surfaces marked by

abrupt changes in facies (Fig. 5.4). Interpreted architectural elements include lobe deposits, channel-fills and drapes (Fig. 5.4).

5.6.1 Zoutkloof area

Unit D/E. Unit D/E is a tabular sandstone package, informally referred to as an interfan (Flint et al., 2011), with a basal interval of interbedded siltstones and very fine-grained sandstones and a sharp top (Fig. 5.4a). The spatial extent of Unit D/E is limited to the Zoutkloof and Roggekraal study area (81 km^2; Figueiredo et al., 2010). Overall, palaeocurrent direction is to the ENE, but climbing ripple-laminated sandstones at Zoutkloof S show some readings to the west (Figs. 5.5, 5.6). Unit D/E is thickest (10 m) in the Zoutkloof N and Roggekraal areas where it comprises amalgamated thick-bedded structureless sandstones (FA 1) (Fig. 5.5). Across strike to the south (Zoutkloof S), a 6 m heterolithic package (FA 3) sharply overlies very fine- and fine-grained structured sandstones (FA 2). Unit D/E is not observed 6 km along strike to the south, which constrains the southward (lateral) pinch-out (Fig. 5.6). Across strike to the north (Roggekraal North; Fig. 5.4b), a 7 m-thick succession of structured sandstone (FA 2) is sharply overlain by structureless sandstones (FA 1).

Interpretation. Overall, the axis of Unit D/E is in the Zoutkloof N and Roggekraal areas, with more off-axis and fringe deposits in the south and north. The stratigraphic changes in facies in the Zoutkloof S and Roggekraal N areas suggest that Unit D/E comprises at least two lobes, and therefore represents a lobe complex (*sensu* Prélat et al. 2009). The lower lobe extends further south than the upper lobe, with lobe off-axis deposits (FA 2) overlain by lobe-fringe deposits (FA 3) in Zoutkloof S and lobe off-axis deposits (FA 2) overlain by lobe-axis deposits (FA 1) in Roggekraal N (Fig. 5.5) suggesting a minor compensational stacking pattern. The lobe axes are amalgamated in the central part of the study area.
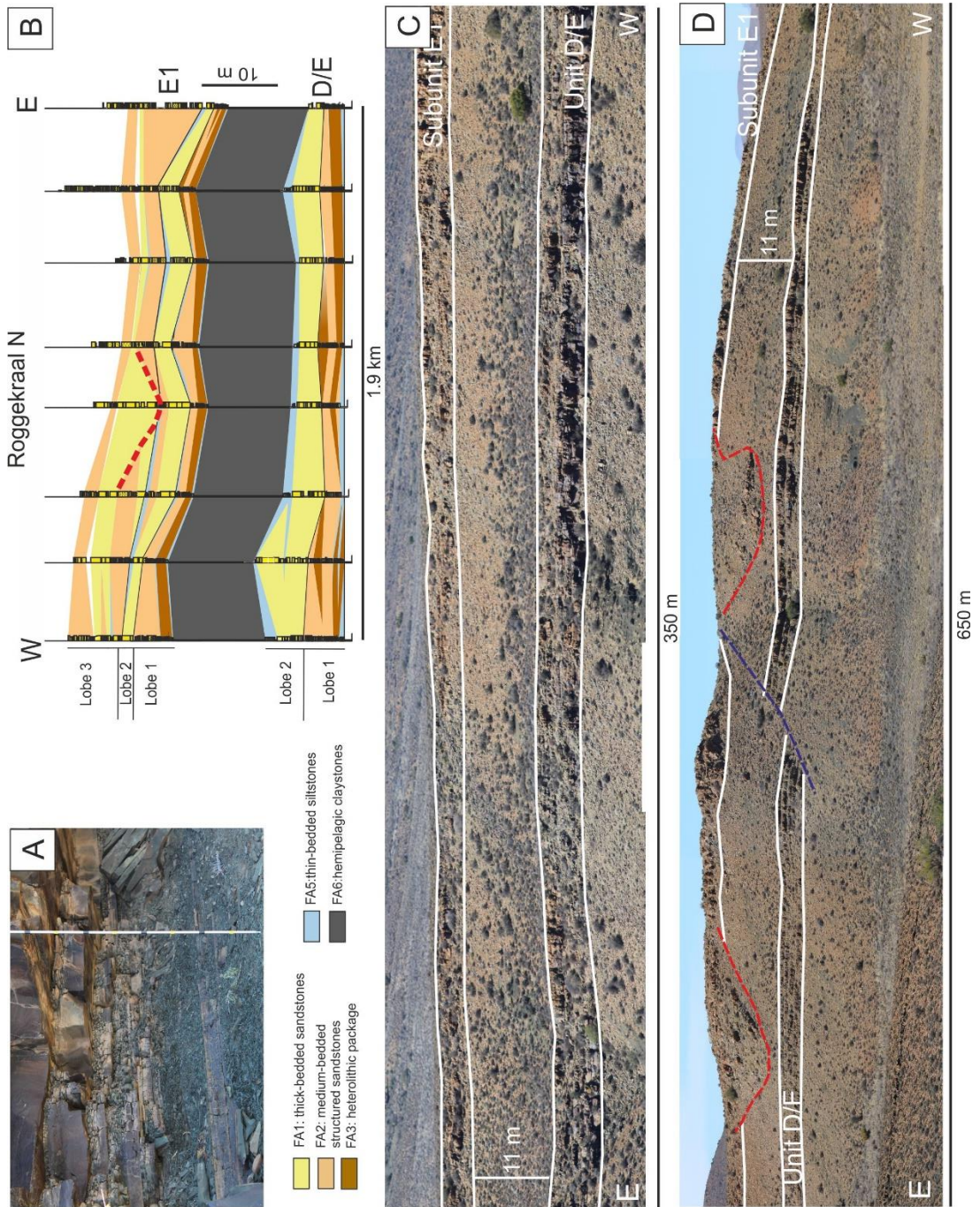
Figure 5.4. Representative photographs and correlation panel of the intraslope lobe complexes of Unit D/E and E1 in the Zoutkloof area and correlation panel for the Roggekraal N area. A) Coarsening- and thickening-upward at the base of the intraslope lobe deposits in Unit D/E. Logging pole with 10 cm gradations as scale. B) Roggekraal N correlation panel showing siltstone intervals that separate individual lobes in Subunit E1 and the two lobes of Unit D/E. Dashed red line represents erosion surface C) Tabular geometries of Unit D/E and Subunit E1 in the Zoutkloof N area. The sand-prone units are separated by a ~11 m thick mudstone. D) E1 channels cut down through E1 lobes and into the underlying claystone (Zoutkloof N).

The westward palaeocurrents in deposits in Zoutkloof S are interpreted to indicate rapid deposition of turbidity currents deflected and reflected off seabed topography at

the fringes of the intraslope lobe (Fig. 5.6). There is no evidence of incision into the Unit D/E deposits and no deposit of this age directly down-dip has been recognized (van der Merwe et al., 2014). The abandonment of Unit D/E suggests that either the sediment routing system avulsed outside of the study area or sand-grade sediment supply ceased prior to the complete infill of the slope accommodation.

Subunit E1. E1 is separated from Unit D/E by a 10-11 m thick mudstone, and has a basal ~0.5 m-thick interval of interbedded mudstone, siltstone and very fine-grained sandstone. The dominant palaeoflow is to the E, which is consistent with regional trends, whereas some deposits show palaeoflow to the W in the Zoutkloof S area (Figs. 5.5 and 5.6). Where thickest (14 m), E1 is characterised by structureless amalgamated sandstones (FA 1) and structured sandstones (FA 2). In Roggekraal N, to the north where E1 is 8 m-thick, 3 packages are identified by sharp contacts with thin-bedded siltstone (FA 5) units. The lowermost unit is dominated by heterolithic deposits (FA 3), the middle is dominated by FA 1, and the upper is dominated by FA 2 (Fig. 5.4b). In contrast, to the south at Zoutkloof S, E1 is thinner (5 m) and comprises heterolithic packages (FA 3) and thin-bedded siltstones (FA 5). E1 is not observed 6 km along strike to the south, which constrains the southward (lateral) pinch-out (Fig. 5.6). Locally, E1 is truncated by erosion surfaces from multiple stratigraphic levels (E1, E2, E3 and Unit F; Figueiredo et al., 2010, 2013; Fig. 5.6). Erosion surfaces within E1 cut down up to 10 m and are overlain by thick-bedded sandstones that have low aspect ratios (10:1 to 15:1; Fig. 5.4). Younger erosion surface commonly have higher aspect ratios (20: 1 to 35: 1; Fig. 5.5) and are overlain by thin bedded, and locally tightly folded, sandstones and siltstones (Figueiredo et al., 2010, 2013), but sand-filled younger channel-fills are also observed.

Interpretation. In Roggekraal N, thin siltstone packages that abruptly separate three axis and off-axis packages indicate the existence of three lobes in the lobe complex (Fig. 5.4). The distribution of the lobe axis and off-axis deposits, and the lobe fringe and distal fringe deposits of the individual lobes, suggest an aggradational to slightly compensational stacking pattern. Deviation from the regional palaeocurrent trend in Zoutkloof S is interpreted to indicate deflection and reflection of turbidity currents off seabed topography. Erosion surfaces overlain by sandstones are interpreted as W-E and NW-SE oriented channel-fills.
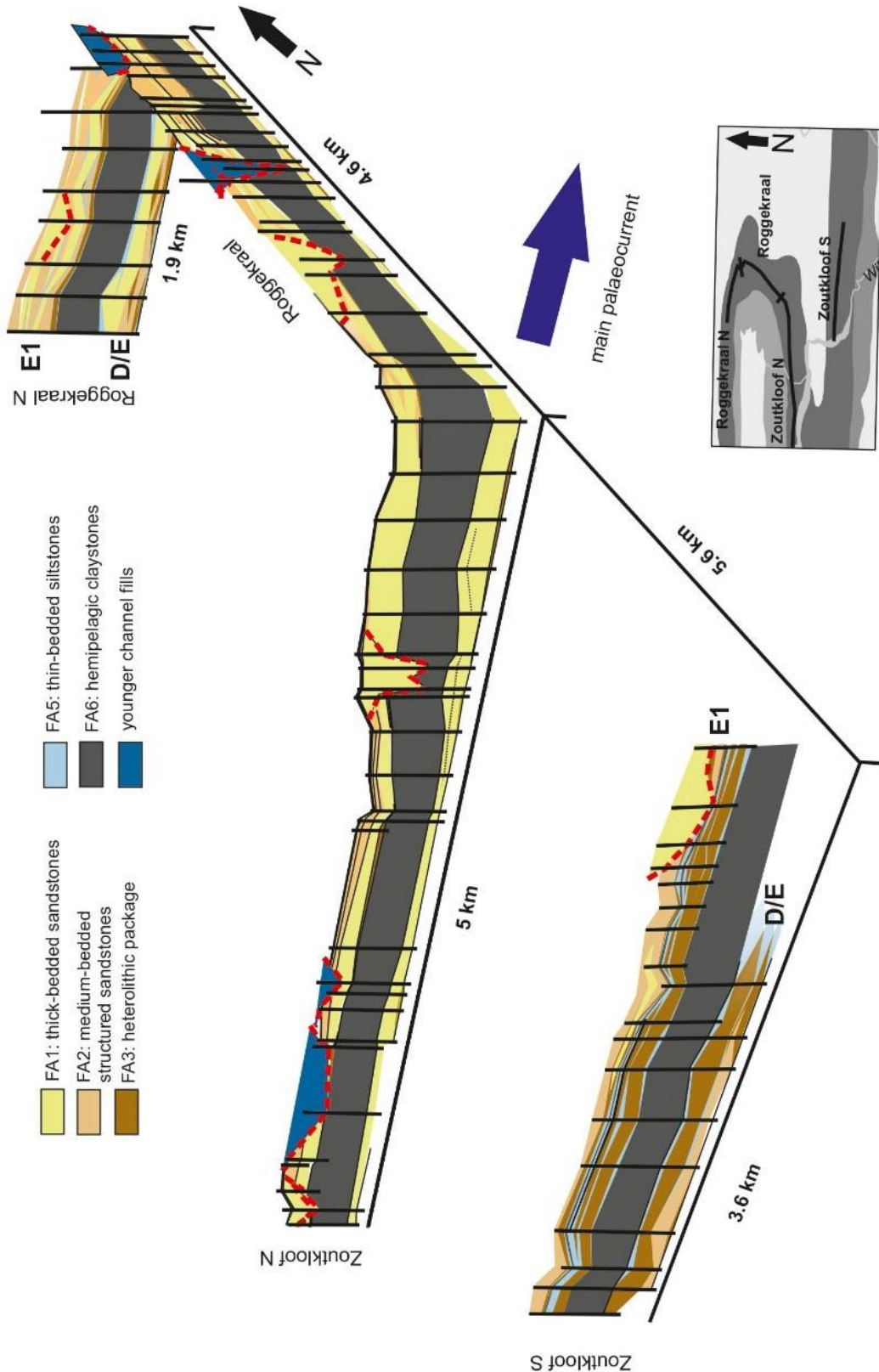
Figure 5.5. Correlation panels for Unit D/E and Subunit E1 in the Zoutkloof area. Overall axis of the lobe complexes of Unit D/E and Subunit E1 is located in the Roggekraal and Zoutkloof N areas. Towards the north and south lateral facies transitions can be observed and correspond to lobe off-axis and lobe fringe deposits. Note incision of Subunit E1 by younger channel-fills.
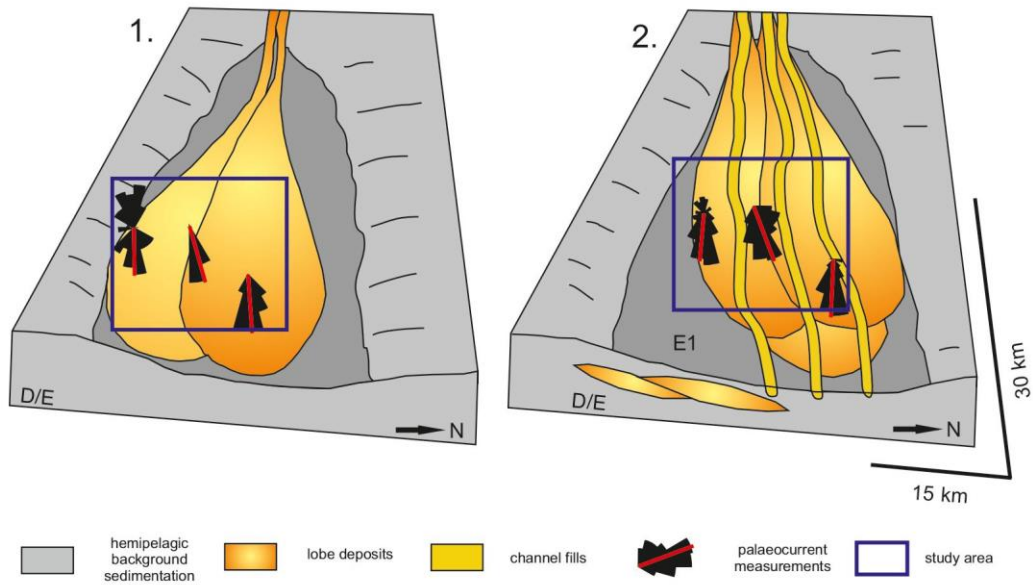
Figure 5.6. Simplified palaeogeographic reconstruction of 1) Unit D/E and 2) overlying Subunit E1 in the Zoutkloof area. Flows show evidence for deflection and reflection.

5.6.2 Geelbek area

Subunit E2. Subunit E2 comprises three packages based on thickness trends, facies distribution, bounding surfaces and palaeocurrents measurements (Figs. 5.7a-d and 8). The mean palaeocurrent direction is to the E, but with local variations (Fig. 5.8). The base of the lower package, E2A, consists of heterolithic deposits (FA 3) overlain by FA 1 and FA 2 beds with abundant dm-scale erosion surfaces (Fig. 5.9a). Commonly, medium-bedded, structured sandstones (FA 2) display more than one sedimentary structure vertically and laterally (planar lamination, ripple lamination and climbing-ripple lamination). Lateral facies transitions in individual beds include ripple-, through wavy-, to planar-lamination, which occur over 10s of metres.

In some beds, palaeocurrent measurements from stoss-side preserved climbing ripple-lamination can display ENE palaeocurrents in the lower section whereas the upper section preserves palaeocurrents to the WSW (e.g. Marker bed 1 (Mb1), see Fig. 5.7, 5.8 and 5.9a). Typically, these beds are thickest in the east and thin westward in an up-dip direction. Sedimentary structures change in the direction of thinning from stoss-side preserved climbing-ripple lamination, through planar lamination with isolated current-ripple forms, to planar laminated sandstones. The bases of some beds with bi-directional palaeocurrents (e.g. Marker bed 2 (Mb2), see Fig. 5.9a)

truncate underlying bedding with siltstones that display soft-sediment deformation structures (Fig. 5.7b).

The middle package, E2B, is defined by a stepped basal erosion surface that incises 6 m into E2A (Fig. 5.8). The overlying sediments comprise highly amalgamated thick-bedded sandstones (FA 1) with rare planar lamination on bed tops (Fig. 5.8). These pass vertically into more clearly stratified but internally structureless fine-grained sandstones close to the (oblique) margin of the cut and can be traced out for over a km away beyond the basal scour surface, where E2B overlies E2A concordantly (Fig. 5.7c). Palaeocurrents from grooves indicate an overall ENE-WSW flow direction (Fig. 5.8).

The upper E2C division is the most laterally extensive of Subunit E2 and the boundary with E2B is marked by a thin siltstone horizon (~10 cm; FA 5; Fig. 5.7d). It comprises basal bipartite beds (FA 4) in its proximal (westerly) section and is largely made up of medium-bedded, structured sandstones (FA 2) that overlie the highly
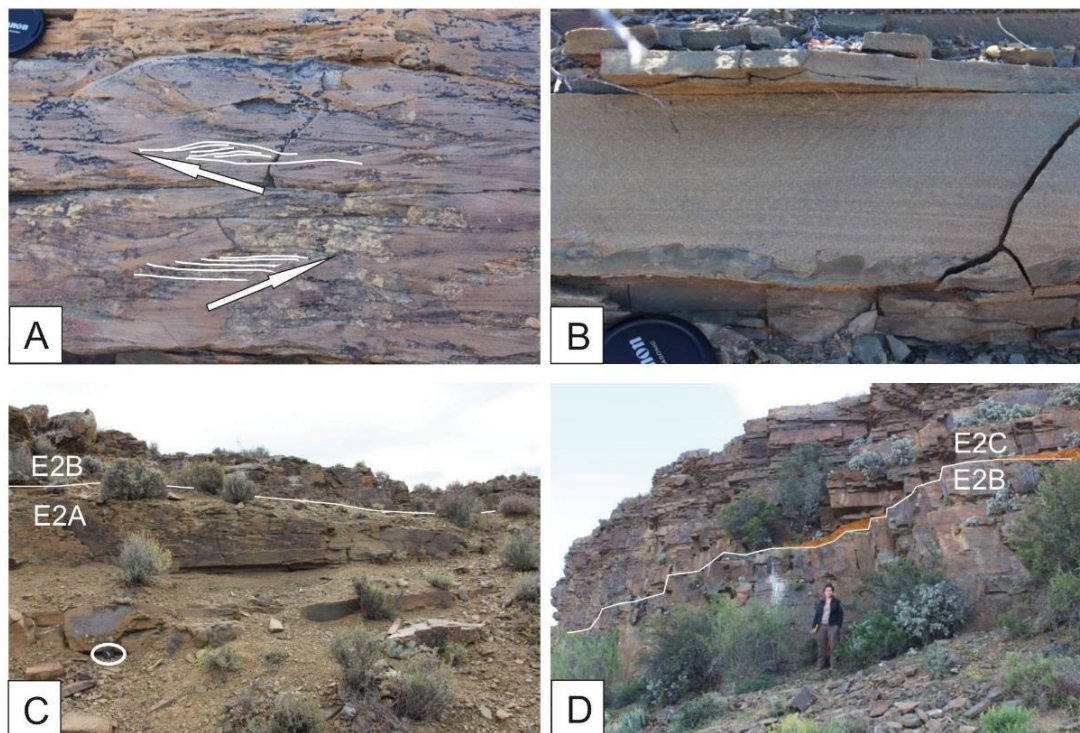
Figure 5.7. Representative photographs of the intraslope complex in the Geelbek area. A) Bed showing climbing-ripple lamination with opposing flow direction patterns. Camera lens cover as scale. B) Deformed mudstone interlayer with flames. Camera lens cover as scale. C) E2B overlies E2A outside of the basal scour surface. Camera lens cover as scale. D) E2B and E2C are separated by a thin (0.1 to 0.2 m thick; indicated by orange overlay) siltstone interval. Geologist (1.6 m) as scale.

amalgamated sandstones of E2B (FA 1). Thin-bedded deposits (FA 3 and FA 5) are rare. Palaeocurrents measured from current- and climbing-ripple lamination indicates an easterly flow direction (Fig. 5.8). In the west, beds are structureless (FA 1), with rare ripple lamination showing easterly palaeocurrents. Structureless sandstone beds onlap westward onto the underlying siltstone, overstepping the E2A and B deposits (Fig. 5.8). Commonly, the onlapping beds show pinching and swelling close to the onlap surface as well as evidence of erosion (rip-up clasts, truncation). Clastic injectites are abundant in the mudstone that underlies the sandstone onlap (Fig. 5.9b).

In the underlying claystone that separates Units D and E, a distinctive 0.4 m-thick intraformational mudclast-rich sandstone bed is used as a local marker bed. The sandstone bed and bounding claystones are present in western part of the outcrop. However, they terminate abruptly eastward against a steep surface overlain by a thin-bedded coarse siltstone and silty claystone succession below where the overlying E2 attains its maximum thickness (Fig. 5.8). The thin-bedded siltstone unit forms a discrete ~30 m-thick unit that thins out over ~700 m to the east; by contrast, the western edge is steep and abrupt (Fig. 5.8).

Interpretation. The high sand-content and tabular geometry, the underlying and overlying channel-levee systems (e.g. Brunt et al 2013b), and the downdip change to thin-bedded turbidites led van der Merwe et al. (2014) to interpret E2 as an intraslope lobe in the Geelbek area. The three divisions of E2 in Geelbek are interpreted here as lobe deposits that stack to form a lobe complex. In E2A, sandstone beds with bidirectional palaeocurrents and up-dip thinning are interpreted to indicate reflection of the flow column (Pickering & Hiscott, 1985; Kneller et al., 1991;Edwards et al., 1994; Kneller et al., 1999). Soft-sediment deformation was triggered either through instability on the open erosional slope or through dewatering due to deposition of overlying strata. This range of features is consistent with a confined setting at the onset of the filling of slope accommodation. The amalgamated deposits of E2B are interpreted to be deposited in a scoured lobe-axis setting. The scour-fill interpretation is preferred to a channel-fill interpretation because no mudstone clast conglomerate facies is observed, the geometries of the structureless sandstone beds are tabular and can be walked out for ~1.5 km away, and the erosion surface shallows in the direction of main palaeocurrent direction. E2C is the most laterally extensive of the subunits. Lack of bidirectional palaeocurrent indicators and dominance of climbing-ripple laminated medium-bedded sandstones indicates a relatively unconfined phase of deposition. Overall, the depocentre of successive E2 lobe deposits shifts slightly to

the W (up slope; Fig. 5.9). These findings conform to subsurface observations made in the Gulf of Mexico indicating temporal evolution of the locus of sedimentation (Prather et al., 2012b).

5.7 Discussion

5.7.1 Mechanisms of slope accommodations

Typically, submarine slope systems are dominated by sediment bypass (e.g. Beaubouef et al., 1999; Gardner et al., 2003; Romans et al. 2009; Hodgson et al., 2011). For lobate bodies to deposit on the submarine slope low gradient areas of high accommodation must be present. Here, the origin of this accommodation is discussed.

The formation of the intraslope lobe complexes of Unit D/E and Subunit E1 in a similar location, albeit slightly offset, demonstrates the presence of accommodation on Zoutkloof part of the palaeoslope through multiple depositional sequences. In the Zoutkloof area, there is no evidence of slide scars, syn-sedimentary tectonic or diapiric deformation of the seabed, or underlying mass transport complexes that could form an area of high accommodation (Figueiredo et al., 2010). However, in the underlying successions (Units A-D) the Zoutkloof area represents an overall off-axis position with abundant silt-prone deposits (levees and lobe fringes), and the main slope channel-levee systems to the south (e.g. Grecula et al., 2003 a; Sixsmith et al., 2004; Figueiredo et al., 2010) feeding sand-prone basin-floor lobe complexes to the east and north east (Di Celma et al., 2011; van der Merwe et al., 2014). Therefore, slope accommodation at Zoutkloof is interpreted to be the result of differential compaction of the underlying fine grained stratigraphy relative to the more sand-rich underlying stratigraphy to the south (Figueiredo et al., 2010) and east (van der Merwe et al., 2014).
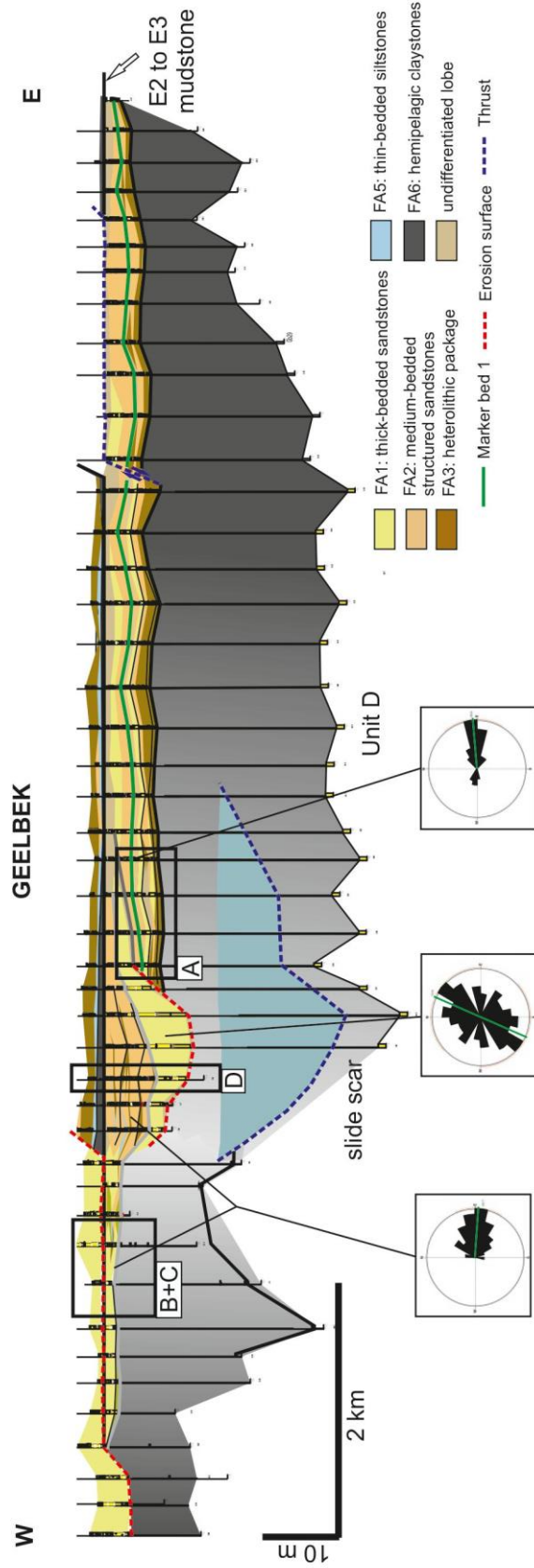
Figure 5.8. . Correlation of subunit E2 in the Geelbek area. Panel is hung from hemipelagic claystone between E2 and E3. Black boxes (A-D) indicate areas shown in detail in Figure 5.9. Note siltstone wedge within the mudstone interval which is interpreted to partially fill a slide scar.
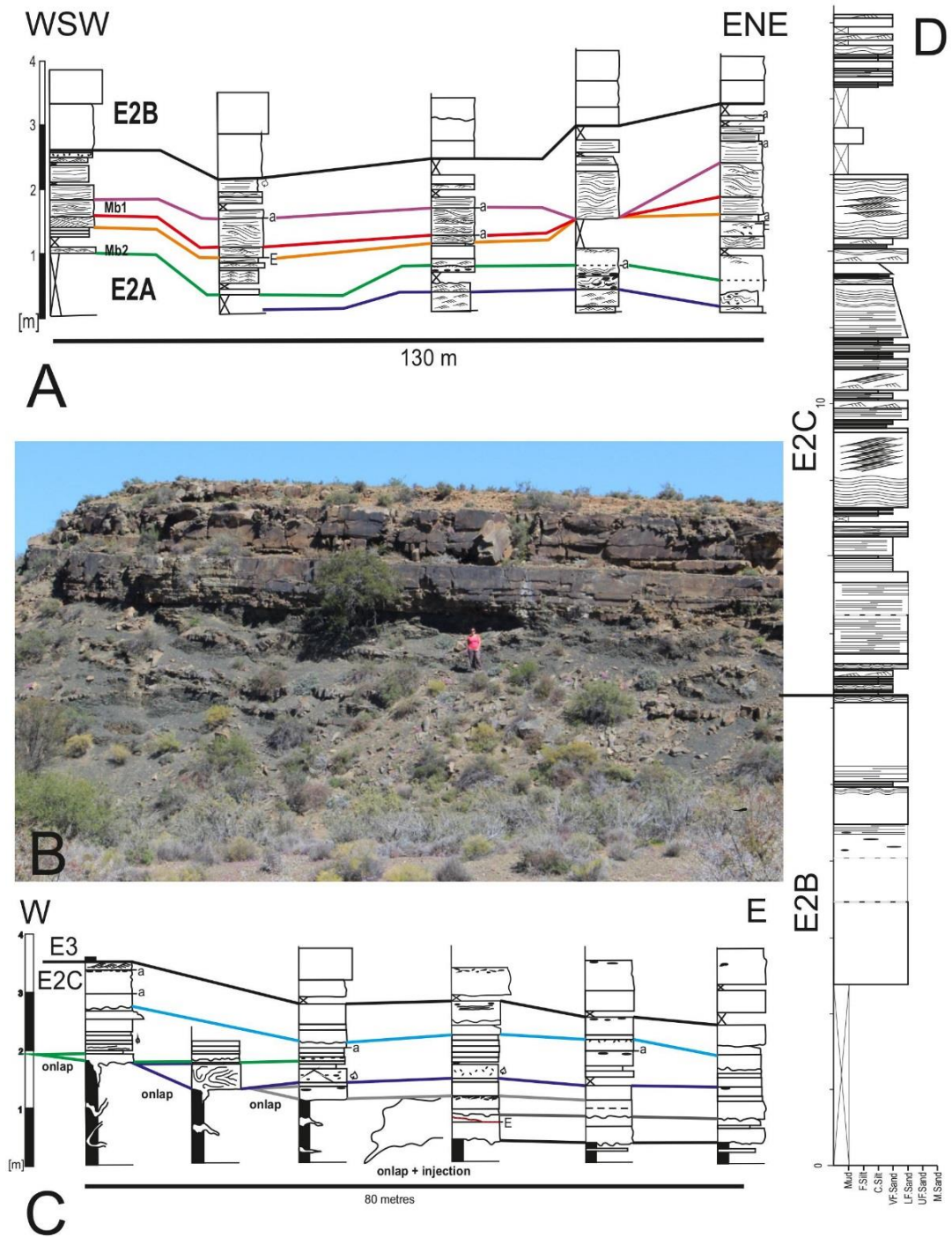
Figure 5.9. Details of the Geelbek correlation panel. A) Detailed correlation panel of E2A. Coloured lines represent bed correlations B) Injected mudstone below E2A with geologist as scale. C) Detailed correlation panel of the E2C onlap zone. 'a' marks amalgamation surfaces, 'E' erosion surfaces. Coloured lines represent bed correlations D) Example graphic log through high-amalgamation zone of E2B overlain by well bedded, structured sandstone beds of E2C.

The geometries of architectural elements, palaeocurrent measurements, and facies distributions in Subunit E2 indicate a depositional setting that evolved from highly- to weakly-confined. E2A was deposited on the partially healed accommodation (Fig. 5.10) and beds show evidence for flow deflection and reflection. E2B deposits show a slightly different main palaeocurrent direction and formed above an erosion surface that cuts into E2A and shallows downdip (Fig. 5.10). E2C shows onlap against the open slope when the accommodation was infilled (Fig. 5.10).

At the regional-scale, sedimentary features in the Geelbek area have been shown to form part of a step in a stepped slope profile with a ramp and sediment bypass ~ 2 km basinward of this area (van der Merwe et al., 2014). A large slide scar has been interpreted at the top of the underlying Unit D in this locality (Brunt et al., 2013b). In this study, an abrupt facies change from claystones with a clast-rich sandstone marker bed to a 30 m-thick asymmetric wedge of thin-bedded siltstone (Fig. 5.8) in strata underlying Subunit E2 has been identified. This is interpreted to indicate the presence of a W-E oriented slide scar that formed near the step-to-ramp transition area prior to the initiation of Unit E, but was only partially healed, and could have modified and amplified the accommodation for the E2 intraslope lobe complex (Fig. 5.10).

5.7.2 Diagnostic criteria for intraslope lobe deposits

The identification of key characteristics of intraslope lobes compared to basin floor lobes can aid their identification in less well constrained subsurface and outcrop datasets (Fig. 5.11a). Geometries and architecture have been compared using published data from basin floor lobes in the Karoo Basin (Fan 3, Tanqua depocentre, Prélat et al., 2009; Unit A, Laingsburg depocentre, Prélat & Hodgson, 2013) with intraslope lobes of Units D/E and E (Table 5.1).
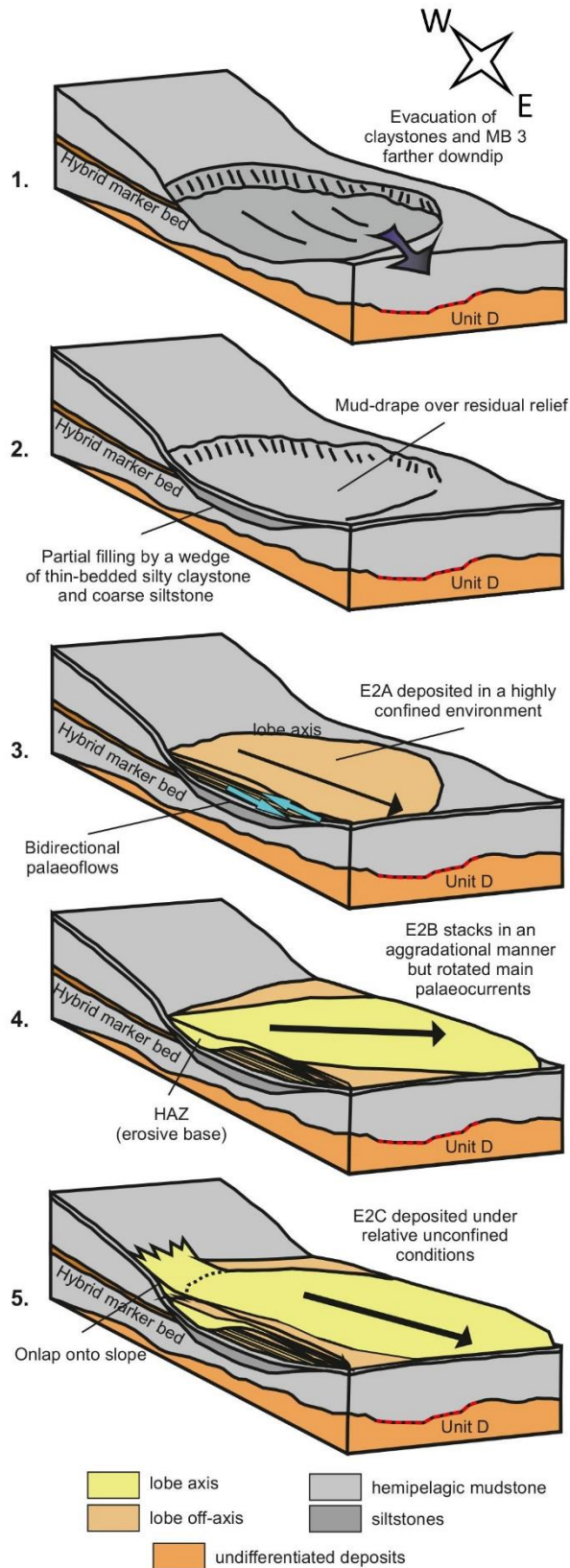
Figure 5.10. Simplified palaeogeographic reconstruction of subunit E2 in the Geelbek area. 1) slide removes hemipelagic claystone and marker bed 3 (MB3). Surface is steep in the west and shallows to the east. 2) thin-bedded siltstone beds partially infill scar, which is also draped by hemipelagic mudstone. 3) deposition of confined sediments of E2A. 4) E2B locally scours into E2A. 5: onlap of E2C deposits to the west. Slope feeder channels are not exposed in the field and therefore not displayed.

	Intraslope lobes	Basin-floor lobes
Depositional setting	Slope	Basin floor/ terminal end of system
Degree of confinement	Weak to high	Unconfined to weak
Stacking patterns	Aggradational to slightly compensational	Compensational
Aspect ratio	Low	High
Sand percentage	Average: 70% (>90% lobe axis; 50% lobe fringe)	Average: 60% (>80% lobe axis; <40% lobe fringe)
Sediment features	Immature sandstones, moderate sorting, micas and mud chips abundant, sediment features reflect highly variable flow patterns, paucity of hybrid beds, depleted of fine grained sediments	Relative mature sandstones, fair to good sorting, abundance of hybrid beds in lobe fringe positions, fines concentrated in lobe fringe deposits, rich on mud clast and carbonaceous material in banded facies

Table 5.1. Comparison chart of the main sedimentological and stratigraphic characteristics of intraslope lobes and basin-floor lobes in the Laingsburg depocentre, Karoo Basin.

Dimensions

The lobe complexes are 6 to 10 km wide, 15 to 25 km long and 10 to 15 m thick. In volume, they are an order of magnitude smaller than dimensions of basin floor lobe complexes quoted in Prélat et al. (2010), which are 10 to 30 km wide and 30 to 100 m thick.

Lobe stacking patterns

Lobes stack to form lobe complexes (Deptuck et al., 2008; Prélat et al., 2009), and the patterns of stacking of lobes within such complexes provide an insight into the degree of confinement (Deptuck et al., 2008; Straub et al., 2009). Generally, an aggradational to slightly compensational style of stacking is observed within intraslope lobes of the Fort Brown Formation (Fig. 5.11). This characteristic is also identified from subsurface studies of recent deepwater systems (Ferry et al., 2005; Barton, 2012). In contrast, basin floor lobes exhibit markedly compensational styles of stacking, indicative of relatively unconfined settings (Prélat et al., 2009; Straub et al., 2009; Groenenberg et al., 2010).

Sedimentary facies and features

Intraslope lobe-axis deposits share similar facies associations with basin floor lobes (e.g. Prélat et al., 2009). Off-axis deposits of intraslope lobes are characterised by an abundance of medium bedded ripple- and climbing ripple-laminated sandstones (Fig. 5.11). Successions of climbing-wavy-climbing lamination or ripple-wavy-ripple lamination are indicative of highly unsteady flows with high rates of sediment fallout. Individual beds can preserve ripple forms and climbing ripple-lamination that yield palaeoflow directions oriented at a high angle or even opposite to each other (Fig. 5.11), indicating deflection and reflection of the turbidity current during sedimentation. Commonly, basin floor, lobe fringe deposits contain numerous bipartite beds (Hodgson, 2009), and these are relatively rare in intraslope lobe fringe deposits. Erosion surfaces mantled with mudclasts are more common in intraslope lobe axis and lobe off-axis deposits than in basin floor lobe systems because proximity to channels and flow confinement leads to more entrainment of fine-grained substrate. Basin floor lobes also display erosion surfaces in the lobe axis, leading to amalgamation of thick-bedded sandstones by removal of intervening thin beds (Stephen et al., 2001; Prélat et al., 2009). However, erosion surfaces in basin-floor lobes are more subtle than in the intraslope lobes. In basin floor lobe systems, facies transitions occur over several kilometres, both frontally and laterally (e.g. Prélat et al. 2009; Groenenberg et al. 2010), whereas in intraslope lobe systems, facies transitions occur over shorter distances (typically over 10+ m), as observed in Unit E2 in the Geelbek area (Fig. 5.9).

Sand percentage

Overall, intraslope lobe deposits are characterised by a higher percentage of sandstone than basin floor lobe deposits because sand becomes trapped preferentially in areas where available accommodation is limited compared to flow depth (Brunt et al., 2004). If the flow height is greater than the relief of the confinement then the upper fine-grained part of the flow can be stripped, which will increase the proportion of sand that is accumulated (Sinclair & Tomasso, 2002; Prather et al., 2012b). Basin floor lobes of Unit A have an average sandstone percentage of 60% , with >80% in lobe axes and < 40% in distal lobe fringe settings (Prélat et al., 2009); intraslope lobes of Unit D/E and E show an average of 75% sandstone, with >90% in lobe axes and <50 % sandstone in lobe fringes (Table 5.1 and Fig. 5.11b).
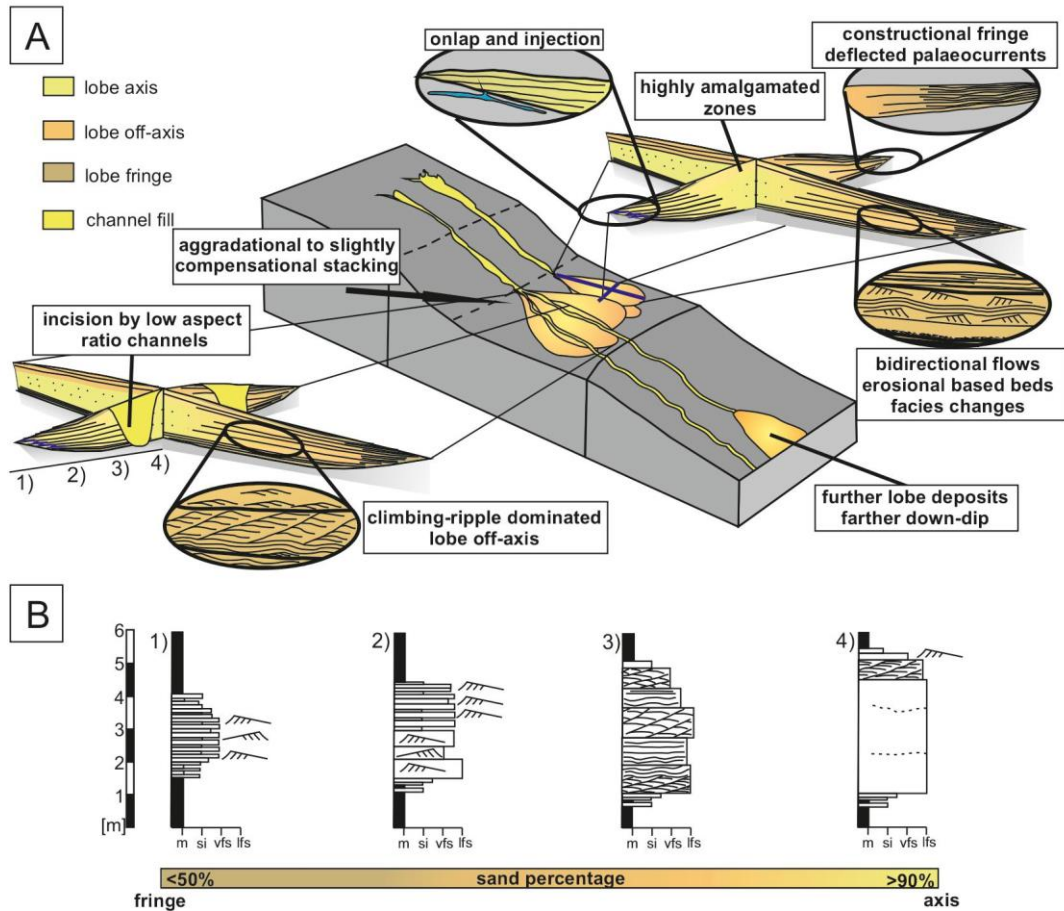
Figure 5.11. A) Block diagram showing the key recognition criteria of intraslope lobes. Aggradational to slightly compensational stacking patterns; onlap combined with injection onto mud-prone slope; highly amalgamated zones in the lobe complex axis; subtle confinement leads to fringes that show aggradational stacking; high degree of confinement leads to preservation of beds with evidence of flow deflection, erosional based beds and abrupt facies changes; climbing-ripple lamination is the dominant facies of the lobe-off axis; incision by low-aspect-ratio channels that originate in the same unit as the intraslope lobes; more lobe deposits can be found down-dip on the basin-floor or on steps basinward on the slope. B) Simplified logs of typical thicknesses and stacking patterns from lobe axis to lobe fringe (downdip and laterally) in intraslope lobes that are observed over a few kilometres. Note position of the schematic logs from fringe (1) to axis (4) in A).

Incision of intraslope lobes by channels

Commonly, intraslope lobes are incised by channels (e.g. Adeogba et al. 2005). Incision of the E1 lobe complex by low-aspect-ratio channel systems of different ages, including E1-aged channels, indicates that when the accommodation had been filled, slope channel systems could develop in response to a lower base level. This indicates that slope accommodation in this area was transient. This is supported by the

identification of thick basin floor lobe complexes of Unit E age farther into the basin by van der Merwe et al. (2014).

5.8 Conclusions

Three exhumed intraslope lobe complexes, constrained by stratigraphic and geographic position based on extensive and detailed correlation and mapping in the Laingsburg depocentre, Karoo Basin, were studied to establish their sedimentological and stratigraphic characteristics.

In the study area, intraslope lobe complexes are 6 to 10 km wide and extend 15 to 25 km in down-dip directions; areal extent is controlled by the area over which slope accommodation was generated. The deposits are sandstone-rich and lack significant siltstone. Stacking patterns are aggradational to slightly compensational depending on the amount of confinement. The lobe axis is dominated by thick-bedded, amalgamated sandstones. The lobe off-axis mainly comprises medium-bedded climbing-ripple laminated sandstones. The lobe fringe is characterised by ripple- and climbing ripple-laminated sandstones that can show flow deflection and reflection, and are interbedded with siltstones. Lateral and vertical facies changes occur over tens of metres and demonstrate highly variable, unsteady depositional flows that interacted with, and were governed by, underlying sea-bed topography and surrounding confinement. Two mechanisms are proposed for the development of accommodation on the Karoo slope: differential compaction and scars formed by mass wasting processes. The presence of intraslope lobe complexes supports regional interpretations that the slope of the Laingsburg depocentre developed a series of steps. These sub-seismic-scale observations and interpretations provide possible analogues to sub-surface examples identified on geophysical data for which information relating to detailed internal sedimentary architecture is not available.

The development of sedimentological and stratigraphic recognition criteria for identification of intraslope lobes will permit improved reconstruction of the stratigraphic evolution of continental margins. However, the depositional architecture will vary across systems depending on the mechanism responsible for slope accommodation, the areal extent of the accommodation, and the ratio of flow size and the degree of confinement.

Chapter 6

Is hybrid bed distribution in basin-floor fans predictable?

6.1 Abstract

Hybrid beds, which are the deposits of flows that show more than one flow regime (turbulent, transitional and/or laminar), have been recognized as important elements of submarine lobe deposits. The range of hybrid bed types has been widely documented, however, quantitative analyses of the distribution of these deposits is rare. Here, extensive exposures supplemented by research borehole data from Unit A of the Laingsburg Formation and Fan 4 of the Skoorsteenberg Formation, South Africa, provide the means to examine geographical and stratigraphic patterns over a range hierarchical scales (from lobe to lobe complex set).

For this purpose, >23,000 individual beds have been evaluated for deposit type and bed thickness, and hybrid beds make up <17 % of all events in a lobe complex. A prominent geographical trend shows that hybrid bed deposits become more prevalent towards the frontal fringes of a lobe complex. Vertical stacking of clean sandstones, thin-bedded heterolithic deposits and hybrid-bed prone deposits is dependent on the dominant stacking pattern (aggradational, compensational, progradational and retrogradational) of lobes within a lobe complex as this controls the vertical stacking of clean sandstones, thin-bedded heterolithic deposits and hybrid-bed prone deposits. Rather than being dominantly controlled by processes on the slope as suggested hitherto, the occurrence and distribution of hybrid beds is interpreted to be controlled by flow transformation processes on the basin-floor.

This has implications for reservoir evaluation and the recognition of lobe stacking patterns in 1D core data sets.

6.2 Introduction

Basin-floor lobes generally comprise three deposit types: turbidites, hybrid beds and debrites (Talling et al., 2004; Hodgson, 2009; Etienne et al., 2012). The distinction of their flow processes and their quantitative importance regarding the overall

succession is important from a hydrocarbon exploration and production perspective. In particular, understanding controlling factors on the geographical and stratigraphic distribution of hybrid event beds introduces bed-scale reservoir heterogeneities due to the vertical juxtaposition of reservoir and non-reservoir lithologies (Davies et al., 2009; Haughton et al., 2009). Core and outcrop data sets (e.g. Haughton et al., 2003; Talling et al., 2004; Ito, 2008; Davies et al., 2009; Haughton et al., 2009; Hodgson, 2009; Jackson et al., 2009; Magalhaes & Tinterri, 2010; Kane & Pontén, 2012; Patacci et al., 2014; Fonnesu et al., 2015) enabled different hybrid bed classifications to be established, and experiments have been conducted to study the flow processes that control hybrid bed deposition (Baas et al., 2009; Sumner et al., 2009; Baas et al., 2011).

Several studies have indicated that hybrid bed deposits occur in the distal parts of submarine fan and lobe settings (Talling et al., 2004; Ito, 2008; Hodgson, 2009; Pyles & Jennette, 2009; Talling et al., 2012a; Etienne et al., 2012; Kane & Pontén, 2012; Grundvåg et al., 2014; Collins et al., 2015; Fonnesu et al., 2015). Where hybrid beds have been observed in more proximal lobe settings (Ito, 2008; Jackson et al., 2009; Patacci et al., 2014; Southern et al. 2015) enhanced erosion and deceleration have been invoked due to processes occurring in the channel-lobe transition zone and basin confinement. Their stratigraphic distribution has been linked to the character of the supply slope and seabed relief. Hybrid beds are suggested to develop during periods of disequilibrium over steep, out-of-grade slopes (Haughton et al., 2003; 2009; Hodgson, 2009), and therefore are dominantly deposited during fan initiation and growth, or initiated by flow expansion in the channel-lobe transition zone (Ito, 2008; Kane & Pontén, 2012). Quantitative analysis on the geographic and stratigraphic distribution, and therefore predictability of these deposits has seldom been attempted. Davis et al. (2009) presented statistical analysis on hybrid bed deposits from the outer Forties Fan, Central North Sea. They assessed >1000 event beds of which 67% were hybrid beds. Their significance in terms of bed thickness was even higher (81%). However, this analysis incorporated data from different field areas. Correlation between the fields was hindered by field-specific fossil assemblages.

Here, we present a quantitative analysis of geographic and stratigraphic hybrid bed distribution trend from an outcrop and core data set from the palaeogeographically well-constrained Fan 4 (Skoorsteenberg Formation, Tanqua depocentre) and Unit A (Laingsburg Formation, Laingsburg depocentre) of the Karoo Basin, South Africa. Specific objectives are to: 1) establish proximal to distal trends of hybrid beds within

a lobe complex; 2) examine stratigraphic trends at lobe complex set, lobe complex and lobe scale; and 3) discuss the factors that control the observed trends.

6.3 Geological Setting

Traditionally, the Karoo Basin has been interpreted as a retroarc foreland basin connected to a magmatic arc and fold-thrust belt (Visser & Prackelt, 1996; Visser, 1997; Catuneanu et al., 1998). More recently, Tankard et al. (2009) suggested that subsidence during the early deep-water phase of deposition pre-dates the effects of loading by the Cape Fold Belt and was instead induced by dynamic topography associated with mantle flow processes coupled with distant subduction of the palaeo-Pacific plate (Pysklywec & Mitrovica, 1999). This study focusses on deposits of the Ecca Group (Wickens, 1994; Flint et al., 2011) from that early deep-water phase of deposition in the Tanqua and Laingsburg depocentres of the southwest Karoo Basin (Fig. 6.1a). In both areas, the Ecca Group represents a shallowing-upward succession of sediments from deep-water to fluvial settings (Flint et al., 2011; Fig 6.2).

6.3.1 Tanqua depocentre

The Tanqua depocentre is located in the southwest of the Karoo Basin adjacent to the Cederberg branch of the Cape Fold Belt (Fig. 6.1a, b). This study focuses on deposits of Fan 4 of the Skoorsteenberg Formation (Fig. 2), one of four sand-prone basin-floor channel-lobe systems (Bouma & Wickens, 1991; Wickens, 1994; Wickens & Bouma, 2000; Johnson et al., 2001; Hodgson et al., 2006; Prélat et al., 2009). Fan 4 is up to 65 m thick (Johnson et al., 2001) and is built of three sand-rich lobe complexes (LC1, 3, 5) that are separated by thin-bedded deposits of lobe complex fringes (LC2, 4; cf. see Chapter 3). Data used for this study were collected from LC1, the basal lobe complex of Fan 4. Palaeocurrents and thickness distributions indicate that sediment was sourced from the southwest and transported north and northeast (Wickens & Bouma, 2000; Hodgson et al., 2006). Outcrops and cores for this study were measured from strategically chosen locations (Fig. 6.1b) in order to collect a data set that provides a 3D constraint on the geographical distribution of hybrid beds.
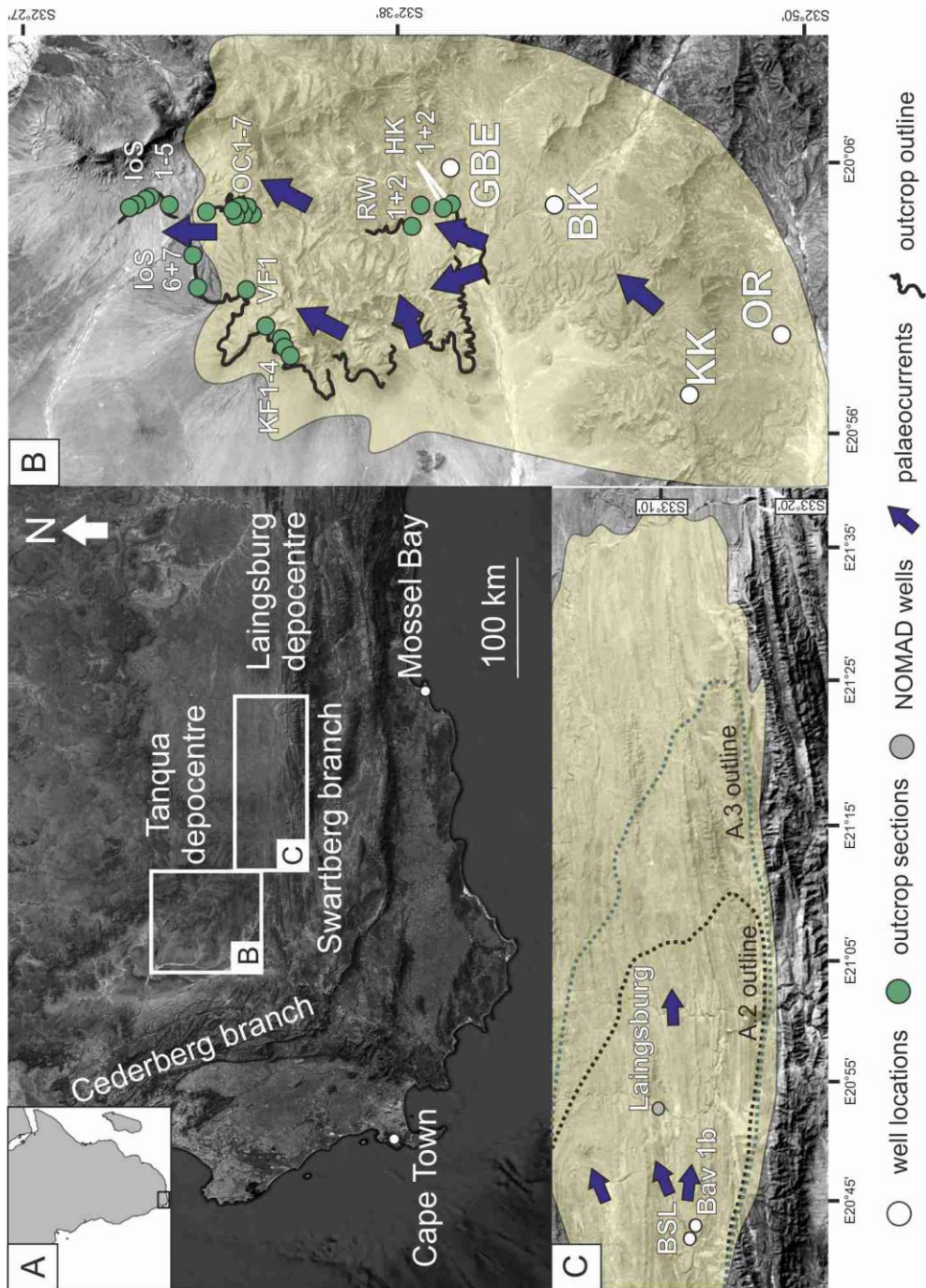
Figure 6.1. A: Geological setting of the two study areas inboard of the two branches of the Cape Fold Belt; B: Schematic outline of the lower lobe complex of Fan 4 (Skoorsteenberg Formation, Tanqua depocentre and outcrop and core locations); C: Schematic outline of Unit A and locations of the BSL and Bav 1b cores. Outlines of A.2 and A.3 are modified after Sixsmith et al., 2004. A more detailed pull-out map can be found at the back of the thesis.
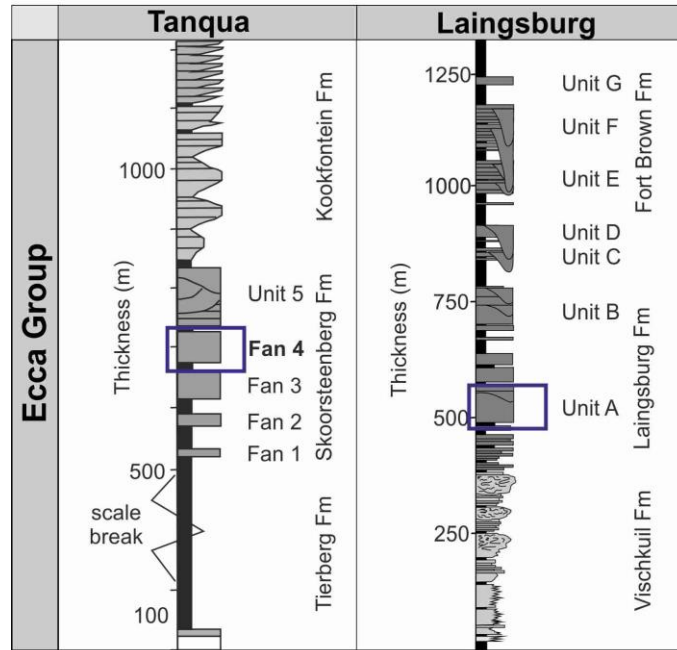
Figure 6.2. Stratigraphy of the Tanqua and Laingsburg depocentre; based on Wild et al. (2009) and Flint et al. (2011). The studied fan systems are highlighted with blue boxes.

6.3.2 Laingsburg depocentre

The Laingsburg depocentre is located approximately 80 km southeast of the Tanqua depocentre, adjacent to the Swartberg branch of the Cape Fold Belt (Fig. 6.1 a, c). The proximal basin-floor system of the Laingsburg Formation is subdivided into Unit A (Sixsmith et al., 2004; Prélat & Hodgson, 2013; Hofstra et al., 2015) and Unit B (Grecula et al., 2003a; Brunt et al., 2013a; Fig. 6.2). Units A and B are separated by a 40 m thick hemipelagic mudstone, which contains a thin sand-prone unit referred to as the A/B Interfan (Grecula et al., 2003a; Fig. 6.2). The stratigraphy of Unit A was subdivided by Sixsmith et al. (2004) into seven sand-prone subunits called A.1 to A.7. The subunits are separated by regional hemipelagic mudstone horizons. In agreement with Prélat & Hodgson (2013), subunits A.4 and A.7 have been re-interpreted as lobe complexes within Subunits A.5 and A.6, respectively, as there is no true hemipelagic mudstone separating them. Long-term progradational-aggradational-retrogradational stacking patterns have been described by several authors (Sixsmith et al., 2004; Flint et al., 2011).The studied cores (BSL and Bav 1b; Fig. 6.1c) were obtained from the 'Skeiding' area within the post-depositional Baviaans anticline and assessed for stratigraphical trends in hybrid bed distribution.

6.4 Methodology

For this study, 23,068 beds were individually assessed for their facies (turbidite, hybrid bed, debrite). The percentage of hybrid beds within subunits and lobe complexes was established in two ways: 1) as percentage of events; and 2) as percentage of bulk thickness. To determine the geographical distribution of hybrid beds ~11,000 beds from Tanqua Fan 4 were evaluated. The data set for this part of the study includes data from four research wells (OR, KK, BK and GBE) as well as outcrop data. The deposits of Fan 4 were examined on a lobe complex scale. Evaluation was limited to the basal three lobe complexes (LC1, LC2 and LC3) as these are extensive across the whole study area. Additionally, their palaeogeography is well known (cf. Hodgson et al., 2006; Chapter 3). To evaluate stratigraphic trends in hybrid bed distribution, ~12,000 beds of the BSL and Bav 1b cores (Laingsburg depocentre) were examined. The core locations are 1.58 km apart, and Bav 1b is located obliquely down-dip of BSL. Distribution was established for subunits A.1 - A.6. To compare detailed distribution trends on lobe complex scale in BSL and Bav 1b, moving averages were established for A.2 and A.3. For this purpose, the sections were divided into equal intervals (in this case 0.9 m) and the proportion of structureless sandstone, structured sandstone, siltstone, hybrid beds, debrites and claystone was determined and depicted graphically next to the core data set.

6.5 Facies

For the purpose of this study, deposits have been classed as turbidites, hybrid beds or debrites. Below a short description of the detailed facies is given. Sedimentary facies and related environments of deposition have been described in detail previously for the Skoorsteenberg Formation (e.g. Morris et al., 2000; Johnson et al., 2001; van der Werff & Johnson, 2003a; Hodgson et al., 2006; Luthi et al., 2006; Prélat at al., 2009; Hodgson, 2009, Jobe et al., 2012; Hofstra et al., 2015; Chapter 3) and Laingsburg Formation (e.g. Grecula et al., 2003a, b; Sixsmith et al., 2004; Hofstra et al., 2015; Chapter 4).

6.5.1 Turbidites

Description. Turbiditic deposits include structureless sandstone, structured sandstone, banded sandstone and siltstones (Fig. 6.3a-g). Structureless sandstones are medium- to thick-bedded (>0.2 to 2 m), moderately to well sorted and lower fine to upper fine grained (Fig. 6.3a, e). Bed bases are sharp, erosive (with or without rip-up clasts present), amalgamated, or loaded and commonly show flute and tool marks. Beds can show weak normal grading, passing to very fine-grained sandstone at their top.

Structured sandstones are thin- to medium-bedded (0.1 to 0.7 m), very fine to fine-grained and well sorted. They display a range of sedimentary structures (Fig. 6.3b, f) including planar lamination, current-ripple lamination, climbing-ripple lamination and rarely wavy laminations. Current-ripple lamination foresets may be draped by silt laminae. Climbing-ripple lamination commonly displays a low angle of climb and stoss-side preservation.

Banded sandstones are thin- to thick-bedded (0.1 to 1.5 m) and display couplets of light and dark bands (Fig. 6.3c). The darker bands are clay-rich and less well sorted than the lighter 'clean' sandstones that commonly load into the darker bands. The thickness of clay-rich bands varies from 1 to 30 mm.

Siltstones are very thin- to thin-bedded (0.01 to 0.2 m) and fine to coarse grained. They are structureless, planar laminated or current-ripple laminated (Fig. 6.3d, g). Current ripple lamination is observed, where the siltstones have a sandy component. Siltstones commonly show bioturbation.

Processes. Medium- to thick-bedded structureless sandstones are interpreted to be deposited by high-density turbidity currents (Kneller & Branney, 1995) with high aggradation rates (Arnott & Hand, 1989; Leclair & Arnott, 2005; Talling et al., 2012), which act to suppress the formation of sedimentary structures (Davis et al., 2009).

Structured thin- to medium-bedded sandstones are interpreted to be deposited by low-density turbidity currents. Planar and current-ripple lamination are produced by reworking through dilute flows along the bed (Allen, 1982; Southard, 1991; Best & Bridge, 1992). Climbing-ripple lamination forms under bedload transport associated

with high aggradation rates (Allen, 1973; Hunter, 1977; Jobe et al., 2012; Talling et al., 2012a). Wavy or sinusoidal lamination has been interpreted to indicate deposition from waning currents with very high rates of suspension fallout (Allen, 1973; Jopling & Walker, 1968; Hunter, 1977).

Banded sandstones are interpreted to form under aggradational but fluctuating flow conditions as in traction carpets of high-density currents (Lowe, 1982, Sumner et al., 2008, Talling et al., 2012a).

Thin-bedded siltstones are interpreted to be deposited by dilute turbidity currents. Planar lamination is a product of traction (Stow and Piper, 1984; Mutti, 1992; Talling et al., 2012a). Structureless beds are formed by direct suspension fallout (Bouma, 1962).

6.5.2 Hybrid beds

Description. Hybrid beds are thin-to thick-bedded (0.05 to 1.5 m) and include a lower and upper division (Fig. 6.4). The lower division is well sorted, fine-to very fine-grained commonly structureless and dewatered sandstone that can have a sharp, loaded or erosive base. Rip- up clasts at the base and dewatering features are common. Mudstone chips (up to 10%) can be observed to the top of the lower division. The upper division is poorly sorted mud-rich and argillaceous. It can comprise plant fragments, mudstone chips, mudstone/siltstone clast and outsized grains compared to the overall grain size of the bed. Characteristically, the fabric is swirly and patchy. In addition, it is often injected by the underlying clean sandstone. In rare cases, the upper division can be mudstone clast-rich well sorted sandstone (cf. D3 of Hodgson, 2009). Mudstone and siltstone clasts and fragments show no preferred orientation.

 Processes. Three models are invoked for the formation of hybrid bed deposits: 1) Deposition by independent debris flows and turbidity currents that were generated almost simultaneously through slope failure (cf. Georgiopoulou et al., 2009); 2) Deposition by co-genetic turbidity current and debris flow through longitudinal flow transformation (cf. Haughton et al., 2003; Talling et al., 2004; Ito, 2008; Davies et al.,
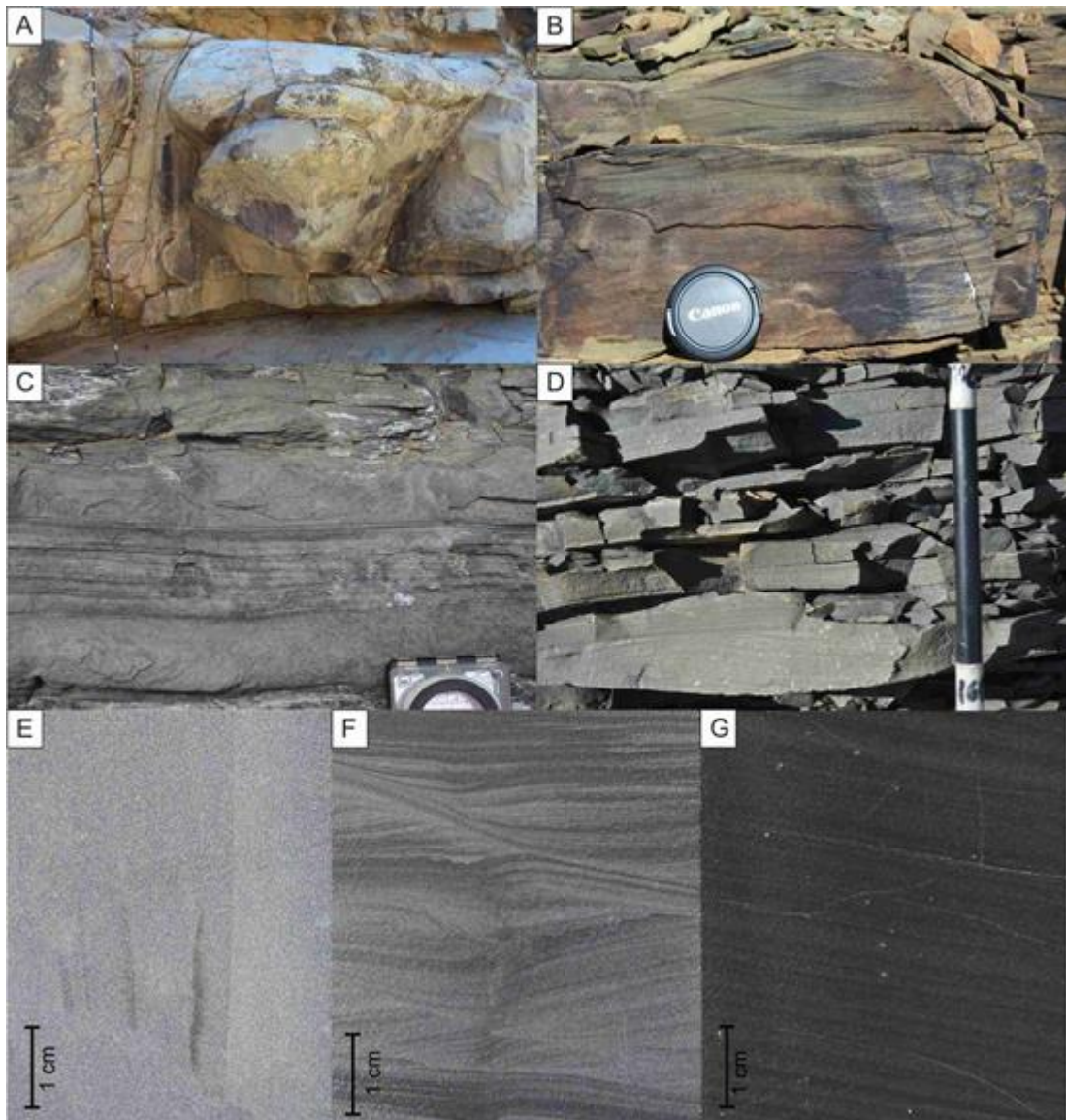
Figure 6.3. Representative photographs from outcrop and core for turbidite facies. A: Structureless sandstone. Logging pole (10 cm increments) as scale. B: Ripple laminated sandstone. Camera lens cover (7 cm) as scale. C: Banded sandstone. Compass as scale. D: Planar and ripple laminated siltstone. Logging pole (10 cm increments) as scale. E: Dewatered structureless sandstone. F: Ripple laminated sandstone. G: Siltstone.

2009; Haughton et al., 2009, Hodgson, 2009; Jackson et al., 2009; Magahlaes & Tinterri, 2010; Patacci et al., 2014); and 3) deposition initiated through grain-size segregation due to deceleration of a supersaturated turbidity current (cf. Baas et al., 2009; Sumner et al., 2009; Kane & Pontén, 2012).

6.5.3 Debrites

Debrites are thick- to thin-bedded (0.2 to 3.0 m), poorly sorted sandstones with a high mud content and outsized quartz grains (upper fine sand). Their fabric is swirly and patchy. Commonly these deposits comprise variable amounts of mudstone chips, mudstone and siltstone clasts, and carbonaceous material that show no preferred orientations. Clast size ranges between 1 and 35 cm in diameter.

Debrites have been interpreted to be deposited by *en-masse* freezing of debris flows (Iverson, 1997; Talling et al., 2012b; Talling et al., 2013).

6.6 Lobe hierarchy

Several studies have recognized that submarine lobe deposits follow a hierarchical pattern (Gervais et al., 2006; Deptuck et al., 2008, Saller et al., 2008; Prélat et al., 2009; Mulder & Etienne, 2010; Prélat et al., 2010; Bernhard et al., 2012; Etienne et al., 2012; Grundvåg et al., 2014). A fourfold hierarchy of lobes in the Karoo Basin was established by Prélat et al. (2009) where 1) a 'bed' represents a single depositional event; 2) one or more beds stack to form a 'lobe element'; 3) several lobe elements that are divided by thin siltstone intervals form a 'lobe'; 4) one or more genetically related lobes stack to form a 'lobe complex'. This hierarchy is expanded by adding a fifth hierarchical unit, the 'lobe complex set', which is formed by several genetically related lobe complexes within the same lowstand systems tract (Prélat and Hodgson, 2013). Lobes and lobe complexes are deposited during discrete periods of channel activity or growth phases (cf. Feeley et al., 1985; Deptuck et al., 2008; Prélat et al., 2009), and are bounded by abrupt facies change to fine-grained strata that are interpreted to indicate avulsion of feeder channel, and compensational stacking (Prélat & Hodgson, 2013).
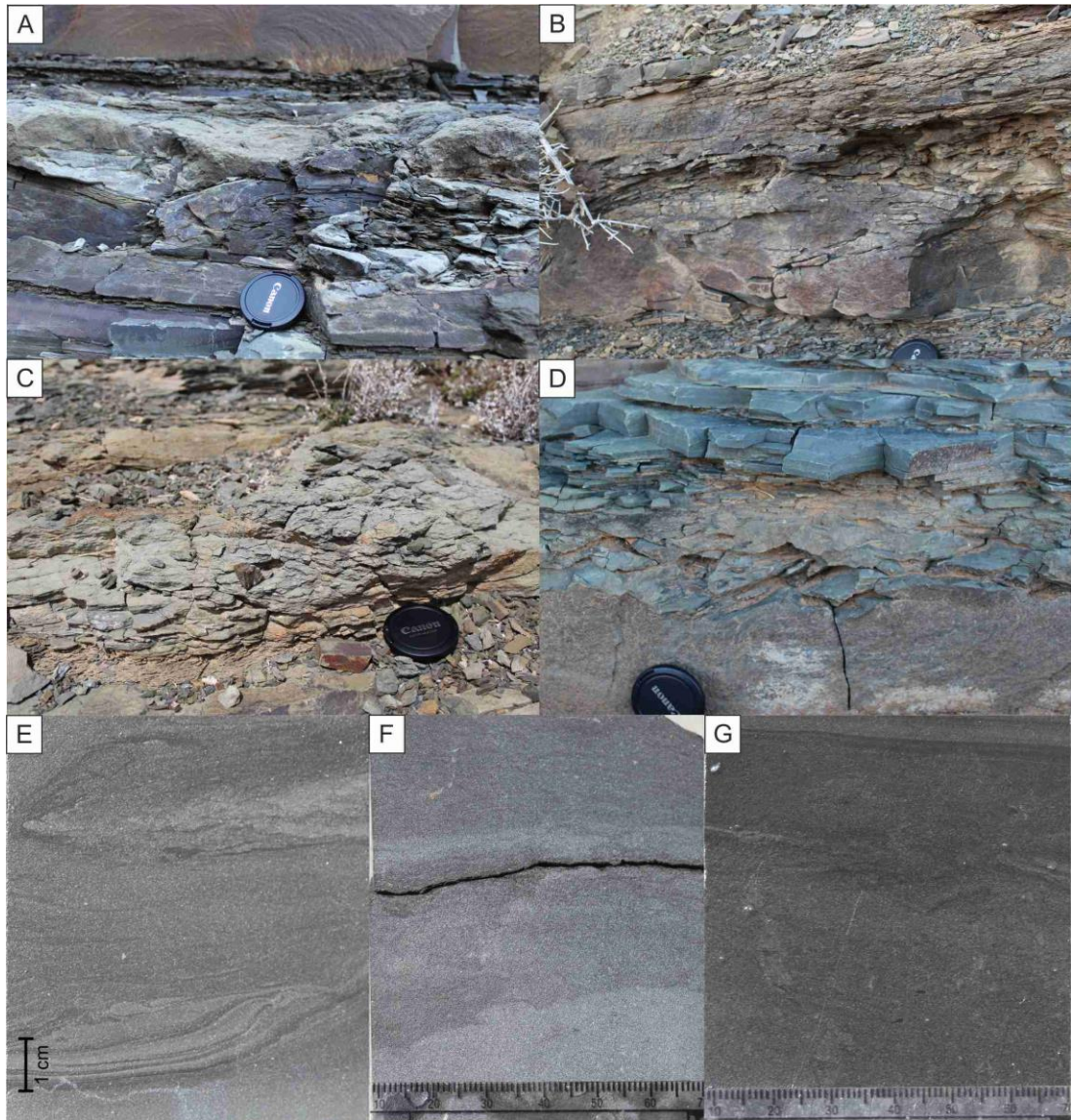
Figure 6.4. Representative photographs of hybrid beds from outcrop and core. A: Hybrid bed (F4) with lower clean division and upper mudstone clast –rich division. Lens cover as scale (~7 cm diameter). B: Hybrid bed showing different weathering of lower clean and upper muddy division. Lens cover as scale (~7 cm diameter). C: Weathered mica-rich upper division with high mud content. Lens cover as scale (~7 cm diameter). D: Hybrid bed. Upper clast rich division overlain directly by thin-bedded siltstone. Lens cover as scale (~7 cm diameter). E-G: Hybrid bed examples from core.

Recognition of this hierarchical division in outcrop and core has been as follows: Hemipelagic intervals mark a true shutdown in clastic sediment supply to the deep basin, and can be correlated regionally (Flint et al., 2011). These are interpreted to represent transgressive and highstand systems tracts, and the sand-prone material between are the lowstand systems tract. In the lowstand systems tract deposits, lobe complexes are between 20-50 m thick and separated by 1) several metre thick siltstone intervals, or 2) several metre thick thin-bedded heterolithic packages. Both types are interpreted as lobe complex fringes (Prélat & Hodgson, 2013; Chapter 3) to

sand-prone lobe deposits elsewhere. Lobes are between 1 m (in distal environments) and 10 m (in axial environments) thick (Prélat et al. 2009, 2010). Individual lobes have been established through identification of 1) 0.2- 1.5 m thick thin-bedded siltstone packages; 2) 0.2- 1.5 m thick thin-bedded heterolithic packages, 3) prominent erosion surfaces, or distinctive facies changes (i.e. structureless thick-bedded sandstones overlain by hybrid bed rich deposits). Siltstone packages are interpreted as distal lobe fringe deposits (Chapter 3, 4; Prélat et al., 2009), whilst the heterolithic packages represent (lateral) lobe fringes (Chapter 3, 4; Prélat et al., 2009). Lobe elements have been assigned by recognition of 1) < 0.2 m siltstone intervals, or 2) facies changes that point to a different lobe sub-environment. Thick-bedded deposits with a major proportion of structureless sandstone are interpreted to represent a lobe axis environment, whereas a higher proportion of medium-bedded structured sandstone deposits are interpreted as lobe off-axis environment. Lobe fringes are characterised by hybrid bed prone successions and packages of thin-bedded interbedded siltstones and sandstones, whereas lobe distal fringes comprise siltstones with minor intercalated thin sandstone beds (< 20% sandstone).

6.7 Results

The proportion of hybrid beds has been evaluated in two respects at different levels of the lobe hierarchy: 1) the percentage of hybrid beds in the total number of events; and 2) the percentage of hybrid beds in the cumulative thickness. The results can be found in Table 1. Overall, of the bed types assessed in the whole dataset, the proportion of hybrid bed deposits is below 5% (4.1% mean; 2.65% median).. 90% of values fall below 17% of hybrid bed occurrence (Fig. 6.5a). However, they show more significance in terms of their proportion of cumulative thickness. Their percentage of bulk thickness averages at <12% (11.4% mean; 6.2% median) with 90% of the values being below 26% of the succession thickness (Fig. 6.5b) whichmeans that hybrid bed typically comprise less than 26% of thickness of a successions.

A | Hybrid bed event distribution

B | Hybrid bed thickness distribution
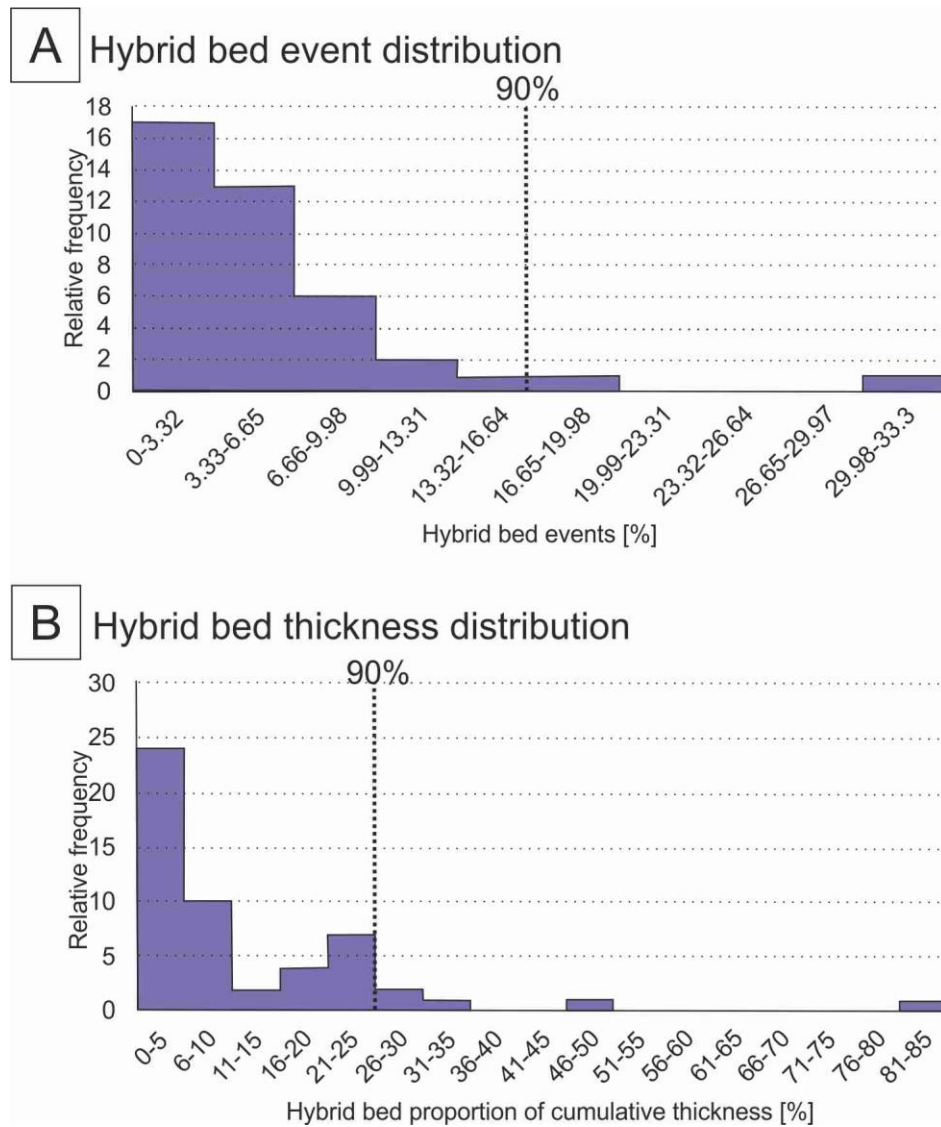
Figure 6.5 Hybrid bed distribution over the complete data set. A: Percentage of hybrid beds relative to all events. B: Hybrid bed proportion of the cumulative thickness

6.7.1 Geographical trends

The palaeogeography of lobe complex 1 (LC1) of Fan 4 is well established (Hodgson et al., 2006; Figure 3.10). Sediment was supplied from the southwest and palaeoflow directions are to the north and northwest (Fig. 6.1). LC1 is ~25 m thick in the south (OR) and thins to 5 m in the north (OC1-6; Sout Rivier) before it pinches out abruptly to the north (OC 7; cf. Chapter 3.6.1). Therefore, a cross-section from south (OR) to north (OC 6) represents a proximal to distal trend (Fig. 6.6a). The percentage of hybrid beds is less than 10% in terms of total events that make up LC1, except for a spike of high percentage (33.3%) in OC 4 (Fig. 6.5b). Deposits of OC 4 represent a frontal lobe fringe pinch-out finger; these deposits have been shown to contain high

amounts of hybrid bed deposits (Chapter 3.7.2). A prominent trend in the proportion of hybrid beds in the bulk thickness of LC1 can be observed (Fig. 6.6c). An approximately linear increase in the percentage of hybrid bed thickness (from 2.1% to 83.3%; cf. Table 6.1) can be observed from the proximal to distal areas of the lobe complex followed by an abrupt decrease.
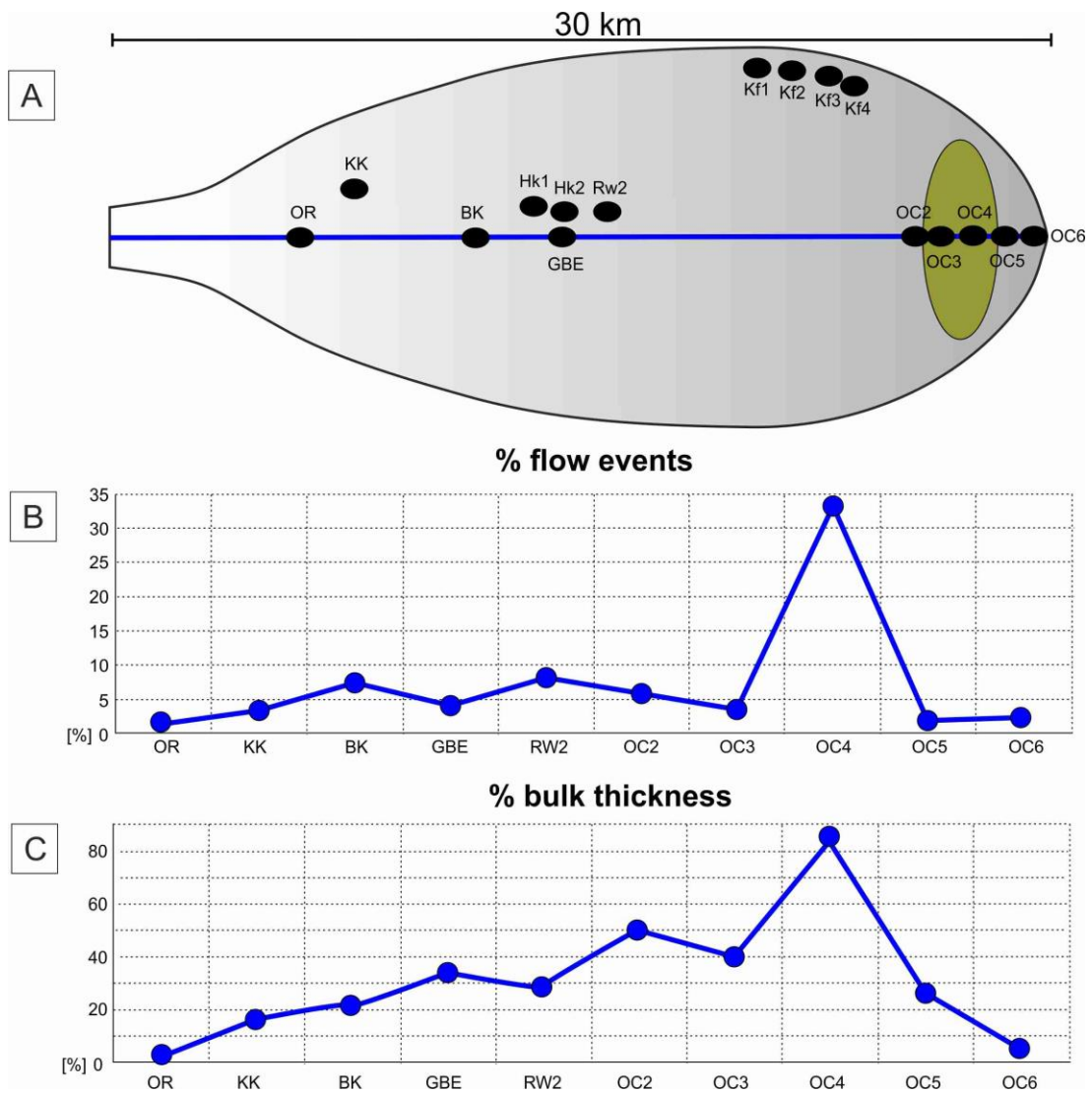
Figure 6.6. A: Schematic distribution of the outcrops over LC1. The green circle points out where hybrid beds are approximately 50% of the deposit thickness. B: Hybrid bed deposits plotted as percentage of all flow events. C: Hybrid bed deposits plotted as percentage of the bulk thickness of the succession.

6.7.2 Stratigraphic trends

Unit A of the Laingsburg Formation comprises six subunits (Sixsmith et al., 2004; Prélat & Hodgson, 2013; Chapter 4.3.1) that are separated by intervals of siltstone and hemipelagic mudstone that have been mapped regionally (Flint et al., 2011). Subunits A.2 and A.3 of Laingsburg Fan A comprise one lobe complex each in the study area, whereas Subunits A.1, A.5 and A.6 comprise two to eight lobe complexes (A.1.1-3; A.5.1-8; A.6.1-2). Due to the well-established stratigraphy and exceptional preservation, the core from research boreholes BSL and Bav 1b (Fig. 6.1) are well-suited for the evaluation of the stratigraphic distribution of hybrid beds.

Hybrid beds account for less than 10 % of beds in all subunits in both locations (Table 6.1). However, evaluation of their proportion of bulk thickness shows that there are considerable variations between the subunits (Table 6.1). In the BSL core, A.1 comprises 7.7 % hybrid beds, A.2 slightly less (4.9%), whereas there is a spike towards 30.2 % in A.3. Subunits A.5 and A.6 contain 8.5% and 8.2% of hybrid beds, respectively. In the Bav 1b core, the largest bulk thickness is A.1 (17.9%) and A.2 (18.2%). The proportion decreases significantly in A.3, which contains only 6.3%. Subunits A.5 and A.6 show similar values with 6.9% (Table 6.1).

The subunits have been subdivided into sand-prone lobe complexes and metres thick thin-bedded heterolithic packages that are interpreted as fringes to lobe complexes (cf. Prélat et al., 2009 Prélat & Hodgson, 2013; Chapter 3.5.1). Several observations can be made (Fig. 6.7): 1) there is no clear trend in stratigraphic distribution of hybrid beds over the lowstand sequence set (Flint et al., 2011), which show a high number of events in A.5.5 for both cores, whereas in cumulative thickness they are most prevalent in A.3 of the BSL core and A.1.1 in the Bav 1b core (Table 6.1); 2) the younger lobe complexes (A.5.5- A.6.2) show an in-phase occurrence of hybrid beds for both cores; 3) the two lobe complexes of A.6 are the only intervals that show the same trends in the occurrence and thickness of hybrid beds in both cores; and 4) hybrid beds are a minor component of a lobe complex fringe, and comprise less than 2% of events and bulk thickness (Fig. 6.7). Reoccurring hemipelagic intervals on the basin-floor that divide the lobe complex sets don't seem to have any affect on the occurrence of subsequent hybrid bed deposits.

Sub-units A.2 and A.3 show a large difference in hybrid bed distribution between the two locations (BSL and Bav1b; Fig. 6.1). This lateral variability has been examined in more detail (Figs. 6.8 a- c). For this purpose, a moving average for facies proportions

has been established and aligned with the corresponding core log. The base and top of A.2 and A.3 are rich in hybrid beds in both cores, however there are differences in the underlying spatial distribution of hybrid beds. The lobe complex in Unit A.2 shows an increasing proportion of hybrid beds from BSL to Bav 1b, which is located down-dip of BSL. The lobe complex of A.3 shows the opposing trend of decreasing hybrid bed proportions down-dip. Overall, there are no obvious vertical trends established from the lobe complexes A.2 and A.3 other then their preferred accumulation in their bases and tops. However, hybrid bed deposit occurrence is not limited to the basal and/or top interval, but occurs throughout the succession, either irregularly as in A.3 at BSL (Fig. 6.8b) or regularly as in A.3 at Bav 1b (every ~10m; Fig. 6.8c).

6.8 Discussion

6.8.1 Proximal to distal trend

A strong geographic trend is evident, showing that hybrid bed occurrence increases to the frontal lobe fringes (up to 30% of events and > 50% of deposit thickness; Fig. 6.6 b,c), before their proportion drops abruptly towards the sand pinch-out of the lobe complex (Fig. 6.6b,c), before their proportion drops abruptly towards the sand pinch-out of the lobe complex (Fig. 6.6b,c).Lateral thin-bedded lobe fringes (Fig. 6.7) contain less than 2% of hybrid beds. Recent studies, as presented in Chapter 3, show that hybrid beds are commonly found in the frontal lobe fringes and are much less common in lateral lobe fringes. The data analyzed for this study supports this model. The distinctly different distribution has been interpreted to be caused by the spatial distribution of primary flow processes. High-density turbidity currents that can transform to hybrid bed deposits are transported farther out to the frontal margins of the lobes, while low-density turbidity currents that deposit structured thin-beds spread out more radially and build up the lateral margins. Geographical distribution over the scale of lobes and lobe complexes is controlled by process (see Chapter 3.8.1). This study has quantified the previously qualitative observation that hybrid bed deposits occur in the distal parts of fan and lobe settings (Talling et al., 2004; Ito, 2008; Hodgson, 2009; Pyles & Jennette, 2009; Talling et al., 2012a; Etienne et al., 2012a; Kane & Pontén, 2012; Grundvåg et al., 2014; Collins et al., 2015; Fonnesu et al., 2015).

Location	Subunit	% hybrid beds of total events	% hybrid beds of cumulative thickness
BSL	A.1	2	7.7
	A.2	4.7	4.9
	A.3	7.2	30.2
	A.5	4.5	8.5
	A.6	0.7	8.2
Bav 1b	A.1	2	17.9
	A.2	6.6	18.2
	A.3	3.5	6.3
	A.5	2.4	6.9
	A.6	0.4	6.9
OR	LC1	1.2	2.1
	LC2	0	0
	LC3	14.5	11.3
KK	LC1	3.2	16.3
	LC2	0	0
	LC3	12	23.7
BK1	LC1	7.4	22.2
	LC2	0	0
	LC3	5.8	8.5
GBE	LC1	4	34.1
	LC2	0	0
	LC3	2.9	11
RW2	LC1	8.2	29.1
	LC2	0	0
	LC3		
OC2	LC1	5.9	49.1
	LC2	0	0
	LC3	11.6	19.5
OC3	LC1	3.4	40.9
	LC2	0	0
	LC3	18.2	19.2
OC4	LC1	33.3	83.3
	LC2	0	0
	LC3	4.2	4
OC5	LC1	1.8	26.1
	LC2	0	0
	LC3		
OC6	LC1	2.2	4.8
	LC2	0	0
	LC3	7.8	8
KF1	LC1	6.8	21.1
	LC2	0	0
	LC3	4.2	6.1
KF2	LC1	4	2.9
	LC2	0	0
	LC3	0.6	1.1
KF3	LC1	3.8	2.4
	LC2	0	0
	LC3		
KF4	LC1	4.6	21.5
	LC2	0	0
	LC3	5.5	5.5
VF	LC1	0	0
	LC2	0	0
	LC3	1.8	2.7

Table 6.1. Proportion of hybrid beds for subunits of Unit A (BSL and Bav 1b; Laingsburg depocentre) and lobe complexes 1-3 of Fan 4 (Skoorsteenberg Formation, Tanqua depocentre). For locations see Figure 6.1 or the pull-out map.
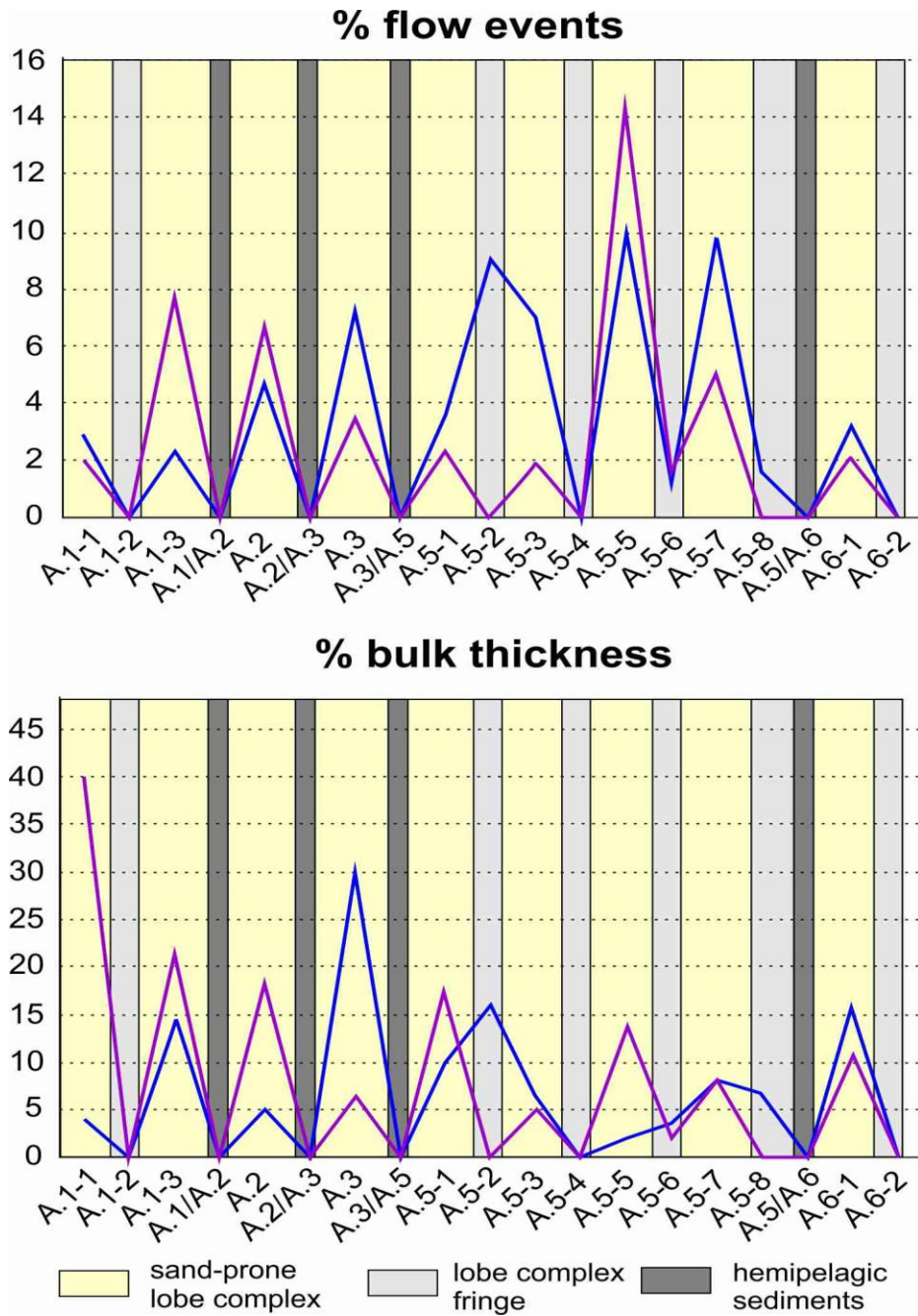
Fig. 6.7. Hybrid bed distribution over the lobe complexes of Unit A. The graphs are linked to their depositional environment. The blue line displays values for BSL, whereas the violet line displays values for Bav 1b.
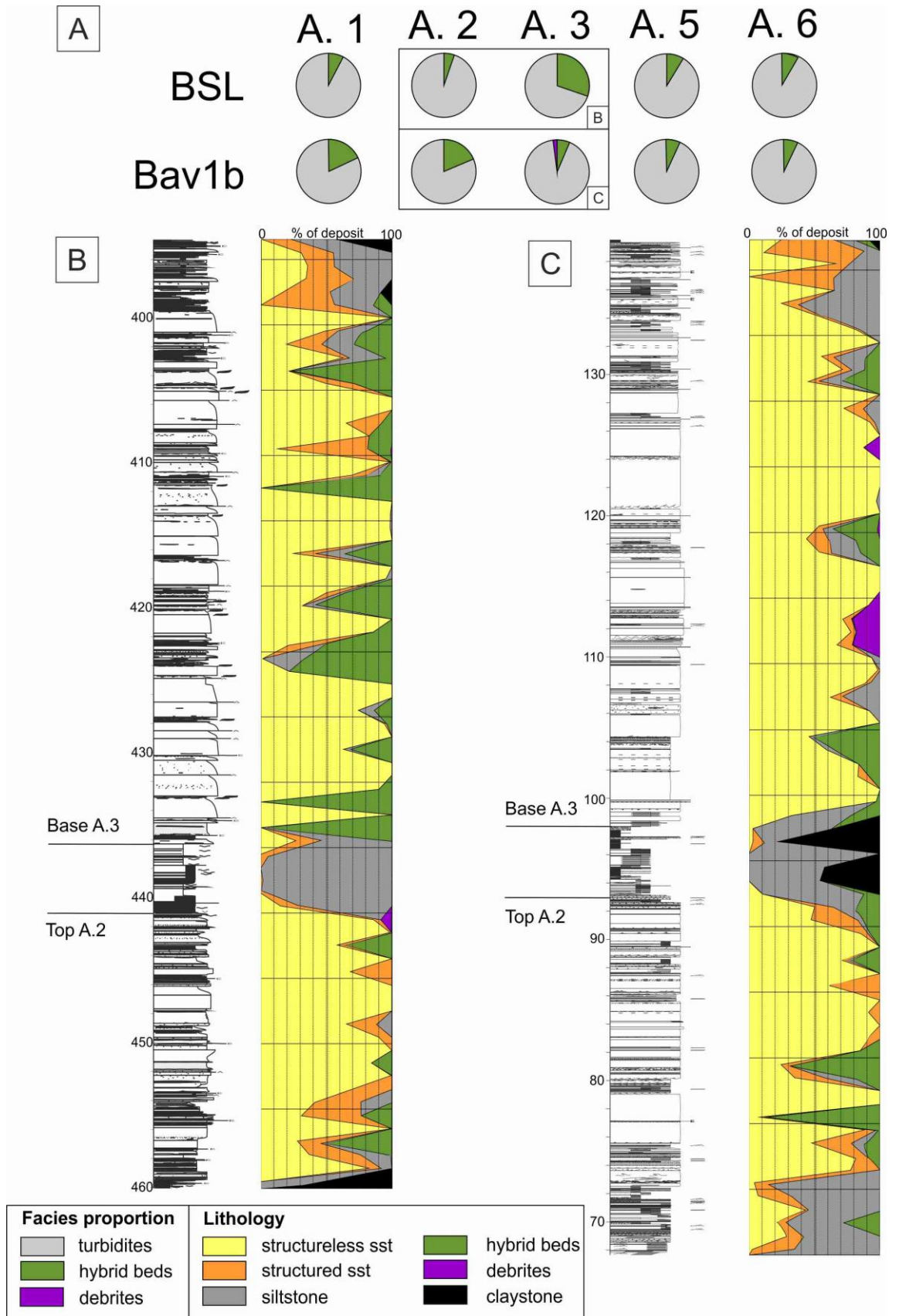
Figure 6.8. A: Facies proportions of subunits A.1- A.2 of Unit A, Laingsburg Formation; B: Core log of Subunits A.2 and A.3 of the BSL core aligned with its lithology composition (moving average); C: Core log of Subunits A.2 and A.3 of the Bav 1b core aligned with its lithology composition (moving average).

6.8.2 Stratigraphic distribution within Unit A

The stratigraphic distribution within the lowstand sequence set (Flint et al., 2011) of Unit A shows no obvious trends. There is an overall increase of hybrid bed occurrence within the sand-prone lobe complexes of Subunit A.5, but the cores show different distribution curves (Fig. 6.9) Hybrid bed deposits are less common in the basal (A.1) and top (A.6) subunits in both core data sets (cf. Table 6.1) compared to A.2-A.5, which contain similar proportions (from 2.4%- 7.2%), although they can make up to 18% of the thickness (A.1 in Bav 1b; Table 6.1 and Fig. 6.8a).

These results contradict the simple model of hybrid bed distribution that has been suggested by several authors (e.g. Haughton et al., 2003, 2009; Hodgson, 2009) proposing that hybrid beds are most common in the basal part of deep-water successions during fan (lobe complex or lobe complex set) initiation and growth. The rationale being that the generation of hybrid beds is associated with the disequilibrium of steep, out-of-grade muddy slopes that would achieve equilibrium over the period of sediment accumulation on the basin-floor fan. Therefore, less muddy material needed to induce longitudinal flow transformation would be entrained through time, therefore hybrid beds would be less common in the younger parts of successions (*sensu* Haughton et al., 2003).
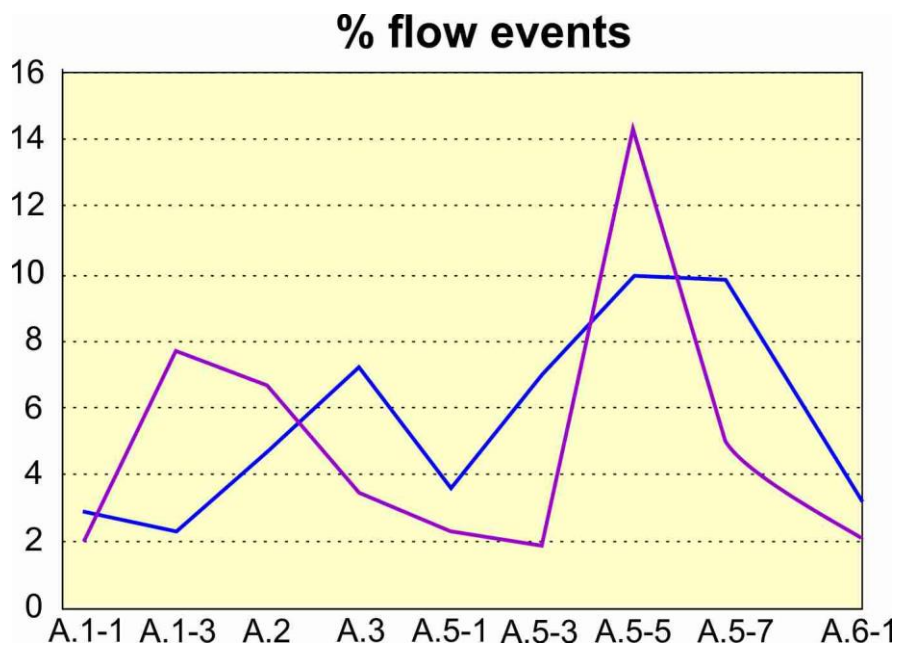
Figure 6.9. Hybrid bed distribution curve for sand-prone lobe complexes of Unit A. The blue line displays values for BSL, whereas the violet line displays values for Bav 1b.

Haughton et al. (2009) suggested that deviation from this model provides important clues to the slope evolution: 1) occurrence of hybrid beds throughout a basin-floor system is connected to a supply slope that never achieved equilibrium; 2) sporadic occurrence through the system can point to intermittent periods where the slope is in disequilibrium due to slope adjustments caused by tectonics or changes in sediment supply. Van der Merwe et al. (2014) and Spychala et al. (2015; Chapter 5.7.2 and 5.8) report a stepped slope profile that influenced the overlying Fort Brown Formation. It is possible that the supply slope during the deposition of Unit A may have been stepped meaning that the slope was always in disequilibrium.

Picot et al. (2016) suggest that channel avulsion is another factor that can generate disruption of the equilibrium profile and is connected to the deposition of lobe complex successions. Ortiz-Karpf et al. (2015) inferred less sandy lobes early during a phase of channel avulsion from seismic amplitude responses due to entrainment of mud before new feeder channels could be established. High angle and up-dip channel avulsion is therefore an important mechanism that could promote the occurrence of hybrid beds at the initiation phase of lobe complexes and therefore also explain sporadic occurrence through a basin-floor system.

Another factor that has been shown to have influence on the distribution of hybrid bed deposits is frontal basin confinement (e.g. Patacci et al., 2014; Southern et al., 2015), which leads to rapid deceleration and expansion of flows. The lobe complexes of the Laingsburg depocentre are interpreted to have experienced minor to no confinement in their axes and subtle confinement to their lateral margins (Sixsmith et al., 2004; Chapter 4) therefore enhanced deceleration (Patacci et al., 2014, Southern et al., 2015) can be eliminated as a controlling factor on the stratigraphic distribution of hybrid beds, particularly in the Skeiding area (Fig. 6.1).

However, the paucity of stratigraphic trends within a lobe complex set suggests that there is a complicated interplay of factors involved in hybrid bed initiation and evolution. The process of flow transformation from turbdity currents to flow that display turbulent as well as laminar behaviour is probably the most important factor. Flow transformation has been reported to occur when turbidity currents erode and entrain substrate material (Haugthon et al., 2003, 2009; Hodgson, 2009, Kane et al., in review) leading to 1) enhanced stratification and eventually to the collapse of the upper part of the flow (MacCave & Jones, 1988; Kane & Pontén, 2012; Kane et al., in review; see Chapter 3.8.1), or 2) longitudinal flow transformation to a co-genetic

turbidity current and debris flow (Haughton et al., 2003; Talling et al., 2004; Ito, 2008; Davis et al., 2009; Haughton et al., 2009; Magahlaes & Tinterri, 2010; Patacci et al., 2014). The entrainment of substrate material does not need to happen on the slope, but may also occur at the channel-lobe transition zone () or on the basin-floor. This could explain why the distribution in Unit A of the Laingsburg Formation is not satisfingly explainable with the simple slope state-induced hybrid bed distribution model suggested by several authors (Haughton et al., 2003, 2009; Hodgson, 2009)

6.8.3 Stratigraphic distribution on the scale of a lobe complex

If avulsion was the main factor governing the distribution of hybrid beds on a lobe complex scale an abundance of hybrid beds in their basal intervals would be predicted. However, at a lobe complex scale there are no obvious trends. Rather, a prominent pattern can be determined once lobes have been identified (Fig. 6.10): 1) thick-bedded structureless sandstone-prone lobes have an irregular distribution of hybrid beds, 2) thin-to-medium bedded structureless and structured sandstone and siltstones deposits that are rich in hybrid beds, and 3) thin-to-medium bedded structured sandstone and siltstone deposits that are poor in hybrid beds (Fig. 6.10). The 1D core data sets conform to the observation from 3D outcrop studies, and has been tested by geographical trend evaluation, that lobes have two fringe types (hybrid bed prone frontal fringes and hybrid bed poor lateral fringes). In addition, it shows that distribution in a 1D vertical succession is impacted by the superposition of lobes and their sub-environments.
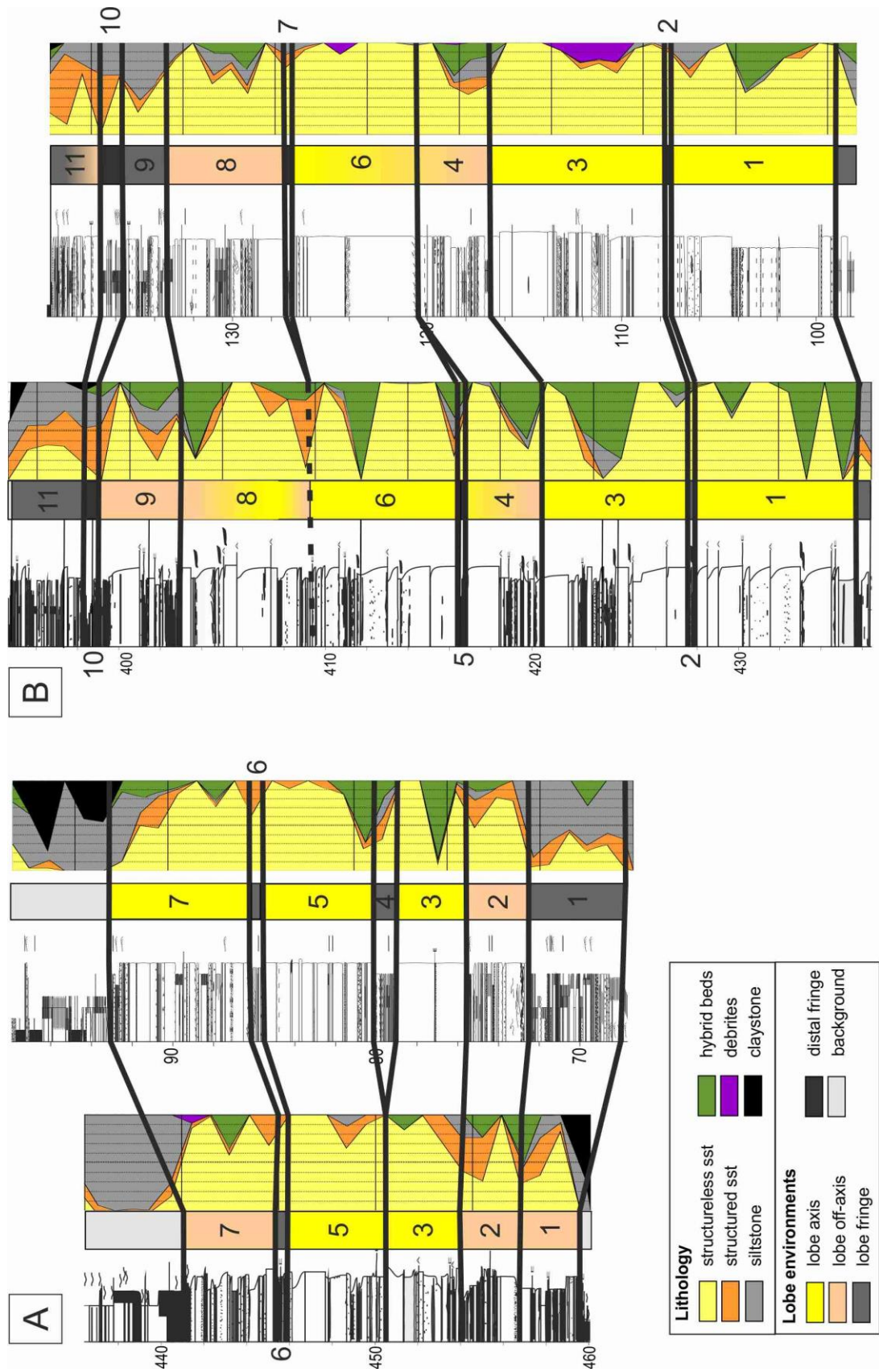
Figure 6.10. Interpretation of individual lobes and their correlation from BSL to Bav 1b. A: Correlation for the lobe complex of Subunit A.2. B: Correlation for the lobe complex of Subunit A.3.

6.8.4 Stratigraphic distribution on the scale of a lobe

Examination of individual lobes shows no clear trend, as (Fig. 6.10) hybrid beds can be found at the base, at the top or in the middle of the lobe. This is interpreted to be due to the stacking of lobe elements, and is well expressed in lobe 8 of Subunit A.3 in Figure 6.9). Prélat & Hodgson (2013) suggested that the stacking of lobe elements can show a wide range of bed thickness patterns (compensational, disorganized, laterally stacked, landward and basinward stepping). Lobe elements and beds are not as laterally extensive as lobes themselves. Therefore, core datasets that are kilometres apart, sample different lobe elements and beds, leading to a range of vertical distributions (Fig. 6.10). This finding implies that lobe elements are comparable to lobes regarding their facies distributions and geometries, i.e. they show similar facies transitions albeit on a smaller scale.

6.8.5 Subsurface implications

Rather than being dominantly controlled by processes on the slope, the occurrence and distribution of hybrid beds is interpreted to be controlled by flow transformation processes on the basin-floor, and the stacking patterns of lobes. Stratigraphic distributions of clean sandstones, thin-bedded heterolithic deposits and hybrid-bed prone deposits is dependent on the dominant stacking patterns of lobes (aggradational, compensational, progradational and retrogradational) within a lobe complex. Therefore, the distribution of reservoir sandstones, and non-reservoir hybrid bed-prone and heterolithic deposits, can be used to infer lobe stacking patterns. Where aggradational stacking patterns dominate, and a core is sited in the axial area, there would be no to rare hybrid beds (Fig. 6.11). If progradational stacking of lobes is dominant, hybrid beds will be abundant on the base and become less frequent upwards in the succession in 1D (Fig. 6.11). Retrogradational stacking patterns would display the opposite distribution with hybrid beds being abundant in the top interval of the succession (Fig. 6.11). However, when compensational stacking is the dominant stacking pattern, reservoir and non-reservoir facies will be less predictable as lobe environments are superimposed in a more complicated manner (Fig. 6.11). In reality, a lobe complex can display more than one stacking pattern. Commonly reported progradational-aggradational-retrogradational stacking of lobes within a lobe complex

(e.g. Sixsmith et al., 2004; Hodgson et al., 2006; Flint et al., 2011) would result in basal and top lobes being hybrid-bed prone, while the aggradational middle section would show no or rare hybrid bed deposits. To sum up, hybrid bed distribution could be used in a 1D data set to form an initial evaluation of the dominant stacking patterns within the system, and the degree of confinement and the sediment supply of the system.
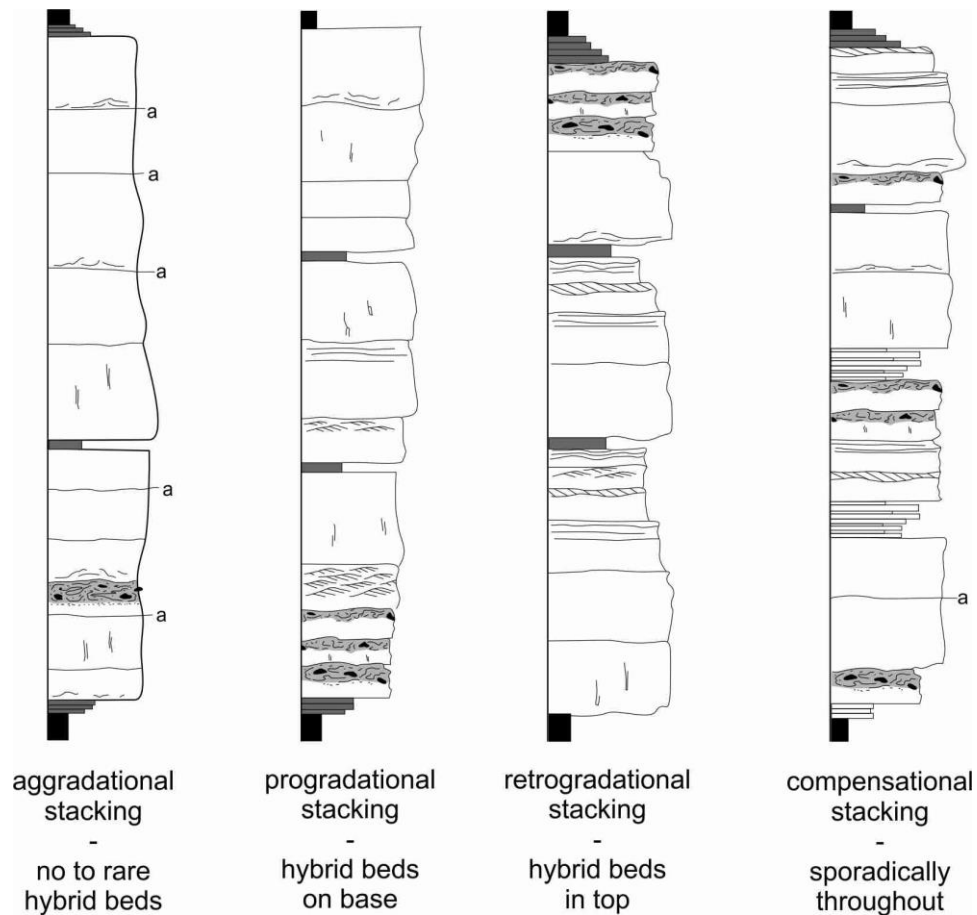
Fig.6.11. Stacking patterns and resulting hybrid bed distribution within an axial setting.

6.9 Conclusion

A well-constrained outcrop and core data set from two unconfined basin-floor fans of the Karoo Basin, South Africa, have permitted the stratigraphic and geographic distribution of hybrid beds to be constrained quantitatively for the first time. In general, hybrid bed deposits average at 4.1% of all flows within the database.Most recorded values (>90%) fall below 17% of hybrid bed events in a lobe complex. Therefore, hybrid beds are not always prevalent, with less degradation of reservoir quality. There

is a strong geographic trend showing that while hybrid beds occur throughout lobes, they are preferentially found in frontal lobe fringes (up to 33% of the total number of events and 83% of deposit thickness). Stratigraphic trends do not support allogenic controls (e.g. confinement, nature of supply slope) on the generation and deposition of hybrid beds. The stratigraphic distribution is strongly influenced by autogenic factors, and in particular the style of stacking patterns of lobe element to lobe complex set scale. Stacking patterns, however, are strongly influenced by allogenic factors like seabed topography and sediment supply and their interplay warrants further investigation.

Chapter 7:

Discussion & Conclusions

Here, the research questions posed in Chapter 1 are addressed, with reference to the results presented in Chapters 3-6. This Chapter concludes with recommendations for potential future research arising from this PhD research.

7.1 What are the sedimentological and stratigraphic expressions of lobe fringes?

The fringes of lobes can stratigraphically separate lobe axis and off-axis deposits as a function of compensational stacking, and can stack to form the fringes of lobe complexes. Lobe fringe deposits are the least well-studied sub-environments of lobes despite showing the widest range of facies configurations (Fig. 7.1a-d). Here, lobe fringe deposits from unconfined to weakly confined settings have been studied to capture the range of sedimentological and stratigraphic expression of lobe fringes (Chapters 3, 4, 5).

Several authors (e.g. MacPherson, 1978; Pickering, 1981, 1983) suggested that lobe deposits show different facies transitions down-dip and across-strike, which could lead to distinctive facies trends and characteristic facies associations for frontal and lateral fringes. This theory has been tested on Fan 4 of the Tanqua depocentre (Chapter 3). Characteristic facies associations and the flow processes are summarized and discussed below.
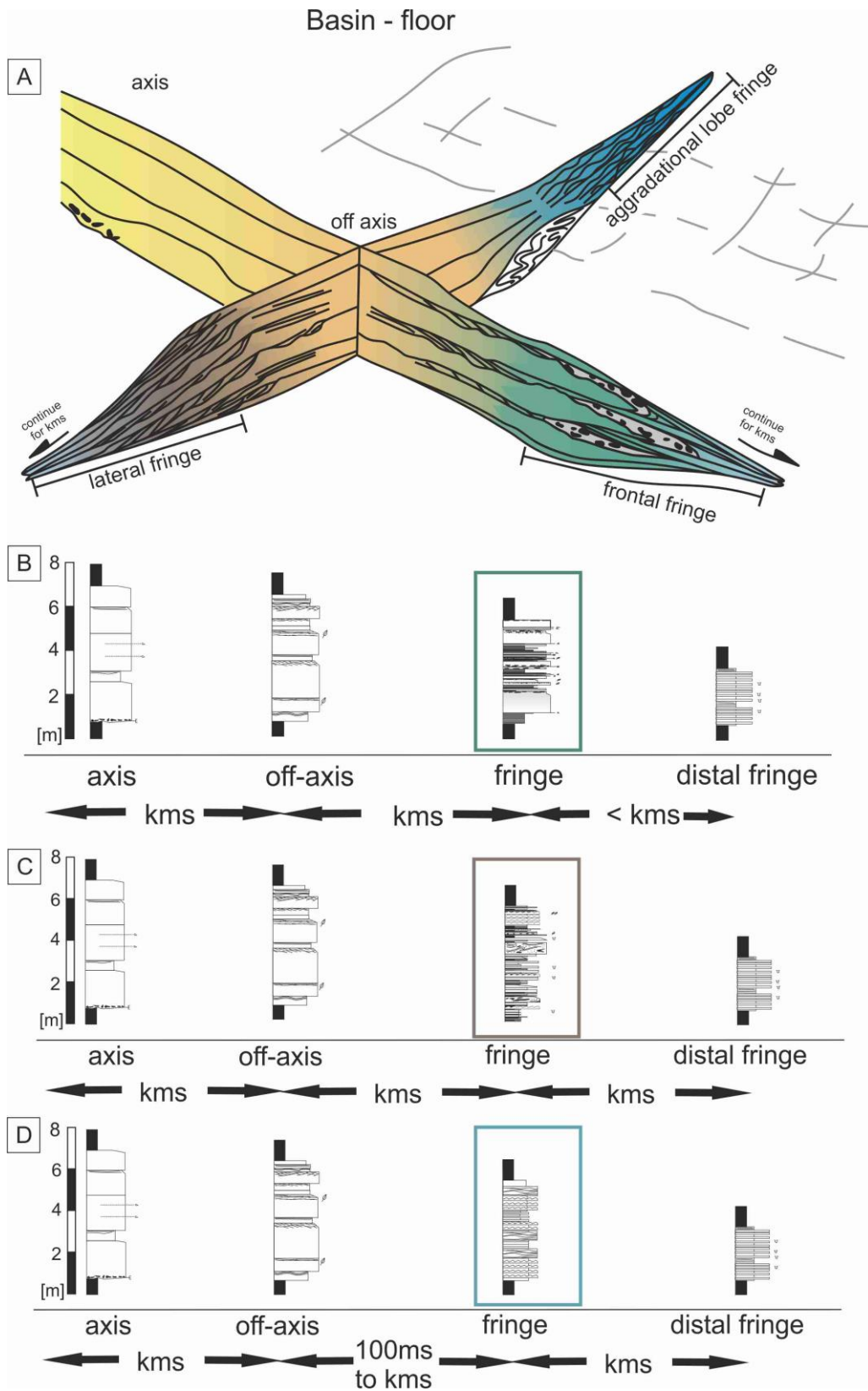
Figure 7.1. A: Range of lobe fringes within unconfined to subtly confined basin-floor settings. B: Frontal fringes are characterised by pinch-and-swell geometries and the occurrence of hybrid bed deposits. C: Lateral fringes are characterised by thin-beds with planar- and ripple-lamination and a tapering geometry. D: Aggradational lobe fringes are lateral fringes under the influence of subtle confinement resulting in modified sedimentology and stacking patterns, e.g. climbing bedforms.

7.1.1 Frontal lobe fringes

The frontal lobe fringe facies association is characterised by dewatered, structureless or planar laminated fine-grained sandstone (Fig. 7.1a, b; Chapter 3.7.2) associated with hybrid beds and rare debrites. In strike section, frontal fringes exhibit prominent depositional pinch-and-swell geometries at lobe scale, with laterally variable bed thickness. Beds thin or pinch out abruptly at the transition to the distal lobe fringe (Fig. 7.1a, b).

Generally, frontal lobe fringes are dominated by deposits from high-density turbidity currents and other high-concentration flows (structureless sandstones, debrites and hybrid beds). In frontal lobe fringes, there is evidence that relatively distal turbidity currents eroded and entrained substrate material, preserved as mudstone clasts and dispersed mud (Hodgson, 2009, Kane et al., in review) that damped turbulence and resulted in the collapse of the upper part of the flow (McCave & Jones, 1988; Kane et al., in review), leading to the deposition of hybrid bed deposits. Deposits of high-density turbidity currents are able to create their own pathways and become successively more elongated down-dip, forming finger-like bodies as observed in the Tanqua depocentre. These finger-like bodies are 1.5 to 2 km long and 200 to 300 m wide. Finger-like pinchouts of frontal lobes are observed within successive lobes of multiple different lobe complexes within the Tanqua depocentre (Bouma & Rozman, 2000; Rozman, 2000; Prélat et al., 2009; Groenenberg et al., 2010). Similar terminations have also been observed within other basin-floor lobe systems (Nelson et al., 1992; Twichell et al., 1992), albeit occasionally misinterpreted as channel-forms (e.g. Van der Werff & Johnson, 2003b) due to their elongated shape in planform view and their concave-up form in outcrop.

7.1.2 Lateral lobe fringes

The lateral lobe fringe facies association is dominated by thin-bedded (>0.2 m) heterolithic deposits of structureless or planar laminated siltstone and wavy, ripple and climbing ripple laminated very-fine grained sandstone (Fig. 7.1 a, c; Chapter 3.7.1). Lobe pinch out occurs over several kilometres through thinning and fining of the deposits away from the lobe axis and lobe off-axis environments (Fig. 7.1a,c). In outcrop, lateral lobe fringes commonly show tabular geometries at the scale of observation.

Generally, lateral lobe fringes are predominantely characterised by deposits from low-density turbidity currents. Luthi's (1981) experiments show that flow velocities are

lowest in these flow marginal areas, and that the decrease in flow thickness is greatest laterally away from the central flow axis. The deposits of the low-density turbidity currents probably form laterally extensive radial deposits that are higher in proportion at the lateral fringe, owing to the forward momentum and lack of lateral spreading of the higher concentration flows.

The expression of lateral lobe fringes has been documented in a relatively unconfined basin-floor setting (Chapter 3.7.1). Studies from more confined areas in the Karoo Basin show that the presence of subtle seabed topography can influence the expression of lobe fringes and the stacking of lobe fringes in lobe complexes. Subtle seabed topography was formed by a lateral intrabasinal slope (Unit A, Laingsburg Formation; Chapter 4) and differential compaction on a stepped slope (E1, Fort Brown Formation; Chapter 5). The lobe fringe facies association in subtle confined environments differs from the lobe fringe facies association proposed from the unconfined Tanqua depocentre (see also Prélat et al., 2009), largely due to evidence for high sedimentation rates (climbing ripples and climbing bedforms; Fig. 7.1 a,d) and the persistent aggradational stacking of facies over tens of metres on lobe complex scale.

7.1.3 Aggradational lobe fringes

Aggradational lobe fringes (Fig. 7.1a, d) comprise a heterolithic facies association. Siltstones make up the bulk of the succession. Sandstone beds show stoss-side preserved climbing ripple-, planar, or wavy-lamination. Ripple morphology is preserved on bed tops, and in cross-section. Successions of these ripples form larger dune-like features. The heterolithic package comprises multiple event beds that stack in the direction of palaeoflow (climbing bedforms). Commonly, interbedded sandstones and siltstones form stacked, aggradational packages up to 10 m thick, which internally show no discernible trends in grain size or bed thickness. Palaeocurrents either show a narrow range parallel to the confining slope (Chapter 4) or deviation from the regional palaeocurrent trend that is interpreted to indicate deflection and reflection of turbidity currents off seabed topography (Chapter 5).

The facies association of aggradational lobe fringes indicates rapid deposition from density-stratified turbidity currents (e.g. Kneller & Buckee, 2000; Peakall et al., 2000), with a thin basal sand-prone section and a thick mud-prone section, that interact with

the confining seabed topography. The sand-prone portion is confined and pinches out, whilst the fine-grained sediment is held aloft and deposited higher up the confining structure. Stoss-side preserved climbing-ripple lamination indicates deposition beneath flows with high aggradation rates (Allen, 1971a; Allen, 1982; Southard, 1991; Jobe et al. 2012). The lateral facies transition between lobe axis and off-axis to fringe is governed primarily by the height of the topography relative to the thickness of the flows (Muck & Underwood, 1990; Pickering & Hilton, 1998, Wynn et al., 2012).

7.2 What is the range of stacking patterns that can be constrained from lobe complexes and lobe complex sets?

Stacking patterns of lobes are proxies for the relationship between sediment supply and seabed topography during the evolution of lobe complexes and lobe complex sets (Piper & Normark, 1983; Mitchum & Van Wagoner, 1991; Schlager, 1993; Twichell et al., 2005; Picot et al., 2016). Seabed topography can be dynamic or static, which can change the degree of confinement experienced by a system over time. Confinement has been documented to be an important allogenic factor in the control of sediment dispersal patterns and lobe stacking patterns (e.g. Piper & Normark, 1983; Smith & Joseph, 2004; Amy et al., 2004, Twichell et al., 2005; Southern et al., 2015; Marini et al. 2015). Sediment supply is governed by climate and tectonics in the hinterland, sea level variations that change accommodation on the shelf (e.g. Mitchum & Van Wagoner, 1991; Schlager, 1993), and topography on the supply slope (e.g. Prather, 1998). Several types of stacking patterns have been documented from lobe successions (e.g. Gervais et al., 2006; Amy et al., 2007; Deptuck et al., 2008; Prather et al., 2012b; Prélat & Hodgson, 2013, Burgreen & Graham, 2014; Grundvåg et al., 2014; Picot et al., 2016): compensational, aggradational, and longitudinal, with either basinward (progradational) and landward (retrogradational) trends (Fig. 7.2). There can be a continuum between these stacking patterns during the growth of a lobe complex set or lobe complex. For example, parts of a lobe complex set or lobe complex can experience the influence of confinement that results in aggradational stacking patterns, whereas away from the confining structure compensational stacking can be prevalent.

Different stacking patterns can be interpreted from 1D datasets and extensive 2D/3D datasets, with different implications for the distribution of heterogeneities and reservoir potential for a system. Where only 1D data are available, interpretations and predictions have to be considered very carefully as recognised thickening/thinning upwards cycles can be biased (e.g. Hiscott, 1981; Anderton, 1995).

Lobes from the Karoo Basin show a range of stacking patterns reported in the literature. Below these stacking patterns and their controlling factors are presented:

7.2.1 Compensational stacking

Deposits of the Laingsburg and Tanqua depocentres are reported to show low to no influence of confinement by seabed topography and compensational stacking can be observed in several of the examined lobe successions, e.g. lobes of Unit A in the Laingsburg depocentre (cf. Chapter 4.7). Compensational stacking patterns can be identified by the paucity of thickening- and thinning-upward cycles, abrupt stratigraphic changes in lobe sub-environments, and lateral thickness variations between stacked lobes. Compensational stacking can be observed across many scales from bed to lobe complex scale (Prélat & Hodgson, 2013) to lowstand sequence sets (van der Merwe et al. 2014). Migration of beds and lobes can be dip parallel, strike parallel or oblique, depending on the exact location of a topographic low. As long as there is no confinement impeding free dispersal of sediment then compensational stacking will be the dominant stacking pattern through a lobe complex (Straub et al., 2009). Compensational stacking in lobe to lobe complex sets is governed by the avulsion of feeder-channels to redirect to a new topographic low after the creation of sufficient depositional relief in a lobe complex.
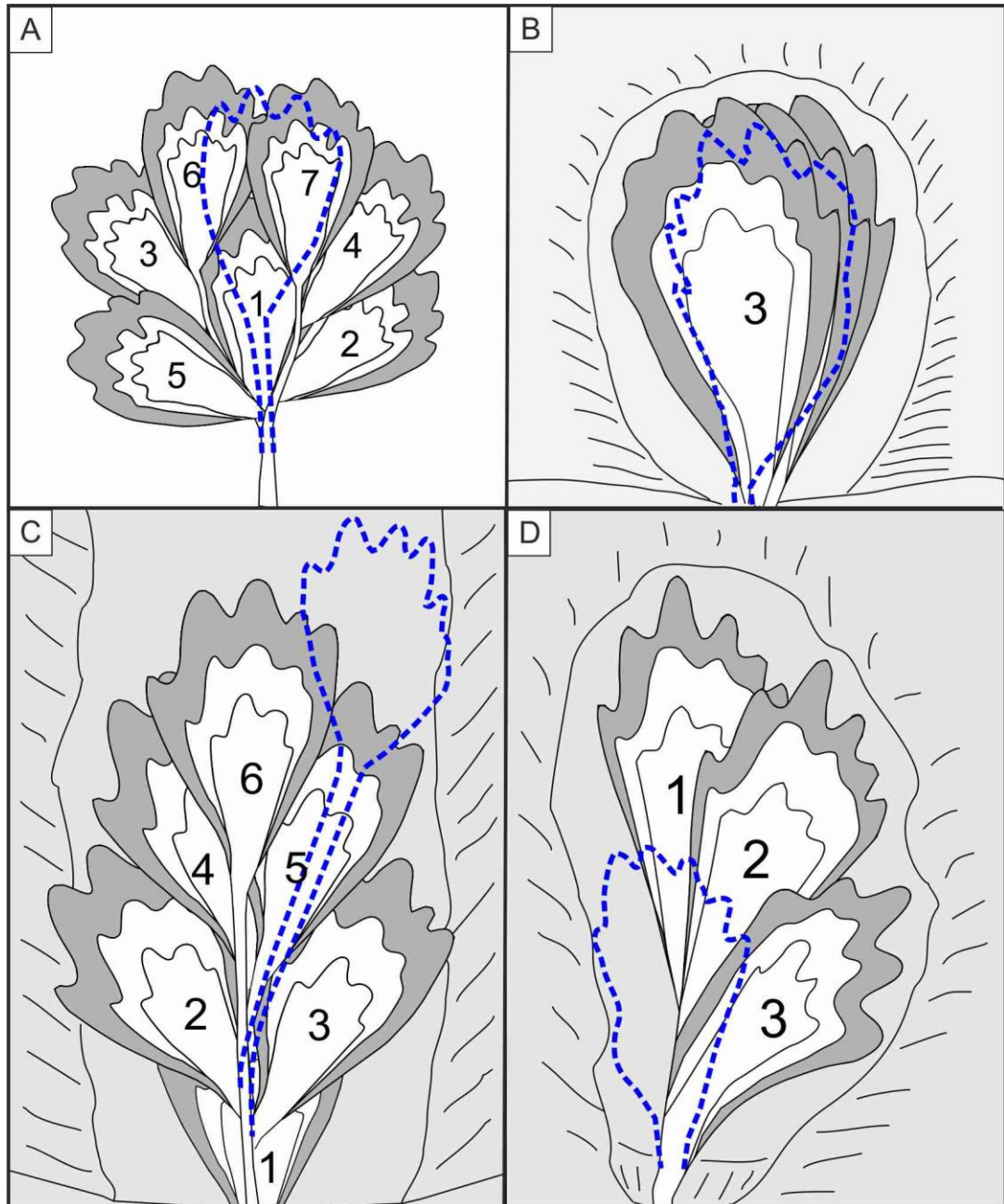
Figure 7.2 Schematic plan view of lobe stacking patterns. A: Compensational stacking; B: Aggradational stacking; C: Progradational stacking; D: Retrogradational stacking. The dashed blue line indicates the locus of deposition of the next lobe.

7.2.2 Aggradational stacking

In the Karoo Basin deposits, aggradational stacking patterns have been observed in settings where accommodation and/or confinement influences sediment dispersal, e.g. on the slope (D/E and E1, Fort Brown Formation; cf. Chapter 5) and through the existence of an intrabasinal lateral slope (Unit A; cf. Chapter 4). The main recognition criterion for aggradational stacking is the vertical superposition of the same lobe sub-

environment over the evolution of a lobe complex (E1, Unit A) and lobe complex set scale (Unit A), with little or no lateral offset. In E1, the axes of intraslope lobes are stacked in the axis of the available accommodation while fringes are stacked at its margin and show influence by confinement (deflected and reflected palaeoflow indicators; Chapter 4, 5). In the case of Unit A, a subtle intrabasinal slope influenced the stacking patterns (Chapter 4). While lobe deposits in the axis of the system show compensational stacking (see above), towards the slope and on the slope there is a vertical accumulation of lobe fringes (therefore termed aggradational lobe fringe).

Aggradational stacking occurs where avulsion is not possible due to the scale of confinement (Burgreen & Graham, 2014) and is commonly observed with lobes deposited in highly confined settings, e.g. mini-basins and ponded basins (e.g. Burgreen & Graham, 2014). When accommodation is filled, the system will either prograde and sediment will spill into the next available mini-basin (fill and spill; e.g. Prather et al., 1998), or, in the case of stepped slope profiles, is transported farther downslope to the next available area of slope accommodation or the basin-floor (van der Merwe et al., 2014). If progradation is not possible deposits will migrate landwards as the break-of-slope successively moves up-slope.

7.2.3 Progradational stacking

Traditionally, the existence of thickening-upward cycles in lobes was interpreted as evidence of progradation (e.g. Mutti, 1974; Ricci Lucchi, 1975). Since then the interpretation of thickening upward cycles as the sole indicator for progradation has been challenged (Hiscott, 1981; Anderton, 1995; Chen & Hiscott, 1999; Macdonald et al., 2011). Hiscott (1981) stated that cycles have been over-interpreted by comparing them with thickening-upward cycles in delta-lobes even though processes of deposition are different. Macdonald et al. (2011) suggested that evidence of increased erosion and bypass needs to be identified in addition to repetitive thickening upward cycles to argue for progradational stacking over aggradational or compensational stacking.

Progradational stacking has been observed in combination with compensational stacking in the Karoo Basin (e.g. Unit A, Laingsburg Formation; Fan 4, Skoorsteenberg Formation), but never as the predominant stacking pattern.

Grundvåg et al. (2014) proposed that progradational stacking can be associated with 1) basin configurations that limit the space for lateral migration of lobes, 2) tectonic

activity that increases the basin-floor gradient, 3) increased rates of sedimentation due to shelf edge progradation and initiation of larger volume flows, and/or 4) high sediment supply rates resulting in rapid shelf-margin accretion. Essentially, progradational stacking has been attributed to high sediment supply rates by Picot et al. (2016), and a combination of shelf edge progradation and high sediment supple rates by Grundvåg et al. (2014). Macdonald et al. (2011) suggest that progradational stacking of lobe elements can be explained by autocyclic growth of the supply channels through progressive confinement. If similar mechanisms could work on lobe scale has not been determined yet. Progradational stacking patterns might also be more common in proximal and base-of-slope settings where there is less accommodation and less space for lateral compensation and the deposition/ preservation of lobe fringe deposits.

7.2.4 Retrogradational stacking

Unit E.2 of the Fort Brown Formation (Laingsburg depocentre; Chapter 5) is a prominent example of landward stacking of lobes caused by low accommodation through healing of a slide scar on the slope. Retrogradational stacking can be identified by the vertical succession of lobe axis deposits overlain by lobe-off axis and eventually frontal lobe fringe deposits. Care must be taken to distinguish this stacking pattern from lateral offset stacking due to autogenic avulsion processes. These findings conform to subsurface observations made in the Gulf of Mexico indicating temporal evolution of the locus of sedimentation (Prather et al., 2012b) and outcrop observations from highly confined basins e.g. the Peïra Cava Basin, France (Amy et al., 2007), where the shift in deposition has been inferred to be caused by aggradation in the depocentre and an up-slope migration of the slope break (Amy et al., 2007). In general, retrogradational stacking patterns can also be caused through decrease in sediment supply at the end of a depositional cycle (e.g. at the end of a LST) when sediment is trapped on the shelf rather than transported to the deep-water. The same stacking has been described at sequence set scale in Unit C by Di Celma et al. (2011), where the upper LST stacks retrogradationally with respect to the lower two LSTs within the Unit C lowstand sequence set.

7.3 What is the stratigraphic and geographic distribution of hybrid beds in submarine lobes?

Over the last decade hybrid beds have been recognised as an important part of the rock record in deep-water environments as indicator for distal fan settings. Many studies on core and outcrop data (e.g. Haughton et al., 2003; Talling et al., 2004; Ito, 2008; Davies et al., 2009; Haughton et al., 2009; Hodgson, 2009; Jackson et al., 2009; Magalhaes & Tinterri, 2010; Kane & Pontén, 2012; Patacci et al., 2014; Fonnesu et al., 2015) have resulted in different hybrid bed classifications. Quantitative analysis on the predictability and significance of these deposits is rare. Exceptionally large exposures supplemented by research borehole data from Unit A of the Laingsburg Formation and Fan 4 of the Skoorsteenberg Formation, South Africa, provided the means to examine geographical and stratigraphical trends over several hierarchical scales (Chapter 6).

Overall, of the bed types assessed in the whole dataset, the proportion of hybrid bed deposits is below 5% (4.1% mean; 2.65% median).. 90% of values fall below 17% of hybrid bed occurrence. This figure differs markedly from the value of 67% that Davies et al. (2009) reported from the outer Forties Fan, Central North Sea. Two main reasons can be invoked for this striking diference: 1) palaeogeographic location of the data set; e.g. the data from the Forties Fan are from the distal end of the system while the data from the Karoo deposits were collected from all over the lobe complex sets; and 2) different degrees of basin confinement. It has been shown that increased frontal basin confinement can lead to increased hybrid bed content through deceleration and expansion of the flows (e.g. Patacci et al., 2014; Southern et al. 2015).
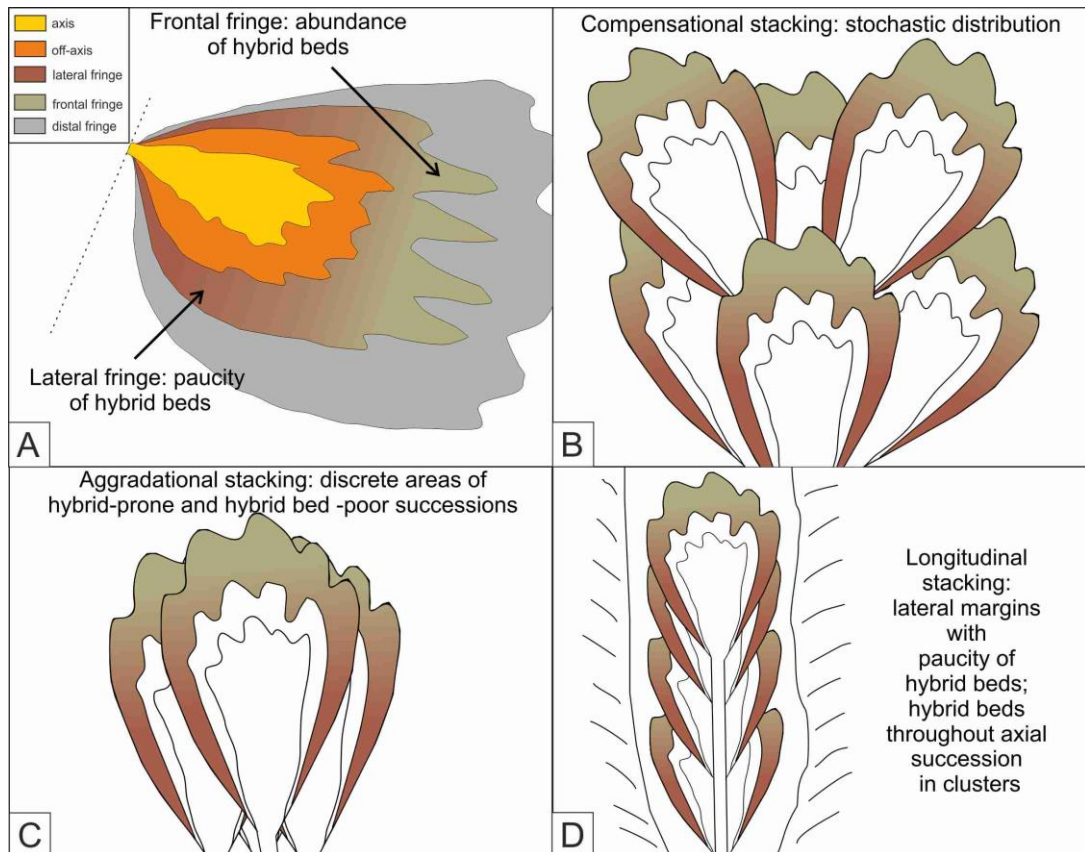
Figure 7.3 A: Distribution of hybrid beds in lobe fringes; B: Stochastic distribution of hybrid beds due to compensational stacking patterns; C: Discrete areas of hybrid-bed rich and hybrid bed-poor successions due to aggradational stacking; D: Marginal hybrid rich successions, axial hybrid bed clusters throughout due to longitudinal stacking.

7.3.1 Proximal to distal trends

A strong geographic trend shows that hybrid beds are mostly accumulated in the frontal lobe fringes (up to 33% of the total number of events and 83% of deposit thickness; Fig.7.3a), before dropping off below 5% at sand pinchout. This result conforms to the qualitative observations made from outcrop and core studies that proposed hybrid beds occur in the distal lobe setting (Talling et al., 2004; Ito, 2008; Hodgson, 2009; Pyles & Jennette, 2009; Talling et al., 2012; Etienne et al., 2012; Kane & Pontén, 2012; Grundvåg et al., 2014; Collins et al., 2015; Fonnesu et al., 2015). The data also support the observation that frontal lobe deposits are hybrid bed-prone (5-30% of events and > 50% of deposit thickness), whereas lateral fringes are hybrid bed-poor (less than 2% of events) as presented in Chapter 3.

7.3.2 Stratigraphic trends

The stratigraphic distribution of hybrid beds has been postulated to be connected with the character of the supply slope and seabed relief. Hybrid beds are suggested to develop during periods of disequilibrium over steep, out-of-grade slopes (Haughton et al., 2003; 2009; Hodgson, 2009). Therefore, the occurrence of hybrid beds is thought to be greater during the initiation and growth phases of lobe complexes and lobe complex sets. The results of the quantitative study from the Karoo Basin do not conform to this model, nor are there any distinctive trends at a lobe complex or lobe scale. Sand-prone lobe complexes show a irregulardistribution of hybrid beds, whereas intercalated thin-bedded packages that represent the fringes of lobe complexes show a paucity in hybrid beds due to the difference in lobe fringe facies association mentioned above (cf. Chapter 3.7). Overall, it can be stated that stacking patterns are a major factor in the vertical distribution of hybrid beds on a lobe complex scale as they govern the stratigraphic trend of lobe axes, lobe off-axes and lobe fringes (Fig. 7.3b-d). Individual lobes show no clear trend. Hybrid beds are found at the base, at the top, or in the middle of the lobe. This is probably due to the stacking of lobe elements, which introduces another level of hierarchy and complexity to lobe successions. In summary, prediction of the stratigraphic distribution of hybrid beds is a complicated problem controlled by multiple allogenic (confinement, nature of supply slope) and autogenic factors (stacking patterns from lobe element to lobe complex set scale).

7.4 Can we apply concepts established from basin-floor lobes to lobe deposits in different stratigraphic and geographic settings?

Lobes have been observed from various settings, including the basin-floor, the base-of-slope and on the continental slope. Depositional and stratigraphic models that have been established from basin-floor lobes of the Karoo Basin (Prélat et al., 2009, 2010; Prélat & Hodgson, 2013; this thesis) have been applied as analogues for a wide range of lobe deposits that are not necessarily in the same stratigraphic and geographical settings. Here, these models are discussed in terms of their application to lobes that have been deposited on the slope (intraslope lobes; Chapter 5):

7.4.1 Hierarchy

Intraslope lobes show the same hierarchical organisation that has been presented from the basin-floor (cf. Prélat et al., 2009; Grundvåg et al., 2014). Beds stack to form lobe elements, these lobe elements stack to form lobes and lobes stack to form lobe complexes. The number of lobes in a lobe complex is controlled by the available accommodation and sediment supply. In the case of the intraslope lobes from the Fort Brown Formation, two to three lobes from individual lobe complexes occupied accommodation generated by differential compaction and a slide scar (cf. Chapter 5). A higher number of intraslope lobes per complex have been described from seismic data sets (e.g. Pirmez et al., 2012; Prather et al., 2012a, b) in salt withdrawal mini-basins.

7.4.2 Lobe sub-environments

The fourfold model of lobe environment subdivision can be applied to intraslope lobe deposits, but needs slight modification to the facies associations. Although the lobe axis is also characterised by thick-bedded structureless sandstones, a higher amount of erosion (several metres instead of several dms) can be observed. Erosion surfaces mantled with mudstone clasts are more common in intraslope lobe axis deposits than in basin floor lobe systems due to proximity to channels and flow confinement leading to more entrainment of fine-grained substrate. Off-axis deposits of intraslope lobes are characterised by an abundance of medium-bedded ripple- and climbing ripple-laminated sandstones. Individual beds can preserve ripple forms and climbing ripple-lamination that yield palaeoflow directions orientated at a high angle or even opposite to each other, indicating deflection and reflection of the turbidity current on topography during sedimentation. Overall, lobe fringes have been observed to consist of thin-bedded heterolithic facies, and hybrid beds are relatively rare. However, more examples need to be assessed to tell whether this is a diagnostic criterion.

7.4.3 Lobe stacking patterns

While basin-floor lobes show the full range of stacking patterns (see Chapter 7.2), intraslope lobes are generally stacked in aggradational to slightly compensational manner or show a retrogradational stacking pattern due to aggradation in the depocentre and an up-slope migration of the slope break. As stacking patterns are thought to provide an insight into the degree of confinement (Deptuck et al., 2008;

Straub et al., 2009) these stacking patterns point to a relatively higher level of confinement for intraslope lobes compared to basin-floor lobes.

In summary, it can be stated that depositional and stratigraphic models developed from basin-floor lobes can be applied to lobes from different geographic settings such as intraslope lobes. However, there are differences in detailed lobe sub-environments and predominant stacking patterns that require slight modifications to the models. Importantly the identification of these differences can be used to aid the identification of intraslope lobes in less well constrained subsurface and outcrop datasets.

7.5 Recommendations for future research

7.5.1 Lobe fringes and hybrid beds in moderate to highly confined settings

The depositional and stratigraphic models for lobe fringes that have been established within this thesis have been derived from submarine lobes deposited in relatively unconfined settings. It has been shown that even subtle confinement can have a major influence on facies, architecture and stacking patterns of lobe fringes (see Chapters 4 and 7.1). It is not clear if there are distinctive lateral or frontal facies trends in more confined basin settings. This warrants further investigation, including lobes in settings where confinement changes through time. Stacking patterns and confinement have been suggested to have strong influence on the geographic and stratigraphic distribution of hybrid beds. While geographic trends for hybrid bed distribution could be established for relatively unconfined lobe deposits in the Karoo Basin (Chapter 6 and 7.3), stratigraphic trends, if any, remain poorly constrained. Basins with a higher degree of confinement favour aggradational or dip-parallel stacking over compensational stacking of lobes. Hence, stratigraphic trends that are controlled by allogenic factors might not be overprinted by autogenic lobe stacking. However, confinement has been shown to enhance erosion and flow deceleration (Patacci et al., 2014; Southern et al., 2015) and will therefore influence the dispersal patterns and occurrence of hybrid beds.

7.5.2 What is the detailed sedimentology of frontal and lateral lobe fringes?

This study has focussed on the establishment of the broad differences between frontal and lateral fringes (Chapter 3). However, their detailed sedimentology and electrofacies character could be further analysed using the core and well log database collected during the Lobe2 research programme. This includes detailed documentation of facies transitions between the sub-environments, rates of change, net:gross values, and their evolution from axis to frontal/lateral fringe. Analysis of these aspects is important from an applied point of view to pinpoint heterogeneities within reservoir rocks. In addition, the transition zone between frontal and lateral fringes has not been studied and is an important part of the story.

7.5.3 Integration of outcrop and seismic data sets

Commonly, studies on submarine lobes are conducted from outcrop or geophysical data sets. While outcrop data sets can provide detailed insights into sedimentary facies and geometries, seismic data sets enable the study of lobes at basin scale. Because the resolution of these data sets is different, the terminology to describe the same hierarchical element differs, e.g. lobes in seismic studies commonly correspond to lobe complexes in outcrops. Integration of outcrop and seismic data sets is rare (e.g. Lin et al., 2014; Pickering et al., 2015) and not applied systematically, but can enable differences and similarities in observation to be determined. For example, in seismic studies distributary channels truncating submarine lobes are regularly described, while they are rarely documented in outcrop. Is this difference caused by outcrop limitations or caused through processes during lobe deposition?

7.5.4 What is the role of changing sediment supply to the architecture and stacking patterns of lobe deposits?

Sediment supply has been acknowledged to be one of the main factors to govern stacking patterns in deep-water lobes (e.g. Schlager, 1993; Picot et al., 2016). Sediment supply is controlled by climate and tectonics of the hinterland (Schlager, 1993) and through relative sea-level changes as sediment can be stored on the shelf during a sea-level highstand. Most deep-water fans have been postulated to be

deposited during lowstands of relative sea level (e.g. Deptuck et al., 2008; Jegou et al., 2008; Covault & Romans, 2009; Prélat et al., 2009; Marchès et al., 2010; Flint et al., 2011). However, there are also examples of deep-water fans that deposited during highstand system tracts (e.g. Schwalbach et al., 1996; Weber et al., 1997; Piper et al., 1999; Normark et al., 2009), including many modern systems. Do lobes deposited during highstand systems tracts that are supplied by longshore systems differ from lobes in river-fed systems, and how do HST fans differ from LST fans?

List of References

Aas, T.E., Howell, J.A., Janocko, M., Jackson, C.A.L., 2010. Control of Aptian palaeobathymetry on turbidite distribution in the Buchan Graben, Outer Moray Firth, Central North Sea. Marine and Petroleum Geology 27, 412-434.

Adeogba, A.A., McHargue, T.R., Graham, S.A., 2005. Transient fan architecture and depositional controls from near-surface 3-D seismic data, Niger Delta continental slope. AAPG Bulletin 89, 627-643.

Allen, J.R.L., 1966 Note on the use of plaster of Paris in flow visualization, and some geological applications. Journal of Fluid Mechanics 25, 331-335.

Allen, J.R.L., 1971a. Instantaneous sediment deposition rates deduced from climbing-ripple cross-lamination. Journal of the Geological Society London 127, 553-561.

Allen, J. R. L.,1971b. Mixing at turbidity current heads, and its geological implications. Journal of Sedimentary Petrology 41, 97–113.

Allen, J.R.L., 1973. A classification of climbing-ripple cross-lamination. Journal of the Geological Society London 129, 537–541.

Allen, J.R.L., 1982. Sedimentary Structures: Their Character and Physical Basis, Vols. 1, 2. Amsterdam: Elsevier. 593pp., 663pp.

Altinakar, M.S., Graf, W.H., Hopfinger, E.J., 1996. Flow structure in turbidity currents. Journal of Hydraulic Research 34, 713-718.

Amy, L.A., McCaffrey, W.D., Kneller, B.C., 2004. The influence of a lateral basin-slope on the depositional patterns of natural and experimental turbidity currents. In Joseph, P., Lomas, S.A (Eds.), Deep-Water Sedimentation in the Alpine Basin of Se France: New Perspectives on the Grès d'Annot and related systems. Geological Society London Special Publication 221, 311-330.

Amy, L.A., Hogg, A.J., Peakall, J., Talling, P.J., 2005. Abrupt transitions in gravity currents. Journal of Geophysical Research 110, F03001.

Amy, L.A., Kneller, B.C., McCaffrey, W.D., 2007. Facies architecture of the Grès de Peira Cava, SE France: landward stacking patterns in ponded turbiditic basins. Journal of the Geological Society London 164, 143-162.

Anderton, R., 1995. Sequences, cycles and other nonsense: are submarine fan models any use in reservoir geology? In: Hartley, A.J., Prosser, D.J.(Eds.), Characterization of Deep Marine Clastic Systems. Geological Society of London, Special Publications 94, 5–11.

Arnott, R.W.C., Hand, B.C., 1989. Bedforms, primary structures and grain fabric in the presence of suspended sediment rain. Journal of Sedimentary Petrology 59, 1062-1069.

Baas, J.H., van Kesteren, W., Postma. G., 2004. Deposits of depletive high-density turbidity currents: A flume analogue of bed geometry, structure and texture. Sedimentology 51, 1053-1088.

Baas, J.H., McCaffrey, W.D., Haughton, P.D.W., Choux, C., 2005. Coupling between suspended sediment distribution and turbulence structure in a laboratory turbidity current. Journal of Geophysical Research 110, 1-20.

Baas, J.H. Best, J.L., Peakall, J., Wang, M., 2009. A phase diagram for turbulent, transitional, and laminar clay suspension flows. Journal of Sedimentary Research 79, 162-183.

Baas, J.H., Best, J.L., Peakall, J., 2011. Depositional processes, bedform development and hybrid bed formation in rapidly decelerated cohesive (mud-sand) sediment flows. Sedimentology 58, 1953-1987.

Badalini, G., Kneller, B., & Winker, C. D., 2000. Architecture and processes in the late Pleistocene Brazos-Trinity turbidite system, Gulf of Mexico continental slope.Deep-Water Reservoirs of the World: SEPM, Gulf Coast Section, 20th Annual Research Conference, 16-34.Bagnold, R. A., 1954. Experiments on a gravity-free dispersion of large solid spheres in a Newtonian fluid under shear. Proceedings of the Royal Society of London A 225, 49-63.

Bagnold, R.A. 1962. Auto-suspension of transported sediment; turbidity currents. Proceedings of the Royal Society of London. Series A, Mathematical and Physical Sciences 265, No. 1322, 315-319.

Bailleul, J., Robin, C., Chanier, F. Guillocheau, F., Field, B., Ferriere, J., 2007. Turbidite systems in the inner forearc domain of the Hikurangi Convergent Margin (New Zealand): New constraints on the development of trench-slope basins. Journal of Sedimentary Research 77, 263-283.

Bakke, K., Kane, I.A., Martinsen, O.J., Petersen, S.A., Johansen, T.A., Hustoft, S., Jacobsen, F.H., Groth, A., 2013. Seismic modeling in the analysis of deep-water sandstone termination style. AAPG Bulletin 97, 1395- 1419.

Baldwin, B., Butler, C.O., 1985. Compaction curves. AAPG Bulletin 69, 622-626.

Barton, M.D., 2012. Evolution of an Intra-Slope Apron, Offshore Niger Delta Slope: Impact of step geometry on apron architecture. In: Prather, B.E., Deptuck, M.E., Mohrig, D., van Hoorn, B., Wynn, R.B. (Eds.), Application of the principles of seismic geomorphology to continental -slope and base-of-slope systems: Case studies from seafloor and near-seafloor analogues. SEPM Special Publication 99, pp. 181- 197.

Beaubouef, R.T., Rossen, C., Zelt, F.B., Sullivan, M.D., Mohrig, D.C., and Jennette, D.C. 1999, Deep-water sandstones, Brushy Canyon Formation, West Texas. AAPG Continuing Education Course Notes, 40, pp. 50.

Beaubouef, R.T., Rossen, C., Lovell, R.W.W., 2007. The Beacon Channel: A newly recognized architectural type in the Brushy Canyon Formation, Texas, USA. In: Nielsen, T.H., Shew, R.D., Steffens, G.S., Studlick, J.R.J. (Eds.). Atlas of Deep-Water Outcrops. AAPG Studies in Geology 56. AAPG and Shell Exploration & Production, pp. 432-444.

Bernhardt, A., Jobe, Z.R., Grove, M., Lowe, D.R., 2012. Palaeogeography and diachronous infill of an ancient deep-marine foreland basin, Upper Cretaceous Cerro Toro Formation, Magallanes Basin, Chile. Basin Research 24, 269-294.

Bersezio, R., Felletti, F., Riva, S., Micucci, L., 2009. Trends in bed thickness and facies of the turbiditic sandstone bodies: unravelling the effects of basin confinement, depositional processes, and modes of sediment supply. In: Kneller, B., Martinsen, O.J., McCaffrey, B. (Eds.), External Controls on the Deep-water Depositional Systems. SEPM Special Publication 92, 303-321.

Best, J., Bridge, J., 1992. The morphology and dynamics of low amplitude bedwaves upon upper stage plane beds and the preservation of planar laminae. Sedimentology 39, 737-752.

Biddle, K.T., Wielchowsky, C.C., 1994. Hydrocarbon traps. AAPG Memoir 60, 219-235.

Booth, J.R., Dean, M.C., DuVernay, A.E., Styzen, M.J., 2003. Paleo-bathymetric controls on the stratigraphic architecture and reservoir development of confined fans in the Auger Basin: central Gulf of Mexico slope. Marine and Petroleum Geology 20, 563-586.

Bouma, A.H., 1962. Sedimentology of some flysch deposits: a graphic approach to facies interpretation. Elsevier, Amsterdam, 168p.

Bouma, A.H., Stelting, C.E., Coleman, J.M., 1985. Mississippi Fan, Gulf of Mexico. In: Bouma, A.H., Normark, W.R., Barnes, N.E. (Eds.), Submarine Fans and Related Turbidite Systems, 143-150.

Bouma, A.H., Wickens, H.d.V., 1991. Permian passive margin submarine fan complex, Karoo Basin, South Africa: possible model to Gulf of Mexico. Gulf Coast Association of Geological Societies 41, 30-42.

Bouma, A.H., 2000. Fine-grained, mud-rich turbidite systems: Model and comparison with coarse-grained, sand-rich systems. In: Bouma, A.H., Stone, C.G. (Eds.), Fine-grained Turbidite Systems. AAPG Memoir 72/SEPM Special Publication 68, 9-19.

Bouma, A.H., Rozman, D.J., 2000. Characteristics of fine grained outer fan fringe turbidite systems. In: Bouma, A.H., Stone, C.G. (Eds.), Fine-grained Turbidite Systems. AAPG Memoir 72/SEPM Special Publication 68, 291–298.

Bourget, J., Zaragosi, S., Mulder, T., Schneider, J.-L., Garlan, T., Van Toer, A., Mas, V., Ellouz-Zimmermann, N., 2010. Hyperpycnal-fed turbidite lobe architecture and recent sedimentary processes: Acase study from the Al Batha turbidite system, Oman margin. Sedimentary Geology 229, 144-159.

Britter, R.E., Simpson, J.E., 1978. Experiments on the dynamics of gravity current head. Journal of Fluid Mechanics 88, 223-240.

Brunt, R.L., McCaffrey, W.D., Kneller, B.C., 2004. Experimental modeling of the spatial distribution of grain size developed in a fill-and-spill mini-basin setting. Journal of Sedimentary Research 74, 438-446.

Brunt, R.L., Hodgson, D.M., Flint, S.S., Pringle, J.K., Di Celma, C., Prélat, A., Grecula, M., 2013a. Confined to unconfined: Anatomy of a base of slope succession, Karoo Basin, South Africa. Marine and Petroleum Geology 41, 206-221.

Brunt, R.L., Di Celma, C.N., Hodgson, D.M., Flint, S.S., Kavanagh, J.P., van der Merwe, W.C., 2013b. Driving a channel through the levee when the levee is high: An outcrop example of submarine down-dip entrenchment. Marine and Petroleum Geology 41, 134-145.

Bugge, T., 1983. Submarine slides on the Norwegian continental margin, with special emphasis on the Storegga area. Continental Shelf Institute Publication 110, 152p.

Bugge, T., Belderson, R.H., Kenyon, N.H., 1988. The Storegga Slide. Philosophical Transactions Royal Society London, Series A 325, 357-388.

Bull, S., Cartwright, J., Huuse, M., 2009. A subsurface evacuation model for submarine slope failure. Basin Research 21, 433-443.

Burgreen, B., Graham, S., 2014. Evolution of a deep-water lobe system in the Neogene trench-slope setting of the East Coast Basin, New Zealand: lobe stratigraphy and architecture in a weakly confined basin configuration. Marine and Petroleum Geology 54, 1-22.

Carr, M., Gardner M.H., 2000. Portrait of a basin-floor fan for sandy deepwater systems, Permian Lower Brushy Canyon Formation, West Texas. In: Bouma, A.H., Stone, C.G. (Eds.), Fine-grained Turbidite Systems. AAPG Memoir 72/SEPM Special Publication 68, 215-232.

Catuneanu, O., Hancox, P.J., Rubidge, B.S., 1998. Reciprocal flexural behaviour and contrasting stratigraphies: a new basin development model for the Karoo retroarc foreland system, South Africa. Basin Research 10, 417-439.

Catuneanu, O., Wopfner, H., Eriksson, P.G., Cairncross, B., Rubidge, B.S., Smith, R.M.H., Hancox, P.J., 2005. The Karoo basins of south-central Africa. Journal of African Earth Sciences 43, 211-253.

Clark, J.D., Pickering, K.T., 1996. Architectural elements and growth patterns of submarine channels: Application to hydrocarbon exploration. AAPG Bulletin 80, 194-221.

Cobain, S.L., Peakall, J., Hodgson, D.M., 2015. Indicators of progradation direction and relative depth in clastic injectites: Implications for laminar versus turbulent flow processes. GSA Bulletin 127, 1816-1830.

Collins, J., Kenyon-Roberts, S., Cullen, B., White, J., Bordas-Le Floch, N., Downey, J. 2015. Arran Field: a complex heterolithic reservoir on the margins of the Forties

Fan System. In: McKie, T., Rose, P.T.S., Hartley, A.J., Jones, D.W., Armstrong, T.L. (Eds.), Tertiary Deep-Marine Reservoirs of the North Sea Region. Geological Society London Special Publication 403, 185-217.

Collinson, J.D., Martinsen, O., Bakken, B., Kloster, A., 1991. Early fill of the Western Irish Namurian Basin: a complex relationship between turbidites and deltas. Basin Research 3, 223-242.

Coussot, P., Meunier, M., 1996. Recognition, classification and mechanical description of debris flows. Earth-Science Reviews 40, 209-227.

Covault, J.A., Romans, B.W., 2009. Growth patterns of deep-sea fans revisited: Turbidite-system morphology in confined basins, examples from the California Borderland. Marine Geology 265, 51-66.

Dakin, N., Pickering, K.T., Mohrig, D., Bayliss, N.J., 2013. Channel-like features created by erosive submarine debris flows: Field evidence from the Middle Eocene Ainsa Basin, Spanish Pyrenees. Marine and Petroleum Geology 41, 62-71.

Davis, C., Haughton, P., McCaffrey, W., Scott, E. Hogg, N., Kitching, D., 2009. Character and distribution of hybrid sediment gravity flow deposits from the outer Forties Fan, Palaeocene Central North Sea, UKCS. Marine and Petroleum Geology, 26, 1919-1939.

Deptuck, M.E., Piper, D.J.W., Savoye, B., Gervais, A., 2008. Dimensions and architecture of late Pleistocene submarine lobes off the northern margin of East Corsica. Sedimentology 55, 869-898.

Di Celma, C.N., Brunt, R.L., Hodgson, D.M., Flint, S.S., Kavanagh, J.P., 2011. Spatial and temporal evolution of a Permian submarine slope channel-levee system, Karoo Basin, South Africa. Journal of Sedimentary Research 81, 579-599.

Dixon, J.F., Steel, R.J., Olariu, C., 2012. River-dominated, shelf-edge deltas: delivery of sand scross the shelf break in the absence of slope incision. Sedimentology 59, 1133-1157.

Dott, R.H., 1963. Dynamics of subaqueous gravity depositional processes. AAPG Bulletin 47, 104-128.

Ducassou, E., Migeon, S., Capotondi, L., Mascle, J., 2013. Run-out distance and erosion of debris-flows in the Nile deep-sea fan system: Evidence from lithofacies and micropalaeontological analyses. Marine and Petroleum Geology 38, 102-123.

Dudley, P.R.C., Rehmer, D.E., Bouma, A.H., 2000. Reservoir-Scale Characteristics of Fine-Grained Sheet Sandstone, Tanqua Karoo Subbasin, South Africa. GCSSEPM Foundation 20th Annual Research Conference. Deep-Water Reservoirs of the World, December 3-6, 200.

Edwards, D.A., 1993. Turbidity Currents: Dynamics, Deposits and Reversals, Lecture Notes in Earth Sciences, no. 44. Springer-Verlag. Berlin.

Edwards, D.A., Leeder, M.R., Best, J.L., Pantin, H.M., 1994. On experimental reflected density currents and the interpretation of certain turbidites. Sedimentology 41, 437- 461.

Enos, P., 1977. Flow regimes in debris flows. Sedimentology 24, 133-142.

Eschard, R., Albouy, E., Gaumet, F., Ayub, A., 2004. Comparing the depositional architecture of basin floor fans and slope fans in the Pab Sandstone, Maastrichtian, Pakistan. In: Lomas, S.A. (Ed.), Confined Turbidite Systems. Geological Society of London, Special Publications 222, pp. 159-185.

Etienne, S., 2012. Caractérisation architecturale haute-résoltion des lobes turbiditiques sableux confinés. Exemple de la Formation des Grès d'Annot (Eocène-Oligocène, SE-France). Unpublished Ph.D. Thesis, Université Bordeaux.

Etienne, S., Mulder, T., Bez, M., Desaubliaux, G., Kwasniewski, A., Parize, O., Dujoncquoy, E., Salles, T., 2012. Multiple scale characterization of sand-rich distal lobe deposit variability: Examples from the Annot Sandstones Formation, Eocene–Oligocene, SE France. Sedimentary Geology 273-274, 1-18.

Faerseth, R. B., Lien, T., 2002. Cretaceous evolution in the Norwegian Sea—a period characterized by tectonic quiescence. Marine and Petroleum Geology 19, 1005-1027.

Feeley, M.H., Bufïler, R.T., Bryant, W.R., 1985. Depositional units and growth pattern of the Mississippi Fan. In: Bouma, A.H., Normark, W.R., Barnes, N.E. (Eds.), Submarine Fans and Related Turbidite Systems. 253–257.

Felix,M., Peakall, J., 2006. Transformation of debris flows into turbidity currents: meachnism infereed from laboratory experiments. Sedimentology 53, 107-123.

Felletti, F., 2002. Complex bedding geometries and facies associations of the turbiditic fill of a confined basin in a transpressive setting (Castagnola Fm., Tertiary Piedmont Basin, NW Italy). Sedimentology 49, 645-667.

Felletti, F., Bersezio, R., 2010. Quantification of the degree of confinement of a turbidite-filled basin: A statistical approach based on bed thickness distribution. Marine and Petroleum Geology 27, 515-532.

Fernandez, R.L., Cantelli, A., Pirmez, C., Sequeiros, O., Parker, G., 2014. Growth patterns of subaqueous depositional channel lobe systems developed over a basement with a downdip break in slope: Laboratory experiments. Journal of Sedimentary Research 84, 168-182.

Ferry, J.N., Mulder, T., Parize, O., Raillard, S., 2005. Concept of equilibrium profile in deep-water turbidite system: effects of local physiographic changes on the nature of sedimentary process and the geometries of deposits. In: Hodgson, D.M., Flint, S.S. (Eds.), Submarine Slope Systems: Processes and Products, Geological Society of London, Special Publications 244, pp. 181-193.

Fiduk, J.C., Weimer, P., Trudgill, B.D., Rowan, M.G., Gale, P.E., Phair, R.L., Korn, B.E., Roberts, G.R., Gafford, W.T., Lowe, R.S., 1999. The Perdido fold belt, northwestern deep Gulf of Mexico, part 2: seismic stratigraphy and petroleum systems. AAPG Bulletin 83, 578-612.

Figueiredo, J.J.P., Hodgson, D.M., Flint, S.S., Kavanagh, J.P., 2010. Depositional environments and sequence stratigraphy of an exhumed Permian mudstone-dominated submarine slope succession, Karoo Basin, South Africa. Journal of Sedimentary Research 80, 97-118.

Figueiredo, J.J.P., Hodgson, D.M., Flint, S.S., Kavanagh, J.P., 2013. Architecture of a channel complex formed and filled during long-term degradation and entrenchment on the upper submarine slope, Unit F, Fort Brown Fm., SW Karoo Basin, South Africa. Marine and Petroleum Geology 41, 104-116.

Fildani, A., Drinkwater, N.J., Weislogel, A., McHargue, T., Hodgson, D.M., Flint, S.S., 2007. Age controls on the Tanqua and Laingsburg deep-water systems: New insights on the evolution and sedimentary fill of the Karoo Basin, South Africa. Journal of Sedimentary Research 77, 901-908.

Fildani, A., Weislogel, A., Drinkwater, N.J., McHargue, T., Tankard, A., Wooden, J., Hodgson, D., Flint,S., 2009. U-Pb zircon ages from the southwestern Karoo Basin, South Africa- Implications for the Permian-Triassic boundary. Geology 37, 719-722.

Fisher, R.V., 1983. Flow transformations in sediment gravity flows. Geology 11, 273-274.

Flint, S.S., Hodgson, D.M., Sprague, A.R., Brunt, R.L., van der Merwe, W.C., Figueiredo, J., Prélat, A., Box, D., Di Celma, C., Kavanagh, J. P., 2011. Depositional architecture and sequence stratigraphy of the Karoo basin floor to shelf edge succession, Laingsburg depocentre, South Africa. Marine and Petroleum Geology 28, 658-674.

Fonnesu, M., Haughton, P., Felletti, F., McCaffrey, W., 2015. Short length-scale variability of hybrid event beds and its applied significance. Marine and Petroleum Geology 67, 583-603.

Frey- Martínez, J., Cartwright, J., James, D., 2006. Frontally confined versus frontally emergent submarine landslides: A 3D seismic characterisation. Marine and Petroleum Geology 23, 585-604.

Fusi, N., Kenyon, N.H., 1996. Distribution of mud diapirism and other geological structures from long-range sidescan sonar (GLORIA) data, in the Eastern Mediterranean Sea. Marine Geology 132, 21-38.

Gamberi, F., Rovere, M., 2011. Architecture of a modern transient slope fan (Villafranca fan, Gioia basin–Southeastern Tyrrhenian Sea). Sedimentary Geology 236, 211-225.

Gamberi, F., Rovere, M., Marani, M., 2011. Mass-transport complex evolution in a tectonically active margin (Gioia Basin, Southeastern Tyrrhenian Sea). Marine Geology 279, 98-110.

Gamundi, O.R., Rossello, E.A., 1998. Basin fill evolution and paleotectonic patterns along the Samfrau geosyncline: the Sauce Grande basin-Ventana foldbelt (Argentina) and Karoo basin-Cape foldbelt (South Africa) revisited. Geologische Rundschau 86, 819-834.

García, M.H., 1990. Depositing and Eroding Sediment-Driven Flows: Turbidity Currents. St. Anthony Falls Hydraulic Laboratory. 179 pp.

García, M.H., 1993. Hydraulic jumps in sediment-driven bottom currents. Journal of Hydraulic Engineering 119, 1094-1117.

García, M., Parker, G., 1993. Experiments on the entrainment of sediment into suspension by a dense bottom current. Journal of Geophysical Research 98, 4793-4807.

García, M.H., 1994. Depositional turbidity currents laden with poorly sorted sediment. Journal of Hydraulic Engineering 120, 1240-1263.

Gardiner, A.R., 2006. The variability of turbidite sandbody pinchouts and its impact on hydrocarbon recovery in stratigraphically trapped fields. In: Allen, M.R., Goffey, G.P., Morgan, R.K., Walker, I.M. (Eds.), The Deliberate Search for the Stratigraphic Trap. Geological Society of London, Special Publication 254, 267-287.

Gardner, M.H., Borer, J.A., Melick, J.J., Mavilla, N., Dechesne, M., and Wagerle, R.N. 2003, Stratigraphic process-response model for submarine channels and related features from studies of Permian Brushy Canyon outcrops, West Texas. Marine and Petroleum Geology, 20, 757-787.

Gee, M.J.R., Masson, D.G., Watts, A.B., Allen, P.A., 1999. The Saharan debris flow: an insight into the mechanics of long runout submarine debris flows. Sedimentology 46, 315-335.

Georgiopoulou, A., Wynn, R., Masson, D.G., Frenz, M., 2009. Linked turbidite-debrite resulting from recent Sahara Slide headwall reactivation. Marine and Petroleum Geology 26, 2021–2031.

Gervais, A., Savoye, B., Mulder, T., Gonthier, E., 2006. Sandy modern turbidite lobes: A new insight from high resolution seismic data: Marine and Petroleum Geology 23, 485-502.

Goldhammer, R.K., Wickens, D.H., Bouma, A.H., Wach, G., 2000. Sequence stratigraphic architecture of the late Permian Tanqua submarine fan complex, Karoo Basin, South Africa. In: Bouma, A.H., Stone, C.G. (Eds.), Fine-grained Turbidite Systems. AAPG Memoir 72/SEPM Special Publication 68, 165-172.

Grant, H.L., (1958). The large eddies of turbulent motions.Journal of Fluid Mechanics 4, 149-190.

Grecula, M., Flint, S.S., Wickens, H.D.V., Johnson, S.D., 2003a. Upward-thickening patterns and lateral continuity of Permian sand-rich turbidite channel fills, Laingsburg Karoo, South Africa. Sedimentology 50, 831-853.

Grecula, M., Flint, S., Potts, G., Wickens, D., Johnson, S., 2003b. Partial ponding of turbidite systems in a basin with subtle growth-fault topography: Laingsburg-Karoo, South Africa. Journal of Sedimentary Research 73, 603-620.

Grecula, M., Hognestad, J., Price, S., Boya Ferrero, M., De Brujin, G., Noraberg, K.T., Engenes, K., Mears, P., Van Ojik, K., McGarva, R., 2015. Interplay of fan-fringe reservoir deteration and hydrodynamic aquifer: understanding the margins of gas development in the Ormen Lange Field. In: McKie, T., Rose, P.T.S., Hartley, A.J., Jones, D.W., Armstrong, T.L. (Eds.), Tertiary Deep-Marine Reservoirs of the North Sea Region. Geological Society London Special Publication 403, 157-183.

Groenenberg, R.M., Hodgson, D.M., Prélat, A., Luthi, S.M., Flint, S.S., 2010. Flow-deposit interaction in submarine lobes: Insights from outcrop observations and realizations of a process-based numerical model. Journal of Sedimentary Research 80, 252-267.

Grundvåg, S.A., Johannessen, E.P., Helland-Hansen, W., Plink-Björklund, P., 2014. Depositional architecture and evolution of progradationally stacked lobe complexes in the Eocene Central Basin of Spitsbergen. Sedimentology 61, 535-569.

Gulliford, A.R., Flint, S.S., Hodgson, D.M., 2014. Testing applicability of models of distributive fluvial systems or trunk rivers in ephemeral systems: Reconstructing 3-D fluvial architecture in the Beaufort Group, South Africa. Journal of Sedimentary Research 84, 1147-1169.

Hadelari, T., Tylosky, S.A., Lemieux, Y., Zantvoort, W.G., Catuneanu, O., 2009. Slope and submarine fan turbidite facies of the Upper Devonian Imperial Formation, Northern Mackenzie Mountains, NWT. Bulletin of Canadian Petroleum Geology 57, 192-208.

Haflidason, H., Sejrup, H.P., Nygård, A., Mienert, J., Bryn, P., Lien, R., Forsberg, C.F., Berg, K., Masson, D., 2004. The Storegga Slide: architecture, geometry and slide development. Marine Geology 213, 201-234.

Hallworth, M.A., Phillips, J.C., Huppert, H.E., Sparks, R.S.J., 1993. Entrainment in turbulent gravity currents. Nature, 362, 829–831.

Hampton, M., 1972. The role of subaqueous debris flow in generating turbidity currents. Journal of Sedimentary Petrology 42, 775-793.

Hampton, M.A., Lee, H.J., Locat, J., 1996. Submarine landslides. Reviews of Geophysics, 34, 33–59.

Hanquiez, V., Mulder, T., Toucanne, S., Lecroart, P., Bonnel, C., Marchès, E., Gonthier, E., 2010. The sandy channel-lobe depositional system in the Gulf of Cadiz:

Gravity processes forced by contour current processes. Sedimentary Geology 229, 110-123.

Hansma, J., Tohver, E., Schrank, C., Jourdan, F., Adams, D., 2015. The timing of the Cape Orogeny: New 40 Ar/39 Ar age constraints on deformation and cooling of the Cape Fold Belt, South Africa. Gondwana Research 32, 122-137.

Harms, J.C., 1974. Brushy Canyon Formation, Texas: A deep-water density current deposit. Bulletin of the Geological Society of America 85, 1763-1784.

Hartog Jager, D.D., Giles, M.R., Griffiths, G.R., 1993. Evolution of Paleogene submarine fans of the North Sea in space and time. In: Parker, J.R. (Ed.), Petroleum Geology of Northwest Europe: Proceedings of the 4th Conference, pp. 59-71.

Haughton, P.D.W., 2000. Evolving turbidite systems on a deforming basin floor, Tabernas, SE Spain. Sedimentology 47, 497-518.

Haughton, P.D.W., Barker, S.P., McCaffrey, W.D., 2003. 'Linked' debrites in sand-rich turbidite systems – Origin and significance. Sedimentology 50, 459-482.

Haughton, P., Davis, C., McCaffrey, W., Barker, S., 2009. Hybrid sediment gravity flow deposits – Classification, origin and significance. Marine and Petroleum Geology 26, 1900-1918.

Heezen, B.C., Ewing, M., 1952. Turbidity currents and submarine slumps, and the 1929 Grand Banks Earthquake. American Journal of Science 250, 849-873.

Heiniö, P., Davies, R.J., 2007. Knickpoint migration in submarine channels in response to fold growth, western Niger Delta. Marine and Petroleum Geology 24, 434-449.

Hess, G.R., Normark, W.R., 1976. Holocene sedimentation history of the major fan valleys of Monterey fan. Marine Geology 22, 233-251.

Hiscott, R.N., 1981. Deep-sea fan deposits in the Macigno Formation (Middle–Upper Oligocene) of the Gordana Valley, Northern Apennines, Italy—Discussion. Journal of Sedimentary Petrology 51, 1015–1033.Hodgson, D.M., Haughton, P.D.W., 2004. Impact of syndepositional faulting on gravity current behaviour and deep-water stratigraphy: Tabernas-Sorbas Basin, SE Spain. In: Lomas, S.A., Joseph, P. (Eds.), Confined Turbidite Systems. Geological Society London Special Publication 222, pp. 135-158.

Hodgson, D.M., Flint, S.S., Hodgetts, D., Drinkwater, N.J., Johannessen, E.P., Luthi, S., 2006. Stratigraphic evolution of fine-grained submarine fan systems, Tanqua depocentre, Karoo Basin, South Africa. Journal of Sedimentary Research 76, 20– 40.

Hodgson, D.M., 2009. Distribution and origin of hybrid beds in sand-rich submarine fans of the Tanqua depocentre, Karoo Basin, South Africa. Marine and Petroleum Geology 26, 1940-1956.

Hodgson, D.M., Di Celma, C.N., Brunt, R.L., Flint, S.S., 2011. Submarine slope degradation and aggradation and the stratigraphic evolution of channel-levee systems. Journal of the Geological Society 168, 625-628.

Hofstra, M., Hodgson, D.M., Peakall, J., Flint,S.S., 2015. Giant-scour fills in ancient channel-lobe transition zones: Formative processes and depositional architecture. Sedimentary Geology 329, 98-114.

Hunter, R.E., 1977. Terminology of cross-stratified sedimentary layers and climbing-ripple structures. Journal of Sedimentary Research 47, 697–706.

Ito, M., 2008. Downfan transformation from turbidity currents to debris flows at a channel-to-lobe transitional zone: The lower Pleistocene Otadai Formation, Boso Peninsula, Japan. Journal of Sedimentary Research 78, 668-682.

Iverson, R.M., 1997. The physics of debris flow. Reviews of Geophysics 35, 245-296.

Jackson, C.A.-L., Zakaria, A.A., Johnson, H.D., Tongkul, F., Crevello, P.D., 2009. Sedimentology, stratigraphic occurrence and origin of linked debrites in the West Crocker Formation (Oligo-Miocene), Sabah, NW Borneo. Marine and Petroleum Geology 26, 1957-1973.

Jegou, I., Savoye, B., Pirmez, C., Droz, L., 2008. Channel-mouth lobe complex of the recent Amazon fan: The missing piece. Marine Geology 252, 62–77.

Jirah, S., Ribidge, B.S., 2014. Refined stratigraphy of the Middle Permian Abrahamskraal Formation (Beaufort Group) in the southern Karoo Basin. Journal of African Earth Sciences 100, 121-135.

Jobe, Z.R., Lowe, D.R., Morris, W.R., 2012. Climbing-ripple successions in turbidite systems: depositional environments, sedimentation rates and accumulation times. Sedimentology 59, 867-898.

Johns, D.R., Mutti, E., Rosell, J., Seguret, M., 1981. Origin of a thick, redeposited carbonate bed in Eocene turbidites of the Hecho Group, South-Central Pyrenees, Spain. Geology 9, 161-164.

Johnson, A. M., 1970. Physical processes in geology: A method for interpretation of natural phenomena; intrusions in igneous rocks, fractures, and folds, flow of debris and ice. Freeman, Cooper and Co, San Fransisco, California, p.571.

Johnson, S.D., Flint, S.S., Hinds, D., Wickens, H.d.V., 2001. Anatomy of basin floor to slope turbidite systems, Tanqua Karoo, South Africa: sedimentology, sequence stratigraphy and implications for subsurface prediction. Sedimentology 48, 987–1023.

Jones, G.E.D., Hodgson, D.M., Flint, S.S., 2013. Contrast in the process response of stacked clinotherms to the shelf-slope rollover. Geosphere 9, 299-316.

Jones, G.E.D., Hodgson, D.M., Flint, S.S., 2015. Lateral variability in clinoform trajectory, process regime, and sediment dispersal patterns beyond the shelf-edge rollover in exhumed basin margin-scale clinothems. Basin Research 27, 657-680.

Jopling, A.V., Walker, R.G., 1968. Morphology and origin of ripple-drift cross-lamination, with examples from the Pleistocene of Massachusetts. Journal of Sedimentary Research 38, 971–984.

Kane, I.A., Kneller, B.C., Dykstra, M., Kassem, A., McCaffrey, W.D., 2007. Anatomy of a submarine channel-levee: An example from Upper Cretaceous slope sediments, Rosario Formation, Baja California, Mexico. Marine and Petroleum Geology 24, 540-563.

Kane, I.A., Hodgson,D.M., 2012. Sedimentological criteria to differentiate submarine channel levee subenvironments: Exhumed examples from the Rosario Fm. (Upper Cretaceous) of Baja California, Mexico, and the Fort Brown Fm., Karoo Basin, S. Africa. Marine and Petroleum Geology 28, 807-823.

Kane, I.A., Pontén, A.S.M., 2012. Submarine transitional flow deposits in the Palaeogene Gulf of Mexico. Geology 40, 1119-1122.

Kane, I.A., Pontén, A.S.M., Vangdal, B. Hodgson, D.M., Eggenhuisen, J.T., in review, Turbidity current transformation in a distal lobe setting: Skoorsteenberg Fm., Tanqua Karoo: Sedimentology.

Kilhams, B., Hartley, A., Huuse, M., Davis, C., 2012. Characterizing the Paleocene turbidites of the North Sea: the Mey Sandstone Member, Lista Formation, UK Central Graben. Petroleum Geoscience 18, 337-354.

King, R.C., Hodgson, D.M., Flint, S.S., Potts, G.J., Van Lente, B., 2009. Development of subaqueous fold belt as a control on the timing and distribution of deepwater sedimentation: An example from the Southwest Karoo Basin, South Africa. In: Kneller, B., Martinsen, O.J., McCaffrey, B. (Eds.), External Controls on Deep-Water Depositional Systems. SEPM Special Publication 92, 261-278.

Klaucke I., Hesse R., Ryan W.B.F, 1997: Flow parameters of turbidity currents in a low-sinuosity giant deep-sea channel. Sedimentology 44, 1093-1102.

Kneller, B., Edwards, D., McCaffrey, W.D., Moore, R., 1991. Oblique reflection of turbidity currents. Geology 14, 250–252.

Kneller, B., 1995. Beyond the turbidite paradigm: Physical models for deposition of turbidites and their implications for reservoir prediction. In: Hartley, A.J. (Ed.), Characterization of Deep Marine Clastic Systems. Geological Society of London, Special Publication 94, 31-49.

Kneller, B.C., Branney, M.J., 1995. Sustained high-density turbidity currents and the deposition of thick massive sands. Sedimentology 42, 607-616.

Kneller, B., McCaffrey, W., 1999. Depositional effects of flow nonuniformity and stratification within turbidity currents approaching a bounding slope: Deflection, reflection, and facies variation. Journal of Sedimentary Research 69, 980-991.

Kneller, B.C., Bennett, S.J., McCaffrey, W.D., 1999. Velocity structure, turbulence and fluid stresses in experimental gravity currents. Journal of Geophysical Research: Oceans 104, 5381-5391.

Kneller, B., Buckee, C., 2000. The structure and fluid mechnics of turbidity currents: A review of some recent studies and their geological implications. Sedimentology 47, 62-94.

Komar, P.D., 1971. Hydraulic jumps in turbidity currents. AAPG Bulletin 82, 1477-1487.

Konsoer, K., Zinger, J., Parker, G., 2013. Bankfull hydraulic geometry of submarine channels created by turbidity currents: relations between bankfull channel

characteristics and formative flow discharge. Journal of Geophysical Research: Earth Surfurface 118, 216–228.

Kuenen, Ph.H., 1948. Troebelingsstroming van hoog soortelijk gewicht. Verslag van de gewone vergadering der Afdeling Natuurkunde, LVII, 3–6.

Kuenen, Ph.H., 1950. Turbidity currents of high density. Report of the 18th Session, International Geological Congress, part 8, London, 44-52.

Kuenen, Ph.H., Migliorini, C.I., 1950. Turbidity currents as a cause of graded bedding. Journal of Geology 58, 91-127.

Kuenen, Ph.H., 1951. Properties of turbidity currents of high density. In: Hough, J.L. (Ed.), Turbidity Currents and the Transportation of Coarse Sediments to Deep Water. SEPM Special Publication 2, 14-33.

Laberg, J.S., Vorren, T.O., 2000. Flow behaviour of the submarine galcigenic debris flows on the Bear Island Trough Mouth Fan, western Barents Sea. Sedimentology 47, 1105-1117.

Laugier, F.J., Plink-Björklund, P., 2016. Defining the shelf edge and the three-dimensional shelf-edge to slope facies variability in the shelf-edge deltas. Sedimentology, doi: 10.1111/sed.12263.

Laursen, J., Normark, W.R., 2003. Impact of structural and autocyclic basin-floor topography on the depositional evolution of the deep-water Valparaiso forearc basin, central Chile. Basin Research 15, 201-226.

Leclair, S.F., Arnott, R.W.C., 2005. Parallel lamination formed by high-density turbidity currents. Journal of Sedimentary Research 75, 1-5.

Levorsen, A.I., 1936. Structural versus structural accumulation. AAPG Bulletin 20, 521-530.

Li, L., Wang, Y., Xu, Q., Zhao, J., Li, D., 2012. Seismic geomorphology and main controls of deep-water gravity flow sedimentary process on the slope of the northern South China Sea. Science China Earth Sciences 55, 747-757.

Li, L., Wang, Y. M., Zhang, L. M., Huang, Z. C., 2010. Confined gravity flow sedimentary process and its impact on the lower continental slope, Niger Delta. Science China Earth Sciences 53, 1169-1175.

Lin, C., Liu, J., Erikkson, K., Yang, H., Cai, Z., Li, H., Yang, Z., Rui, Z., 2014. Late Ordovician, deep-water gravity-flow deposits, palaeogeography and tectonic setting, Tarim Basin, Northwest China. Basin Research 26, 297-319.

Lopez-Mir, B., Muñoz, J.A., Senz, J.G., 2014. Restoration of basins driven by extension and salt tectonics: Example from the Cotiella Basin in the central Pyrenees. Journal of Structural Geology 69, 147-162.

Lowe, D.R., 1979. Sediment gravity flows: their classification and some problems of application to natural flows and deposits. In: Doyle, L.J., Pilkey, O.H. (Eds.), Geology of Continental slopes. SEPM Special Publication 27, 79-82.

Lowe, D.R., 1982. Sediment gravity flows: II. Depositional models with special reference to the deposits of high-density turbidity currents. Journal of Sedimentary Petrology 52, 279-297.

Lowe, D.R., Guy, M., 2000. Slurry-flow deposits in the Britannia Formation (Lower Cretaceous), North Sea: a new perspective on the turbidity current and debris flow problem. Sedimentology 47, 31-70.

Luthi, S., 1980. Die Eigenschaften nichtkanalisierter Trübeströme: Eine experimentelle Untersuchung. Eclogae geologicae Helvetiae 73, 881-904.

Luthi, S., 1981. Experiments on non-channelized turbidity currents and their deposits. Marine Geology 40, M59-M68.

Luthi, S.M., Hodgson, D.M., Geel, C.R., Flint, S.S., Goedbloed, J.W., Drinkwater, N.J., Johannessen, E.P., 2006. Contribution of research borehole data to modelling fine-grained turbidite reservoir analogues, Permian Tanqua-Karoo basin-floor fans (South Africa). Petroleum Geosciences 12, 175-190.

Macdonald, H.A., Peakall, J., Wignall, P.B., Best, J., 2011. Sedimentation in deep-sea lobe-elements: implications for the origin of the thickening-upward sequences. Journal of the Geological Society London 168, 319-331.

MacPherson, B.A., 1978. Sedimentation and trapping mechanism in upper Miocene Stevens and older turbidite fans of Southeastern San Joaquin Valley, California. AAPG Bulletin 62, 2243-2274.

Magalhaes, P., Tinterri, R., 2010. Stratigraphy and depositional setting of slurry and contained (reflected) beds in the Marnoso-arenacea Formation (Langhian-Serravallian) Nrothern Apenninnes, Italy. Sedimentology 57, 1685-1720.

Marchand, A.M.E., Apps, G., Li, W., Rotzien, J.R., 2015. Depositional processes and impact on reservoir quality in deepwater Palaeogene reservoirs, US Gulf of Mexico. AAPG Bulletin 99, 1635-1648.

Marchès, E., Mulder, T., Gonthier, E., Cremer, M., Hanquiez, V., Garlan, T., Lecroat, P., 2010. Perched lobe formation in the Gulf of Cadiz: Interactions between gravity processes and contour currents (Algarve Margin, Southern Portugal). Sedimentary Geology 229, 81-94.

Marini, M., Milli, S., Moscatelli, M., 2011. Facies and architecture of the Lower Messinian turbidite lobe complexes of the Laga Basin (central Appennines, Italy). Journal of Mediterranean Earth Sciences 3, 45-72.

Marini, M., Salvatore, M., Ravnås, R., Moscatelli, M., 2015. A comparative study of confined vs. semi-confined turbidite lobes from the Lower Messinian Laga Basin (Central Apennines, Italy): Implications for assessment of reservoir architecture. Marine and Petroleum Geology 63, 142-165.

Marini, M., Patacci, M., Felletti, F., McCaffrey, W.D., 2016. Fill to spill stratigraphic evolution of a confined turbidite mini-basin succession, and its likely well bore expression: The Castagnola Fm, NW Italy. Marine and Petroleum Geology 69, 94-111.

Marr, J.G., Harff, P.A., Shanmugam, G., Parker, G., 2001. Experiments on subaqueous sandy gravity flows: the role of clay and water content in flow dynamics and depositional structures. GSA Bulletin 113, 1377–1386.

Masson, D.G., Van Niel, B., Waever, P.P.E., 1997. Flow processes and sediment deformation in the Canary Debris Flow on the NW African Continental Rise. Sedimentary Geology 110, 163-179.

Masson, D.G., Canals, M., Alonso, B. Urgeles, R., Huhnerbach, V., 1998. The Canary Debris Flow: source area morphology and failure mechanisms. Sedimentology 45, 411-432.

McCaffrey, W.D., Kneller, B.C., 2001. Process controls on the development of stratigraphic trap potential on the margins of confined turbidite systems and aids to reservoir evaluation. AAPG Bulletin 85, 971-988.

McCaffrey, W.D., Choux, C.M., Baas, J.H., Haughton, P.D.W., 2003. Spatio-temporal evolution of velocity structure, concentration and grain-size stratification within

experimental particulate gravity currents. Marine and Petroleum Geology 20, 851-860.

McCave, I.N., Jones, K.P.N., 1988. Deposition of ungraded muds from high-density non-turbulent turbidity currents. Nature 333, 250-252.

McKay, M.P., Weislogel, A.L., Fildani, A., Brunt, R.L., Hodgson, D.M., Flint, S.S., 2015. U-PB zircon tuff geochronology from the Karoo Basin, South Africa: implications of zircon recycling on stratigraphic age controls. International Geology Review 57, 393-410.

Meiburg, E., Kneller, B., 2010. Tubidity currents and Their Deposits. Annual Review of Fluid Mechanics 42, 135-156.

Miall, A.D., 1988. Facies architecture in clastic sedimentary basins. In: Kleinspehn, K.L., Paola (Eds.), Frontiers in Sedimentary Geology: New Perspectives in Basin Analysis. 67-81.

Middleton, G.V., 1966a. Experiments on density and turbidity currents: I. Motion of the head. Canadian Journal of Earth Sciences 3, 627-637.

Middleton, G.V., 1966b. Experiments on density and turbidity currents: II. Uniform flow of density currents. Canadian Journal of Earth Sciences 3, 523-546.

Middleton, G.V., Hampton, M.A., 1973. Part I. Sediment gravity flows: Mechanics of flow and deposition. Pacific Section SEPM, 1-38.

Middleton, G.V., 1993. Sediment deposition from turbidity currents. Annual Review of Earth & Planetary Seciences 21, 89-114.

Mienert, J., Vanneste, M., Bünz, S., Andreassen, K., Haflidason, H., Sejrup, H.P., 2005. Ocean warming and gas hydrate stability on the mid-Norwegian margin at the Storegga Slide. Marine and Petroleum Geology 22, 233-244.

Migeon, S., Ducassou, E., Le Gonidec, Y., Rouillard, P., Mascle, J., Revel-Rolland, M., 2010. Lobe construction and sand/mud segregation by turbidity currents and debris flows on the western Nile deep-sea fan (Eastern Mediterranean). Sedimentary Geology 229, 124-143.

Migeon, S., Mulder, T., Savoye, B., Sage, F., 2012. Hydrodynamic processes, velocity structure and stratification in natural turbidity currents: Results inferred from field data in the Var Turbidite System. Sedimentary Geology 245, 48-62.

Mitchum, R.M., Van Wagoner, J.C., 1991. High-frequency sequences and their stacking patterns: sequence-stratigraphic evidence of high-frequency eustatic cycles. Sedimentary Geology 70, 131-160.

Mohrig, D., Whipple, K. X., Hondzo, M., Ellis, C., Parker, G., 1998. Hydroplaning of subaqueous debris flows. GSA Bulletin 110, 387–394.

Mohrig, D., Marr, J.G., 2003. Constraining the efficiency of turbididty current generation from submarine debris flows and slides using laboratory experiments. Marine and Petroleum Geology 20, 883-899.

Morris, W.R., Scheilhing, M.H., Wickens, DeV., Bouma, A.H., 2000. Reservoir architecture of deepwater sandstones: examples from the Skoorsteenberg Formation, Tanqua Karoo Sub-Basin, South Africa. In: Weimer,P., Slatt, R.M., Bouma, A.H., Lawrence, D.T. (Eds.), Deep-water reservoirs of the world: Gulf Coast Section SEPM Foundation. Twentieth Annual Research Conference, 1010-1032.

Morris, E.A., Hodgson, D.M., Flint, S.S., Brunt, R.L., Butterworth, P.L., Verhaeghe, J., 2014a. Sedimentology, stratigraphic architecture and depositional context of submarine frontal lobe complexes. Journal of Sedimentary Research 84, 763-780.

Morris, E.A., Hodgson, D.M., Brunt, R.L., Flint, S.S. 2014b. Origin, evolution and anatomy of silt-prone submarine external levées. Sedimentology 61, 1734-1763.

Muck, M.T., Underwood, M.B., 1990. Upslope flow of turbidity currents: A comparison among field observations, theory, and laboratory models. Geology 18, 54-57.

Mulder, T., Cochant, P., 1996. Classification of offshore mass movements. Journal of Sedimentary Research 66, 43-57.

Mulder, T., Alexander, J., 2001. Abrupt change in slope causes variation in the deposit thickness of concentrated particle-driven density currents. Marine Geology 175, 221-235.

Mulder, T., Etienne, S., 2010. Lobes in deep-sea turbidite systems: State of the art. Sedimentary Geology 229, 75-80.

Mulder, T., 2011. Chapter 2-Gravity processes and deposits on the continental slope, rise and abyssal plains. In: Hüneke, H., Mulder, T. (Eds.), Developments in Sedimentology: Deep-Sea Sediments 63, 25-148.

Mutti, E., 1974. Examples of ancient deep-sea fan deposits from Circum-Mediterranean Geosynclines. In: Dott, R.H., Shaver, R.H. (Eds.), Modern and Ancient Geosynclinal Sedimentation. SEPM Special Publication 19, 92-105.

Mutti, E., Ricci Lucchi, F., 1975. Signification de certaines unites sequentielles dans les series à turbidites. Bulletin de la Société Géologique de France 16, 577–582.

Mutti, E., 1977. Distinctive thin-bedded turbidite facies and related depositional environments in the Eocene Hecho Group (South-central Pyrenees, Spain). Sedimentology 24, 107-131.

Mutti, E. and Sonnino, M., 1981. Compensation cycles: a diagnostic feature of turbidite sandstone lobes. International Association of Sedimentologists, 2nd European Meeting, Bologna, Abstracts (pp. 120-123).

Mutti, E., Normark, W.R., 1987. Comparing examples of modern and ancient turbididte systems: Problems and concepts. In: In Leggett, J.K. and Zuffa, C.G. (Eds.), Marine Clastic Sedimentology: Concepts and Case Studies. Graham & Trotman, London, 1-38.

Mutti, E., 1992. Turbidite Sandstones, Agip -Instituto di Geologia, Università di Parma, Italy, 275p.

Nelson, C.H., Twichell, D.C., Schwab, W.C., Lee, H.J., Kenyon, N.H., 1992. Upper Pleistocene turbidite sand beds and chaotic silt beds in the channelized, distal, outer-fan lobes of the Mississippi fan. Geology 20, 693–696.

Nagatomo, A., Archer, S., 2015. Termination geometries and reservoir properties of the Forties Sandstone pinch-out, East Central Graben, UK North Sea. In: McKie, T., Rose, P.T.S., Hartley, A.J., Jones, D.W., Armstrong, T.L. (Eds.), Tertiary Dee-Marine Reservoirs of the North Sea Region.Geological Society of London, Special Publication 403, 133-155.

Normark, W.R. 1970. Channel piracy on Monterey Deep-Sea Fan. Deep-Sea. Deep-Sea Research and Oceanographic Abstracts 17, 837-846.

Normark, W.R., Piper, D.J.W., 1972. Sediments and growth pattern of Navy Deep-Sea Fan, San Clemente Basin, California Borderland. The Journal of Geology 80, 198-223.

Normark, W.R., 1978. Fan valleys, channels, and depositional lobes on modern submarine fans: Characters for recognition of sandy turbidite environments. AAPG Bulletin 62, 912-931.

Normark, W.R., Piper, D.J.W., Hess, G.R., 1979. Distributary channels, sand lobes, and mesotopography of Navy Submarine Fan, California Borderland, with applications to ancient fan sediments. Sedimentology 26, 749-774.

Normark, W.R., Paull, C. K., Caress, D.W., Ussler, W., Silter, R., 2009. Fine-scale relief related to Late Holocene channel shifting within the floor of the upper Redondo Fan, offshore Southern California. Sedimentology 56, 1690-1704.Nygård, A., Sejrup, H.P., Haflidason, H., King, E.L., 2002. Geometry and genesis of glacigenic debris flows on the North Sea Fan: TOBI imagery and deep-tow boomer evidence. Marine Geology 188, 15-33.

Oliveira, C. M., Hodgson, D. M., Flint, S. S., 2009. Aseismic controls on in situ soft-sediment deformation processes and products in submarine slope deposits of the Karoo Basin, South Africa. Sedimentology 56, 1201-1225.

Oliveira, C.M.M., Hodgson, D.M., Flint, S.S., 2010. Distribution of soft-sediment deformation structures in clinoform successions of the Permian Ecca Group, Karoo Basin, South Africa. Sedimentary Geology 235, 314-330.

Oluboyo, A.P., Gawthorpe, R.L., Bakke, K., Hadler-Jacobson, F., 2014. Salt tectonic controls on deep-water turbidite depositional systems: Miocene, southwestern Lower Congo Basin, offshore Angola. Basin Research 26, 597-620.

Ortiz-Karpf, A., Hodgson, D.M., McCaffrey, W.D., 2015. The role of mass-transport complexes in controlling channel avulsion and the subsequent sediment dispersal patterns on an active margin: The Magdalena Fan, offshore Colombia. Marine and Petroleum Geology 64, 58-75.

Ouchi, S., Ethridge, F.G., James, E.W., Schumm, S.A., 1995. Experimental study of subaueous fan development. In: Hartley, A.J., Prosser, D.J. (Eds.), Characterization of Deep Marine Clastic Systems. Geological Society Special Publication 4, 13-29.

Parker Gay, S., 1989. Gravitational Compaction, A Neglected Mechanism in Structural and Stratigraphic Studies: New Evidence from Mid-Continent, USA. AAPG Bulletin 73, 641-657.

Patacci, M., Haughton, P.D.W., McCaffrey, W.D., 2014. Rheological complexity in sediment gravity flows forced to decelerate against a confining slope, Braux, SE France. Journal of Sedimentary Research 84, 270-277.

Peakall, J., McCaffrey, B., Kneller, B., 2000. A process model for the evolution, morphology, and architecture of sinous submarine channels: Perspectives. Journal of Sedimentary Research 70, 434-448.

Peakall, J., Sumner, E., 2015. Submarine channel flow processes and deposits:A process-product perspective. Geomorphology 244, 95-120.

Pickering, K. T., 1981. Two types of outer fan lobe sequence, from the late Precambrian Kongsfjord Formation submarine fan, Finnmark, North Norway. Journal of Sedimentary Research 51, 1277-1286.

Pickering, K. T., 1983. Transitional submarine fan deposits from the late Precambrian Kongsfjord Formation submarine fan, NE Finnmark, N. Norway. Sedimentology 30, 181-199.

Pickering, K.T., Hiscott, R.N., 1985. Contained (reflected) turbidity currents from the Middle Ordovician Cloridorme Formation, Quebec, Canada: an alternative to the antidune hypothesis (flysch succession). Sedimentology 32, 373-394.

Pickering, K.T., Hiscott, R.N., Hein, F.J., 1989. Deep marine environments: Clastic sedimentation and tectonics. Unwin Hyman, London, 416 pp.

Pickering, K.T., Hilton, V.C., 1998. Turbidite systems of Southeast France. Application to hydrocarbon prospectivity. Vallis Pr., London, 229pp.

Pickering, K.T., Corregidor, J., 2005. Mass-transport complexes (MTCs) and tectonic control on basin-floor submarine fans, middle Eocene, South Spanish Pyrenees. Journal of Sedimentary Research 75, 761-783.

Pickering, K.T., Corregidor, J., Clark, J.D., 2015. Architecture and stacking patterns of lower-sloep and proximal basin-floor channelized fans, Middle Eocene Ainsa System, Spanish Pyrenees: An integrated outcrop-subsurface study. Earth-Science Reviews 144, 47-81.

Picot, M., Droz, L., Marsset, T., Dennielou, B., Bez, M., 2016. Controls on turbidite sedimentation: Insights from a quantitative approach of submarine channel and lobe architecture (Late Quaternary Congo Fan). Marine and Petroleum Geology 72, 423-446.

Piper, D.J.W., Normark, W.R., 1983. Turbidite depositional patterns and flow characteristics, Navy Submarine Fan, California Borderland: Sedimentology 30, 681-694.

Piper, D.W.J., Hiscott, R.N., Normark, W.R., 1999. Outcrop-scale acoustic facies analysis and latest Quaternary development of Hueneme and Dume submarine fans, offshore California. Sedimentology 46, 47-78.

Piper, D.J.W., Normark, W.R., 2009. Processes that initiate turbidity currents and their influence on turbidites: A marine geology perspective. Journal of Sedimentary Research 79, 347-362.

Pirmez, C., Imran, J., 2003. Reconstruction of turbidity currents in Amazon Channel. Marine and Petroleum Geology 20, 823-849.

Pirmez, C., Prather, B.E., Mallarino, G., O'Hayer, W.W., Droxler, A.W., Winker, C.D., 2012. Chronostratigraphy of the Brazos-Trinity depositional system, Western Gulf of Mexico: Implications for deepwater depositional models. In: Prather, B.E., Deptuck, M.E., Mohrig, D., van Hoorn, B., Wynn, R.B. (Eds.), Application of the Principles of Seismic Geomorphology to Continental -Slope and Base-of-Slope Systems: Case Studies from Seafloor and Near-Seafloor Analogues. SEPM Special Publication 99, pp. 112- 143.

Plink-Björklund, P., Steel, R., 2002. Sea-level fall below the shelf edge, without basin-floor fans. Geology 30, 115-118.

Posamentier, H.W., Kolla, V., 2003. Seismic geomorphology and stratigaphy of depositional elements in deep-water settings. Journal of Sedimentary Research 73, 367-388.

Prather, B.E., Booth, J.R., Steffens, G.S., Craig, P.A., 1998. Classification, lithologic calibration, and stratigraphic succession of seismic facies of intraslope basins, Deep-Water Gulf of Mexico. AAPG Bulletin 82, 701-728.

Prather, B.E., Pirmez, C., Sylvester, Z., Prather, D.S., 2012a. Stratigraphic response to evolving geomorphology in a submarine apron perched on the upper Niger Delta Slope. In: Prather, B.E., Deptuck, M.E., Mohrig, D., van Hoorn, B., Wynn, R.B. (Eds.), Application of the Principles of Seismic Geomorphology to Continental -Slope and Base-of-Slope Systems: Case Studies from Seafloor and Near-Seafloor Analogues. SEPM Special Publication 99, pp. 145- 161.

Prather, B.E., O'Byrne, C., Pirmez, C., Sylvester, Z., 2016. Sediment partitioning, continental slopes and base-of-slope systems. Basin Research, DOI: 10.1111/bre.12190

Prather, B.E., Pirmez, C., Winker, C.D. 2012b. Stratigraphy of linked intraslope basins: Brazos-Trinity System Western Gulf of Mexico. In: Prather, B.E., Deptuck, M.E., Mohrig, D.,van Hoorn, B., Wynn, R.B. (Eds.), Application of the Principles of Seismic Geomorphology to Continental -Slope and Base-of-Slope Systems: Case Studies from Seafloor and Near-Seafloor Analogues. SEPM Special Publication 99, pp. 83- 109.

Prélat, A., Hodgson, D.M., Flint, S.S., 2009. Evolution, architecture and hierarchy of distributary deep-water deposits: a high-resolution outcrop investigation from the Permian Karoo Basin, South Africa. Sedimentology 56, 2132-2154.

Prélat, A., Covault, J.A., Hodgson, D.M., Fildani, A., Flint, S. S. 2010. Intrinsic controls on the range of volumes, morphologies, and dimensions of submarine lobes. Sedimentary Geology 232, 66-76.

Prélat, A., Hodgson, D.M., 2013. The full range of turbidite bed thickness patterns in submarine lobes: controls and implications. Journal of Geological Society of London 170, 1-6.

Pringle, J.K., Brunt, R.L., Hodgson, D.M., Flint, S.S., 2010. Capturing stratigraphic and sedimentological complexity from submarine channel complex outcrops to digital 3D models, Karoo Basin, South Africa. Petroleum Geoscience 16, 307-330.

Prior, D.B., Bornhold, B.D., Johns, M.W., 1984. Depositional characteristics of a submarine debris-flow. Journal of Geology 92, 707-727.

Puigdefàbregas, C., Gjelberg, J., Vaksdal, M., 2004. The Grès d'Annot in the Annot syncline: outer basin-margin onlap and associated soft-sediment deformation. In: Joseph, P., Lomas, S.A. (Eds.), Deep-Water Sedimentation in the Alpine Basin of Se France: New Perspectives on the Gres d'Annot and related systems. Geological Society of London Special Publication 221, 367-388.

Pyrcz, M.J., Catuneanu, O., Deutsch, C.V., 2005. Stochastic surface-based meodeling of turbidite lobes. AAPG Bulletin 89, 177-191.

Pyles, D.R., 2008. Multiscale stratigraphic analysis of a structurally confined submarine fan: Carboniferous Ross Sandstone, Ireland. AAPG Bulletin 92, 557-587.

Pyles, D.R., Jennette, D.C., 2009. Geometry and architectural associations of co-genetic debrite–turbidite beds in basin-margin strata, Carboniferous Ross Sandstone (Ireland): Applications to reservoirs located on the margins of structurally confined submarine fans. Marine and Petroleum Geology 26, 1974-1996.

Pysklywec, R.N., Mitrovica, J.X., 1999. The role of subduction-induced subsidence in the evolution of the Karoo Basin. The Journal of Geology 107, 155-164.

Ricci Lucchi, F., 1967. Trasporti gravitativi sinsedimentari nel Tortoniano dell'Appennino Romagnoldo (Valle Del Savio). Committee Mediterranean Neogene Stratigraphy, Proceedings IV Session, Giornale de Geologia, series 2, 1-30.

Ricci Lucchi, F., 1975. Depositional cycles in two turbidite formations of the northern Apennines. Journal of Sedimentary Research 45, 3-43.

Rittenhouse, G., 1972. Stratigraphic-trap classification: Geologic exploration methods. In: Gould, H.R. (Ed.), Stratigraphic Oil and Gas Fields—Classification, Exploration Methods, and Case Studies. AAPG Memoir 16, 14-28.

Romans, B.W., Hubbard, S.M., and Graham, S.A. 2009, Stratigraphic evolution of an outcropping continental slope system, Tres Pasos Formation at Cerro Divisadero, Chile. Sedimentology 56, 737-764.

Rowan, M.G., Lawton, T.F., Giles, K.A., Ratliff, R.A., 2003. Near-salt deformation in La Popa basin, Mexico, and the northern Gulf of Mexico: A general model for passive diapirism. AAPG Bulletin 87, 733-756.

Rozman, D.J., 2000. Characterization of a fine-grained outer submarine fan deposit, Tanqua-Karoo Basin, South Africa. In: Bouma, A.H., Stone, C.G. (Eds.), Fine-grained Turbidite Systems. AAPG Memoir 72/SEPM Special Publication 68, 279-290.

Rubidge, B.S., 1991. A new primitive dinocephalian mammal-like reptile from the Permian of southern Africa. Palaeontology 34, 547-559.

Saller, A., Werner, K., Sugiaman, F., Cebastiant, A., May, R., Glenn, D., Barker, C., 2008. Characteristics of Pleistocene deep-water fan lobes and their application to an upper Miocene reservoir model, offshore East Kalimantan, Indonesia. AAPG Bulletin 92, 919–949.

Salles, L., Ford, M., Joseph, P., 2014. Characteristics of axially-sourced turbidite sedimentation on an active wedge-top basin (Annot Sandstone, SE France). Marine and Petroleum Geology 56, 305-323.

Schlager, W., 1993. Accommodation and supply- a dual control on stratigraphic sequences. Sedimentary Geology 86, 111-136.

Schwalbach, J.R., Edwards, B.D., Gorsline, D.S., 1996. Contemporary channel-levee systems in active borderland basin plains, California Continental Borderland. Sedimentary Geology 104, 53-72.

Sclater, P.A.F., Christie, J.G., 1980. Continental stretching: an explanation of the post-mid-Cretaceous subsidence of the central North Sea basin. Journal of Geophysical Research 85, 3711-3739.

Sheldon, N.D., Retallack, G.J., 2001. Equation for compaction of paleosols due to burial. Geology 29, 247-250.

Simpson, J.E., Britter, R.E., 1979. The dynamics of the head of a gravity current advancing over a horizontal surface. Journal of Fluid Mechanics 94, 477-495.

Simpson, J.E., 1997. Gravity currents in the environment and the laboratory. 2nd Edition, Cambridge University Press. New York. 258 pp.

Sinclair, H.D., 2000. Delta-fed turbidites infilling topographically complex basins: A new depositional model for the Annot Sandstones, SE France. Journal of Sedimentary Research 70, 504-519.

Sinclair, H.D., Tomasso, M., 2002. Depositional evolution of confined turbidite basins. Journal of Sedimentary Research 72, 451-456.

Sixsmith, P.J., 2000. Stratigraphic development of a Permian turbidite system on a deforming basin floor: Laingsburg Formation, Karoo basin, South Africa. Ph.D. thesis, University of Liverpool, Liverpool.

Sixsmith, P.J., Flint, S.S., Wickens, H.D., Johnson, S.D., 2004. Anatomy and stratigraphic development of a basin floor turbidite system in the Laingsburg Formation, Main Karoo Basin, South Africa. Journal of Sedimentary Research 74, 239-254.

Smith, R., 1987a. Structure and deformation history of the Central Wales Synclinorium, northeast Dyfed: evidence for a long-lived basement structure. Geological Journal 22, 183-198.

Smith, R., 1987b. The griestoniensis zone turbidite system, Welsh Basin. In Leggett, J.K. and Zuffa, C.G. (Eds.), Marine Clastic Sedimentology: Concepts and Case Studies. Graham & Trotman, London, 89-107.

Smith, R., Møller, N., 2003. Sedimentology and reservoir modelling of the Ormen Lange field, mid Norway. Marine and Petroleum Geology 20, 601-613.

Smith, R., 2004 a. Silled sub-basins to connected tortuous corridors: Sediment distribution systems on topographically complex sub-aqueous slopes. In: Lomas, S.A. (Ed.), Confined Turbidite Systems. Geological Society London Special Publication 222, 23-43.

Smith, R., 2004 b. Turbidite systems influenced by structurally induced topography in the multi-sourced Welsh Basin. In: Lomas, S.A., Joseph, P. (Eds.), Confined Turbidite Systems. Geological Society London Special Publication 222, 209-228.

Smith, R., Joseph, P., 2004. Onlap stratal architectures in the Grès d'Annot: geometric models and controlling factors. In: Joseph, P., Lomas, S.A. (Eds.), Deep-Water Sedimentation in the Alpine Basin of Se France: New Perspectives on the Gres d'Annot and related systems. Geological Society London Special Publication 221, 389-399.

Sømme, T.O., Helland-Hansen, W., Martinsen, O., Thurmond, J.B., 2009. Relationships between morphological and sedimentological parametres in source-to-sink systems: a basis for predicting semi-quantitative characteristics in subsurface systems. Basin Research 21, 361–387.

Southard, J.B., 1991. Experimental determination of bed-Form stability. Annual Review of Earth and Planetary Science 19, 423-55.

Southern, S.J., Patacci, M., Felletti, F., McCaffrey, W.D., 2015, Influence of flow containment and substrate entrainment upon sandy hybrid event beds containing a co-genetic mud-clast rich division. Sedimentary Geology 321, 105-122.

Spikings, A.L., Hodgson, D.M., Paton, D.A., Spychala, Y.T., 2015. Palinspastic restoration of an exhumed deep-water system: a workflow to improve paleogeographic reconstructions. SEG Interpretation 3 (4), SAA71-SAA87.

Sprague, A.R., Sullivan, M.D., Campion, K.M., Jensen, G.N., Goulding, F.J., Garfield, T.R., Sickafoose, D.K., Rossen, C., Jennette, D.C., Beaubouef, R.T., Abreu, V., Ardill, J., Porter, M.L., Zelt, F.B., 2003. The physical stratigraphy of deep-water strata: a hierarchical approach to the analysis of genetically related stratigraphic elements for improved reservoir prediction (Abstract) AAPG Annual Meeting. AAPG Bull., 87, 10.

Spychala, Y.T., Hodgson, D.M., Flint, S.S., Mountney, N.P., 2015. Constraining the sedimentology and stratigraphy of submarine intraslope lobe deposits using exhumed examples from the Karoo Basin, South Africa: Sedimentary Geology 322, 67-81.

Stacey, M. W., Bowen, A.J., 1988. The vertical structure of density and turbidity currents: Theory and observations. Journal of Geophysical Research 93, 3528-3542.

Stearns, D.W., 1978. Faulting and forced folding in the Rocky Mountains foreland. In: Matthew, V. III (Ed.), Laramide Folding Associated with Basement Block Faulting in the Western United States. GSA Memoirs 151, 1-37.

Stephen, K.D., Clark, J.D., Gardiner, A.R., 2001. Outcrop-based stochastic modelling of turbidite amalgamation and its effects on hydrocarbon recovery. Petroleum Geoscience 7, 163-172.

Stevenson, C.J., Talling, P.J., Wynn, R.B., Masson, D.G., Hunt, J.E., Fren, M., Akhmetzhanhov, A., Cronin, B.T., 2013. The flows that left no trace: investigating very large-volume turbidity currents that bypassed sediment through submarine channels without eroding the seafloor. Marine and Petroleum Geology 41, 186-205.

Stevenson, C.J., Talling, P.J., Sumner, E.J., Masson, D.G., Frenz, M., Wynn, R.B., 2014. On how thin submarine flows transported large volumes of sand for hundreds of kilometres across a flat basin plain without eroding the sea floor. Sedimentology 61, pp.1982-2019.

Stewart, S.A., Clark, J.A., 1999. Impact of salt on the structure of the Central North Sea hydrocarbon fairways. Petroleum Geology Conference series 5, 179- 200.

Stow, D.A.V., Bowen, A.J., 1980. A physical model for the transport and sorting of fine-grained sediment by turbidity currents. Sedimentology 27, 31-46.

Stow, D.A.V., Piper, D.J.W., 1984. Deep-water fine-grained sediments: facies models. In: Stow, D.A.V., Piper, D.J.W. (Eds.), Fine-grained Sediments: Deep-water Processes and Facies. Geological Societyof London, Special Publication 15, pp. 611-646.

Stow, D.A.V., 1996. Deep seas. In: H.G. Reading (Ed.), Sedimentary environments: processes, facies and stratigraphy, Blackwell Sciences, Oxford, 395–453.

Straub, K.M., Paola, C., Mohrig, D., Wolinsky, M.A.,George, T., 2009. Compensational stacking of channelized sedimentary deposits. Journal of Sedimentary Research 79, 673-688.

Sullivan, M.D., Foreman, J.L., Jennette, D.C., Stern, D., Jensen, G.N., Goulding, F.J., 2004. An integrated approach to characterization and modeling of deep-water reservoir, Diana Field, Western Gulf of Mexico. In: Grammer, G.M., Harris, P.M., Eberli, G.P. (Eds.), Integration of outcrop and modern analogs in reservoir modelling. AAPG Memoir 80, 215-234.

Sumner, E.J., Amy, L.A., Talling, P.J., 2008. Deposit structure and processes of sand deposition from decelerating sediment suspensions. Journal of Sedimentary Research 79, 529-547.

Sumner, E.J., Talling, P.J., Amy, L.A., 2009. Deposits of flows transitional between turbidity current and debris flow. Geology 37, 991-994.

Swart, R., 1994. Late Precambrian outer-fan turbidites from Namibia – vertical and lateral characteristics. Journal of African Earth Sciences 18, 3-13.

Talling, P.J., Amy, L.A., Wynn, R.B., Peakall, J., Robinson, M., 2004. Beds comprising debrite sandwiched within co-genetic turbidite: origin and widespread occurrence in distal depositional envrionments. Sedimentology 51, 163-194.

Talling, P.J., Amy, L.A., Wynn, R.B., Blackbourn, G., Gibson, O., 2007. Evolution of turbidity currents deduced from extensive thin turbidites: Marnoso Arenacea Formation (Miocene), Italian Apennines. Journal of Sedimentary Research 77, 172-196.

Talling, P.J., Masson, D.G., Sumner, E.J., Malgesini, G., 2012a. Subaqueous sediment density flows: Depositional processes and deposit types. Sedimentology 59, 1937-2003.

Talling, P.J., Malgesini, G., Sumner, E.J., Amy, L.A., Felletti, F., Blackbourn, G., Nutt, C., Wilcox, C., Harding, I.C., and Akbari, S., 2012b, Planform geometry, stacking pattern, and extrabasinal origin of low strength and intermediate strength cohesive debris flow deposits in the Marnoso-arenacea Formation, Italy: Geosphere, v. 8, p. 1207-1230.

Talling, P.J., 2013. Hybrid submarine flows comprising turbidity current and cohesive debris flow: Deposits, theoretical and experimental analyses, and generalized models 9, 460-488.

Tankard, A., Welsink, H., Aukes, P., Newton, R., Stettler, E., 2009. Tectonic evolution of the Cape and Karoo basins of South Africa. Marine and Petroleum Geology 26, 1379-1412.

Tinker, J., de Wit, M., Brown, R., 2008. Mesozoic exhumation of the southern Cape, South Africa, quantified using apatite fission track thermochronology. Tectonophysics 455, 77-93.

Twichell, D.C., Schwab, W.C., Nelson, C.H., Kenyon, N.H., Lee, H.J., 1992. Characteristics of a sandy depositional lobe on the outer Mississippi fan from DeaMARC IA sidescan sonar images. Geology 20, 689–692.

Twichell, D.C., Cross, V.A., Hanson, A.D., Buck, B.J., Zybala, J.G., Rudin, M.J., 2005. Seismic architecture and lithofacies of turbidites in Lake Mead (Arizona and Nevada, U.S.A.), an analogue for topographic complex basins: Journal of Sedimentary Research, v. 75, p. 134-148.

van der Merwe, W.C., Hodgson, D.M., Flint, S.S., 2009. Widespread syn-sedimentary deformation on a muddy deep-water basin-floor: the Vischkuil Formation (Permian), Karoo Basin, South Africa. Basin Research 21, 389-406.

van der Merwe, W.C., Flint, S.S., Hodgson, D.M., 2010. Sequence stratigraphy of an argillaceous, deepwater basin-plain succession: Vischkuil Formation (Permian), Karoo Basin, South Africa. Marine and Petroleum Geology 27, 321-333.

van der Merwe, W.C., Hodgson, D.M., Flint, S.S., 2011. Origin and terminal architecture of a submarine slide: a case study from the Permian Vischkuil Formation, Karoo Basin, South Africa. Sedimentology 58, 2012-2038.

van der Merwe, W.C., Hodgson, D.M., Brunt, R.L., Flint, S.S., 2014. Depositional architecture of sand-attached and sand-detached channel-lobe transition zones on an exhumed stepped slope mapped over a 2500 km^2 area. Geosphere 10, 1076-1093.

van der Werff, W., Johnson, S., 2003a. High resolution stratigraphic analysis of a turbidite system, Tanqua Karoo Basin, South Africa: Marine and Petroleum. Geology 20, 45-69.

van der Werff, W., Johnson, S., 2003b. Deep-sea fan pinch-out geometries and their relationship to fan architecture, Tanqua Karoo basin (South Africa). Geologische Rundschau 92, 728-742.

Vernai, P., 1998. Three-dimensional seismic stratigraphic expression of Pliocene-Pleistocene turbidite systems, Northern Green Canyon (Offshore Louisiana), Northern Gulf of Mexico. AAPG Bulletin 82, 986-1012.

Viljoen, J.H.A., 1992. Lithostratigraphy of the collingham formation (Ecca group), including the Zoutekloof, Buffels river and Wilgenhout river members and the Matjiesfontein chert bed. In: Geological Survey, South African Committee for Stratigraphy–Lithostratigraphic Series No. 22, p. 10.

Viljoen, J.H.A., 1994. Sedimentology of the collingham formation, karoo Supergroup, south Africa. Journal of Geology 97, 167–183.

Visser, J.N.J., 1997. Deglaciation sequences in the Permo-Carboniferous Karoo and Kalahari basins of the southern Africa: a toll in the analysis of cyclic glaciomarine basin fills. Sedimentology 44, 507-521.

Visser, J.N.J., Prackelt, H.E., 1996. Subduction, mega-shear systems and Late Palaeozoic basin development in the African segment of Gondwana. Geologische Rundschau 85, 632-646.

Weber. M.E., Wiedicke, M.H., Kudrass, H.R., Hübscher, C., Erlenkeuser, H., 1997. Active growth of the Bengal Fan during sea-level rise and highstand. Geology 25, 315-318.

Wickens, H.d.V., 1994. Basin floor fan building turbidites of the southwestern Karoo Basin, Permian Ecca Group. PhD Thesis, Port Elizabeth University, South Africa, 233pp.

Wickens, H.d.V., Bouma, A.H., 2000. The Tanqua Fan Complex, Karoo Basin, South Africa – outcrop analogue for fine-grained, deepwater deposits. In: Bouma, A.H., Stone, C.G. (Eds.), Fine-grained Turbidite Systems. AAPG Memoir 72/SEPM Special Publication 68, 153–165.

Wild, R.J., Hodgson, D.M., Flint, S.S., 2005. Architecture and stratigraphic evolution of multiple, vertically-stacked slope-channel complexes, Tanqua depocentre, Karoo Basin, South Africa. In: Hodgson, D.M., Flint, S.S. (Eds.), Submarine Slope Systems, Processes and Products. Geological Society London Special Publication 244, 89–112.

Wild, R., Flint, S.S., Hodgson, D.M., 2009. Stratigraphic evolution of the upper slope and shelf edge in the Karoo Basin, South Africa. Basin Research 21, 502-527.

Wilson, D., Davies, J.R., Waters, R.A., Zalasiewicz, J.A., 1992. A fault-controlled depositional model for the Aberystwyth Grits turbiditic system. Geological Magazine 129, 595-607.

Wilson, A., Flint, S., Payenberg, T., Tohver, E., Lanci, L., 2014. Architectural styles and sedimentology of the fluvial lower Beaufort Group, Karoo Basin, South Africa. Journal of Sedimentary Geology 84, 326-348.

Wood, A., Smith, A.J., 1958. The sedimentation and sedimentary history of the Aberystwyth Grits (Upper Llandoverian). Quarterly Journal of the Geological Society 114, 163-195.

Woodcock, N.H., 1979. Sizes of submarine slides and their significance. Journal of Structural Geology 1, 137-142.

Wynn, R.B., Weaver, P.E., Masson, D.G., Stow, D.A.V., 2002. Turbidite depositional architecture across three interconnected deep-water basins on the north-west African margin. Sedimentology 49, 669-695.

Wynn, R.B., Talling, P.J., Masson, D.G., Le Bas, T.P., Cronin, B.T., Stevenson, C.J., 2012. The influence of subtle gradient changes on deep-water gravity flows: A case study from the Moroccan Turbidite System. In: Prather, B.E., Deptuck, M.E., Mohrig, D., Van Hoorn, B., Wynn, R.B (Eds.), Application of the Principles of Seismic Geomorphology to Continental-Slope and Base-of-Slope Systems: Case Studies from Seafloor and Near-Seafloor Analogues. SEPM Special Publication 99, 347-369.

Yang, S.-Y., Kim, J.W., 2014. Pliocene basin-floor fan sedimentation in the Bay of Bengal (offshore northwest Myanmar). Marine and Petroleum Geology 49, 45-58.

Zakaria, A.A., Johnson, H.D., Jackson, C.A.L., Tongkul, F., 2013. Sedimentary facies analysis and depositional model of the Palaeogene West Crocker submarine fan system, NW Borneo. Journal of Asian Earth Science 76, 283-300.

Appendix A

Methods

A.1 Creation of isopach maps with ArcGIS

Isopach maps for palaeogeographical reconstructions were constructed using the Geostatistical Wizard of ArcGIS. Input data were collected and prepared in Excel.

A.1.1 Data preparation with Excel

- Data can be loaded into ArcGIS directly from Excel
- Be aware that in the column headers all the top row symbols are forbidden except for the underscore
- All column headers must start with a letter
- If Excel file is open before ArcGIS the document is live and changes made to Excel can be seen in ArcGIS when refreshing it

Object ID	LogName	LogCode	X_Base	Y_Base	A1_Total	A2_Total	A3_Total	A5_Total	A.6_Total
1	Skeidingen 1	SK1	471633	6324409	19	22	15	105.5	26
2	Skeidingen 2	SK2	474177	6323462	20.5	24	25	109	26
3	Rietfontein 1	RF1	473247	6327299	22.5	23.5	39.5	101.5	24
4	Doornkloof 1	DK1	462193	6330990	8.5	33	38.5	53.5	20
5	Doornkloof 2	DK2	461431	6330838	14.5	39	23	47	20
6	Doornkloof 3	DK3	462571	6330976	9.5	40	31	48	20
7	Doornkloof 4	DK4	463809	6330939	18	34	29	29.5	24.5

Table A.1. Representative chart of thickness data preparation for the creation of isopach maps in ArcGIS.

A.1.2 Importing data into ArcGIS

- Use the Add button to load data into ArcGIS
- Display the data by right clicking on it in the contents panel and 'display XY data'
- Choose the relevant thickness column as your z field

A.1.3 Plotting data in ArcGIS

- Use the Geostatistical analyst
- Choose the Geostatistical Wizard
- Under methods on the left choose Kriging/CoKriging
- Choose your dataset and your field, e.g. A1_Total
- Click 'Next'
- Next click on 'Order of trend removal' and choose 'constant'
- Click 'Next'
- Now a value for 'Exploratory Trend Surface Analysis' needs to be supplied. With low values interpolation between the important data is weak, while with high numbers all data is taken into account, but might be overinterpreted. Data points turn green or red after typing in a value according to their loading. Green: loading is good. Red: loading is bad.
- Click in 'Finish'

A.1.4 Using the data:

- Click right on your Kriging result in the content panel, choose properties and go to symbology
- Click on 'Classify'
- Under 'Classification' use 'Equal Intervals' under 'Methods'
- Costum Min/Max needs to be turned to true and defined under the 'Breaks' section
- Use appropriate amount of classes
- Click 'Ok'
- Colours, contours and/or filling can all be customised now if needed
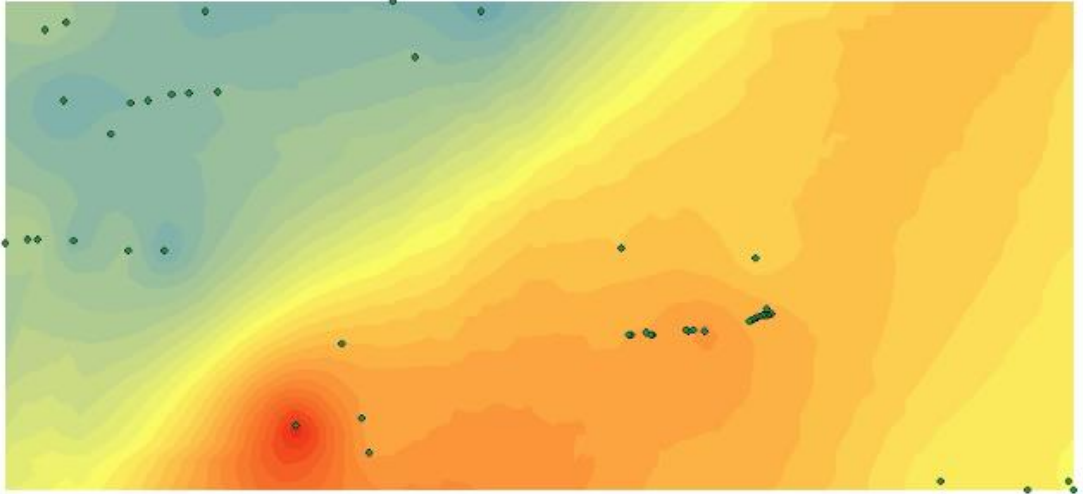
Figure A.1. Example of isopach map created with ArcGIS.

A.2 Statistical analysis

Statistical analysis was conducted to establish unbiased evaluation of hybrid bed distribution (see Chapter 6). For this purpose over 23,000 individual beds were entered recording bed thickness, deposit type (turbidite, hybrid bed or debrite) and detailed sedimentology and proportions of clean division versus debritic division in case of hybrid beds. Distribution of hybrid beds was studied in relation to the total number of events of subunits and lobe complexes and in relation to the bulk thickness of deposits. Data from the 3D constrained dataset of the Tanqua depocentre was used to establish proximal to distal trends of hybrid bed distribution, whereas the Laingsburg depocentre dataset was used to establish stratigraphic trends (Fig. A.2). Furthermore, for selected lobe complexes moving stratigraphic averages were established. For this purpose, each succession was divided into equal intervals and the proportion of structureless sandstone, structured sandstone, siltstone, hybrid beds, debrites and claystone was determined and depicted graphically next to the core data set.
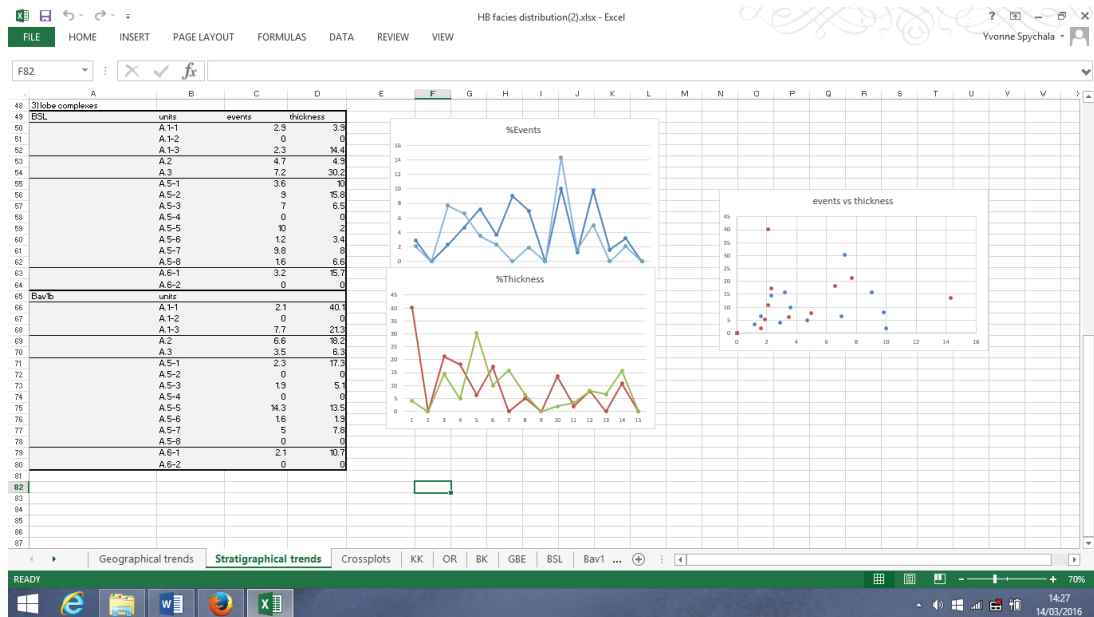
Fig. A.2. Screenshot of raw data evaluation for establishment of stratigraphic trends of the Laingsburg depocentre (BSL and Bav 1b cores).

Appendix B

Outcrop and well locations

B.1 Unit A, Laingsburg Formation

B.1.1 Outcrop

Name	Abbrevation	Easting	Northing
Skeidingen 1	SK1	471633	6324409
Skeidingen 2	SK2	474177	6323462
Rietfontein 1	RF1	473247	6327299
Doornkloof 1	DK1	462193	6330990
Doornkloof 2	DK2	461431	6330838
Doornkloof 3	DK3	462571	6330976
Doornkloof 4	DK4	463809	6330939
Doornfontein 1	DF1	466988	6330577
Doornfontein 2	DF2	465737	6330567
Jakkalsfontein 1	JF1	468861	6336167
Jakkalsfontein 2	JF2	467856	6336120
Jakkalsfontein 3	JF3	467276	6336071
Dapperfontein 1	DAF1	466447	6335840
Dapperfontein 2	DAF1	465808	6335784
R354	R354	463464	6335832
Steekweglagte1	SWL1	475787	6337379
Steekweglagte2	SWL2	475029	6339345
Roggekraal	RK1	478101	6339001
Waterkloof	WK1	468441	6338988
Wilgerhoutfontein	WHF1	463573	6338603
Wilgerhoutfontein 2	WHF2	462806	6338345

Table B.1 UTM positions of outcrop section in Unit A, Laingsburg Formation.

B.1.2 Well locations

Name	Abbrevation	Easting	Northing
ZKNL1	ZKNL1	465129	6334675
BSL1	BSL1	472480	6325243
DK1	DK1	461570	6331811
Bav_1b	Bav_1b	473948	6324692

Table B.2 UTM positions of well locations in Unit A, Laingsburg Formation.

B.2 Unit D/E and E, Fort Brown Formation

B.2.1 Outcrop

Name	Abbrevation	Easting	Northing
Zoutkloof	ZK 1	480586	6337532
	ZK2	480521	6337310
	ZK3	480423	6337125
	ZK4	480295	6336928
	ZK5	480256	6336702
	ZK6	480199	6336491
	ZK7	480150	6336439
	ZK8	480100	6336334
	ZK9	480081	6336290
	ZK10	479946	6336154
	ZK11	479709	6336036
	ZK12	479501	6335939
	ZK13	479442	6335919
	ZK14	479408	6335863
	ZK15	478577	6335739
	ZK16	478316	6335661
	ZK17	478232	6335651
	ZK18	478105	6335618
	ZK19	477850	6335536
	ZK20	477800	6335517
	ZK21	477205	6335371
	ZK22	476767	6335169
	ZK23	476732	6335132
	ZK24	476469	6335050
	ZK25	476265	6335047
	ZK26	476111	6334978
	ZK27	482739	6332782
	ZK28	482839	6332844
	ZK29	483044	6332819
	ZK30	483187	6332817
	ZK31	483332	6332806
	ZK32	483421	6332789
	ZK33	483550	6332787
	ZK34	483753	6332808
	ZK35	483909	6332797
	ZK36	482499	6332818
	ZK37	482398	6332794
	ZK38	482185	6332792
	ZK39	481805	6332816
	ZK40	481442	6332792
	ZK41	480886	6332705
	ZK42	480553	6332684
	ZK43	480366	6332678
	ZK44	480096	6332681

Table B.3 UTM positions of outcrops of Unit D/E and E1, Fort Brown Formation.

Name	Abbrevation	Easting	Northing
Roggekraal	Rk 1	480598	6337937
	Rk2	480766	6338076
	Rk3	480838	6338198
	Rk4	481098	6338501
	Rk5	481134	6338942
	Rk6	481086	6339100
	Rk7	480808	6339236
	Rk8	480738	6339314
	Rk9	480667	6339557
	Rk10	480540	6339690
	Rk11	480716	6339735
	Rk12	480844	6339736
	Rk 13	481021	6339766
	Rk14	481215	6339789
	Rk15	481475	6339836
	Rk16	481517	6339961
	Rk17	481435	6340022
	Rk 18	481298	6340066
	Rk19	481112	6340117
	Rk20	480887	6340198
	Rk21	480587	6340281
	Rk22	480272	6340349
	Rk23	477988	6340392
	Rk24	479751	6340461
	Rk25	479475	6340526
	Rk26	479262	6340551
	Rk27	479072	6340590
	Rk28	478811	6340631
	Rk29	478590	6340635
	Rk30	478320	6340615
	Rk31	478098	6340600
	Rk32	477915	6340572

Table B.4 UTM positions of outcrops of Unit D/E and E1, Fort Brown Formation.

Name	Abbrevation	Easting	Northing
Geelbeck	GB1	498630	6323836
	GB2	498643	6323901
	GB3	498710	6323996
	GB4	499017	6323895
	GB5	499033	6323879
	GB6	499054	6323769
	GB7	499055	6323723
	GB8	499090	6323677
	GB9	499130	6323593
	GB10	499185	6323597
	GB11	499283	6323595
	GB12	499354	6323597
	GB13	499425	6323587
	GB14	499512	6323563
	GB15	499618	6323581
	GB16	499707	6323599
	GB17	499774	6323610
	GB18	499861	6323623
	GB19	499915	6323633
	GB20	500012	6323648
	GB21	500124	6323672
	GB22	500228	6323655
	GB23	500358	6323667
	GB24	500439	6323648
	GB25	500517	6323657
	GB26	500699	6323633
	GB27	500778	6323633
	GB28	500872	6323695
	GB29	500968	6323667
	GB30	501065	6323692
	GB31	501154	6323690
	GB32	501209	6323686
	GB33	501318	6323704
	GB34	501406	6323612
	GB35	501563	6323597
	GB36	501701	6323637
	GB37	501943	6323699
	GB38	498483	6323791
	GB39	498294	6323754
	GB40	498322	6323759
	GB41	497691	6323793
	GB42	497479	6323809
	GB43	497163	6323791
	GB44	497095	6323774
	GB45	496933	6323728

Table B.5 UTM positions of outcrops of E2, Fort Brown Formation

B.3 Fan 4, Skoorsteenberg Formation

B.3.1 Outcrop

Name	Abbrevation	Easting	Northing
Klipfontein	KF1	404403	6394541
	KF2	405023	6395007
	KF3	405436	6395235
	KF4	405805	6395895
Hammerkranz	HK1	412507	6386232
	HK2	412728	6386061
Sout Rivier	OC1	412427	6396751
	OC2	412303	6397253
	OC3	412535	6397613
	OC4	412181	6397733
	OC5	412093	6398031
	OC6	412434	6398045
	OC7	412258	6399662
Isle of Sky	IoS 1	412274	6403598
	IoS 2	412287	6403592
	Ios 3	412998	6402611
	IoS 4	413307	6402164
	Ios 5	412541	6401486
	Ios6	408229	6399925
	Ios7	410012	6400198
Rondawell	RW1	412136	6387342
	RW2	411594	6388076
Grootfontein	GF1	403753	6389844
Vaalfontein	VF1	407876	6397379

Table B.6 UTM positions of outcrops of Fan 4 Skoorsteenberg Formation.

B.3.2 Well locations

Name	Abbrevation	Easting	Northing
Bloukopp	BK1	412244	6379944
Gemsbock East	GBE	415220	6386072
Koppieskraal	KK	402466	6372470
Ongeluks River	OR	405625	6367897
Nomad Cores	NB2	410274	6383578
	NS1	413782	6395109
	NS2	416234	6386267
	NS3	414799	6377911

Table B.7 UTM positions of well locations of Fan 4 Skoorsteenberg Formation.
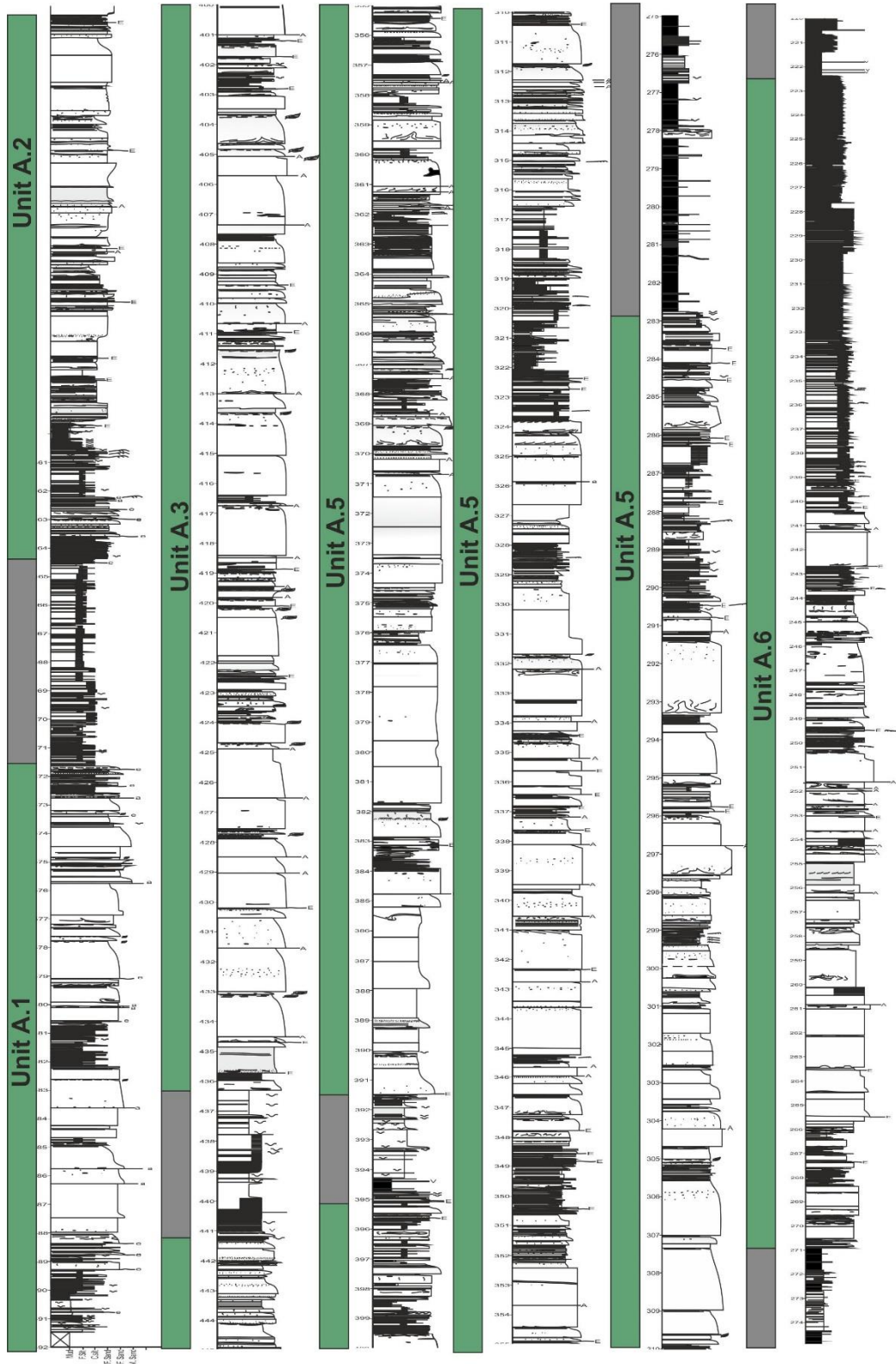
Appendix C

Core logs

C.1 BSL

Figure C.1. Core log of the BSL core, Unit A, Laingsburg Formation

C.1.1 Description

Core interval:	492-222.4 m
Total thickness:	269.6 m
Unit A.1:	29.9 m
Unit A.2:	21.9 m
Unit A.3:	41.4 m
Unit A.5:	109.1 m
Unit A.6:	48.4 m
Box:	41-98

492-490.1 m: Thin-bedded coarse- and fine grained siltstones. Beds are commonly bioturbated. The package is topped by a hemipelagic claystone interval.

490.1-488.0 m: Two thickening and coarsening upward packages. Both packages start with planar laminated fine-grained siltstone and coarsen to fine-grained sandstones. Minor erosional surfaces are observed within both packages.

488.0-482.2 m: Medium- to thick-bedded structureless sandstones. Some beds comprise mudstone-chips either in their bases or tops. The packages is divided into two divisions by 0.2 m of fine- to coarse grained siltstone.

482.2-480.6 m: Heterolithic package comprising structured very fine-grained sandstone interbedded with fine- and coarse-grained siltstone. Bioturbation of siltstones and soft sediment deformation of sandstones is observed.

480.6- 472.8 m: Predominately medium-to thick-bedded fine-grained sandstone beds. Planar lamination is observed at the tops of beds. Normal grading is common. Carbonaceous matter is observed at the top of individual beds. Amalgamation and erosional surfaces are common.

472.8- 464.6 m: The lower part of this package is characterised by very fine to fine-grained sandstone interbedded with fine- and coarse grained siltstone. Some sandstone beds are climbing-ripple laminated, while others show soft-sediment deformation. The upper part is characterised by planar laminated coarse siltstone.

464.6- 460.1 m: Very fine to fine-grained sandstone interbedded with fine- and coarse grained siltstone. Sandstones can be ripple laminated, cross-laminated or structureless. Siltstones are commonly planar laminated and can show bioturbation.

460.1- 459.7 m: Planar laminated claystone package.

459.7-441.0 m: Thick- to thin-bedded very fine- and fine-grained sandstone beds. The majority of beds show sedimentary structures (planar lamination, current ripple lamination, wavy lamination). Beds can comprise mudstone chips and mudstone clasts. Soft-sediment deformation and dewatering are common. Some beds show banding with mudstone chips orientated on the clay-rich bands.

441.0-437.8 m: Coarse- and fine-grained siltstone package. A few sandstone beds are intercalated in the silt-prone interval. Siltstones display planar lamination. Bioturbation is common.

437.8-436.2 m: Bioturbated silty claystone to fine siltstone package.

436.2-424.0 m: This package is dominated by thick-bedded fine-grained sandstone. Individual thick-bedded sandstone packages are separated by thin intervals of thin-bedded very fine-grained sandstones and siltstones. Carbonaceous material is found at bed tops, while mudstone and siltstone clasts are located at the base of beds.

424.0- 422.5 m: Medium- to thin-bedded very fine- to fine grained sandstone interbedded with siltstones. Sandstone beds comprise abundant mudstone and siltstone clasts and mudstone chips. Dewatering features are observed.

422.5- 402.9 m: Thick- to medium bedded normal graded fine-grained sandstone beds. Some beds show planar or current ripple laminated tops, while others comprise sub-rounded mudstone clasts at their tops. Dewatering at the bases of beds is common. Some beds comprise mudstone clasts at their bases. Amalgamation and erosion surfaces are common. Thin-bedded siltstone intervals are intercalated and separate individual packages.

402.9-401.1 m: Medium-bedded very fine-grained sandstone interbedded with thin-bedded siltstone. Sandstones increase in mud-content to the top and comprise mudstone clasts.

401.1- 399.6 m: Thick-bedded normal graded fine-grained sandstone, planar and current ripple to climbing ripple laminated with some floating subrounded mudclasts

399.6- 394.8 m: Very fine- and fine grained sandstone interbedded with coarse- and fine-grained siltstone. Sandstone beds show current ripple and cross-lamination, dewatering and soft-sediment deformation. Siltstones are planar laminated and can be bioturbated. The interval is topped by claystone.

394.8-391.6 m: Bioturbated coarse- and fine siltstone interval. Normal grading is observed.

391.6-384.8 m: This package comprises dominantly structureless thick-bedded normal graded very fine-sandstones.

384.8-382.0 m: Medium- to thin-bedded sandstones intercalated with siltstone and claystone deposits. Mud-content in sandstone beds increases upwards. The upper division of these beds comprise mudstone chips, dewatering features and mudstone clasts. Carbonaceous material can also be observed.

382.0-368.9 m: Thick- to medium-bedded normal graded very fine- to fine-grained sandstone. Mudstone chips in the matrix are common. Rare banding and ripple lamination is observed. The uppermost sandstone beds show abundance on soft-sediment deformation and carbonaceous material.

368.9-367.0 m: Thin-bedded fine-grained sandstone beds interbedded with coarse- and fine-grained siltstones. Sandstones are current ripple, wavy or climbing ripple laminated. Siltstone beds are planar laminated.

367.0 - 361.3 m: Medium- to thin-bedded very-fine sandstone. Individual beds show planar and/or current ripple lamination. Some beds show banding that can be discontinuous.

361.3- 354.9 m: Medium- to thin-bedded very fine to fine-grained sandstone that is commonly normal graded. Sandstones are intercalated with thin-bedded planar laminated siltstones. Sandstone beds show abundant sedimentary structures (planar lamination, current ripple lamination). Soft-sediment deformation is common.

354.9-352.4 m: Thick- to medium bedded sandstones that re dominantly structureless.

352.4- 348.2 m: Thin-bedded very fine-grained sandstone interbedded with coarse-grained siltstone. Planar lamination is the dominant sedimentary structure.

348.2- 329.2 m: Thick- to medium bedded normal graded fine-grained sandstones intercalated with thin siltstone intervals that separate individual packages. Sandstone beds are mostly structureless, but some tops are planar laminated and ripple lamination is rarely observed. Amalgamation and erosional surfaces are common. Sandstone beds can comprise a high amount of mudstone chips in their matrix.

329.2- 327.9 m: Thin-bedded very fine-grained sandstone interbedded with coarse-grained siltstone. Planar lamination and current ripple lamination are the dominant sedimentary structures.

327.9-323.9 m: Thick- to medium-bedded fine-grained sandstones. Tops can be planar or cross-laminated. Dewatering features on bases of beds are common. Mudstone chips are abundant on in the sandstone matrix.

323.9-316.7 m: Thin-bedded very fine- to fine grained normal graded sandstone interbedded with fine- and coarse-grained siltstone. Siltstone beds are planar laminated, whereas sandstone beds are planar, current ripple or climbing-ripple laminated.

316.7-291.4 m: Thick- to medium bedded normal graded fine-grained sandstone packages intercalated with thin-bedded heterolithic packages of very fine-grained sandstone and siltstone that are current ripple and climbing ripple laminated. Thick-bedded sandstone deposits commonly show dewatering features on their bases.

291.4- 285.9 m: Heterolithic package of interbedded very fine-grained sandstone and siltstone. Siltstone beds are planar laminated, whereas sandstone beds are planar, current ripple or climbing-ripple laminated.

285.9-282.8 m: Medium to thin-bedded sandstone with dominantly planar lamination at their tops. Normal grading is common, but inverse grading occurs as well.

282.8- 270.95 m: Claystone package with intercalated fine-grained siltstones and sand-grained clastic injectites.

270.95-264.95 m: Medium bedded fine-grained sandstone intercalated with heterolithic packages of very fine-grained sandstone and siltstone. Thin-bedded sandstones are planar or ripple laminated, while siltstones are mostly planar laminated. Medium-bedded sandstones are structureless and show increase in mud-content to their tops that can also have swirly fabric with incorporated mudstone chips and mudstone clasts.

264.95- 250.3 m: Thick- to medium-bedded normal graded sandstone. Beds are commonly structureless with dewatering features. Some beds show planar, current ripple or climbing-ripple lamination.

250.3- 242.8 m: Basal division comprises thin-bedded structured (planar and current ripple lamination) sandstone interbedded with siltstone. Upwards the package consists of medium- to thick-bedded fine-grained sandstone with abundant mudstone

clasts throughout the beds. These beds are separated by thin siltstone intervals. The top division of the package is made up by heterolithic deposits of very fine-grained sandstone and siltstone.

242.98- 240.4 m: Thick-bedded fine grained sandstones. Tops can be planar laminated.

240.4- 233.3 m: Very thin- to thin-bedded very fine-grained sandstone interbedded with fine- and coarse-grained siltstone. Sandstone beds are planar or current ripple laminated.

233.3- 222.4 m: Package of dominantly coarse siltstone that can be intercalated with thin very fine-grained sandstone and fine siltstone.

C.1.2 Interpretation

The well is located in a proximal axial setting of Unit A (Fig. C.2). The core log comprises Subunits A.1- A.6. Subunit A. 1 consists of 12 distinguishable lobes that show compensational stacking of lobes axes and fringe deposits. A.1 is separated from A.2 by a ~12 m thick siltstone package. Subunit A.2 comprises 8 lobes. Deposits from predominantly lobe axis alternate with lobe fringe deposits. Subunits A.2 and A.3 are separated by a 4.5 m thick claystone/siltstone package. A.3 consists of 15 lobes. Deposits show dominantly lobe axis and off-axis facies. A.3 and A.5 are separated by 3 m of silty claystone. Subunit A.5 is the thickest subunit of Unit A (~110 m). It comprises 38 lobes. Subunits A.5 and A.6 are separated by a 12m thick claystone package with clastic sills and dykes. A. 6 consists of 13 lobes and a thick lobe fringe complex at the top.
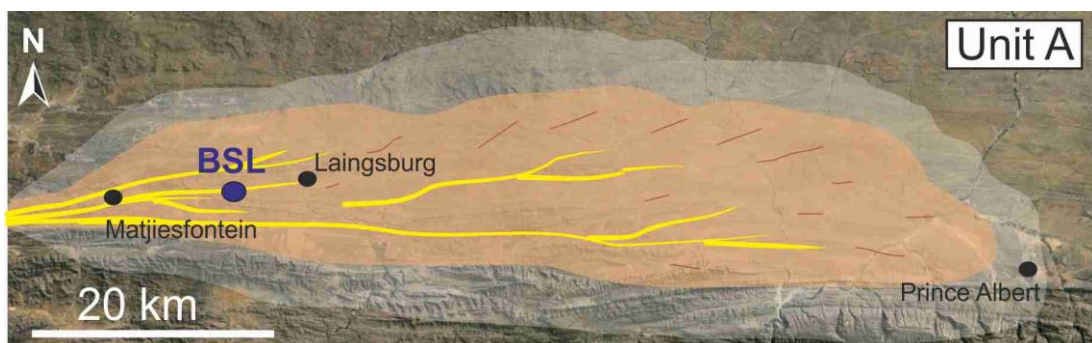

Figure C.2. Laingsburg depocentre showing the position of BSL. The BSL core is located in a proximal axial setting of Unit A.

C.2 ZKNL
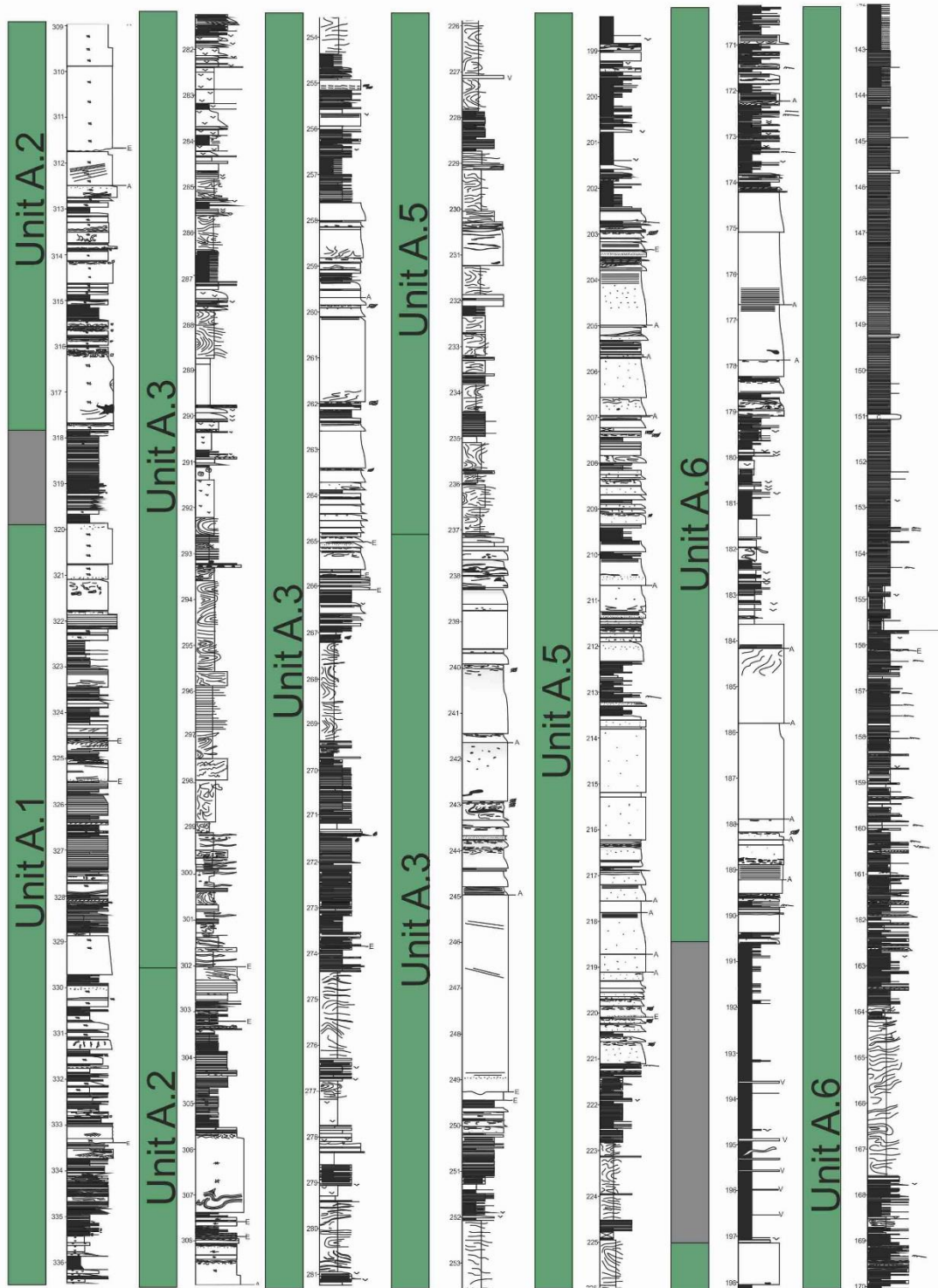

Figure C.3. Core log of ZKNL core, Unit A, Laingsburg Formation

C.2.1 Description

Core interval: 335.8- 167.6 m

Total thickness: 168.2 m

Unit A.1:   12.8 m

Unit A.2:   20.4 m

Unit A.3:   65 m (35 m of deformed facies)

Unit A.5:   34.5 m (14.1 m of deformed facies)

Unit A.6:   23 m

Box: 32-64

335.8-323 m: Thin to medium-bedded very fine sandstone interbedded with coarse and fine siltstone. Thin-bedded sandstone deposits are current ripple and climbing-ripple laminated, while medium-bedded sandstone deposits are structureless with some dewatering features. Siltstone beds are structureless or planar laminated and can display bioturbation.

323-322.4 m: Package of interbedded silty claystone and fine siltstone.

322.4-319.9 m: Medium-bedded very fine- to fine grained sandstone. Beds are structureless or planar laminated. Normal grading is common. Beds show relative high amount of mudstone chips at their bases and tops and rare intraformational siltstone clasts.

319.9-317.9 m: Dominantly thin-bedded coarse siltstone interbedded with fine siltstone. Normal grading is observed.

317.9-315.4 m: Thick-bedded fine-grained sandstone bed overlain by thin-bedded very fine-grained sandstones. All beds show swirly fabric at their top and carbonaceous material.

315.4-314.7 m: Coarsening upward heterolithic package. Thin-bedded coarse siltstone is overlain by thin-bedded structureless or wavy laminated very-fine grained sandstone interbedded with fine siltstone.

314.7-305.6 m: Thick- to medium-bedded fine- to very fine-grained sandstone, separated by packages of thin-bedded siltstone or heterolithic packages of interbedded siltstone and sandstone. Thick-bedded sandstone deposits are

structureless, while medium-bedded sandstone deposits can have current ripple laminated tops, dewatering features and mudstone chips.

305.6-302.8 m: Thin-bedded fine and coarse siltstone interbedded with rare thin-bedded very fine-sandstone. Some beds are bioturbated.

302.8-302.0 m: Coarsening upward package. The base comprises thin-bedded coarse siltstone overlain by medium-bedded very fine-grained sandstone with cross-lamination.

302.0-274.3 m: Folded coarse and fine siltstone with interbedded thin-bedded very-fine sandstone deposits. Siltstones can show bioturbation. The package also comprises minor intervals with disintegrated sandstones encased by siltstone.

274.3-269.8 m: Thin-bedded coarse and fine siltstone interbedded with few thin-bedded very-fine grained sandstone.

269.8-267.1 m: Folded coarse and fine siltstone

267.1- 258.7 m: Basal coarsening upward package comprising thin-bedded siltstone and very fine- to fine-grained sandstone. This package is overlain by medium- to thick-bedded fine-grained sandstone packages that are separated by siltstone-prone intervals. Planar lamination is the dominantly sedimentary structure and occurs on bed tops. Dewatering features are common. Individual beds can comprise mudstone chips and/or mudstone clasts.

258.7-254.3 m: Thin-bedded fine and coarse siltstone intercalated with medium-bedded planar laminated very fine-grained sandstone.

254.3-252.0 m: Folded coarse and fine siltstone.

252.0- 249.3 m: Coarsening upward package. Basal thin-bedded fine siltstone is overlain by thin-bedded coarse siltstone and eventually thin-bedded very fine-grained sandstone.

249.3-244.2 m: Highly amalgamated fine-grained sandstone package. The top is planar laminated.

244.2-237.1 m: Medium- to thick-bedded fine- to very fine-grained sandstone. The majority of beds show increasing mud content to the top. Commonly the tops show swirly fabric and carbonaceous material and/or mudstone chips. Some beds comprise a high amount of mudstone and intraformational clasts.

237.1-222.9 m: Folded coarse and fine siltstone with interbedded thin-bedded very-fine sandstone deposits. Siltstones can show bioturbation. The package also comprises minor intervals with disintegrated sandstones encased by siltstone.

222.9-221.3 m: Thin-bedded fine siltstone interbedded with coarse siltstone.

221.3-213.6 m: Thickening- upward package comprising thin- to thick-bedded fine- to very fine-grained sandstone. The basal thin-bedded sandstone deposits have tops with swirly fabric and carbonaceous material, while overlying medium-bedded sandstone deposits show planar and current ripple- laminated. The uppermost thick-bedded sandstone deposits show no structures.

213.6-212.3 m: Fine and coarse siltstones intercalated with rare current ripple laminated very fine-grained sandstone.

212.3-202.5 m: Thin- to medium-bedded fine- to very fine-grained sandstone intercalated with thin-bedded siltstone packages. Tops show swirly fabric with carbonaceous material, planar lamination, current ripple lamination or climbing ripple lamination. Normal grading and amalgamation is common.

202.5- 190.7 m: Claystone intercalated with thin-bedded fine and coarse siltstone, ash layers. Clastic injections are common.

190.7- 183.6 m: Medium-bedded fine-grained sandstone, overlain by thick-bedded fine-grained sandstone. In the lower part beds comprise mudstone chips and mudstone clasts (at their bases). Thick-bedded sandstones in the upper half show dewatering features and planar laminations.

183.6-179.7 m: Claystone interbedded with fine and coarse siltstone. Bioturbation is common.

179.7-174.1 m: Basal part coarsens and thickens upward from thin-bedded siltstones to medium-bedded structured sandstones. Upper part is thick-bedded and structureless except for planar lamination. Deposits are normal graded.

174.1- 167.6 m: Heterolithic package comprising very fine-grained sandstone (planar, current ripple and climbing ripple laminated), planar laminated coarse siltstone and structureless/planar laminated fine siltstone.

C.2.2 Interpretation

The well is located in a lateral off-axis to fringe position of Unit A (Fig.C.4). The core log comprises Subunits A.1-A.6. Subunit A.1 is deposited in an overall fringe setting and consists of 9 distinguishable lobes that are commonly deposited in lobe lateral fringe environments. Subunit A.2 is overall deposited in an off-axis position. The subunit comprises 13 lobes that show compensational stacking of axis, off-axis, fringe and distal fringe deposits. The boundary to Subunit A.3 is marked by an erosion surface that is overlain by slide deposits. These slide deposits are 34 m thick. The lobe-dominated part of Subunit A.3 comprises 10 lobes and a fringe complex. The lobes show compensational stacking of deposits from axis, off-axis and fringe environments. The top of Subunit A.3 is characterised by an erosion surface that is overlain with the slide deposits of A.5 (~ 14 m thick). The lobate part of Subunit A.5 comprises 8 lobes that are deposited in predominantly in off-axis settings. Subunits A.5 and A.6 are separated by a ~11 m thick claystone package that comprises sills and dykes. Subunit A.6 has a basal package of two lobes (axis/off-axis) that is separated by a second package of sandstone-rich lobes by a distal fringe complex. Upwards A.6 comprises a thick fringe complex that includes a ~4 m thick slide deposit.
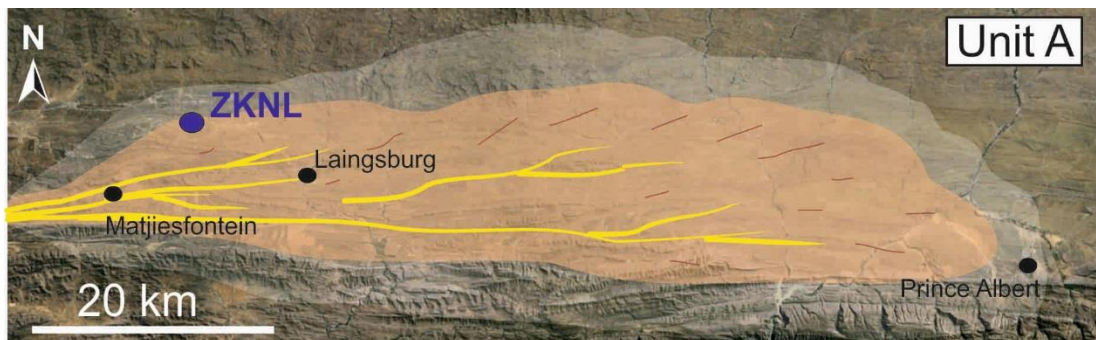

Figure C.4. Laingsburg depocentre showing the position of ZKNL. The ZKNL core is located in a lateral off-axis to fringe setting of Unit A.
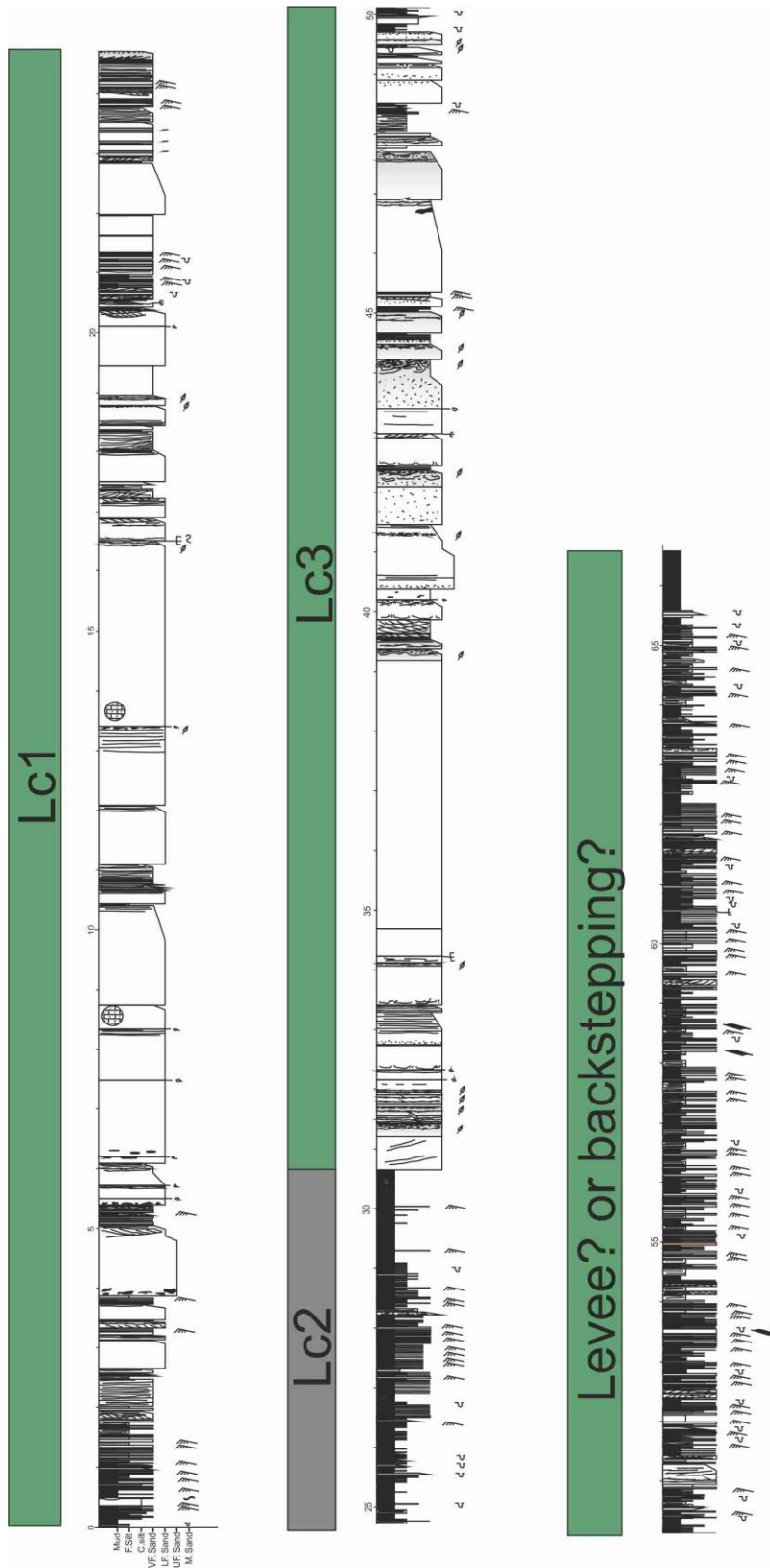
C.3 OR

Figure C. 5. Core log of OR core, Fan 4, Skoorsteenberg Formation

C.3.1 Description

Core interval: 136.13-72.95 m
Total thickness: 63.2 m
Lower Fan 4:   24.7 m
Upper Fan 4:   34.9 m
Box: 17-30

136.13-133.53 m: The lower subunit has a basal heterolithic package (2.6 m) consisting of claystone, siltstone and current ripple/planar laminated laminated very fine-grained sandstone.

133.53-130.23 m: A 3.2 m thick package of structured very fine- to fine-grained sandstone, occasionally with erosive basal surfaces.

130.23 m: A 13.6 m thick unit that consists of banded and planar laminated sandstone, occasionally topped by current ripple laminations. Some bed tops are rich in plant matter.

130.23-116.63 m: A 1m thick heterolithic package consisting of claystone, bioturbated siltstone and current ripple laminated sandstone.

116.3-112.3 m: A 4.3 m thick succession of fine-grained structureless and structured sandstone, capped by a mudstone chips-rich hybrid bed

**112.3-106.5 m:** A 5.8 m thick claystone/siltstone unit with thin (<0.1 m) interbedded very fine-grained sandstones separates the lower and upper subunit of the fan.

106.5-102.9 m: The upper part has a basal package (3.6 m) of banded and planar laminated sandstone.

102.9-98.4 m: An amalgamated package (4.5 m) of structureless sandstone overlies an erosion surface that truncates the underlying package.

98.4-88.4 m: Interbedded medium- to thick-bedded carbonaceous hybrid beds, banded sandstone and climbing-ripple laminated sandstone.

88.4-72.95 m: The top package of the upper subunit comprises 15.45m of interbedded bioturbated claystone/siltstone as well as current and climbing-ripple laminated very fine- to fine-grained sandstone.

C.3.2 Interpretation

The well is located in a proximal and axial setting of Fan 4 (Fig. C.6), which comprises three lobe complexes. The lower and upper parts of Fan 4 are separated by a ~6 m thick claystone/siltstone package. The lower part of Fan 4 comprises lobe axis deposited that alternate with lobe fringe deposits. Overall 9 lobes are distinguished. The upper part comprises lobe off-axis and lobe fringe deposits that are compensationally stacked. The top is built up by external levee.
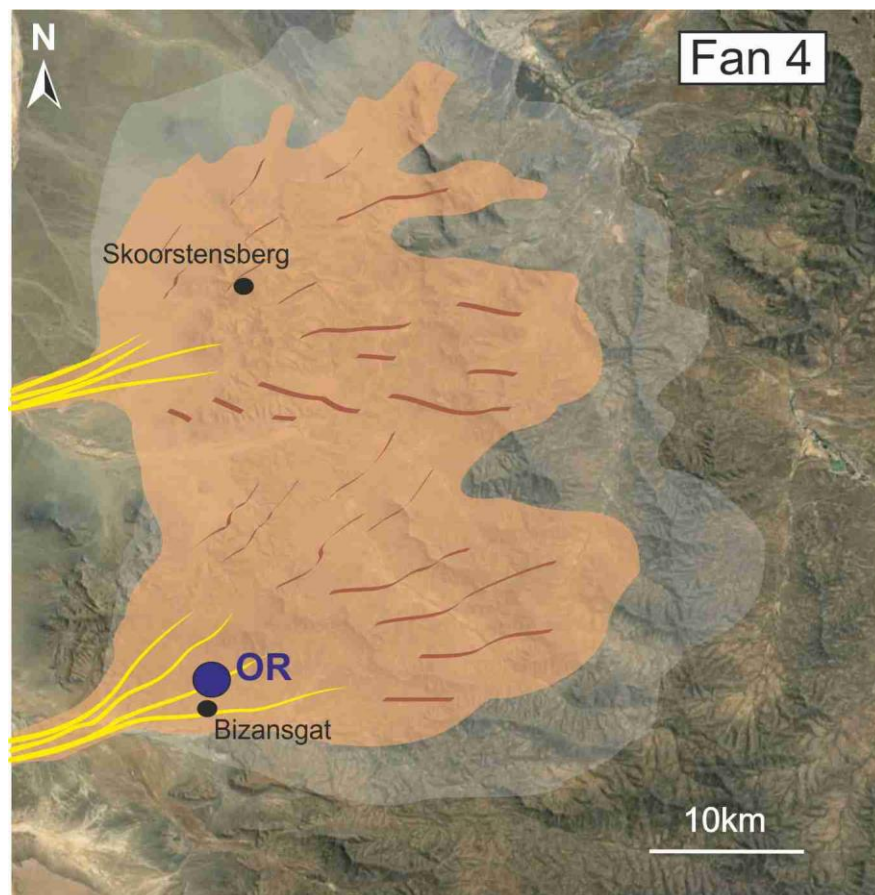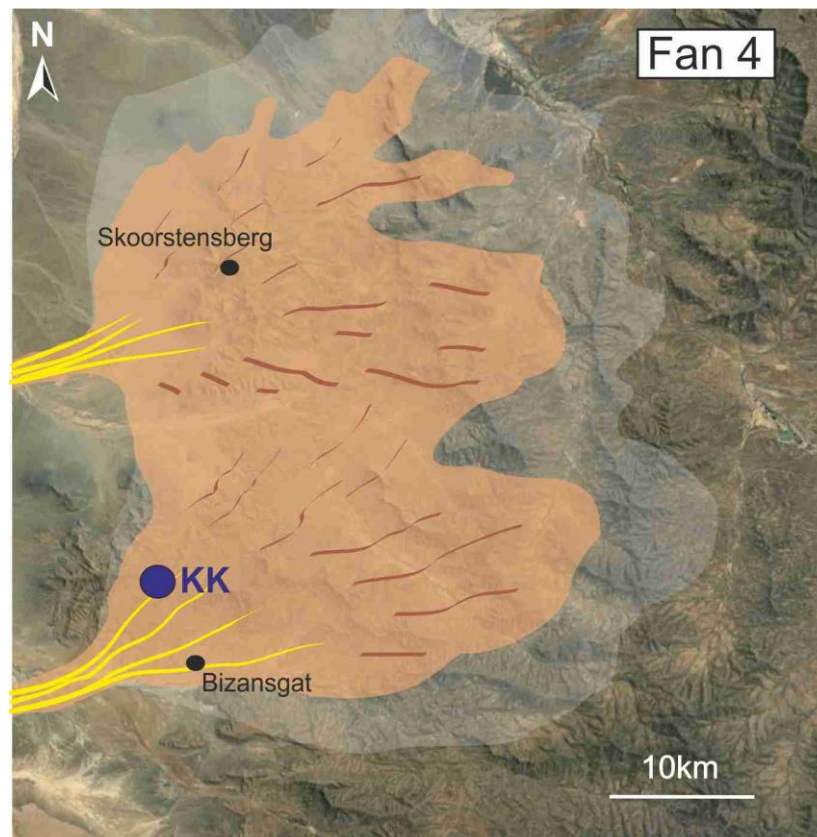

Figure C.6. Tanqua depocentre showing the position of OR in Fan 4. The OR core is located in a proximal and axial position of Fan 4.

C.4 KK
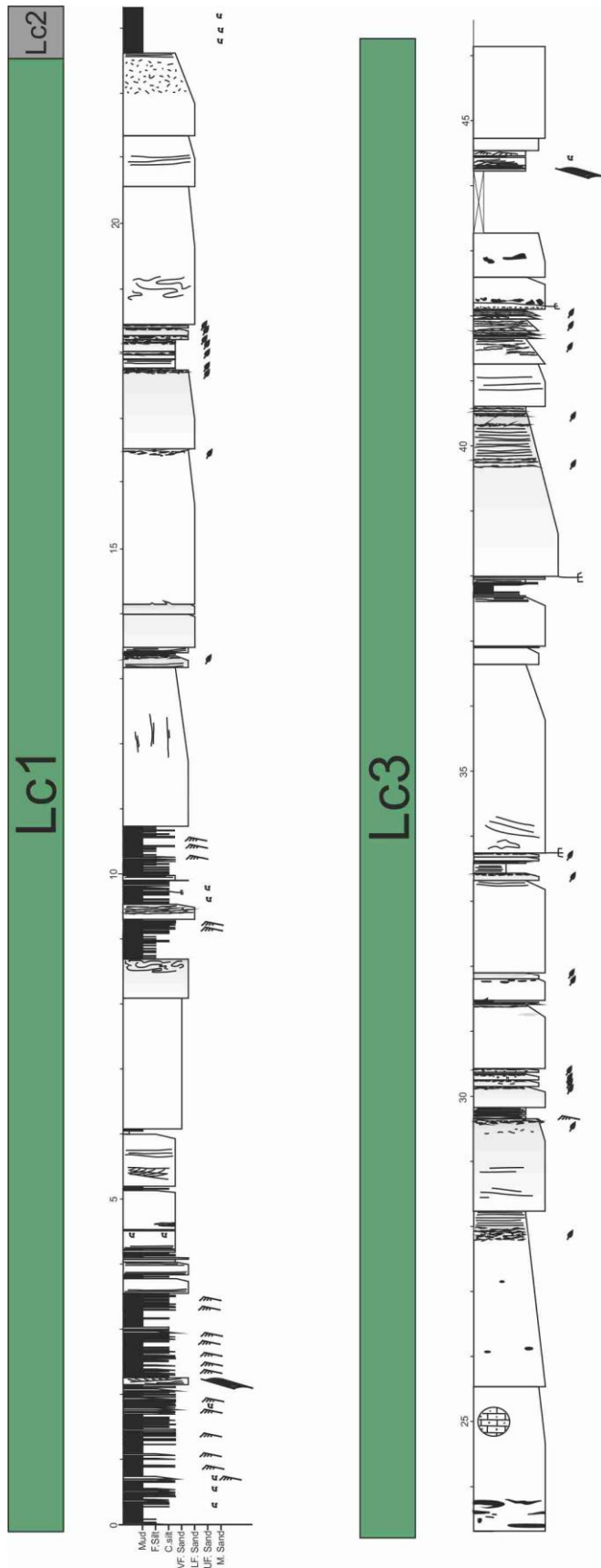
Figure C.7. Core log of the KK core, Fan 4, Skoorsteenberg Formation

C.4.1 Description

Core interval: 45.88-0 m
Total thickness: 45.88 m
Lower Fan 4:   22.5 m
Upper Fan 4:   22.7 m
Box: 1-11

45.88-41.68 m: The basal part of the lower subunit is made up by bioturbated claystone and siltstone as well as current and climbing-ripple laminated very fine-grained sandstone.

41.68-37.28 m: The basal part is overlain by structured very fine- and fine-grained sandstone (4.4 m thick) either structureless or ripple to planar laminated.

37.28-35.28 m: This package comprises current ripple laminated very fine-grained sandstones, planar laminated siltstones that can be bioturbated, silty claystone and a rare banded fine-grained sandstone bed.

35.28-27.58 m: A thinning upwards succession that is dominated by carbonaceous hybrid beds interbedded with fine-grained structureless sandstone with dewatering features.

27.38-23.18 m: The upper 4.2 m of the lower subunit comprises structureless and structured sandstones that show a weak thinning upward trend.

23.18-22.48 m: The subunits are separated by a 0.6 cm thick thin-bedded claystone/siltstone unit.

22.48-20.38 m: The upper subunit has a basal structureless bed (2.1 m) with erosive base overlain by mudstone rip-up clasts.

20.38-12.18 m: A thinning upwards package (8.2 m) comprising carbonaceous hybrid beds interbedded with banded and structured sandstone beds. Some of the hybrid beds have planar laminated vfs caps (< 0.1 m).

12.18-8.28 m: This unit is characterised by thick-bedded structureless and medium-bedded normally graded structured fine-grained sandstones.

8.28-8.0 m: A 0.3 m thick predominately silty mudstone unit truncated by an erosion surface.

8.0-4.8 m: Normally graded banded carbonaceous fine-grained sandstone beds.

4.8-3.9 m: Not recovered.

3.9-0 m: Very fine-grained thin-bedded structured sandstone overlain by thin- to thick-bedded structureless fine-grained sandstone.

C.4.2 Interpretation

The well is located in a proximal axial setting of Fan 4 (Fig. C.8). The lower and upper sand-rich lobe complexes of Fan 4 are separated by a~0.5 m thick claystone package (distal lobe complex). The lower part comprises 6 lobes. Lobe axis deposits alternate with lobe lateral fringe deposits. The upper part consists of 6 lobes. Lobe axis deposits alternate with thin lobe fringe and distal fringe deposits. The top of Fan 4 is not recovered.

Figure C.8. Tanqua depocentre showing the position of KK in Fan 4. The KK core is located in a proximal and axial position of Fan 4.

C.5 BK
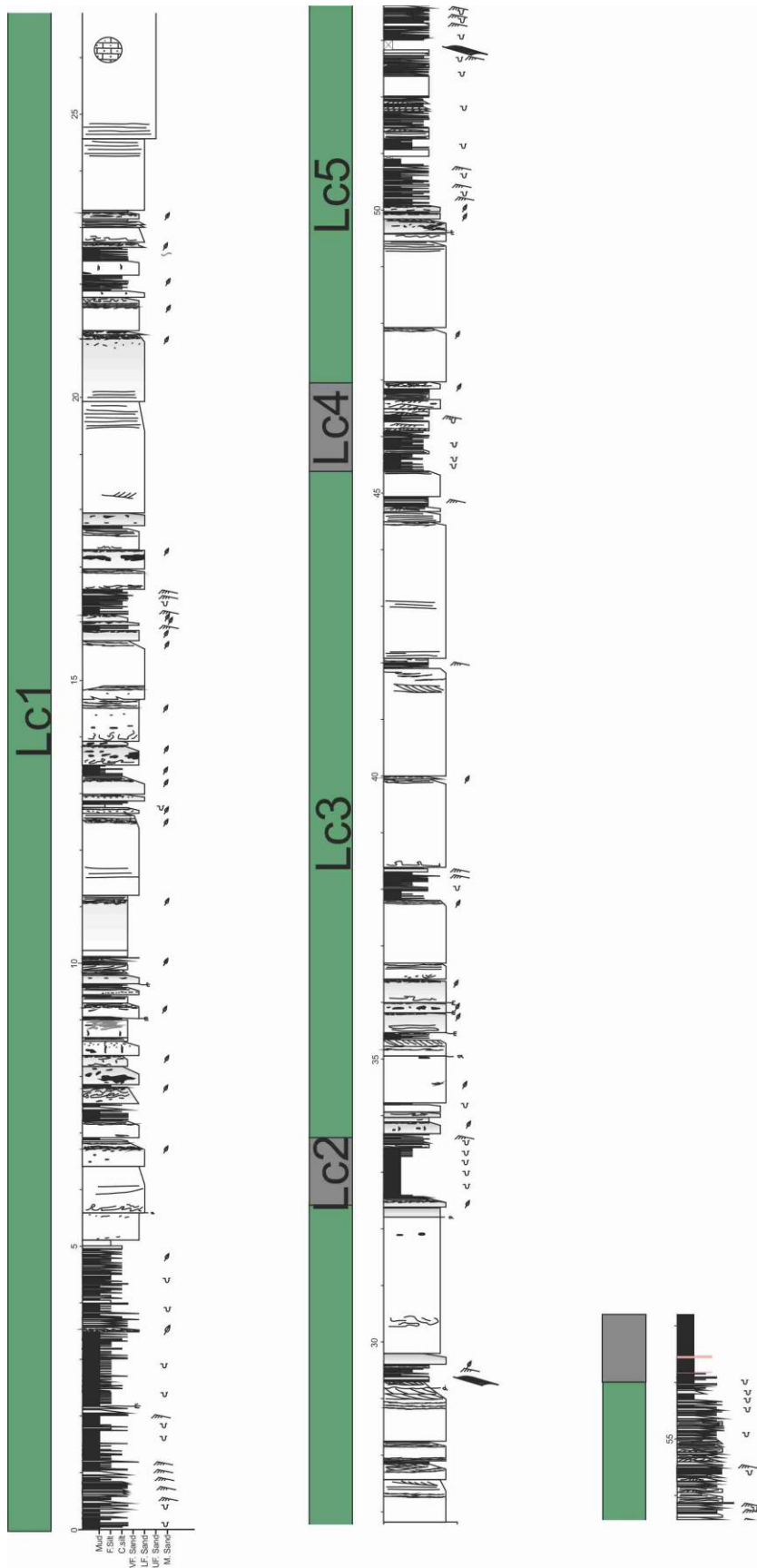
Figure C.9. Core log of BK1 core, Fan 4, Skoorsteenberg Formation

C.5.1 Description

Core interval: 108.73-52.76 m

Total thickness: 56 m

Lower Fan 4:   32.5 m

Upper Fan 4:   22.4 m

Box: 24-37

108.73-103.73 m: The basal interval (5 m) of the lower subunit is made up by a heterolithic package that comprises thin-bedded bioturbated claystones and siltstones as well as current ripple laminated very fine-grained sandstone beds. Rare erosion surfaces and sandstones with argillaceous bed tops are present.

10.3.73-91.3 m: The overlying part of the lower subunit is dominated by carbonaceous and mudstone clast-rich hybrid beds intercalated with structured very fine- to fine-grained sandstone, banded sandstone and thin (<0.5 m) heterolithic units. Some beds show dewatering features at their bases.

91.3-77 m: The upper unit comprises a succession of structureless sandstone with dewatering features, planar laminated fine-grained sandstone, and banded sandstones with ripple and climbing-ripple lamination at their tops. Rare hybrid beds with upper argillaceous carbonaceous divisions are intercalated.

77-75.9 m: A 1.1 m thick thin-bedded claystone/siltstone unit separates the lower and upper fan. The interval comprises 0.6 m of claystone.

75.9-71.4 m: The upper subunit comprises abundant clast-rich hybrid beds in its basal unit (4.5 m) that are associated with structureless and banded sandstones and topped by a heterolithic package comprising ripple-laminated very fine-grained sandstone, fine siltstone and silty claystone.

71.4-64.4 m: The next 7 m are dominated by banded sandstone. Alternating argillaceous and clean sandstone bands can form the last 10-15 cm of otherwise structureless sandstone beds. Sandstone bands can overlying climbing-ripple laminated divisions of sandstone beds, when beds are amalgamated with each other.

64.4-62.9 m: A 1.5 m thick package of heterolithic strata consisting of dominantly ripple laminated very fine- to fine-grained sandstone, planar laminated siltstones and silty claystone.

62.9-59.8 m: A 3.1 m thick succession of fine-grained banded sandstone, planar laminated sandstone and carbonaceous hybrid beds on top.

59.8-53.5 m: The top comprises 6.3 m of interbedded bioturbated claystone and siltstone as well as current ripple and climbing-ripple laminated very fine-grained sandstone.

C.5.2 Interpretation

The well is located in an off-axis/fringe position for the lower lobe complex of Fan 4 and in an off-axis position for the upper lobe complex of Fan 4 (Fig. C.10). The lower and upper lobe complexes are separated by a 0.7 m thick mudstone package (distal lobe complex). The lower lobe complex has a basal fringe complex that is overlain by 12 lobes. Off-axis deposits alternate with lobe frontal fringe deposits. The upper part comprises 5 lobes and a fringe complex at its top. Off-axis deposits are intercalated by lobe frontal fringe deposits.
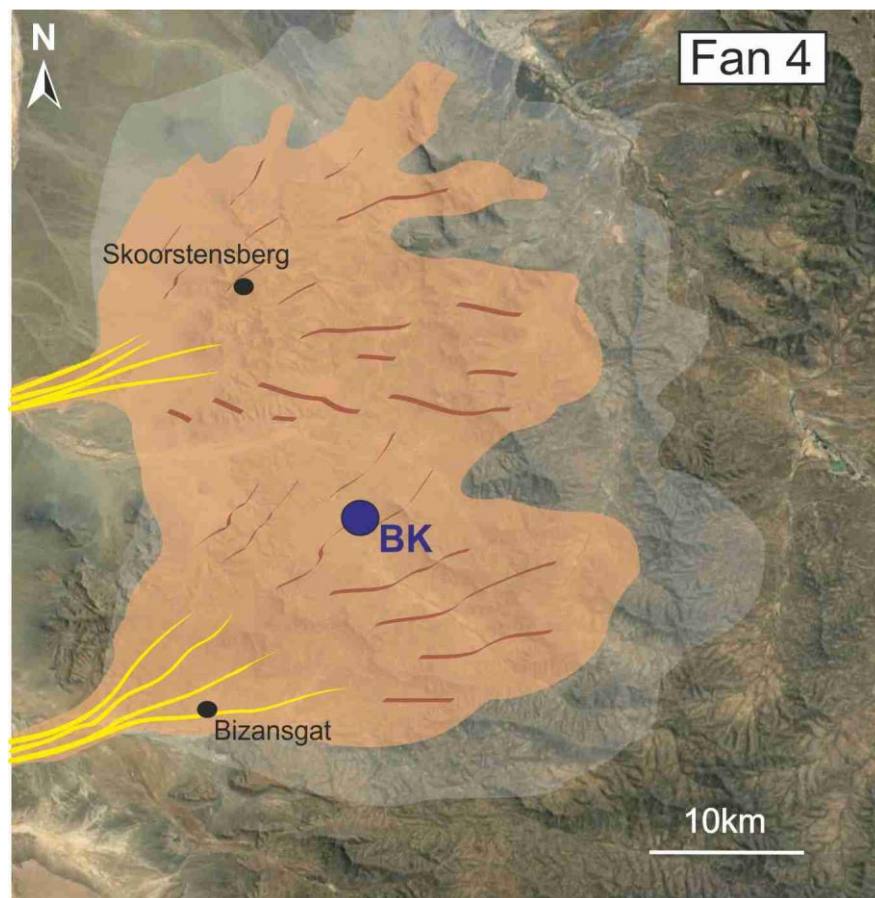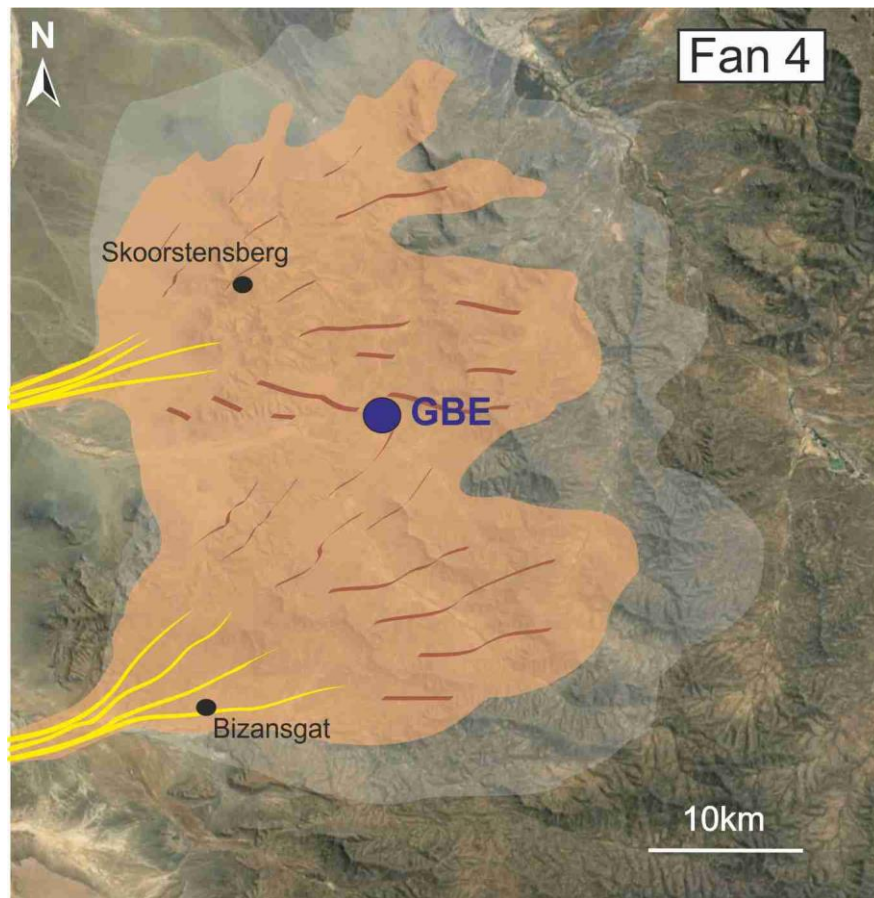

Figure C.10. Tanqua depocentre showing the position of BK in Fan 4. The BK core is located in an off axis/fringe position of Fan 4.

C.6 GBE
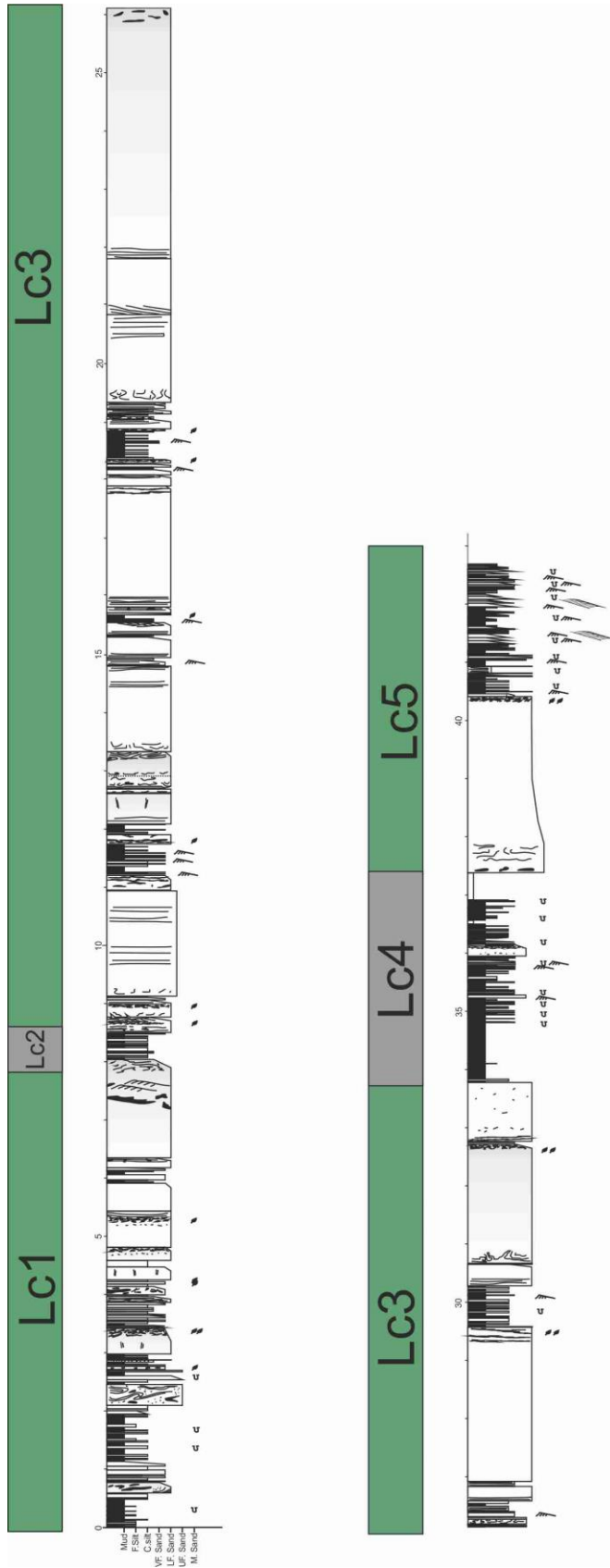
Figure C.11. Core log of GBE core, Fan 4, Skoorsteenberg Formation

C.6.1 Description

Core interval: 123.20-81.61 m
Total thickness: 42.6m
Lower Fan 4:   11.1 m
Upper Fan 4:   30.6 m
Box: 19-28

123.2-119 m: The lower subunit starts with a basal heterolithic unit that comprises bioturbated claystone and siltstone, current ripple laminated very fine-grained sandstone and interbedded hybrid beds. The thickness of the mudstone clasts-rich and carbonaceous hybrid beds are variable (<0.1 m to 0.3 m).

119-112 m: This interval comprises three packages that comprise hybrid beds with argillaceous carbonaceous upper divisions and subsequent planar laminated to banded sandstones. These packages thicken upwards and are separated by ~ 0.5 m thick heterolithic packages of interbedded siltstone and sandstone.

112-111.1 m: The lower and upper subunit are separated by a 0.9 m thick thin-bedded claystone/siltstone unit.

111.1-89.4 m: The upper subunit is dominated by structured sandstone (planar and current ripple laminated), structureless sandstone and banded sandstone, that are separated in packages by heterolithic intervals.

89.4-85.8 m: A 3.6 m thick heterolithic package comprising ripple laminated very fine-sandstone, bioturbated siltstone and silty claystone as well as rare mudstone chip-rich sandstone beds.

85.8-82.8 m: Amalgamated fine-grained sandstone package with rip-up clasts and dewatering features at the base and high proportion of organic matter content at the top.

82.8-81.61 m: The top of the upper subunit is preserved by another heterolithic package with bioturbated claystone and siltstone as well as current and climbing-ripple laminated very fine-grained sandstone.

C.6.2 Interpretation

The well is located in a fringe position for the lower lobe complex of Fan 4 and in an off-axis/axis position for the upper lobe complex of Fan 4. The lower and upper lobe complexes are separated by a 0.5 m thick claystone package intercalated with very thin sandstones (distal lobe complex). The lower part has 8 lobes that represent deposits from lobe frontal fringe and lateral fringe settings. The upper part comprises 7 lobes and two fringe complexes. Lobe axis deposits are intercalated with lobe frontal fringe deposits.

Figure C.12. Tanqua depocentre showing the position of GBE in Fan 4. The KK core is located in a fringe position for lower Fan 4 and off-axis/axis position of upper Fan 4.

Appendix D

Unit A –additional correlation panels
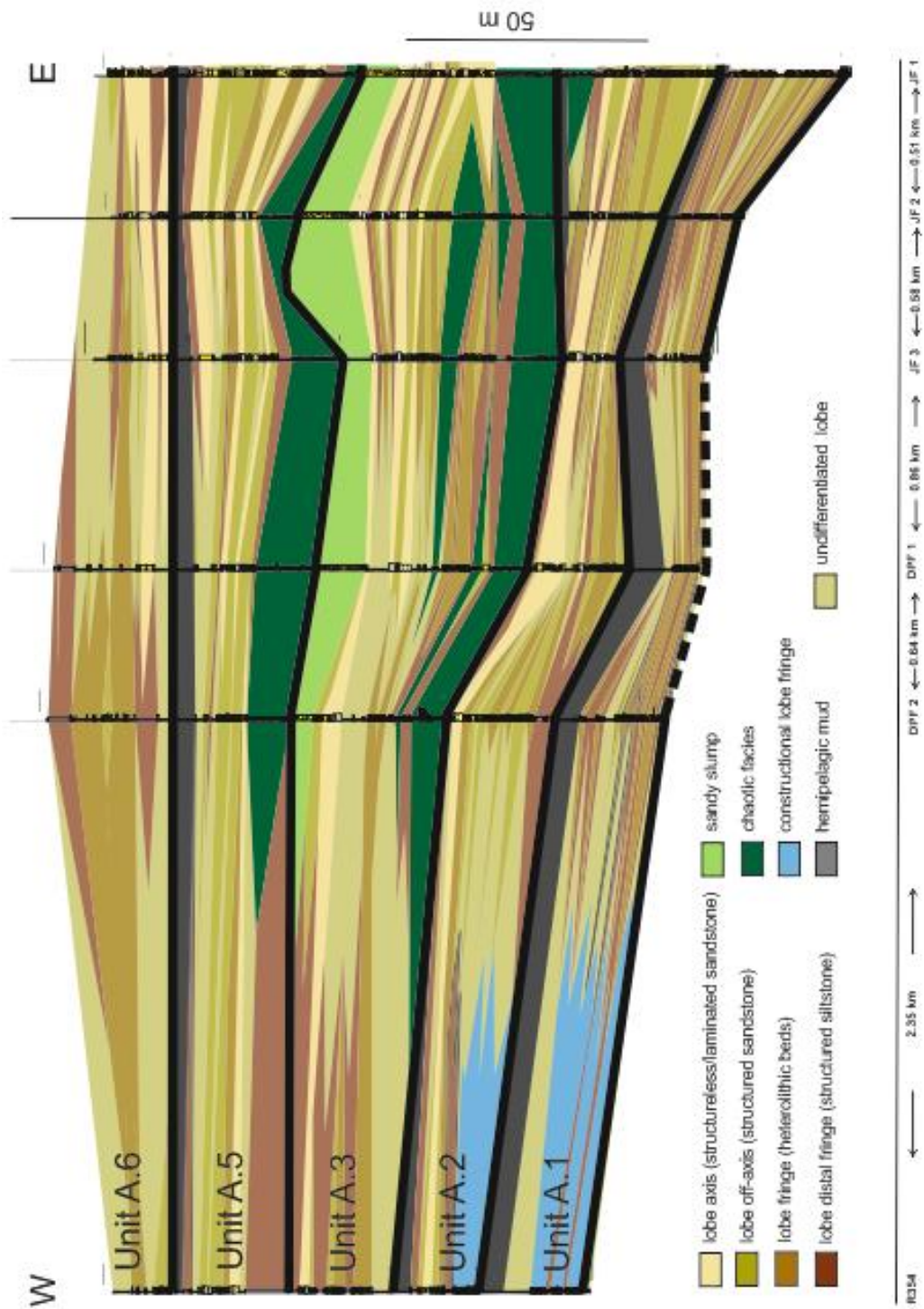
Figure D.1. Additional correlation panel of Unit A, Laingsburg Formation showing the Dapperfontein-Jakkalsfontein limb; DPF: Dapperfontein; JF: Jakkalsfontein
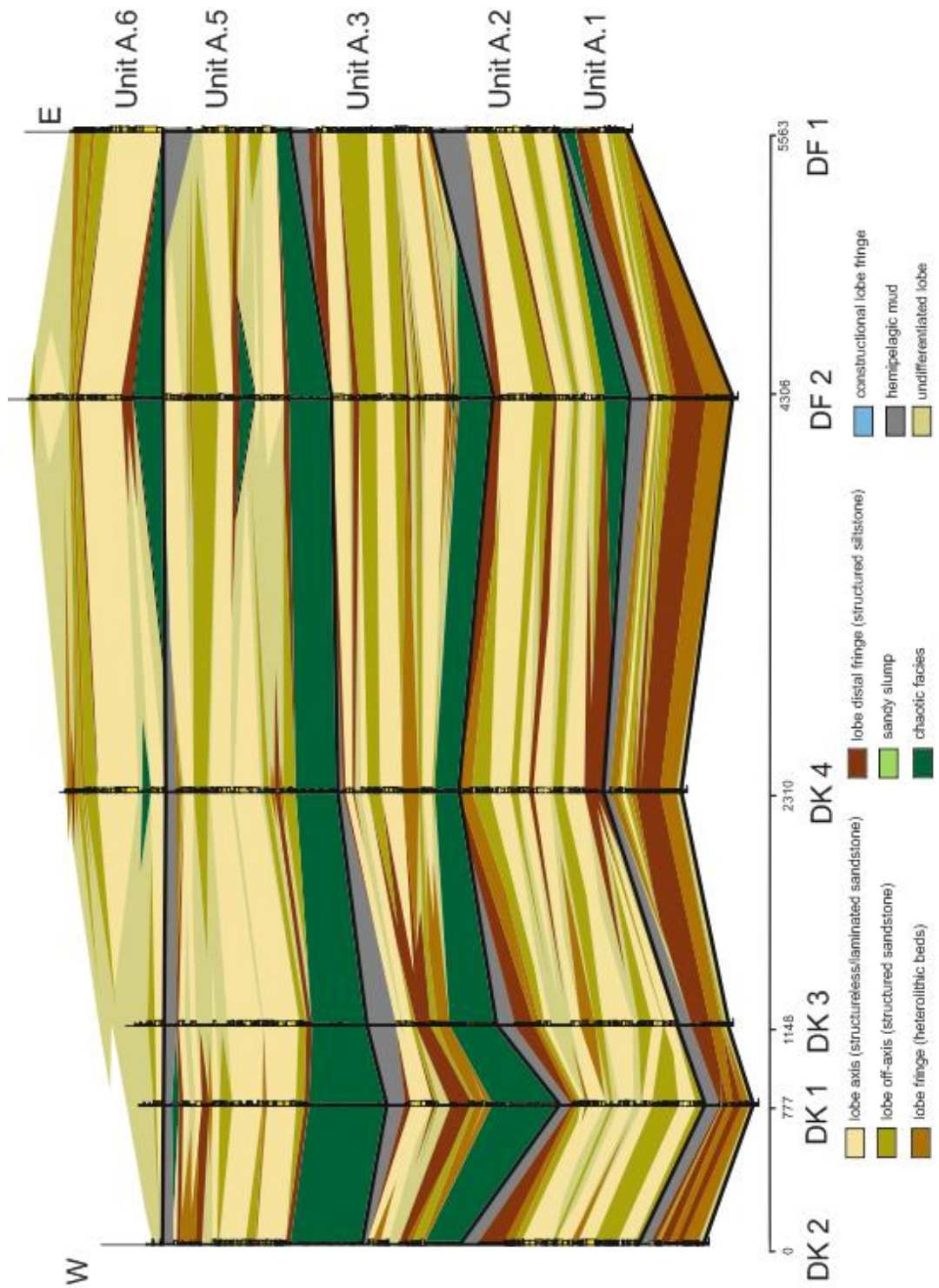
Figure D.2. Correlation panel of Unit A, Laingsburg Formation showing the Doornkloof-Doornfontein limb. DK: Doornkloof; DF: Doornfontein

Appendix E
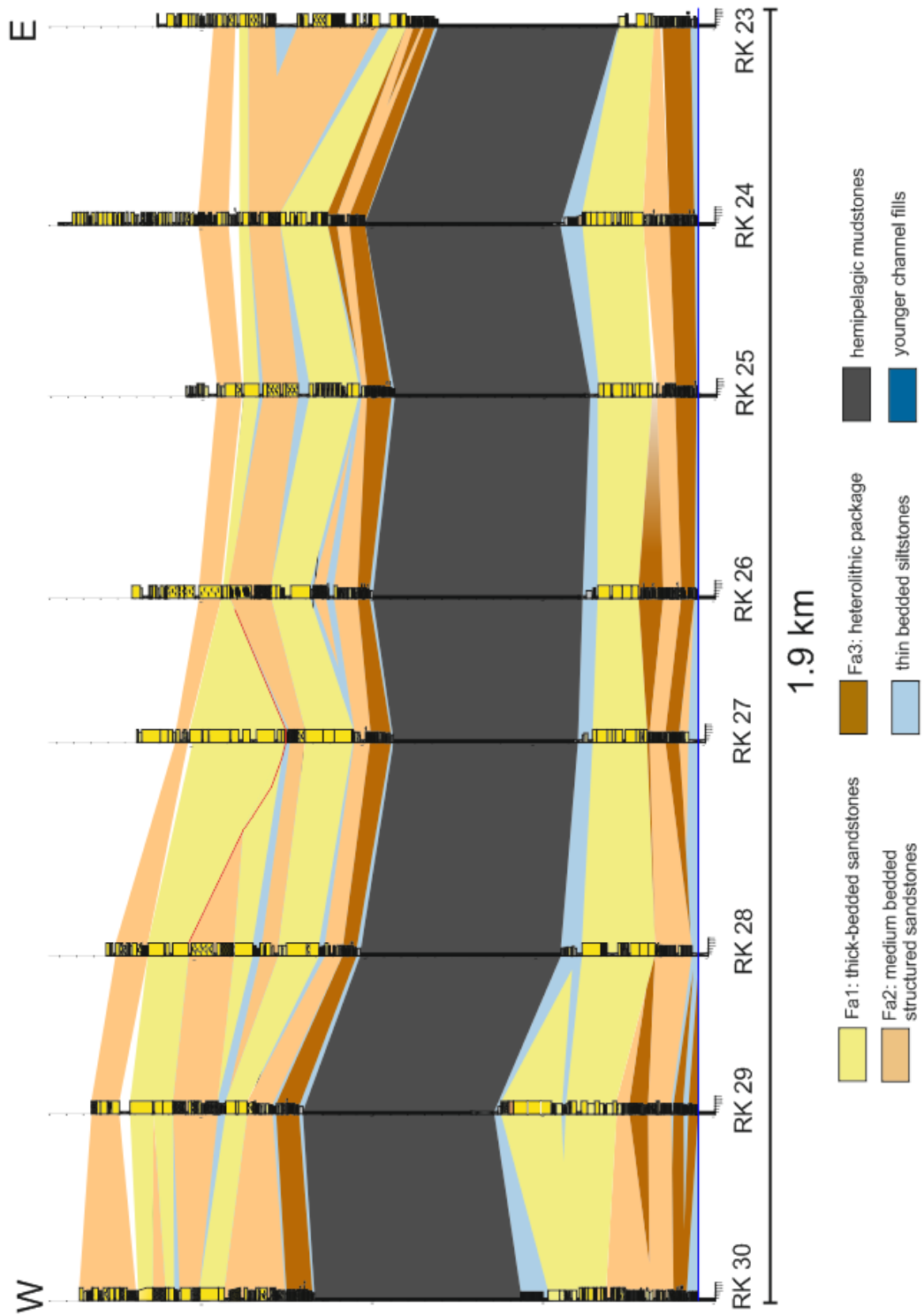
Intraslope lobe- additional correlation panels

Figure E.1. Roggekraal N correlation panel of Unit D/E and E1, Fort Brown Formation; RK: Roggekraal
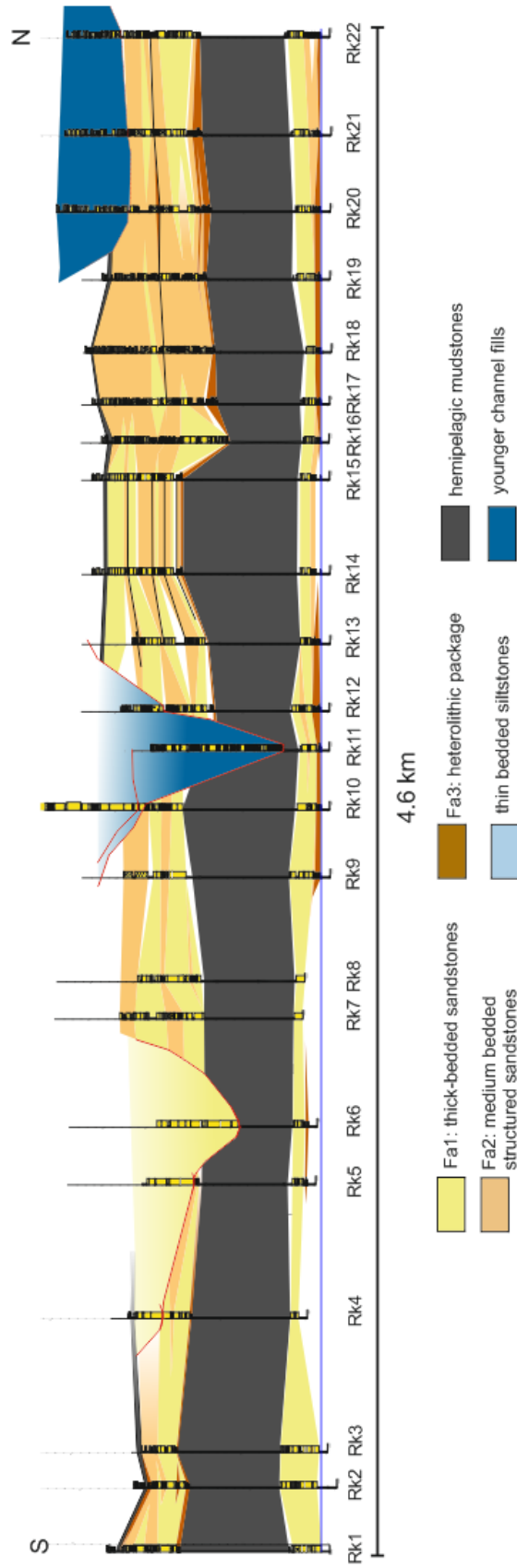
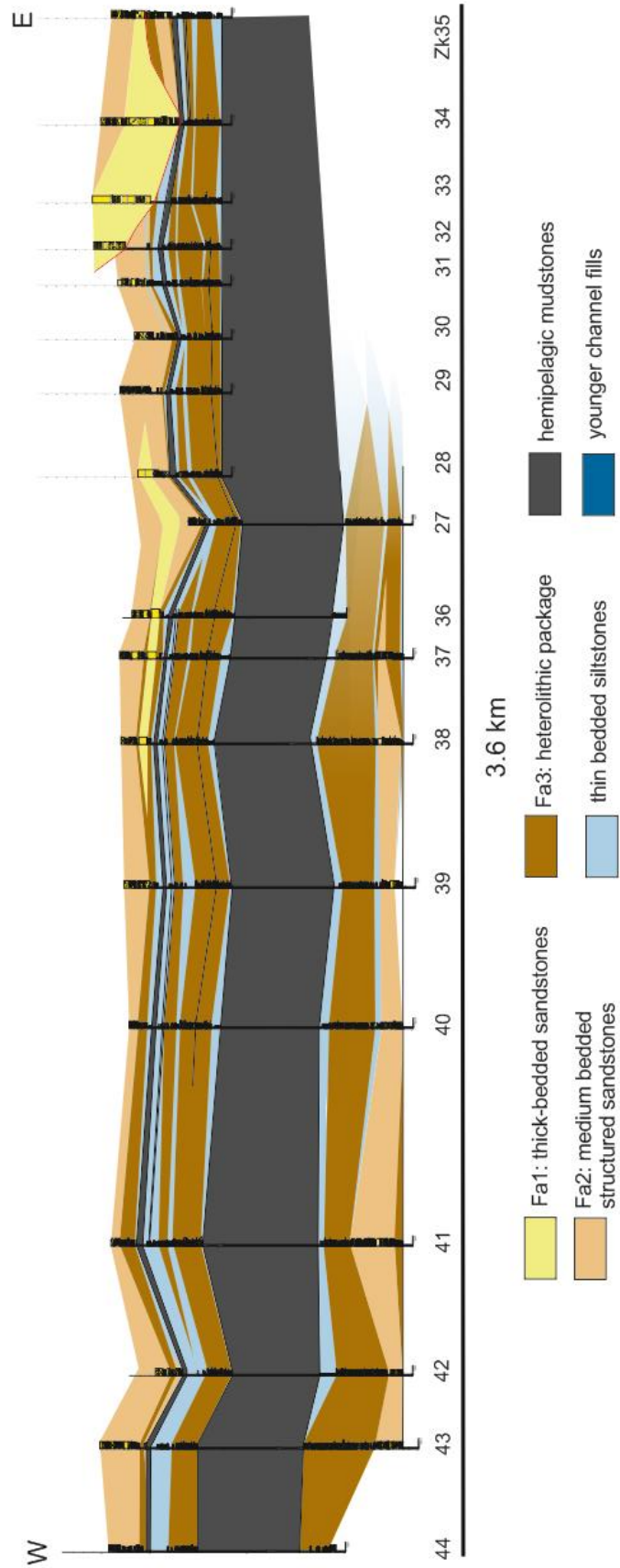*Figure E.2. Roggekraal correlation panel of Unit D/E and E1, Fort Brown Formation; RK: Roggekraal*
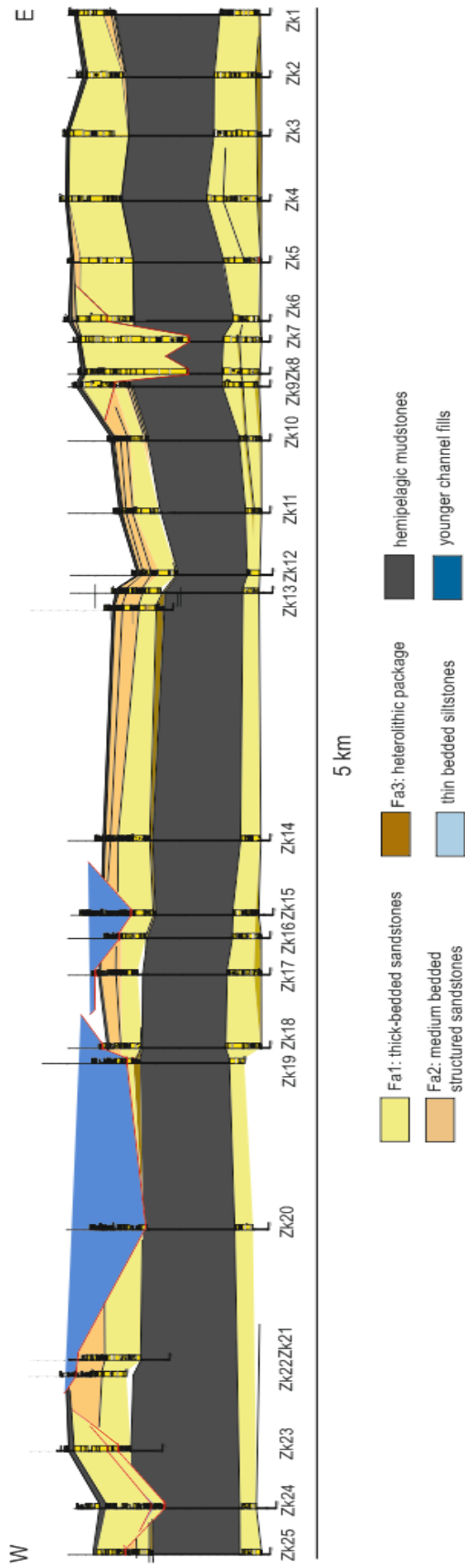
Figure E.3. Zoutkloof North correlation panel of Unit D/E and E1, Fort Brown Formation; Zk: Zoutkloof

Figure E.4. Zoutkloof South correlation panel of Unit D/E and E1, Fort Brown Formation; Zk: Zoutkloof

Tanqua depocentre

10 km

N

KB1-7

IoS1
IoS2
IoS3
IoS4
IoS5

IoS6   IoS7
VF   OC7+8
KF5   OC1-6

KF3   KF4
KF2
KF1   KF6
KF7

NS1

GF1

GF2   RW2
GF3   RW1
GF4
SF4   GF5   HK1
SF3   HK2   GBE
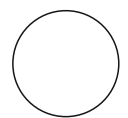   SF1   NS2
SF2   NB2

BK

NS3

KK1

well locations

Fan 4
Skoorsteenberg
Formation

NS4

OR1

Laingsburg depocentre

WHF2 WHF1 WK1
DAF
2 1
R354
3 2 1
JF
ZKNL

DK-1
2 1 3 4 DF2 DF1
DK

SWL2 RK16-32
RK1 RK1-15
SWL1 ZK1-14
ZK15-25
ZK26-44

BSL-1
Bav-1b
SK1
SK2

GB1-45

N

10 km
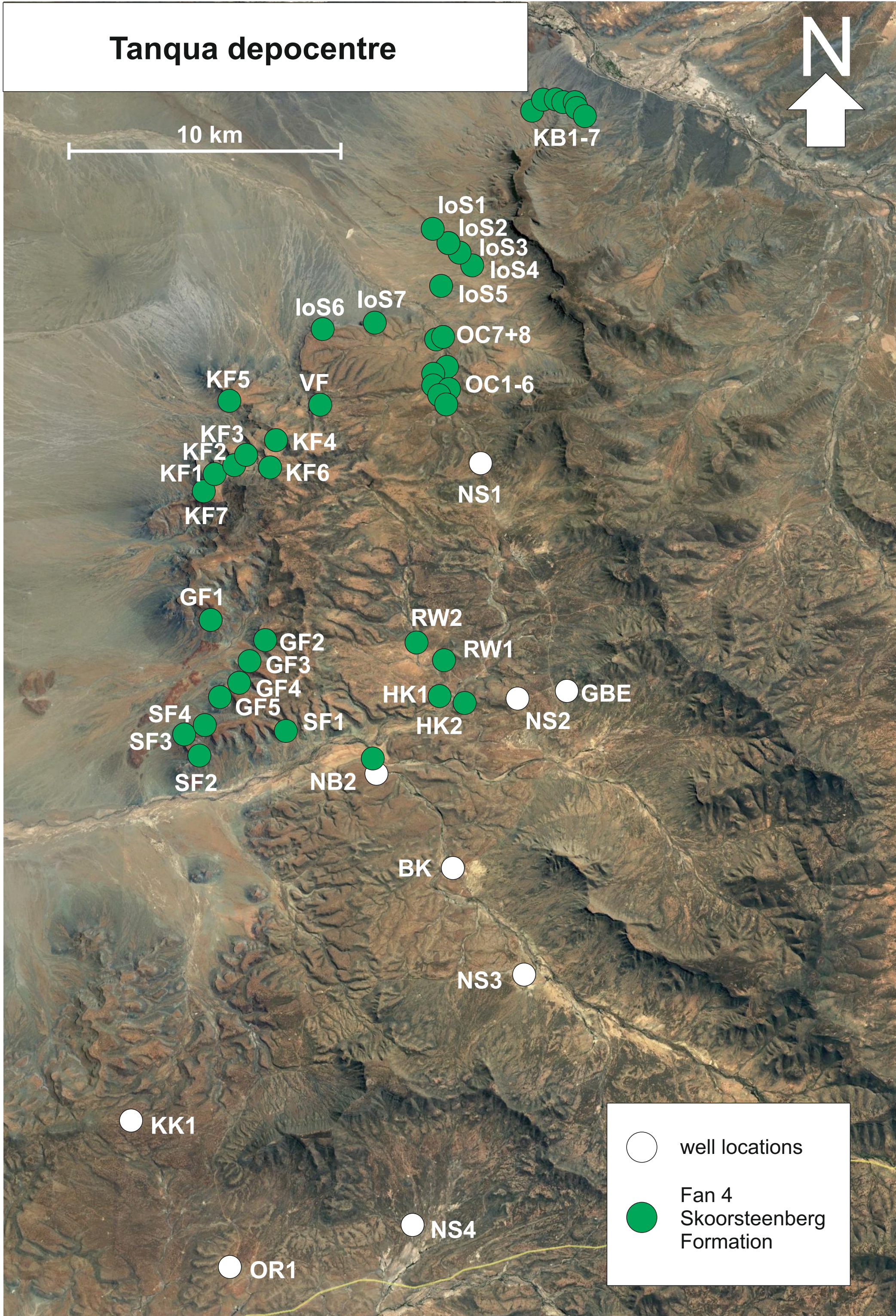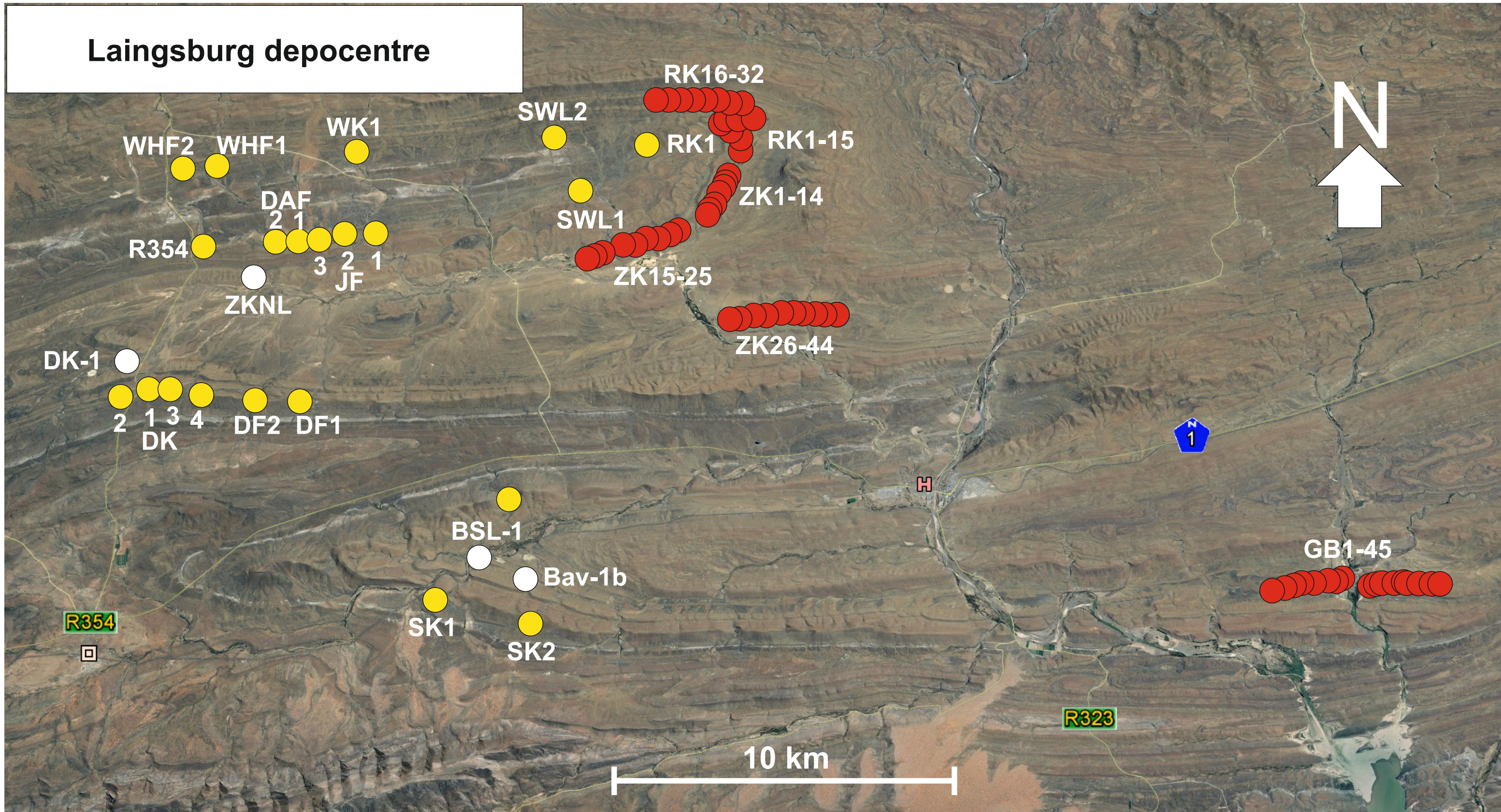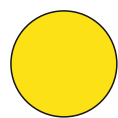
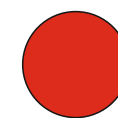○ well locations   ● Laingsburg Formation   ● Fort Brown Formation